THE UNIVERSITY
of EDINBURGH

Regulation and Effects of IRF-1 and p53 Ubiquitination

Vivien Landré

Doctor of Philosophy

The University of Edinburgh

June 2013

Declaration

I hereby declare that I am the author of this thesis. The work herein is entirely my own unless otherwise clearly indicated and acknowledged. I can confirm that this thesis has been submitted for the degree of Doctor of Philosophy and no part of this work has been submitted for any other degree or professional qualification.

Vivien Landré

27th of June 2013

Acknowledgements

First of all I want to thank my great supervisor Kathryn for her patience, guidance and for always believing in me. I am very grateful to her for giving me the opportunity to join her research group and sharing her passion for science with me in endless discussions. A huge thank you to all lab members of the Ball and Hupp group, for all the help, but also the pub nights, tea breaks and always having someone to chat to. I need to especially thank Vikram, Emma and Magda for their help and support, particularly when I was starting out in the lab. Thanks also to Vikram, for his constant interest in my project, as well as for allowing me to work with him and to learn from him. A big thank you to Chandra for mentoring me on the arts of molecular dynamics with incredible patience, I moreover thank everyone in his lab for helping me cope with computational science, especially Thomas, Gloria and Jianguo. I am also very grateful to Nick Gilbert for taking so much time to teach me and to help me to set up assays. I thank Ted for his constant interest in my research and valuable advice along the way, Dimitris for his supervision and the opportunity to go to Dundee to map ubiquitination sites and my fellow PhD students, Terry and Magda, for countless coffee breaks to help me keep my sanity! Thanks to all the people that helped me writing this thesis by proof reading and giving me advice, Kathryn, Terry, Magda, James and CarrieAnne. Lastly, I also want to thank all the amazing people in my life who made me the person I am, most importantly my family, especially my mum, my sister and my dad for their unconditional love and support, Gabriel for being so wonderful to me and the best of friends that I have met over the years and that never felt far away - no matter if in Edinburgh, Germany, Norway, Austria or Lao - and were always there for me when I needed a 'science break' Josefine, Franziska, Katharina, Kjersti and James.

Abstract

Protein ubiquitination is a key regulator of both protein stability and activity, and is involved in the regulation of a vast variety of cellular pathways. The ubiquitination system therefore provides an exciting target for drug development aiming to regulate the function of specific proteins. Our understanding of ubiquitin signalling is far from complete; and if we are to exploit this system for the benefit of human health, it is important to gain a better understanding of this complex posttranslational modification system as well as the effect of ubiquitination on the target protein. The E3 ligases MDM2 and CHIP were implicated in the control of the two transcriptional activators (TAs) IRF-1 and p53, that normally function to maintain health at the cellular and organismal level. Research carried out as part of my PhD has focused on gaining a mechanistic understanding of the ubiquitination process in particular the relationship between the E3 ligase and its substrate. Broadly, the mechanisms of E3 ligase regulation have been linked to substrate specificity and then to the physiological outcome of site-specific ubiquitination of the DNA binding domain of the TAs IRF-1 and p53. More specifically I have; (i) identified a mechanism by which the E3 ligase activity of the CHIP U-box can be allosterically regulated by ligand binding to its TPR domain. (ii) Residues on IRF-1 that are targeted by MDM2 and CHIP have been mapped, revealing that both ligases modify sites exclusively in IRF-1's DNA binding domain (DBD). Furthermore, I showed that, in its DNA bound conformation, IRF-1 is neither bound nor ubiquitinated by the ligases, suggesting a mechanism by which IRF-1 ubiquitination and possibly degradation can be regulated through its DNA binding state. And lastly, (iii) I have shown that both IRF-1 and p53, which have ubiquitin acceptor lysines in their DBD, bind DNA more stably when ubiquitinated. Modelling suggests that interactions between a positively charged surface area of ubiquitin and the negatively charged DNA can stabilises the TA-ubiquitin complex. DBD ubiquitination sites are required for full transactivation potential of both TAs, supporting a role of ubiquitin in their activation. p53 is ubiquitinated in response to activation by IR or Nutlin-3 and these ubiquitinated forms of p53 are localised in the cell nucleus associated with chromatin and do not lead to protein degradation. Taken together, the data imply that p53 and IRF-1 DNA binding ability, and thereby activity, can be modulated by ubiquitin modification.

Abbreviations

aa	Amino acid
AMP	Adenosine monophosphate
ATP	Adenosine triphosphate
ATM	Ataxia-telangiectasia Mutated
BAX	Bcl-2 associated protein X
bp	Base pair
BSA	Bovine serum albumin
DMSO	Dimethyl sulphoxide
DNA	Deoxyribonucleic acid
DTT	Dithiothreitol
E.coli	*Escherichia coli*
EDTA	Ethylenediaminetetraacetic acid
GST	Glutathione S-transferase
HEPES	4-(2-hydroxyethyl)-1-piperazineethanesulfonic acid
His	Histidine
HRP	Horse radish peroxidase
IFN	Interferon
ITPG	Isopropyl-β-thio-galactoside
IR	Ionising radiation
kDa	Kilodalton
mAb	Monoclonal antibody
MEF	Mouse embryonic fibroblast
mRNA	Messenger RNA
OD	Optical density
pAb	Polyclonal antibody
PAGE	Polyacrylamide gel electrophoresis
RNA	Ribonucleic acid
rpm	Revolutions per minute
SDS	Sodium dodecyl sulphate
Tris	2-amino-2-hydroxymethyl-propane-1,3-diol
wt	Wild type

Table of Contents

Figures

Tables

Chapter 1: Introduction

1.1 Ubiquitination

Protein ubiquitination, first discovered in 1975 by Aaron Ciechanover, Avram Hershko and Irwin Rose [1, 2], was shown to play a major role in proteasomal degradation of proteins. One or several ubiquitin molecules, a protein consisting of 76 amino acids, are attached to a lysine on a target substrate. A chain of a minimum of four ubiquitin molecules is recognised by the 26S subunit of the proteasome and subsequently unfolded and degraded [3]. Degradation of proteins by the ubiquitin/proteasome pathway (UPS) is the most prevalent mechanism of controlled protein degradation in cells. Levels of many proteins are tightly controlled to ensure their function and enable a quick and controlled response to stresses or stimuli. This is especially important for proteins involved in mechanisms ensuring cellular homeostasis, e.g. proteins that play a role in the cell stress response, cell cycle and cell death pathways. In addition to these functions, the UPS plays an important role in the elimination of misfolded and aggregated proteins from the cell. However, although ubiquitination as a signal for degradation is the best-studied function for this modification, since its discovery almost endless roles for ubiquitination in the regulation of all kinds of cellular pathways have emerged. For example, ubiquitination has been shown to be involved in endocytosis, signal transduction, DNA repair, autophagy, cell death pathways and more (Table 1-1) [4-8]; thus it is, as it's name suggests, ubiquitously involved in most cellular processes. Ubiquitination is not only the most common but also the most diverse posttranslational modification. This is due to the complexity of the system. As mentioned above, a chain of at least four ubiquitins attached to a target protein can lead to its degradation, however this is only one of many possibilities for the outcome of an ubiquitination reaction. Chains of up to three ubiquitins are common and in most cases do not lead to degradation of the substrate, but can alter its function or localisation. Ubiquitin chains are linked through any of the seven lysines in the molecule (K6, K11, K27, K29, K33, K48, K63) [9], or less commonly through the N-terminal methionine residue of ubiquitin

(M1;[10]). Different chain linkages have been shown to be involved in different cellular processes and, additionally, chains can consist of a mix of different linkages or can even be branched [11, 12]. Branched chains do not associate with the proteasome and therefore do not signal substrate degradation [11, 12].

Adding even more complexity to the system, other ubiquitin like proteins (Table 1-1) have been identified and can be used separately or as part of a mixed ubiquitin chain. This results in almost endless possibilities of protein modification by this system [13], inevitably leading to the question of how such a complex system of modification is controlled. In recent years advances have been made in understanding the regulation of ubiquitination for many proteins, however, many details of how the system is controlled remain elusive.

Considering the complexity of the ubiquitin system, it is not surprising that up to 5% of the human genome encodes proteins involved in ubiquitination pathways [14]. There are two main ubiquitin E1 enzymes, around 30-40 E2s and hundreds of E3 ligases with more being characterised all the time [14]. Protein ubiquitination exclusively appears in eukaryotes, where it is highly conserved from yeast to human, with only three conservative changes in the ubiquitin protein [5]. Although, no ubiquitination like modification system has been identified in prokaryotes, homology searches have identified enzymes in the sulphur pathway of *Escherichia coli* that have similarity to the E1 enzyme of the ubiquitination cascade. This protein, MoeB, is involved in the biosynthesis of the molybdenum cofactor, Moco [15]. Moreover, other proteins involved in the moco and thiamine pathways of different bacteria species have been shown to have similarity to E1 and also E2 enzymes. These proteins are believed to be evolutionarily more ancient than the ubiquitin pathway in eukaryotes, suggesting that they might have formed the origin from which the ubiquitin system has evolved [5, 16, 17].

As ubiquitination is involved in the control of many cellular processes at different levels, it is not surprising that its dysregulation plays a major role in the development of a wide range of diseases, including cancers, neurodegenerative disorders such as Parkinson’s disease, Huntington’s disease and Alzheimer’s disease, type 2 diabetes

and in certain severe types of mental retardation (such as Angelman syndrome) [5, 18]. Thus, a large effort is being made to study this system, its regulation and dysregulation in disease, aiming to find novel drugs and drug targets.

1.1.1 Ubiquitination reaction

The ubiquitination cascade comprises three enzymes E1, E2 and E3 (Fig 1-1). In an initial step, the ubiquitin-activating enzyme (E1) activates ubiquitin by adenylating the C-terminus and forming a thioester bond between a cysteine residue in its active site and the C-terminal glycine of ubiquitin. This step is ATP dependent. For full activity of the E1, it has to non-covalently bind to and adenylate another ubiquitin molecule [19, 20]. In the second step, the ubiquitin linked to the E1 is transferred to the E2, where it is again linked to an active cysteine via a thioester bond. The ubiquitin 'charged' E2 binds an E3 ligase, and in a last step, the E3 catalyses the transfer of ubiquitin from the E2 onto a substrate [21]. There are three classes of E3 ligases the RING-, U-Box and the HECT- domain proteins. HECT domain E3 ligases bind to specific E2 enzymes and contain an active site cysteine residue that forms a thioester bond with ubiquitin in an intermediate step, the ubiquitin then transfers directly from the E3 to the substrate [6, 22, 23]. U-box and RING domain E3 ligases, on the other hand, are unusual enzymes as they lack a catalytic site and are believed to act as a scaffold, positioning the substrate, E2 and ubiquitin and thereby allowing transfer of ubiquitin to the substrate. One round of this cascade leads to addition of one ubiquitin to a lysine of the substrate protein, in many cases not only one, but a chain of ubiquitins is attached to a target protein. Different theories have been proposed to explain how these chains are formed. It has been suggested that preformed ubiquitination chains are attached to the substrate; this is supported by the fact that free, unanchored ubiquitin chains are present in the cell [24]. However, no evidence has been given for this concept and *in vitro,* where addition of ubiquitin to a protein appears to be sequential. The most likely mechanism seems to be several

rounds of the reaction described above, where one of the lysines in the ubiquitin already attached to the substrate serves as the ubiquitin acceptor in the second round, and therefore the chain is elongated round by round [24]. This model raised the question of the need for a so-called E4 enzyme, which is responsible for chain elongation after an E3 ligase has facilitated the transfer of the first ubiquitin to a substrate [25]. It is clear that the formation of an ubiquitin chain would require major conformational changes in the enzymes or enzyme complex involved in the process, allowing the machinery to build and move along an ubiquitin chain. It is thus possible that an E3 ligase can also act as an E4. Multi-protein E3 complexes and E3 oligomerisation has been observed in cells, and these could be involved in the formation of ubiquitination chains. In this case, a different protein or a different molecule of the same E3 in a complex could act as the E4 [25-28]. As discussed later, interplay between distinct E3-E2 pairs appears to be important in controlling chain linkages and length.

In most cases ubiquitin is attached to a lysine of a target protein, however, ubiquitin linked via the formation of esters or thioesters to threonine and serine or cysteine residues respectively has also been observed. Additionally, ubiquitin can be conjugated to the N-terminal α-NH_2 group of protein. These atypical linkages have been shown to serve mainly as signals for degradation [29-31].

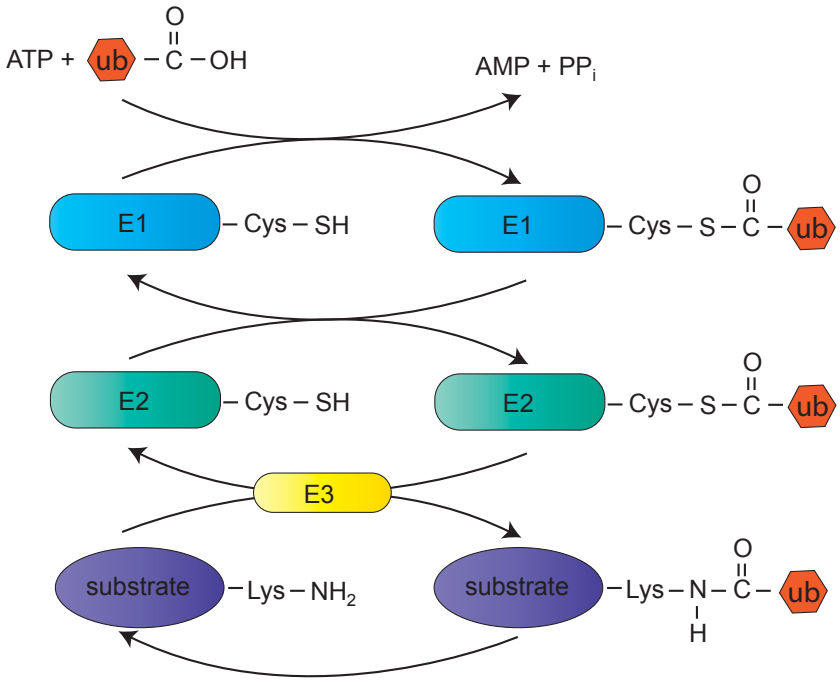

Figure 1-1 Ubiquitination cascade (adapted from Passmore and Barford, 2004 [28]) Overview of the ubiquitination reaction involving three enzymes, E1 (ubiquitin activating enzyme), E2 (ubiquitin conjugating enzyme) and E3 (E3 ligase).

1.1.1.1 Chain linkages

Ubiquitin chains linked via K48 and K11 in ubiquitin are the most common; however, chains linked via any of the 7 lysine residues and the N-terminal methionine have been observed *in vivo* and a chain of at least 4 ubiquitins linked by either residue have been shown to associate with the proteasome [9]. A proteomic study in budding yeast revealed the relative abundance of the different chain linkages in the following order K48 (29%), K11 (28%), K63 (17%), K6 (11%), K27 (9%), K29 (3%) and K33 (3%) [32]. Remarkably, the most studied K48 linkage was as abundant as linkage via K11. Roles of ubiquitin chains linked by K11 are less well understood, however, it is has been the focus of intensive research over the past years, and its roles are now increasingly better understood. Additionally, it has to be noted, that the ratio of chain linkages may vary in different species, under stress conditions or during disease. Little is known about the abundance of linear ubiquitination chains, where the C-terminus of one chain is attached to the N-terminus of another by a 600 kDa E3 ligase complex called the linear ubiquitin chain assembly complex (LUBAC), which consists of HOIL-1, HOIP and Sharpin [10]. Modification of proteins by linear ubiquitination chains has been shown to be involved in different cell signalling pathways [33]. Chains are not always linked by only one residue on ubiquitin; mixed chains have been observed, as well as branched chains, where one ubiquitin molecule is linked to two further ubiquitins molecules (Fig 1-2) [11, 12]. This raises questions regarding the control, function and specificity of the different chain types. It has been suggested that in many cases, ubiquitination is unspecific and that lysines on the substrate are targeted randomly. If this is the case, it is difficult to imagine that chain elongation could be more specific, targeting specific lysine residues on ubiquitin. However, more and more evidence is being found that specific linkages signal for specific events, for example linkages via K63, have been shown to play a major role in cell signaling/kinase activation [34, 35]; and it is thus widely accepted that ubiquitin chain linkages are generated specifically. Furthermore, in many cases ubiquitination of lysine residues has been shown to be specific to either a certain residue or domain of a protein [8]. This illustrates how the system must be controlled on several levels to ensure correct substrate modification with the right length and linkage of the chain. Not only one,

but many lysines within one substrate can be modified by either one ubiquitin or an ubiquitin chain, resulting in multi-mono or multi polyubiquitination (Fig 1-2).

1.1.1.2 Ubiquitin Structure

The 76 amino acid containing protein ubiquitin is folded in a compact β-grasp fold [36], which is conserved among all ubiquitin like (UBL) proteins, and contains a 6 amino acid long flexible C-terminal tail (Fig 1-3). Ubiquitin is extremely stable, tolerating temperatures up to 100°C and has a half life of about 10 hours in cultured cells [4]. Overall ubiquitin adopts a very rigid conformation, with only certain residues within its binding pockets displaying limited flexibility to allow protein-protein interactions [8]. Ubiquitin contains seven lysine residues, which are involved in chain formation. All ubiquitin lysines are exposed and scattered over the surface of the protein (Fig 1-3a). Ubiquitin has three hydrophobic patches, which mediate interactions with its binding partners and the proteasome (see Fig 1-3b) [8]. The hydrophobic patch around Ile^{44}, Leu^{8}, Val^{70} and His^{68} is involved in the majority of interactions with ubiquitin binding proteins (UBP) and the proteasome [37-39]. Another hydrophobic surface lies around the residues Ile^{36}, Leu^{71} and Leu^{73} and is important for recognition by some HECT E3 ligases and involved in the interaction of ubiquitin molecules within an ubiquitin chain [40-42]. The hydrophobic patch around Gln^{2}, Phe^{4} and Thr^{14} has been identified as being required for cell division in yeast [39], and interacts with certain proteins including the ubiquitin-specific protease (USP) domain of some DUBs [41]. The TEK box, which is required for K11 linked chain elongation by the anaphase promoting complex (APC/C) and UbcH10, and mitotic degradation in higher eukaryotes, consists of the residues Thr^{12}, Thr^{14}, Glu^{34}, Lys^{6} and Lys^{11}[8, 43]. X-Ray and NMR structures of ubiquitin chains reveal significant differences in the three-dimensional structure and exposed surface of chains with different linkages (Fig 1-3c) [8, 44-46]. While chains linked by K48 or K11 have a closed and compactly packed conformation, chains linked by K63 and M1 exhibit a more open conformation and expose surface residues that are buried in the K48 and K11 chains, with no contact points of the ubiquitin molecule besides the

linkage site. This more open conformation gives the ubiquitin chains flexibility and allows them to adjust their conformation despite the very rigid structure of ubiquitin [4, 8].

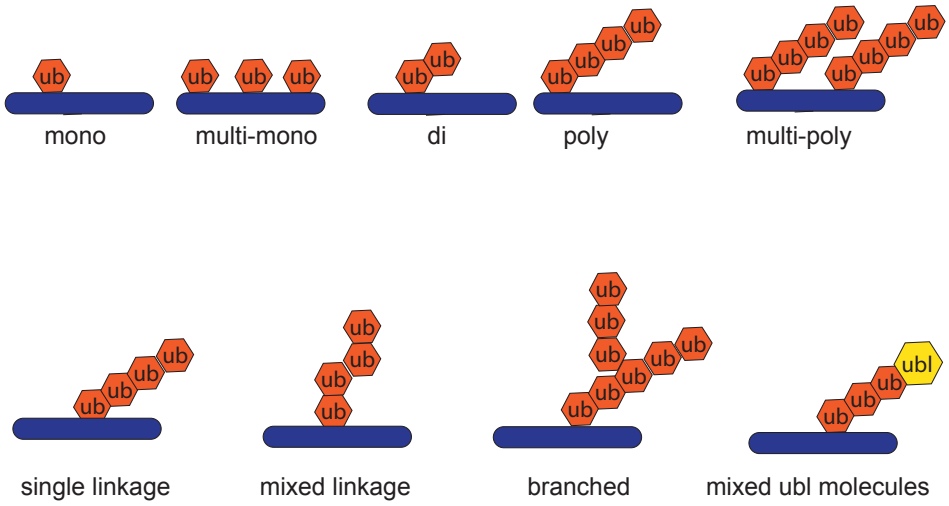

Figure 1-2 Types of ubiquitination

Protein ubiquitination can result in an array of outcomes. If a single ubiquitin molecule is attached to a substrate, it is described as mono-ubiquitination and this generally does not lead to proteasomal degradation. Several ubiquitin molecules can be attached to a protein as a chain, resulting in polyubiquitination. Often multiple ubiquitin molecules or chains are linked to different lysine residues on a target protein, resulting in multi- mono or multi-polyubiquitination. Ubiquitin chains can consist of different linkages or even different types of ubiquitin like modifiers, giving a vast array of diversity to the system.

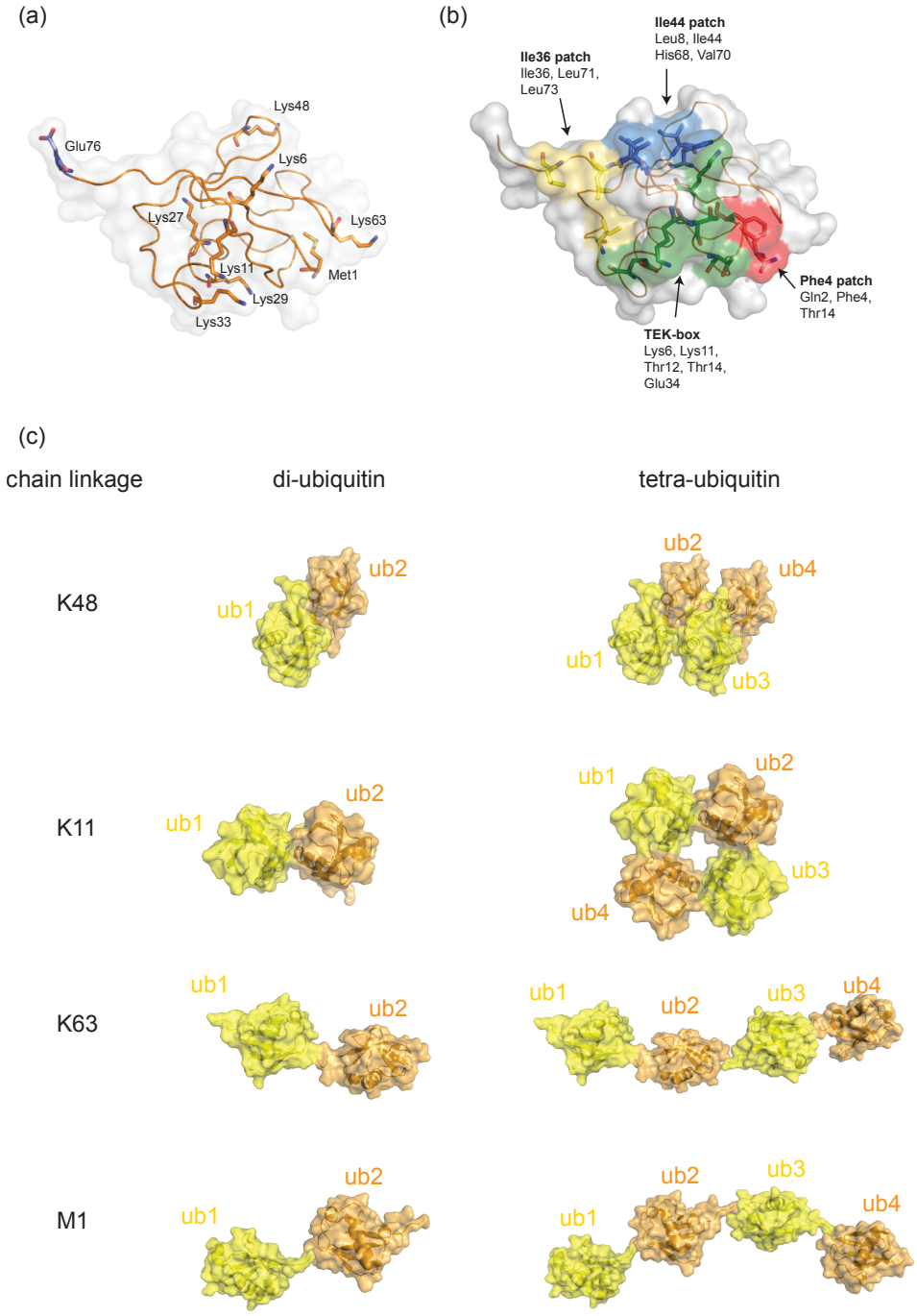

Figure 1-3 Structure of ubiquitin and ubiquitin chains

(a) Ubiquitin structure (PDB: 1ubq [36]) as ribbon with linkage sites indicated by sticks. Residues for chain elongation are in orange and C-terminal glycine in blue. (b) Ubiquitin surface with patches involved in protein-protein interactions highlighted. (c) Structures of ubiquitin chains linked by K48 (PDB:1aar [45]), K11 (PDB:2xew [44]), K63 (PDB:2jf5 [47]) and M1 (PDB:2w9n [47]). Tetra ubiquitin chains were modelled using the respective di-ubiquitin crystal structure.

1.1.2 E2 - E3 interaction

The endless possibilities of ubiquitination events show that the mechanisms leading to ubiquitination have to be controlled tightly to ensure creation of the right molecular signal. Many details about the exact regulation, and how specificity is controlled, remain unknown. It appears that the E3 ligase is mainly responsible for substrate specificity, while chain linkage and length are achieved through the interplay of specific E2-E3 pairs [12, 48]. It has been shown that many E3 ligases can interact with a set of different E2 enzymes resulting in the formation of different types of ubiquitin chains or mono-ubiquitination of the substrate. The E3 ligase complex of BRCA1 and BARD1 for examples has been shown to interact with at least 10 different E2 enzymes. Some of these E3-E2 pairs are required for attachment of the first ubiquitin while other pairs result in the formation of various chain linkages [49, 50]. In this case, the E2 determines whether a certain E3 ligase has the ability to act as an E4 ligase and promote polyubiquitin chain formation or is restricted to act as a monoubiquitination ligase. Some E2s are connected to a certain chain specificity e.g. Ube2G2 has been shown to assemble K48 linked chains while Ube2S is specific to forming K11 linked chains [8]. HECT E3 ligases seem to play a bigger role in determining chain specificity when compared to RING E3 ligases, because they directly bind to and transfer ubiquitin to the substrate. RING E3 ligases on the other hand act as a building block forming a complex of E3, E2, ubiquitin and substrate and facilitating the transfer of ubiquitin from the loaded E2 onto the target residue [12, 24, 48].

Recently the crystal structure of a charged E3-E2-ubiquitin complex has been solved [46] (Fig 1-4). The structure gives insight into the packing of the complex leading to ubiquitination. It shows that the E3 interacts not only with the E2, but also with the E2 bound ubiquitin, resulting in a tightly packed complex of the three molecules. The E3 now directs the ubiquitin to a target lysine, which can be on the E3 ligase itself resulting in autoubiquitination, a lysine on a target substrate or a different ubiquitin molecule. A distinct set of E2-E3 enzymes can, in many cases not only lead to ubiquitination of one specific lysine, but several different residues in one protein. While the static crystal structure does not reveal the degree of flexibility of the

complex, analysis of the UbcH5c–ubiquitin complex by both NMR and SAXS (small-angle X-ray scattering) [39] has shown that the E2-ub conjugate is very flexible and can exhibit a range of conformations in solution. Taken together these experiments suggest that even though all members of the complex interact with each other, the complex is not static and can adopt different conformations, explaining how one E3 ligase can mediate ubiquitination of several different residues within a target protein.

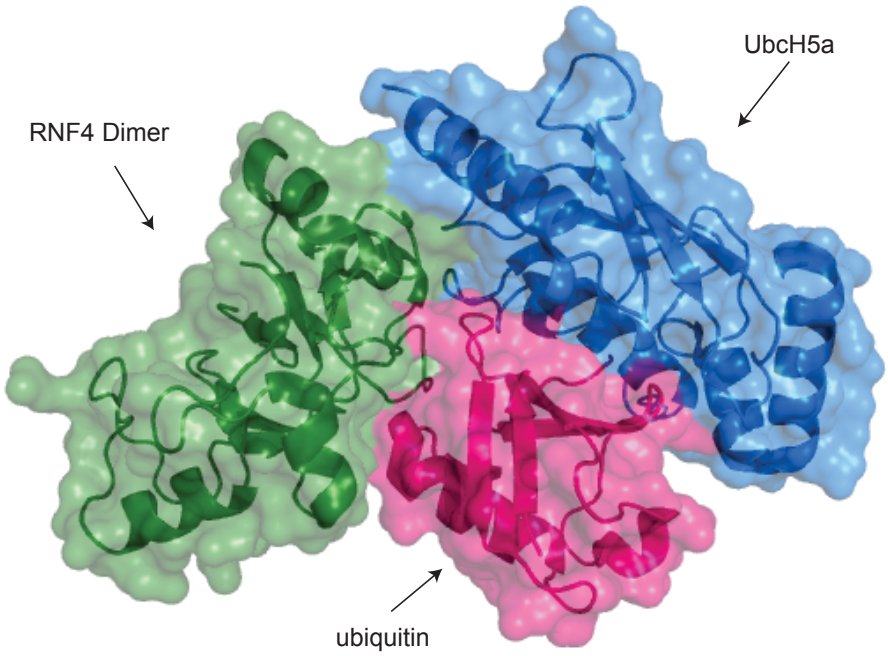

Figure 1-4 Structure of the E3 ligase RNF bound to ubiquitin charged UbcH5a
Crystal structure of the E3 ligase RNF4 (green) in complex with the E2 UbcH5a (blue) and ubiquitin (pink) (PDB:4AP4 [46]). The complex is an intermediate of the ubiquitination cascade; in the next step ubiquitin is transferred from the E2 onto a residue on the target substrate.

1.1.3 Ubiquitin binding proteins

Apart from being recognised and bound by the proteasome, ubiquitin and ubiquitin chains can interact with a variety of different proteins, which have an ubiquitin-binding domain (UBD). These proteins recognise the ubiquitin modification and act as effector molecules that transduce the signal to downstream cellular events. Around 200 proteins in the cell are estimated to contain a UBD with which they can bind ubiquitin, either when it is attached to a protein or free as a single molecule or chain [37]. The different UBDs differ greatly and so far, 16 distinct tertiary structures have been identified that bind to ubiquitin. The domains differ in size from 30-150 residues and are specific to either a certain surface region of ubiquitin or a specific chain linkage [51]. Some UBDs are specific to one of the three hydrophobic patches of ubiquitin (see Fig 1-3) and can therefore only bind ubiquitin, if this patch is not buried by protein interactions with the ubiquitin substrate or a different ubiquitin molecule in a chain. Detailed information of how UBD can distinguish between different linkages is still missing. One example of how chain specificity can be achieved is through the repeat of several UBDs in one ubiquitin binding protein [52]. Consequently some ubiquitin interacting proteins consist of tandem repeats of the ubiquitin interacting motif (UIM), which recognises the patch around the Ile^{44} residue on ubiquitin. Since packing of the ubiquitination chains differs remarkably (see Fig 1-3c) and the distance between two ubiquitin molecules is distinctive for a specific chain linkages, two UIM motifs separated by a spacer of a specific length can recognise different types of chains [8, 51]. Ataxin-3 for example has two repeats of this motif connected by a small spacer, these two UIM can recognise ubiquitin molecules that are connected by a K48 linkage and are therefore packed tightly [53]. A sub-unit of the BRCA1-E3 ligase Rap80, on the other hand, has two UIM separated by a longer spacer; these domains can recognise ubiquitin molecules in an extended conformation for example in K63 linked chains [54]. Another mechanism by which UBDs can recognise specific chain linkages is by contacting two ubiquitin molecules at the same time. In this case, the patches on ubiquitin bound by the UBD are only exposed in a conformation next to each other in chains with a certain linkage [55, 56]. Interestingly, residues around the linkage site itself are, in most cases, not involved in the interaction of the ubiquitin binding domain and ubiquitin. The

linkage rather is important to predict the packing and orientation of the ubiquitin molecules, which is recognised by the UBDs [8].

1.1.4 Deubiquitination enzymes

Ubiquitination is a reversible modification and around 100 deubiquitinating enzymes (DUBs) have been identified so far, with human cells containing around 55 DUBs [8, 57]. These enzymes remove ubiquitin conjugates from substrates and depolymerise ubiquitin chains. This is an important mechanism to ensure that the ubiquitin signal can be controlled carefully in response to stresses or stimuli. DUBs are divided into five main classes, one metalloprotease class and four Cys protease classes [58]. One main function of a subset of DUBs is to protect ubiquitin from degradation by the proteasome; these DUBs are associated with the proteasome and remove ubiquitin from the substrate before it can itself be unfolded and degraded [38]. The cell thereby recycles ubiquitin, ensuring that cellular levels of the protein remain high, saveguarding cellular resources. The other important function of DUBs is to specifically deubiquitinate certain substrates and thereby control the ubiquitination state of certain proteins in response to stimuli [8]. These DUBs tend to be linkage unspecific and act on a certain set of substrates. An example of fine control of the activation state of a protein by E3 and DUB activity is NF-κB. Activation of NF-κB relies on ubiquitination of different proteins by K63 linked chains while deactivation of NF-κB is achieved by deubiquitination of these proteins and ubiquitination of NF-κB by K48 linked chains leading to its proteasomal degradation. Strikingly, the same protein, A20, is responsible for both events; it has both DUB and E3 ligase activity and removes the K63 chains responsible for NF-κB activation with its DUB activity and simultaneously ubiquitinates NF-κB, targeting it for degradation [8, 52, 59-61].

1.1.5 Ubiquitin like modification

Ubiquitin is the leading member of a class of small molecules that modify proteins, which are collectively called ubiquitin like (UBL) proteins. All UBL proteins contain a β-grasp fold as their three dimensional core structure and are attached to substrates via a similar cascade to ubiquitin. So far nine classes of UBL proteins have been identified; these are SUMO, NEDD8, ISG15, FUB1, FAT10, Atg8, Atg12, Urm1, and Ufm1 (Table 1-2) [62]. It is likely that additional UBL molecules will be identified in the future. Despite sharing the same three-dimensional structure, UBL proteins have a low sequence similarity, but are believed to have evolved from a common ancestor (Table 1-2) [5]. UBL proteins are involved in regulation of DNA replication, signal transduction, cell cycle control, embryogenesis, cytoskeletal regulation, metabolism, stress response, homeostasis and mRNA processing and others [62]. UBL modification can inhibit ubiquitination by targeting the same lysine residue, and also can work hand in hand with ubiquitination by forming mixed chains that contain different UBL modifiers [5, 13, 62].

Additionally, ubiquitin like domains (ULD) within bigger polypeptides have been identified. These domains fold in the same way as other UBL proteins but are not processed or attached to other proteins. These ULD can be recognised by proteins with UBD and, similarly to other ubiquitin like modifiers, ULDs can trigger the interaction with ubiquitin binding proteins [5].

1.1.5.1 SUMO

SUMOylation is the best-studied UBL modification apart from ubiquitination. Like ubiquitin, SUMO can form polymers and is involved in a variety of cellular pathways, including the control of genome stability, signal transduction, targeting to, and formation of, nuclear compartments, cell cycle and meiosis [62-66]. SUMO chain formation is achieved mainly through SUMO residue K11 [67]. Three isoforms have been confirmed in humans; these are SUMO-1, SUMO-2 and SUMO-3. SUMO binding proteins containing a so called SUMO-interaction motif (SIM) have been identified and shown to have a higher affinity for SUMO than ubiquitin binding proteins for ubiquitin [65]. SUMO and ubiquitin both target lysine residues and are therefore two mutually exclusive modifications. Nevertheless, both have been shown

to work in synergy, e.g. some proteins were shown to be SUMOylated in a first step, which in turn serves as a signal for ubiquitination in a second step leading to proteasomal degradation [5, 65, 67].

SUMOylation can affect the activity of its target proteins by changing their affinity for their binding partners. One example of this is the DNA glycosylase (TDG), which when SUMOylated undergoes conformational changes that decrease its DNA binding affinity [68, 69].

1.1.5.2 NEDD8

NEDD8 is another UBL protein with 55% sequence identity to ubiquitin. Only limited substrates have been identified for NEDDylation, however, it has become the focus of more intense research in recent years. The transcription factor p53 has been shown to be modified by NEDD8, via a mechanism that is dependent on its E3 ligase MDM2 and leads to transcriptional inactivation of this transcription factor [70]. Another important role of NEDDylation is the activation of the superfamily CRL E3 ligases [71]. NEDDylation of CRL ligases is essential for their activation. Many of these CRL ligases are involved in development of cancers and other diseases. The NEDDylation pathway, including NEDD8-activating enzyme, NAE and the two NEDD8 E2 enzymes UBC12 and UBE2F therefore provide an interesting protein for research aiming to identify novel drug targets [72-74].

1.1.5.3 ISG15

ISG15 was the first ubiquitin like protein identified after ubiquitin in the late 1980s and has been shown to play a role in the innate immune response to viruses. ISG15, its E1 (ISG15-activating) and its E2 (ISG-conjugating) enzymes are strongly induced by type I interferon. Despite being the first UBL protein to be identified, details about its function and regulation remain elusive [5].

Table 1-1 Ubiquitin like modifications [5, 62]

Ubiquitin like modification	Identity with ubiquitin (%)	Function
Ubiquitin	100	Linkage dependent (Table 1-1).
Smt3 (SUMO1, SUMO2, SUMO3)	18	Nuclear transport, DNA replication and repair, mitosis and signal transduction.
NEDD8 (Rub1)	55	Cell cycle control and embryogenesis. May be involved in the formation of aggresomes.
ISG15	32 and 37 *	Modifies STAT1, SERPINA3G/SPI2A, JAK1, MAPK3/ERK1, PLCG1, EIF2AK2/PKR, MX1/MxA, and RIG-1. Displays antiviral activity.
FUBI (MNSF-β or FAU)	38	Translation Gene expression. Viral infectious cycle. Endocrine pancreas development. Cellular protein metabolic processes.
FAT10	32 and 40*	Protein degradation. Activation of innate immunity. Mediates mitotic non-disjunction and chromosome instability in cancers. Caspase-dependent apoptosis.
Atg8	ND	Expression of kappa-type opioid receptor. Intra-Golgi traffic and transport. Intracellular transport of GABA (A) receptors. Apoptosis. Formation of autophagosome.
Atg12	ND	Autophagic vacuole assembly. Negative regulation of type I interferon production.
Urm1	ND	Unknown
UFM1	ND	Ufmylation, unknown function

* Values listed for both two ubiquitin-related domains within the protein. ND=not detectable

1.1.6 Ubiquitin Function

1.1.6.1 Degradation

As describe previously, the best-studied function of ubiquitination is its role in proteasomal degradation. Ubiquitin chains are used as a molecular tag, marking proteins to be recognised and degraded by the proteasome. In the majority of cases, a chain of four ubiquitin molecules linked by either K48 or K11 is both necessary and sufficient for proteasomal degradation. Longer ubiquitination chains increase the affinity for the proteasome and thereby the probability of binding and degradation [8, 75].

Interestingly, tetra-ubiquitin chains of K48 and K63 linkage show the same affinity for the proteasome [76], but while proteins tagged with K48 linked tetra ubiquitin are degraded, proteins attached to a chain linked by K63 are usually not degraded. This has been explained by the structural differences of the chains. As described above K48 chains have a more compact conformation compared to K63 linked chains, and this affects the affinity of the chains for different DUBs. Consequently, K63 chains are deubiquitinated at a faster rate compared to K48 chains, releasing the substrate before the proteasome has unfolded and cleaved it, K48 linked chains, on the other hand, have a slower conversion rate by DUBs and thereby longer residency at the proteasome, favouring degradation [51, 77]. Strikingly, a study by Pickart *et al* showed that chains linked via any of the lysines in ubiquitin bind to the proteasome *in vitro,* suggesting a role in degradation for all of them. *In vivo* chains linked via K11, K29, K48 and K63 have been shown to be involved in signalling protein degradation in different studies [9, 78]. However, the presence of mixed chains makes the investigation of effects of a particular type of chain experimentally challenging, and more work is necessary to confirm the exact roles of different linkages in the degradation of proteins. In certain cases, interactions of the E3 with the proteasome are required for efficient degradation of a protein, suggesting a role of the E3 ligase in delivering the substrate to the proteasome [79]. Other studies suggested that in certain cases mono-ubiquitination is sufficient to signal proteasomal degradation [80-82]. Taken together these studies highlight the fact that

no rigid rule can be applied to the system and that many, often unknown factors, are involved in determining the fate of a protein modified with ubiquitin.

In addition to being the key player in proteasomal degradation, ubiquitination has now been identified as playing a role in autophagy and lysosomal degradation. Accordingly ubiquitin chains, predominantly linked by K63, have been shown to target mainly membrane proteins for degradation via the lysosome [83, 84]. Additionally, mono-ubiquitination of plasma membrane proteins e.g. receptor tyrosine kinases lead to recruitment of members of the endocytic pathway and thereby triggering endocytosis and lysosomal degradation of the kinase [38, 85-88]. Autophagy is important in removal of harmful protein aggregates from the cell, as these aggregates can often be too bulky to be processed by the proteasome. Autophagy receptors that can bind to ubiquitin and autophagy specific ubiquitin like modifiers have been identified, e.g. p62/SQSTM1 and NBR1 [89]. These findings link ubiquitin to the autophagy system, highlighting the role of ubiquitination in the elimination of protein aggregates from the cell.

1.1.6.2 Protein-protein interactions

Ubiquitination can affect protein-protein interactions through four mechanisms (Fig 1-5). (i) It can function indirectly by leading to a conformational change in the protein allowing or inhibiting binding of a binding partner [5]. (ii) The most common mechanism by which ubiquitin mediates interactions between two proteins is by directly being involved in the interaction, providing or extending the molecular surface for the interaction [5, 82]. (iii) Ubiquitin can inhibit binding of another protein by occupying the binding site, and thereby sterically preventing an interaction. However, there are only a few examples of this mechanism *in vivo*. Or (iv) free ubiquitin chains, that are not attached to either of the proteins, can mediate or disrupt interactions [5, 82].

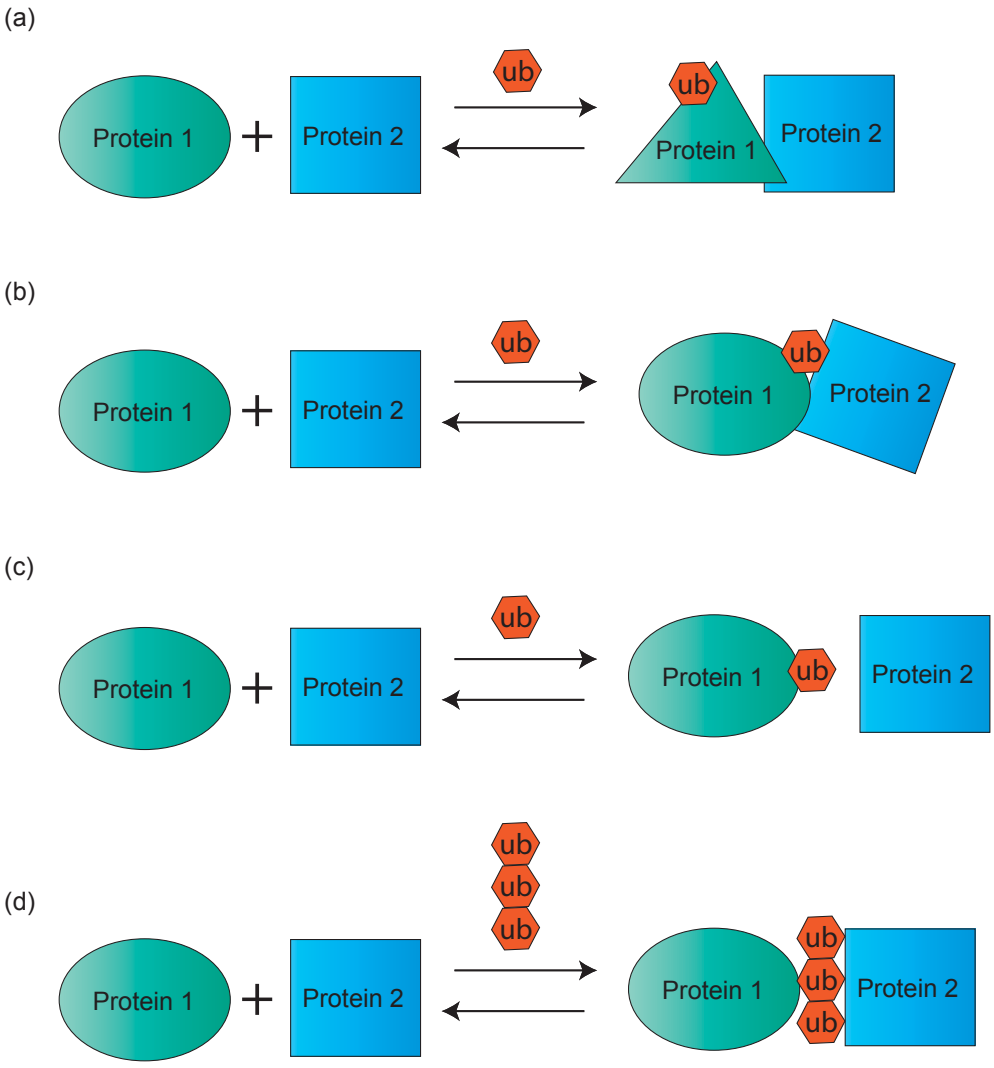

Figure 1-5 Effect of ubiquitin on protein-protein interactions [5]
(a) Ubiquitination of a protein can lead to allosteric changes that allow or inhibit interaction with a binding partner. (b) Ubiquitin can extend the binding surface of a protein interaction and thereby increase the binding affinity of two proteins. (c) Ubiquitin can be attached to a binding interface on a protein and thereby sterically inhibit binding to other proteins. (d) Free ubiquitination chains present in the cell can act as a scaffold in building a protein complex of proteins that have a UBD.

1.1.6.3 Cellular localisation

Ubiquitination has been shown to affect protein localisation. This happens either through ubiquitin binding to a surface important for localisation thereby masking it, or ubiquitin mediating conformational changes leading to unmasking of a protein surface area e.g. a nuclear export signal [5]. Additionally, ubiquitination can affect protein interactions that are important for localisation of a protein. Not only the localisation of ubiquitin substrates are affected by ubiquitin, but also the localisation of the E2 can be effected. Localisation of Ube2E3/UbcM2, for example, has been shown to be dependent upon its ubiquitin binding state; only when the E2 is charged with ubiquitin through a thioester bond, is it recognised by the transport factors of the importin family and shuttled into the nucleus [90].

1.1.6.4 Protein activity

A combination of any of the above can result in a change in protein activity, for example activity of a transcription factor can be suppressed or terminated by its polyubiquitination and subsequent degradation, as occurs in the control of p53 levels through its E3 ligase MDM2. In other cases ubiquitination can lead to a conformational change in a protein that can, for example, affect the catalytic site of an enzyme or its ability to bind other proteins. Moreover, ubiquitin can be directly involved in protein-protein interactions and trigger the formation of large multi molecular complexes by recruitment of proteins with UBDs.

1.2 Transcription

Transcription, the process of enzymatic RNA synthesis from a DNA template, is the first step of all gene expression. Its proper function and regulation is critical for homoestasis, cell growth and differentiation, and consequently dysregulation of this process is involved in the development of numerous kinds of diseases. A brief outline of the transcription event is shown in Fig 1-6. In order for transcription to occur, Pol II (RNA Polymerase II) has to associate with DNA upstream of an open reading frame and synthesise a complementary strand of RNA. However, other than in bacterial cells, where the RNA polymerase can initiate promoter specific transcription, eukaryotic Pol II is dependent on general transcription factors (GTFs) to start transcription [91, 92]. Transcriptional activators (TAs) that contain a domain with specific DNA binding ability are recruited to their specific consensus sequence at a gene promoter. In addition to the DNA binding domain, TAs comprise a transactivation domain (TAD) which binds other components of the transcription machinery, including cofactos, GTFs and Pol II, consequently bringing these factors together at the chromatin to form a preinitiation complex. Next transcription is initiated and Pol II moves along the gene and synthesises an RNA transcript in a process called elongation. During transcriptional elongation, transcription factors can either stay bound to the promoter sequence and another Pol II can be recruited to this pre-assembled recruitment platform, initiating another round of transcription or the transcription factor dissociates from the DNA and terminates transcriptional initiation [91].

During elongation other factors involved in chromatin modification, RNA chain synthesis and RNA processing and export associate with Pol II. As the DNA is tightly packed into nucleosomes these have to be removed or remodelled in order for the Pol II to move along a certain DNA sequence (Fig 1-6b) [91, 93, 94]. After Pol II has moved along and transcribed a DNA sequence, DNA repacked into a chromatin structure. Components of the RNA processing (RnP) machinery associate with the Pol II complex and conduct pre-messenger RNA maturation [91, 92]. Transcription is terminated when Pol II associates with the termination machinery and the newly synthesised mRNA is exported out of the nucleus for translation (Fig 1-6c) [91, 92].

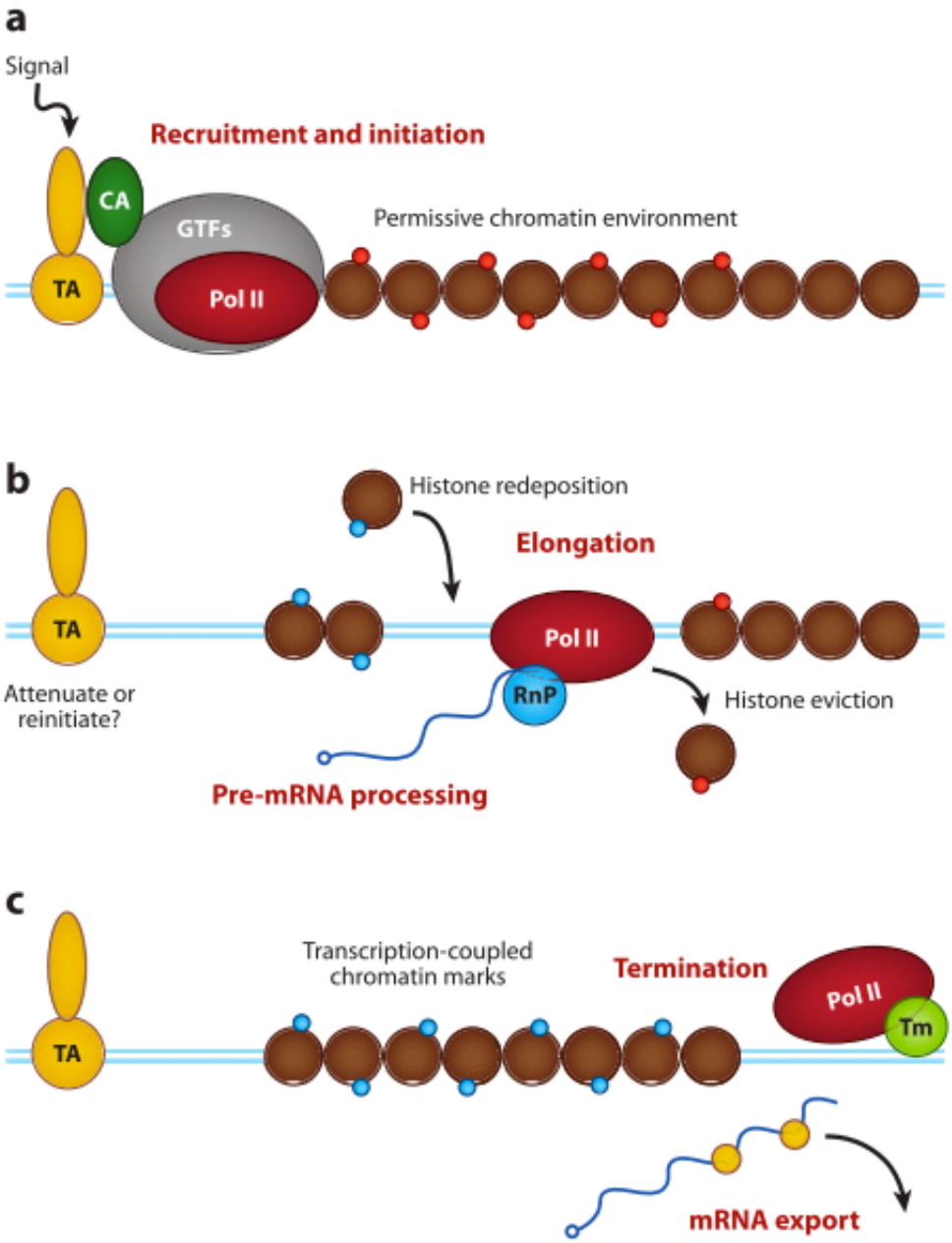

Figure 1-6 Simplified overview of transcription (adapted from Geng et al., 2012)[91] (a) Binding of a transcription factor to its target promoter leads to the recruitment of coactivators (CA), general transcription factors (GTFs) and RNA Polymerase II (Pol II) that form a complex at the promoter and initiate transcription. (b) During the elongation phase, RNA is synthesised by Pol II, which is processed by Pol II associated components of the RNA processing (RnP) machinery. During elongation, histones have to be repositioned to allow sliding of the Pol II complex along the gene. (c) Transcription is terminated by association of the Pol II with the termination machinery (Tm) and transcription-coupled chromatin marks stay on the newly transcribed gene. Newly synthesised mRNA is exported out of the nucleus.

1.3 The UPS in control of transcription

Degradation of proteins by the UPS and transcription as the first step in protein expression appear to be two entirely contradictory events. However, an important role of the UPS in the control of several parts of the transcription machinery has become apparent in recent years. Strikingly a study by Auld *et al. [95]* showed that almost all transcriptional active genes in yeast are associated with one or several parts of the proteasome. The exact role and mechanism by which the proteasome is involved in transcriptional regulation remain unclear, however, different studies have suggested roles of the proteasome in almost every phase of the transcription process [91]. It has been proposed that the proteasome is required to regulate transcription by degrading components of the pre-initiation complex when no longer required thereby allowing transcription to progress, furthermore the 19S subunit was shown to be required for transcriptional elongation [91, 96, 97], while the 20S subunit is required for termination [91, 98].

One interesting example of how the UPS is involved in the control of the transcription machinery is ubiquitination dependent degradation of the Polymerase II (Pol II) in response to DNA damage. This is a very important process as it allows other proteins to access the site of DNA damage in order to repair the active genes or alternatively trigger a cells death response. When an active Pol II encounters a place of DNA damage it first recruits the NER (nucleotide excision repair) machinery to the site of DNA damage as part of the TCR (transcription-coupled DNA repair) pathway [99-102]. If DNA repair by this pathway fails, however, the stalled polymerase is recognised and polyubiquitinated by the E2/E3 complex Rsp5 and UbcH5 leading to Rpb1 ubiquitination and Pol II degradation. It has been suggested that the ubiquitin chain formation acts as a 'molecular clock', only if the DNA damage cannot be repaired by the TCR pathway is the Pol II stalled long enough for the ubiquitin chain to be elongated and thus recognised by the proteasome [99]. Removal of the Pol II complex allows components of the global genome repair (GGR) pathway to be recruited to the site of DNA damage and to repair the damage [103].

It has been proposed that the ubiquitination/degradation model to remove stalled Pol II from the site of transcription is a more general mechanism by which Pol II can be removed from the DNA and can not only work as part of the TCR pathway, but also when for example factors like TFIIS are unable to resume an arrested transcription complex [99, 103].

Interestingly, the Rsp5/UbcH5 complex can only recognise Pol II in a specifically phosphorylated state. The Pol II binds to the promoter it is in its non-phosphorylated form and is phosphorylated at residue serine 5 within its CTD repeats during transcriptional initiation, this phosphorylation inhibits binding of Rsp5 (E3) to Pol II. Only when Pol II is further phosphorylated at serine residue 2 during elongation is it recognised by Rsp5, this ensures that no DNA unbound Pol II is targeted for ubiquitination and destruction by the E3 ligase [99, 104-106].

In addition to targeting stalled Pol II the Rsp5/UbcH5 complex also specifically binds to and ubiquitinates Pol II during the elongation phase. This is achieved by binding of UbcH5 (E2) to the 'switch Ă domain' of pol II [107], strikingly this domain is unstructured unless Pol II is present in complex with DNA and RNA, allowing recognition of this domain by UbcH5 only when in its structured and thus DNA bound, active conformation [99].

Besides Pol II numerous other factors involved in transcription were shown to be regulated by the UPS system. A link between the transactivation and degron domain, for example, has been made in a number of transcription factors and this phenomena is conserved in prokaryotes (which do not have a UPS system) [91], demonstrating the significance of the connection between TA activity and stability (see 5.1 for detail of how transcription factor function is regulated by the UPS).

1.4 Interferon regulatory factor -1

Interferon regulatory factor-1 (IRF-1) is the founding member of the IRF family, a class of transcription factors consisting of ten members in vertebrates (with IRF-10 being non-functional in human and mice [108]). IRF-1 was the first member identified from this family in the late 1980s as a protein that binds to the virus-inducible enhancer element of the IFNβ gene [109]. All members of this family share a structurally similar N-terminal DNA binding domain (DBD), which forms a helix-turn-helix structure and possesses five invariant tryptophan repeats that are essential for their DNA binding ability (Fig 1-7) [110]. All IRF DBDs recognise a characteristic IFN-stimulated response element (ISRE) with the consensus sequence 5'-AAN NGA AA-3' [111]. Even though members of the IRF family share the same ISRE element, the specific binding site, often consisting of a repeat of this consensus site, differ between the different factors. The C-terminus of the IRFs is less well conserved and often functions as an interface for protein-protein interactions [112]. Members of the IRF family were identified through their role as transcriptional regulators in the type I interferon pathway and play an important role in the cells antiviral response. Recently a close connection between the innate and adaptive immune system has been established, and numerous IRFs were shown to play an important role in the development and regulation of several types of immune cells. Additionally, some IRFs including IRF-1, have been linked to the cellular response to oncogenesis and the development of certain cancers [113]. IRF-1 is involved in the DNA damage response, apoptosis, cell cycle control and tumour suppression [113-115]. This is in addition to its role in immunity where it is important for the T-cell response, regulation of IFN and IFN-responsive genes and the antiviral response [116, 117]. IRF-1 was shown to be required for NK (natural killer) cell development in bone marrow stroma cells, by leading to transcription of IL-15 [118]. Accordingly, studies IRF-1 -/- mice demonstrated a severely abrogated number of NK cells [119, 120].

Additionally, IRF-1 is required for the T^{H1} immune response and IRF-1 -/- mice have a deficiency of IL-12 which is required for T^{H1} differentiation and are thus more vulnerable to infection by e.g. *Listeria monocytogenes* and *Leishmania major* [121,

122]. Moreover, IRF-1 -/- mice display a reduced incidence and severity of inflammatory disorders and allergies, implicating a role of IRF-1 in the control of inflammation and autoimmunity as IRF-1 -/- mice [123]. (See 1.4.3 for details of IRF-1's role in cancer development).

1.4.1 Structure

IRF-1 consists of three main-domains and several sub-domains. The main domains are the DNA-binding domain, the transactivation domain and the enhancer domain (Fig 1-8). So far only the structure of the N-terminal DBD has been solved [124], and the structure of the central and C-terminal region remains elusive. Sequence analysis suggests that the central and C-terminus of IRF-1 are intrinsically disordered. The relatively new concept of protein disorder predicts that certain proteins remain unstructured or do not form a distinctive three-dimensional structure spontaneously, until they form complexes with other proteins [125]. This contrasts the 'structure–function paradigm', which predicts that after translation, all proteins fold into a specific shape and that this shape is essential for a protein to be able to perform its function. It is now believed that disorder can be essential to the function of a protein, allowing it to interact with a range of different binding partners [126]. Programs predict that 40% of all human proteins contain such disordered sequences and that 25% are completely disordered [125]. This is supported by the fact that thousands of structures in the PDB databank are known to contain disordered chains or motifs, which only become structured in the presence of binding proteins or ligands [126]. In the case of IRF-1, its C-terminal disordered regions could allow it to interact with a range of different regulatory proteins that affect its function in response to an array of stimuli [127].

1.4.1.1 DNA-binding domain

IRF-1's N-terminal DNA binding domain (aa 1-120) is highly conserved not only across the IRF family, but also across different species. It was crystallised bound to the natural positive regulatory domain I (PRD I), a binding element from the interferon-β promoter (Fig 1-7) [124]. This was the first crystal structure of an IRF DBD and revealed the characteristic helix-turn-helix motif, with conserved

tryptophan repeats contacting the DNA. The structure shows that the main DNA interactions are with a short GAAA core sequence, explaining the occurrence of repeats of this sequence in the IRF response elements. The main residues contacting the major groove in the GAAA sequence are Arg^{82}, Cys^{83}, Asn^{86} and Ser^{87}, with Arg^{82} being completely conserved along the IRF family members. Mutants with either a single mutation from Trp^{11} to Arg or residues Tyr^{109}, Leu^{112} and Pro^{113} mutated to Ala are unable to bind to DNA; however it is not clear if this is due to direct interactions of these residues with the DNA or if these mutations lead to a gross change in the DBD conformation that prevents binding [124]. Although IRF-1 was crystallised bound to DNA as a monomer, footprinting studies by Spink and Evans [128] showed that after initially binding as a monomer, two IRF-1 molecules are present at one IRF-1 binding site of the inducible nitric-oxide synthase (iNOS) promoter. The product of this gene is important for nitric oxide production under different inflammatory conditions. Binding of a second IRF-1 molecule to the promoter extends occupancy on the DNA in both the 5' and 3' direction in footprinting studies, suggesting that binding of the second molecule leads to conformational changes of the DNA-DBD interaction of the first monomer. Additionally, binding of the second IRF-1 monomer was shown to be dependent on the first protein, suggesting cooperative binding of the two molecules [128]. A model of the two IRF-1 monomers, based on the findings of this study, is shown in Figure 1-7 and does not suggest that the DBDs of the two monomers have any points of contact. This implies that the binding cooperativity is not due to dimerisation of the two molecules, but rather that IRF-1 induced conformational changes in the DNA, which were observed in the IRF-1 crystal structure [124], increases the affinity of the IRF-1 DBD for the second binding site on the promoter. However, as the C-terminal region of IRF-1 is not present in the crystal structure, the possibility of dimer formation through the contact of residues in this part of the protein cannot be excluded.

Adjacent to IRF-1 DBD lies its nuclear localisation signal (aa 117-141) [129]. It is predicted to be located within an exposed surface area and is required for the import of IRF-1 into the nucleus, where IRF-1 binds DNA and acts as a transcriptional

regulator. Deletion of this region leads to localisation of IRF-1 mainly in the cytoplasm and thus its inactivation [129].

1.4.1.2 Mf2 domain

Recently, residues 106–140 have been identified to serve as a multi protein binding interface for IRF-1 and named multi-functional domain 2 (Mf2) [127]. The sequence of this domain suggests that it is strongly disordered and proteins binding to this domain differ in their amino acid specificity. Thus, this domain appears to be a *bona fide* example of how the flexibility of a highly disordered domain can allow interaction with an array of different interaction partners. Proteins that interact with this domain include the IRF-1 E3 ligase CHIP, NPM1, TRIM28, and YB-1 [127, 130].

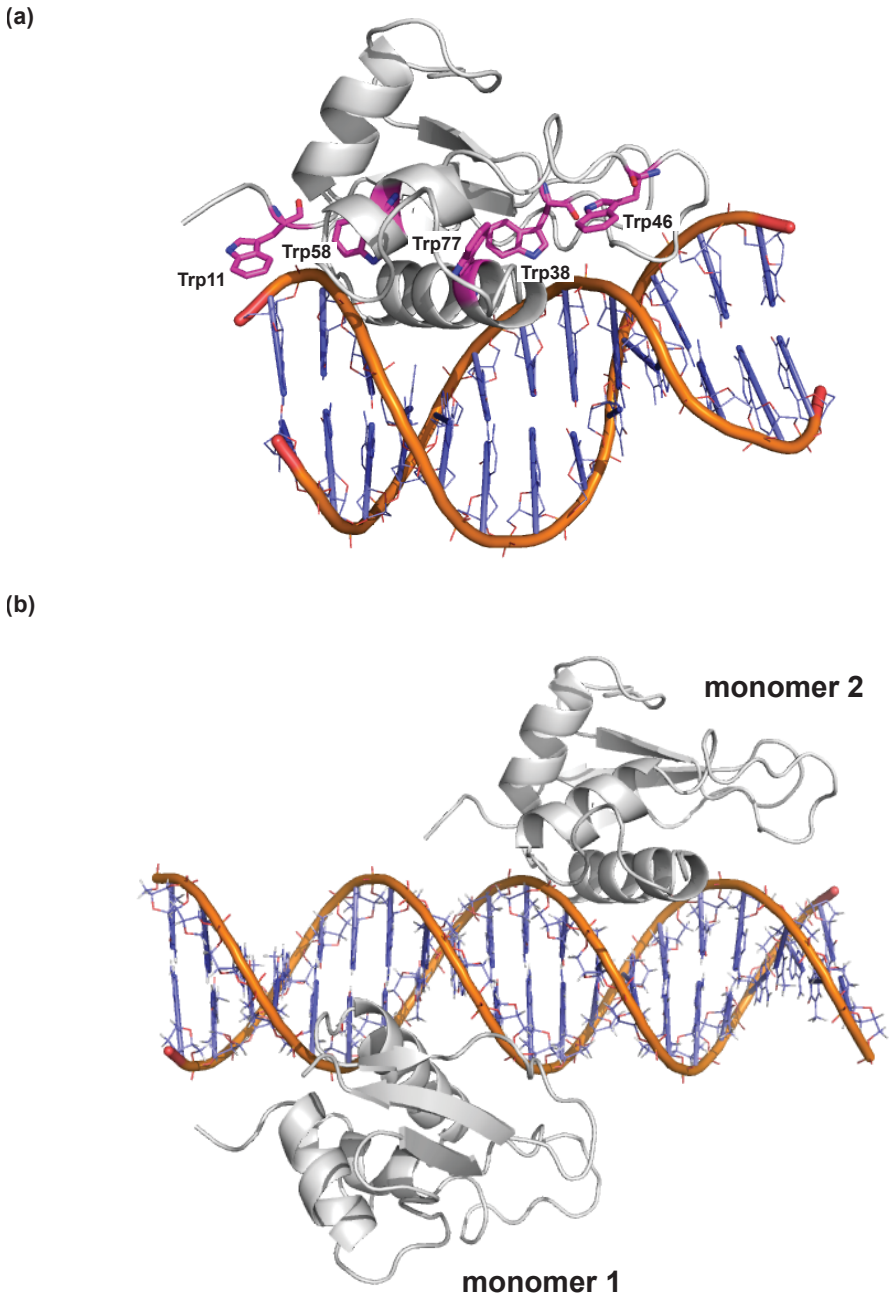

Figure 1-7 IRF-1 DBD bound to its consensus sequence

(a) Crystal structure of the IRF-1 DBD in complex with DNA, with tryphtopan repeats shown as sticks. (b) Model of cooperative binding of two IRF-1 monomers to the iNOS promoter (model based on the crystal structure and data from a study by Spink and Evans) [124, 128].

1.4.1.3 Transactivation domain

The transactivation domain of IRF-1 was mapped to a region between residues 185-256. Deletions and fusion studies showed that this region is both required and sufficient for transactivation i.e. a GAL-4 protein fused to this region shows higher activity in a CAT-reporter assay when compared to wild type GAL-4 [129, 131].

No structural information is available for this domain of the protein, however, it is predicted to be more ordered than the central region of IRF-1 and to form a loop-helix-loop-sheet [132]. Interestingly, a mutant lacking this domain acts as a dominant negative in cells, similar to the IRF-2 protein, which shares high homology with the IRF-1 DBD, but lacks a sequence similar to IRF-1's transactivation domain.

1.4.1.4 Enhancer Domain

Studies on the C-terminal region of IRF-1 demonstrated that even though it is neither required for transactivation nor able to promote transactivation on its own, it is able to 'enhance' IRF-1's transactivation activity. Further studies revealed several distinct functions of this domain. It carries a repressor domain, which is important for IRF-1 dependent Cdk2 repression that is mainly dependent on an LXXLL coregulator signature motif at residues 306-310 [133]. Additionally, molecular chaperones of the Hsp70 family that play an important role in maintaining IRF-1's cellular function, bind to the LXXL motif [112]. The enhancer domain is required for efficient growth inhibition by IRF-1, and deletion or mutation of this region results in a loss of growth suppressor activity [133]. It further encompasses a binding site for p300; IRF-1 binding to p300 leads to acetylations and thus activation of p53. Thereby p53 and IRF-1 synergise to regulate expression of p21, in a mechanism that is independent of IRF-1's DNA binding ability and merely relies on its ability to bind to p300 [134].

Furthermore, the enhancer domain has been shown to play an important role in the control of IRF-1 degradation by the ubiquitin proteasome pathway; it contains both the ubiquitination and degradation signal, but, interestingly, is not subject to modification by ubiquitin itself. Surprisingly, the two signals can be uncoupled, and removal of the last 25 amino acids of IRF-1 leads to inhibition of its degradation

whilst it is still polyubiquitinated. Only removal of the last 70 amino acids leads to inhibition of both ubiquitination and degradation [135].

A study by the Ball group has shown that the activity of the enhancer can be activated by binding of nanobodies to the 25 C-terminal residues of IRF-1 (301-325), also called the multi functional domain 1 (Mf1). Binding of nanobodies to this region results in an up to 8-fold increase in expression of IRF-1 responsive promoter, which is accompanied by an increase in the rate of IRF-1 degradation [136]. This link between activity and degradation is noteworthy, as several transcription factors were shown to be most active when least abundant and it would therefore be interesting to study how this link between activation and degradation is mediated in the case of IRF-1 [137].

1.4.1.5 Dimerisation domains

IRF-1 has been shown to heterodimerise with IRF-8 leading to repression of IRF-1 transcriptional activity [138, 139]. The interface between IRF-1 and IRF-8 has been mapped to residues 164-219 on IRF-1 using deletion mutants [129].
The physiological relevance and occurrence of IRF-1 homodimers remains unclear. A study by Kirchhoff *et al*. suggest that IRF-1 forms homodimers *in vivo* through a dimerisation motif at residues 91-114 [140]. However, *in vitro* IRF-1 is present as a monomer in solution, as shown by density gradient centrifugation and native PAGE (unpublished data, Ball group). Furthermore, IRF-1 was crystallised in its monomeric form, however as mentioned earlier, footprinting studies suggest cooperative binding at the iNOS promoter, which could be due to an additional homodimersiation domain outside the IRF-1 DBD.

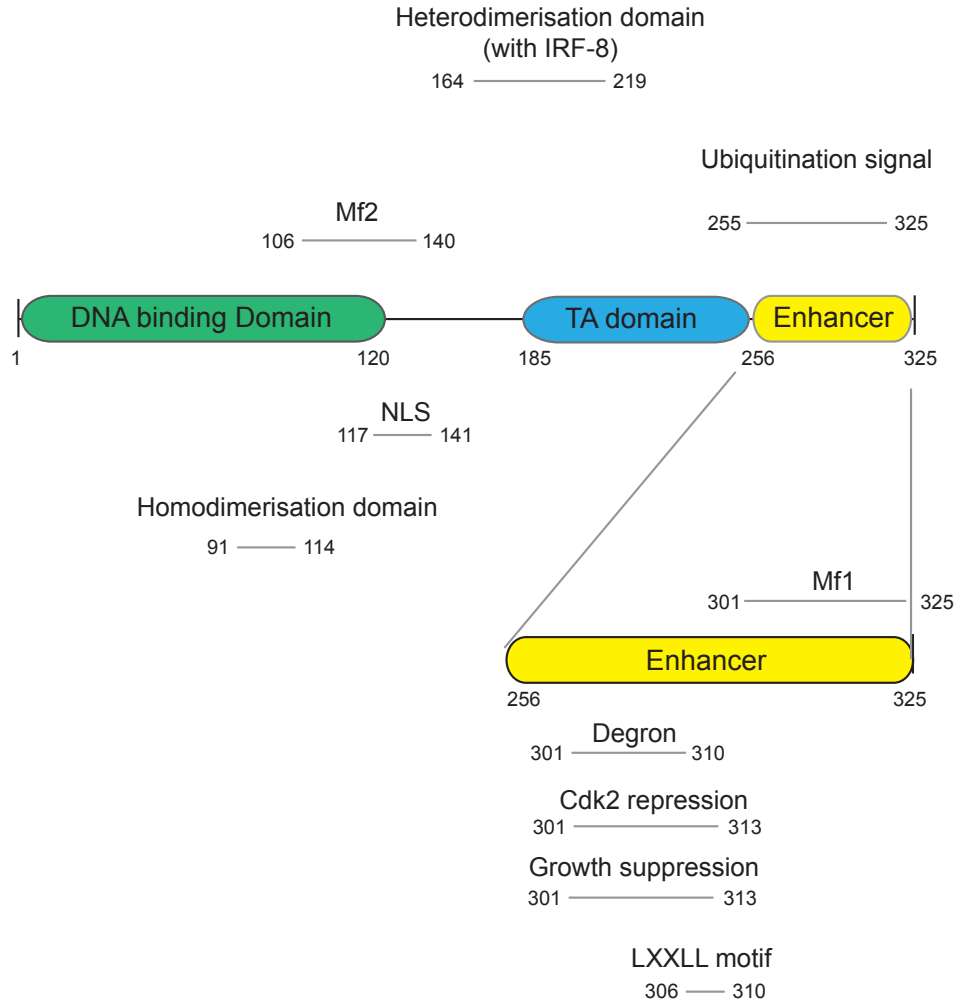

Figure 1-8 Functional domains of human IRF-1

NLS = nuclear localisation signal, Mf = multi-functional domain

1.4.2 Activation

IRF-1 is activated in response to a number of inhibitory cytokines, as well as by dsRNA, interferons (IFNs), and genotoxic stress [141, 142]. Upon activation, IRF-1 can stimulate the expression of a wide range of target genes; this is dependent on several factors including cell type, stage of development and stimulus [143]. The best-studied pathway of IRF-1 activation is through IFN-γ treatment or viral attack. IFN-γ is a cytokine, which is produced by activated T cells or NK cells. IRF-1 activation by IFN-γ is dependent on the JAK/STAT pathway and stimulates expression of IFN-β [109, 144], 2-5A synthetase [145, 146], and RNA dependent protein kinase [147, 148] along with other proteins. IFN-γ binds to the IFN-γ receptor or IFNGR on the outer cell membrane. Binding to the receptors leads to activation of the Janus protein kinase 1 or 2 (JAK1 or JAK2), which is associated with the intracellular part of the trans membrane receptor. After auto- and/or trans phosphorylation of specific residues within JAK, the kinase phosphorylates the downstream targets signal transducers and activators of transcription (STAT) 1 and 2. The activated STATs trigger the formation of a transcriptional activator complex called IFN-γ-activated factor (GAF - also termed IFN-α-activated factor AAF), consisting of a homodimer of tyrosine-phosphorylated STAT1 [149, 150]. This complex translocates into the nucleus, where it binds a specific DNA sequence, called the GAS element, which in turn facilitates transcription of several IFN-stimulated genes, including IRF-1 [149].

A study by Pamment *et al.*[141] showed that activation of IRF-1 in response to DNA damage is dependent on the ATM-kinase. Further, induction of IRF-1 protein and mRNA after radiation is defective in ATM deficient cells; however, the response to viral mimics remains intact. This suggests that the ATM-signalling pathway plays a role in IRF-1 induction after DNA damage, but not in virally infected cells [141].

1.4.3 IRF-1 in cancer

IRF-1 has been identified as playing a role in the development of different cancers and has thus been classified as a tumour suppressor protein. The first study connecting IRF-1 with the regulation of oncogenesis was from Harada *et al.* (1993) and demonstrated that the phenotype of NIH3T3 cells, which underwent transformation by IRF-2 overexpression, could be reverted by over expression of IRF-1 [151]. Later studies in mouse embryonic fibroblasts (MEFs) showed that IRF-1 -/- cells were defective in DNA damage-induced cell cycle arrest [152].

IRF-1 is involved in apoptosis and thereby helps elimination of pre-cancerous cells. In activated matured T lymphocytes IRF-1, and not p53, is required for DNA damage induced cell death [153], while in thymocytes apoptosis is dependent on p53 and not IRF-1. Furthermore, IRF-1 has been implicated in apoptosis that is triggered by factors other than DNA damage, like IFN-γ [154-156]. The exact IRF-1 target proteins involved in apoptosis remain elusive, but factors like caspases and tumor necrosis factor-related apoptosis-inducing ligand (TRAIL), are believed to play an important role [120, 157].

In an oncogenic transformation assay, introduction of activated c-Ha-Ras leads to transformation of IRF-1 -/- MEFs but not wild-type cells (where at least two oncogenes are required for transformation) [158]. In mouse studies, IRF-1 deficiency does not have a substantial effect on tumour formation, however in combination with expression of c-Ha-Ras or deletion of p53 the incidence of tumour development increases dramatically *in vivo*. Together these studies demonstrate a tumour suppressor activity of IRF-1. Consistent with these observations, defects in IRF-1 activity, through loss or mutation of the IRF-1 gene or through overexpression of IRF-1 repressors e.g. Y-box protein (YB-1) or tripartite motif-containing 28 (TRIM-28), have been linked to the development and progression of different cancers, including leukaemia, myelodysplastic syndrome (MDS), oesophageal, gastric and breast cancers [159-163]. The IRF-1 gene maps to chromosome 5q31.1 [161] and cytogenetic abnormalities in this region have been found in several diseases, e.g. 11% of sporadic breast cancers show a loss of chromosome 5q12-31 [164]. A study

by Doherty *et al*. showed that 30% of neo-plastic breast tissues lack IRF-1 [159]. Furthermore, several point mutations in the IRF-1 gene were identified in cancer samples. The COSMIC (Catalogue of somatic mutations in cancers) lists 23 mutations in the IRF-1 gene (from 7859 samples), 14 of these are missense mutation, with 7 affecting residues in the highly conserved DBD of IRF-1 [165].

Taken together the biochemical and clinical studies indicate that IRF-1 is an important regulator of cellular growth control and cell death, and that its loss or dysregulation can play a role in the formation and progress of different malignancies.

1.4.4 Ubiquitination of IRF-1

IRF-1, like most other transcriptional regulators, has a very short half-life of 20-30 minutes in cultured cells. Thus, levels of IRF-1 are controlled very tightly to ensure proper function *in vivo*. IRF-1 is ubiquitinated leading to degradation by the proteasome, a pathway important in controlling cellular levels of IRF-1 [135, 166]. However, many details of this pathway and how it is controlled remain unknown. The Ball group has shown that the rate of IRF-1 ubiquitination and degradation is mainly mediated through its C-terminal enhancer domain. As mentioned earlier the enhancer comprises a degradation and an ubiquitination signal (Fig 1-8) and these two processes can be uncoupled as demonstrated by a mutation study by Pion *et al*. [135]. The only E3 ligase that has been identified for IRF-1 is C-terminus of Hsc70 interacting protein (CHIP) [130]. CHIP is a U-box E3 ligase that binds to Hsp70 and targets misfolded proteins for degradation, thereby linking the ubiquitin pathway to the chaperone machinery in cells. Recently CHIP has also been shown to act as a 'direct' E3 ligase binding to substrates and promoting their ubiquitination directly in the absence of Hsp70. Under unstressed conditions, CHIP has a positive effect on IRF-1 steady state levels in cells. However, under stress conditions, including heat or heavy metal stress, CHIP was shown to directly bind to and ubiquitinate IRF-1, leading to its degradation. A basal E3 for IRF-1 turnover remains unidentified.

1.5 p53

The transcription factor p53 was first described in 1979 and has since been shown to play a major role in the cell's response to oncogenic stresses and in tumour suppression [167-169]. It is one of the most commonly mutated proteins in human cancers, with around 50 % of all malignancies carrying a mutation in the p53 gene. p53 is crucial in the prevention of cancer development as it has been found to control over 100 target proteins involved in regulation of growth control, DNA repair, cell-cycle, apoptosis, angiogenesis, metastasis, nitric oxide production and also protein degradation, in response to oncogenic and other cellular stress signals [170-173]. p53 activity is tightly controlled by the rate of its degradation through the ubiquitin – proteasome pathway. In unstressed cells p53 proteins is constantly ubiquitinated and degraded by the UPS leading to low level of the protein in the cell. Only in response to a wide variety of stresses e.g. DNA damage, hypoxia, nitric oxide, nutrition deprivation, heat/cold shock and or oncogene activation, is degradation of p53 inhibited and its level increase dramatically leading to up-regulation of its target genes. Many of these gene products are involved in the prevention of cancer development by either leading to growth arrest or cell death [171]. How the exact p53 response is determined and regulated (i.e. apoptosis vs. growth arrest and senescence) has not been completely understood yet. Recently, the importance of p53 in the control of the cellular metabolism has become apparent, the tumour suppressor was shown to be involved in control of glycolysis, oxidative phosphorylation, glutaminolysis, insulin sensitivity, nucleotide biosynthesis, mitochondrial integrity, fatty acid oxidation, antioxidant response, autophagy and mTOR signalling [174]. p53, for example, inhibits the glucose transporter GLUT1 and GLUT4 and insulin receptors leading reduced uptake of glucose into the cell. p53 furthermore activates transcription of TIGAR and stimulates degradation of phosphoglycerate mutase (PGM) , together this contributes to reduced glycolysis and opposes the Warburg effect, which described a high rate of glycolysis followed by lactic acid fermentation in the cytosol of cancerous cells. [174]. Strikingly, a study by Li *et al.* [175] showed that p53 function in metabolism is sufficient for its function as a tumour suppressor protein, the study utilised transgenic mice with mutations in the p53 core domain that avert its ability to activate transcription of genes involved in apoptosis and growth

arrest, the mutants protein, however, is still able to regulate metabolic genes and its tumour suppressive function is unaffected. This is an intriguing observation and suggests that the relatively recently discovered role of p53 in the adaptation of the cells metabolism under stress conditions plays a crucial part in p53's role in the prevention of oncogenesis.

The importance of p53 as a tumour suppressor has been demonstrated in several studies with either p53 -/- or +/- mice or mice carrying different mutant p53 genes. Transgenic mice lacking either one or both p53 genes or carrying a mutation that renders the protein transcriptionally inactive are prone to tumour formation and have a dramatically reduced life expectancy [176-180].

MDM2 (murine double minute 2) is the main and best-studied E3 ligase involved in p53 turnover. Under normal conditions, p53 levels are controlled by a complex feedback regulated system and dysregulation can lead to excessive p53 ubiquitination and degradation, thereby inhibiting its function as a tumour suppressor protein. This can result in uncontrolled cell growth and cancer development. Therefore, inhibiting MDM2 mediated ubiquitination of p53 and thus stabilising p53 levels is a major interest for research aiming to reactivate the p53 pathway in cancer cells.

Like IRF-1, p53 has several intrinsically disordered domains; this equips the transcription factor with conformational plasticity and allows it to adopt a wide range of different structures in response to different binding partners. Motifs on p53 have been shown to interact with more than three hundred different proteins in the cell [181]. p53 thereby interconnects different signalling pathways and acts as an important hub protein. The list of p53 interactions partners consists of p53 activators, inhibitors and effectors of its function. p53 is a multi-domain protein and consists of a DNA binding domain, a transactivation domain, a tetramerisation domain and several other sub-domains and motifs that are important in controlling p53 activity and degradation.

1.5.1 Structure

1.5.1.1 DNA binding domain

The structure of the p53 core domain (DNA binding domain) has been studied extensively, it was first crystallised in 1994 in complex with DNA [182] and several others structures, either free, bound to domains of signalling proteins or in complex with DNA have been solved since. The p53 DBD can be subdivided into two motifs, one binding the major and the other one the minor groove of p53's target DNA. The binding site of the minor groove is stabilised through a zinc ion, which is tetrahedrally coordinated by the residues Cys^{176}, His^{179}, Cys^{238} and Cys^{242}. The zinc ion stabilises the interactions between p53 and DNA and loss of this ion leads to a decrease in thermodynamic stability and an increase in aggregation and fluctuation in neighbouring loops, in turn resulting in a decrease of p53 DNA binding specificity [183, 184]. A p53 tetramer specifically recognises a repeat of the consensus sequence: 5'-RRRCWWGYYY-3' (R=A,G; W=A,T; Y=C,T), which can be separated by a spacer of 0-13 base pairs [185]. Crystallographic studies showed that binding of a p53 tetramer to a repeat of this sequence leads to a twisting and bending of the DNA molecule [186]. The main residues on p53 involved in DNA-protein interactions include Lys^{120}, Ser^{241}, Arg^{248}, Arg^{273}, Ala^{276}, Cys^{277} and Arg^{280} [182, 187]. Several residues within the DBD of p53 are subject to posttranslational modifications, which can have an effect on p53 activity and/or DNA binding specificity. One example is acetylation of Lys^{120} by the acetyltransferases hMOF and TIP60 in response to DNA damage. This modification reportedly leads to specific transcription of factors required for apoptosis like BAX and PUMA and initiates apoptosis. Mutation of Lys^{120} to Arg or depletion of the acetyltransferase inhibits the ability of p53 to activate BAX and PUMA, but does not have an effect on expression of other p53 target proteins that are involved in cellular growth arrest [188, 189]. Several missense mutations on the p53 DNA binding domain have been implicated in the development of human cancers, the most common mutations are Arg^{175}, Tyr^{220}, Gly^{245}, Arg^{248}, Arg^{249}, Arg^{273}, Arg^{282} (Fig 1-8b) [170].

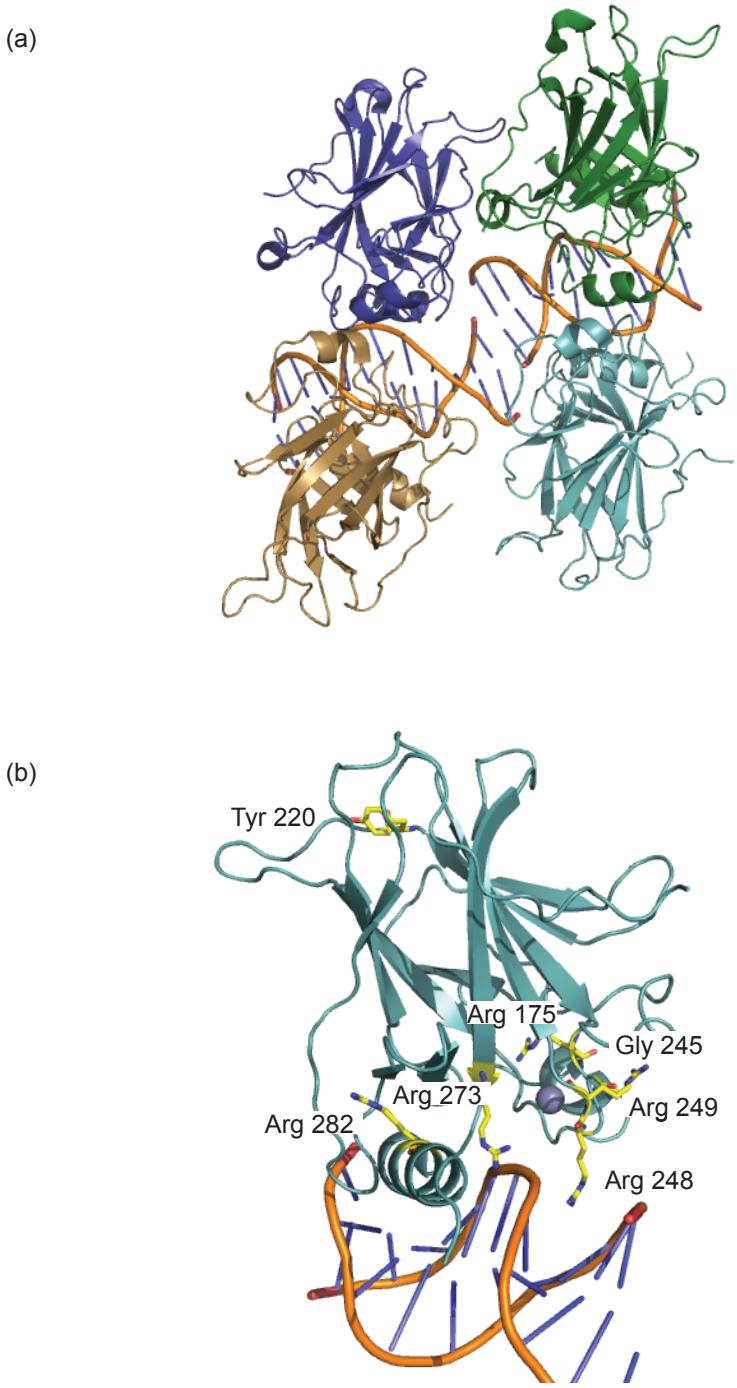

Figure 1-9 Structure of p53s DBD

(a) Tetrameric structure of the p53 core domain, monomers are presented in different colours as cartoon (b). The main sites of p53 mutations observed in human cancers are indicated as yellow sticks.

1.5.1.2 Transactivating domain

The p53 transactivating domain is located at its extreme N-terminus and exhibits a natively unfolded region. It can be divided into two subdomains TAD1 (aa 1-40) and TAD2 (aa 40-61) [190, 191]. The TAD domains are followed by a proline rich region (aa 64-92), which contains five PXXP motifs [191]. PXXP motifs are known to mediate protein-protein interactions through binding of Src homology domains; however, the function of this motif in p53 is not understood well. Mutational studies on this domain suggest that rather than playing a role as a protein-docking site, the length of this domain is essential for p53's function as a tumour suppressor protein [134], implying that it plays a role as a molecular spacer that separates two functional domains [192].

The TAD motifs serve as a binding site for many p53 interacting proteins, including components of the transcription machinery [193-195] and coactivators such as p300 and CREB-binding protein (CBP) [196, 197]. It also provides one of the two binding sites for MDM2 and the MDM4 binding site [198-201]. Interestingly, the binding site for the coactivator p300 and CBP, which is essential for proper p53 function partly overlaps with the binding site of MDM2, making binding of these two p53 regulators mutually exclusive. p300 is believed to acetylate histones and thereby relax the chromatin structure, favouring binding of factors like p53 [202]. Additionally, it directly targets p53 for acetylation in its DNA binding domain, which leads to activation. MDM2 on the other hand inhibits p53 function by targeting it for degradation, in addition to blocking the binding site of the p53 activator p300 (see section 5.1.2 for details about MDM2). The p53 N-terminus is subject to several posttranslational modifications in response to different stresses and these are important in p53 control. Several serine and threonine residues within the transactivation domain are targeted by different kinases, and phosphorylation of these sites can affect the affinity of proteins that compete for binding to this domain, and thereby affect p53 activity. For example, phosphorylation of Thr^{18} or Ser^{20} decreases binding affinity of MDM2 to p53, and studies suggest that this same modification can increase the affinity of the interaction between p53 and p300 [134, 201, 203, 204].

1.5.1.3 Tetramerisation domain

p53 forms reversible tetramers through residues in its C-terminus (aa 326-356). The structure of a p53 tetramer (C-terminal domain only) was solved by NMR and crystallography studies [205-208]. The structure can be described as a dimer of dimers and *in vitro* studies on p53 biogenesis showed that dimers form during translation on the polysome while tetramers are formed in solution by dimerisation of the preformed dimers [209]. The tetramerisation domain is built of a short β-strand and an α-helix; upon dimerisation two monomers form an intermolecular β-sheet and an antiparallel helix. The main residues involved in formation of the intermediate dimer are Leu^{330}, Ile^{332} and Phe^{341}. Two of these dimers then associate, through their helices by mainly hydrophobic interactions, forming a four-helix bundle tetramer. p53 binds DNA in its tetrameric form and mutations of residues that are essential for tetramer formation lead to decreased or complete loss of p53 activity.

1.5.1.4 C-terminal domain

The C-terminal region of p53 is important for control of p53 activity and subject to several posttranslational modifications, including acetylation, ubiquitination, phosphorylation, SUMOylation, methylation, and NEDDylation. These modifications regulate p53 function and cellular protein levels [210-212]. Structurally, the C-terminus is intrinsically disordered, but several crystal structures of peptides from this domain bound to other proteins have been solved, suggesting that it can fold into a specific structure when interacting with binding partners. An example of this is a peptide consisting of p53 residues 367-388, which is unstructured in isolation, but takes up a helical conformation when bound to the calcium-dependent dimeric S100B(ββ) protein and a β-turn-like conformation when acetylated at Lys^{382} and associated with the bromodomain of CBP [213, 214]. One of many other proteins that bind to this region is HAUSP/USP7, a deubiquitinase that has been shown to deubiquitinate p53, thereby working together with different E3s in controlling the ubiquitination state of this transcription factor [215].

The C-terminus of p53 has additionally been shown to bind DNA non-specifically through electrostatic interactions of several lysine residues. These low affinity interactions inhibit binding of the core domain to specific p53 promoter sequences [216], and acetylation of the C-terminal lysines leads to a gradual loss of this non-specific DNA binding capacity [217]. A mechanism has been proposed in which the C-terminal non-specific binding ability of p53 is involved in linear diffusion on DNA, a process where p53 slides along searching for its target sequence [218]. Consistent with these findings, it was shown that the last 30 amino acids of p53 are essential for efficient binding and transactivation of target genes in the context of chromatin or large molecules of DNA [218, 219].

1.5.2 p53 in Cancer

The transcription factor p53 is part of a small protein family that consists of two other members p63 and p73. All three proteins share structural and functional homology, but while p63 and p73 play roles in normal cellular development, p53's most important role appears to be prevention of tumour development. Strikingly, it has been demonstrated that p53 is either non-functional or functions incorrectly in most human cancers [170, 172]. Under normal conditions levels of the protein are kept low, but in response to stresses like carcinogen-induced DNA damage, abnormal proliferative signals, hypoxia or loss of cell adhesion, p53 is activated and regulates different cellular processes to guard against tumorigenesis. p53 can trigger a range of cellular responses including cell-cycle arrest, senescence, DNA damage repair, inhibition of angiogenesis, differentiation and apoptosis. p53 functions either through its transactivation activity, leading to expression of specific target genes, or by binding to other regulatory proteins and thereby altering their function. The nature of the cellular response to p53 activation, depends on several factors like cell type, oncogenic cell composition, type of stress, level of p53 expression and interactions of p53 with specific proteins [170, 173]; however, the most common cellular response to p53 activation is growth arrest and apoptosis. p53 can activate the

expression of target genes that result in growth arrest of the cell either in the G1 phase, before DNA replication, or before mitosis in the G2 phase. Growth arrest allows the cell to repair DNA damage. In other cases, presumably when DNA damage is beyond repair, p53 triggers apoptosis, by inducing the expression of a wide range of cell death effectors [173].

Consistent with the observations of p53 function, mouse models that are p53-deficient develop multiple, spontaneous tumours at an early age [220-222]. As mentioned earlier, genetic alteration of the p53 gene is the most common mutation in human cancers. Most mutations occur in the core DNA binding domain, either in residues that directly contact DNA or are important for the structure of the domain. p53 mutants have been shown to be kinetically unstable and unfold spontaneously taking up a characteristic mutant conformation. These mutant proteins are often not degraded by the cell efficiently, either because they are not recognised effectively by the respective E3 ligase or because the degradation pathways are non functional due to loss of p53 wt function. This can lead to accumulation of mutant p53 in the cell. Since p53 is active in its tetrameric form, some p53 mutants have a dominant-negative effect over wild type p53 as one mutant molecule in a mixed p53 tetramer can inhibit its function [170, 223].

Activation of p53 in tumour cells in order to achieve cell death by apoptosis is a major interest in the development of drugs targeting cancerous cells. The approaches can be divided into three different groups, depending on the status of p53 used in the cell and are: (i) reactivation of mutant p53 [223, 224]; (ii) targeting negative regulator of p53 function by the development of antagonists or activating positive regulators of p53 [225], (iii) exogenous p53 expression, e.g. by adenovirus- mediated gene transfer [226]. Two studies in transgenic mice have independently shown that restoration of p53 function can lead to apoptosis of cancer cells and thus tumour regression *in vivo*. These results indicate that efforts to treat human cancers by reactivation of p53 are a promising therapeutic strategy [227, 228].

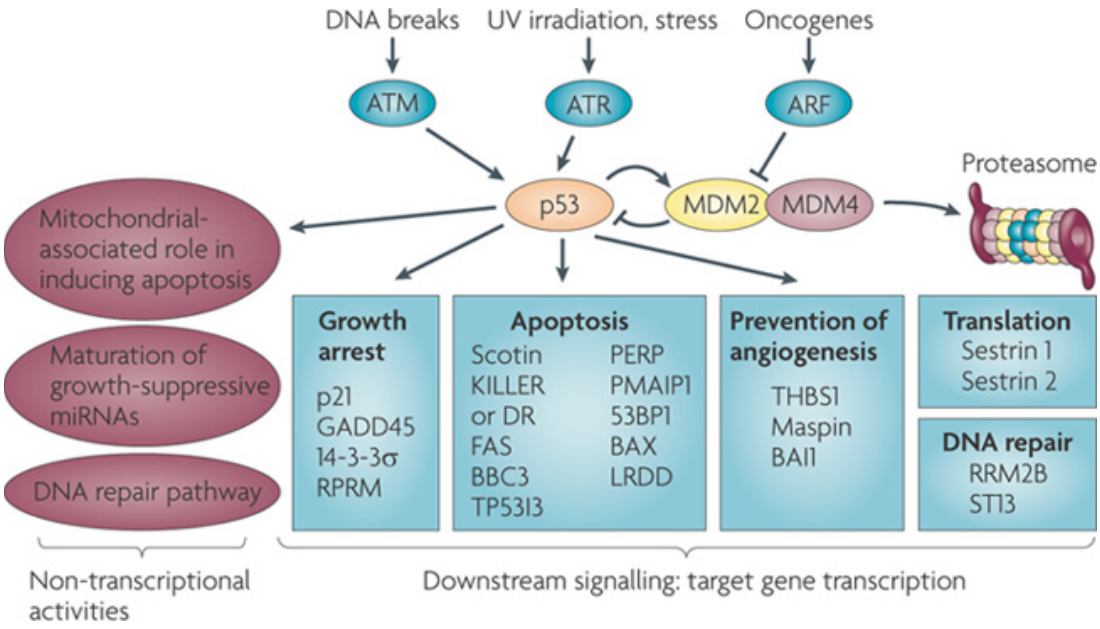

Figure 1-10 Overview of p53 function [229]

Different stimuli like DNA breaks, UV, stress or oncogenes lead to p53 activation by different signalling pathways. p53 is either activated directly by phosphorylation or indirectly by blocking the negative regulators of p53, MDM2 and MDM4, thus leading to an increase in p53 activity. Activated p53 leads to transcription of a range of target genes including several genes that are involved in growth arrest, apoptosis, DNA repair, translation and prevention of angiogenesis. In addition to its role as a transcriptional activator, p53 has been shown to exhibit other non-transcriptional function in a range of cellular pathways (left hand side).

1.5.3 Ubiquitination of p53

p53 levels and therefore its activity is tightly controlled by the rate of its degradation. Under normal conditions p53 is constantly transcribed and translated, however levels are kept low by almost immediate degradation of the protein. Thus, p53 has a very short half-life of only around 20 minutes under unstressed conditions. In response to stresses, e.g. oncogenic or genotoxic stresses, p53 degradation is inhibited and its half-life increases to several hours [230, 231].

So far 15 E3 ligases have been implicated in p53 ubiquitination. Our understanding of the regulation and function of most of these, however, is limited. E3 ligases identified as targeting p53 include MDM2, Pirh2, ARF-BP1/MULE, E4F1, Trim24, CHIP, Cullin complexes and others that still await full validation.
The best studied E3 for p53 ubiquitination is MDM2. This RING finger containing E3 ligase catalyses the ubiquitination of several lysine residues within p53 [232] and has been shown to be a very important factor in controlling p53 protein levels. MDM2 works in synergy with its homolog MDM4 (or MDMX), which shares structure and sequence homology with MDM2 but has no E3 ligase activity [200, 233]. Different studies suggest that MDM2 and MDM4 can form heterodimers, which stabilise MDM2 and increase its inhibitory effect on p53 [234, 235].

In addition to controlling p53 activity by ubiquitination, which leads to proteasomal degradation, MDM2 also competes with the p53 activator p300 for binding to p53 and thereby inhibits p300-mediated enhancement of p53 activity. Interestingly, MDM2 is also a direct transcriptional target of p53 [236, 237]. This results in a negative feedback loop, where p53 ubiquitination is inhibited in response to cell stress, leading to its activation and thus expression of MDM2, which in turn ubiquitinates p53 and thereby down regulates its levels and terminates the signal. Mass spectrometry analysis and mutational studies have identified several lysines in the C-terminal and core domain of p53 to be subject to modification by ubiquitin [232, 238], however, the exact molecular signals of ubiquitination at different lysine residues remain elusive. Studies on the effect of ubiquitination of different residues in its C-terminal domain have resulted in conflicting results. The initial study that

identified six C-terminal lysines as a target for ubiquitination suggested that these residues are essential for proteasomal degradation of p53 [238]. In contrast, results of a recent mutational study in mouse embryonic stem cells showed that the C-terminal lysines are not required for degradation of p53 under normal cellular conditions or during DNA damage [239]. Another study by Lohrum *et al*. suggested that monoubiquitination of the C-terminus of p53 serves as a nuclear export signal, resulting in shuttling of p53 out of the nucleus [240]. So far most studies have either used multiple site mutants or a p53 ubiquitin fusion protein; these artificial modifications of p53 could have effects on the protein e.g. conformational changes that affect the experimental outcome. In summary, more work is necessary to dissect and completely understand how p53 activity and degradation are controlled by ubiquitination at distinct lysine residues.

Strikingly, MDM2 has also been shown to act as an activator of p53 following DNA damage. This effect is dependent on the ATM kinase, which phosphorylates MDM2 at Ser^{395} promoting interaction of MDM2 with p53 mRNA [241]. Interaction between the MDM2 RING domain and p53 mRNA inhibits MDM2 E3 ligase activity and promotes p53 translation, leading to an increase in p53 levels [242]. Thus, MDM2 can act both as an inhibitor and activator of p53.
In conclusion, MDM2 is viewed as the key regulator of p53 activity and its regulation has therefore been studied extensively. In addition to carrying mutations in the p53 gene itself, many cancers have a dysfunctional p53 degradation pathway, leading to excessive degradation of the p53 WT protein and thus loss of its tumour suppressor activity. Reactivating p53 by developing drugs that affect the regulation of its degradation is therefore a major research interest.

1.5.4 CHIP

The ubiquitin ligase CHIP (C-terminal of Hsp70-interacting protein) plays an important role in the protein quality control system of cells. This system recognises misfolded proteins, which are then either refolded by chaperones or degraded via the ubiquitin proteasome pathway. CHIP forms a link between the two pathways by functioning as a Hsp70 co-chaperone [243] that also interacts with Hsp90. CHIP facilitates ubiquitination of Hsp70/90 bound client proteins leading to their proteasomal degradation thereby tilting the machinery towards the degradation rather than the refolding pathway [244-246]. The protein quality control system forms a very important mechanism in the cell, ensuring healthy cellular functions, especially in stress situations. Malfunction of the cells degradation pathways can lead to the accumulation of misfolded proteins and these aggregates can cause diseases, like neurofibrillary tangles in Alzheimer's disease and the Lewy bodies in Parkinson disease [247]. In addition to functioning as an E3 ligase for chaperone bound client proteins, a role of CHIP as a direct E3 ligase is emerging, where CHIP binds to substrates independently of Hsp70 and facilitates their ubiquitination [130]. Details of the control and regulation of these two distinct functions for CHIP are, however, largely unknown. In addition to its E3 ligase function, CHIP can also act as a molecular chaperone that promotes or maintains protein structures independently of Hsp70 [248, 249].

Structurally, CHIP is comprised of two distinct domains: (i) the catalytically active C-terminal U-box domain (aa 227-297), which is structurally related to the RING finger domain, but is stabilised through hydrogen bonds instead of by zinc binding [245, 250]. And (ii) the N-terminal tetratricopeptide repeat (TPR) domain (aa 25-130), which is responsible for chaperone interactions [245] (Fig 1-11). TPR domains are multipurpose structural modules that are highly conserved from *E.coli* to human. These domains were shown to be involved in the assembly of multi-protein complexes and function in a wide array of cellular processes including transcriptional control, mitochondrial transport, kinase signalling, protein folding, immunity and viral replication [251-253]. The TPR and U-box domains are linked by a flexible linker region, also called charged or middle domain [254].

The structure of mouse (aa 25-304, [254]) and zebrafish (aa 112-284, [255]) CHIP was solved by two groups independently. Both structure confirm that CHIP forms a homodimer, however both structures differ significantly. While the zebrafish structure, which lacks the TPR domain, shows a symmetric dimer, the mouse structure, which was solved in complex with an TPR bound Hsp90 peptide, shows an asymmetric dimer with considerable differences in the orientation of the charged middle domains. These differences in the structures could be due to the fact that the zebrafish structure was solved in the absence of the N-terminal TPR domain, which could be important for the over all conformation of the protein. Additionally, an H/D exchange study on full length CHIP suggested that CHIP forms a symmetric dimer in solution [256]. The dimer interface encompasses the U-Box and central domain in both crystal structures [254, 255]. Several ubiquitin conjugating enzymes (E2s) are known to interact with the U-box of CHIP, and these can facilitate the formation of polyubiquitination chains linked by K48, K11 or K63, depending on the E2 [12, 245]. CHIP was shown to negatively control p53 levels in cells and to act as an E3 ligase for IRF-1 under specific stress conditions [130, 257].

CHIP function was implicated in tumour suppression by studies showing that CHIP protein and mRNA levels are negatively correlated with breast cancer malignancy [250].

1.5.5 MDM2

The oncoprotein MDM2 (murine double minute) is the most important regulator of p53 function and was shown to regulate p53 activity on multiple levels. The best-studied role of MDM2 in p53 control is its ability to target p53 for ubiquitination by its E3 ligase activity [258, 259]. However, MDM2 was shown to regulate p53 through several other mechanisms, including blocking interactions between p53 and co-activators at target promoters [197, 260]. Moreover, MDM2 has been suggested to promote degradation of the ribosomal proteins L26 and L11 and thereby inhibiting p53 translation [261]. Interestingly, MDM2 was also shown to positively affect p53 levels by binding to p53 mRNA, which stimulates p53 protein synthesis and inhibits MDM2 E3 ligase activity [242], furthermore, MDM2 can act as an ATP-dependent molecular chaperone towards p53 [262, 263].

MDM2 consists of several distinct domains that are involved in protein-protein interactions and exhibit different functions. The N-terminal hydrophobic pocket is required for interaction with several proteins, including p53, and binds to the peptide consensus sequence FxxxWxxL [199, 264]. The central region of MDM2 comprises of an acidic amino acid rich domain, which interacts with a number of enzymes involved in signalling that contain the general consensus sequence: SxxLxGxxxF [198, 265, 266]. At the MDM2 C-terminus lies its RING domain, which is, like other RING domains, stabilised by coordination of two zinc ions. In addition, the MDM2 RING encompasses a P-Walker motif, which is essential for its ATP-dependent molecular chaperone function [262, 267]. MDM2 is believed to form heterodimers with its close homolog MDM4 (also called MDMX) *in vivo* [268], as well as homodimers. MDM4 also was shown to act as a negative regulator of p53 function, however, it does not exhibit E3 ligase activity and the exact mechanism by which it regulates p53 is unclear [234, 269-272]. MDM4 has been shown to act as a substrate for MDM2 mediated ubiquitination leading to its degradation [273-275].

The structure of several MDM2 sub-domain have been analysed by NMR and/or crystallisation, i.e. the C-terminal RING domain as a heterodimer with the MDM4 RING and as a homodimer [268 , 276] , the zinc-finger domain [277] and the N-

terminal hydrophobic pocket [278, 279] . So far it has however not been possible to solve the structure of full length MDM2, the reason for this is most likely a high amount of intrinsically disordered regions that are difficult to analyse.

MDM2 interacts with two distinct binding sites on p53, the higher affinity interaction between its hydrophobic pocket and the Box I motif on p53 leads to allosteric changes in MDM2 that stimulate binding of the acid domain to the second p53 binding site within its core domain (Box V) with weaker affinity. This site is the "ubiquitination signal" on p53 and binding to this site is required for efficient p53 ubiquitination by MDM2 [198, 265, 266, 280].

In addition to controlling p53 function, MDM2 can regulate the levels and activity of a number of other proteins both positively and negatively. So are IRF-2 and pRb (retinoblastoma protein) ubiquitinated and degraded in a MDM2 dependent manner [281, 282]. The activity of p65 and p73 are modulated by MDM2, without necessarily leading to protein destruction [283-288].

MDM2 has become the focus of intensive research as a target for the development of drugs aiming to reactivate p53 function in cancer cells. Several small molecules have been identified that either disrupt the interactions between p53 and MDM2, modulate MDM2 protein expression or inhibits MDM2's E3 ligase function and at least one of these drugs is currently being tested in clinical trials [289].

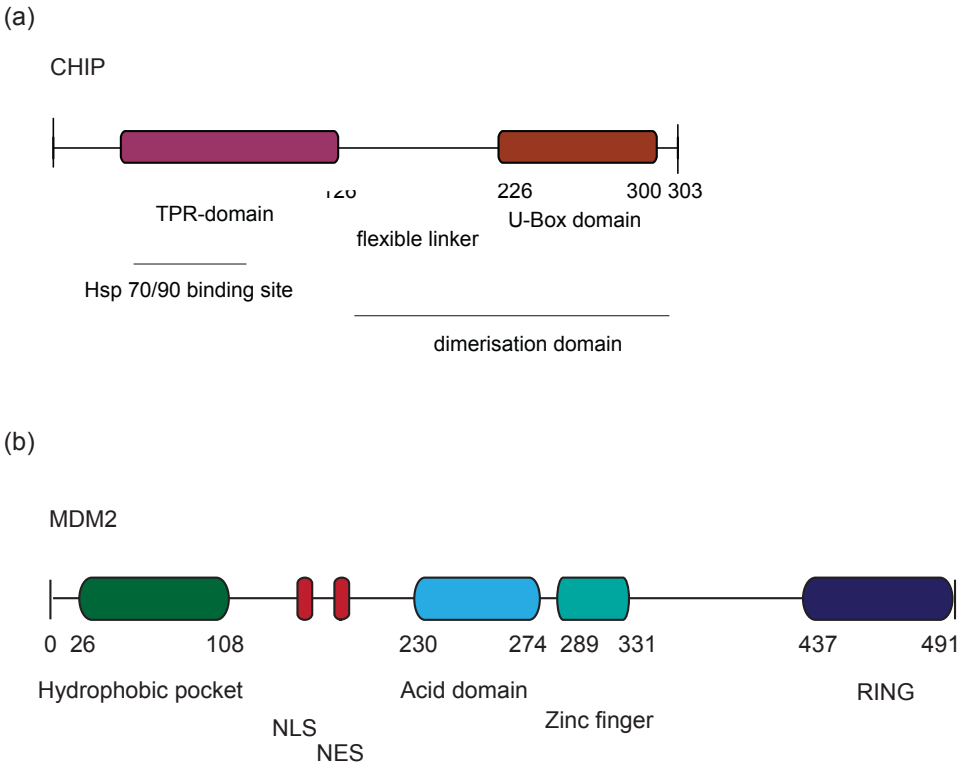

Figure 1-11 Functional domains of CHIP and MDM2

NLS = nuclear localisation signal, NES = nuclear export signal

1.6 Objective of this thesis

The scope of this thesis was to gain a better understanding of the regulation, mechanism and effects of p53 and IRF-1 ubiquitination. To do this, I studied three main areas: Firstly, the regulation of the two E3 ligases CHIP and MDM2, which have been implicated in the control of the tumour suppressors p53 and IRF-1. This was done by studying the structure/function relationship, as well as the effects of ligand binding to the E3 ligases (chapter 3). Secondly, I wanted to establish the mechanism of IRF-1 ubiquitination in more detail, therefore, I mapped the sites of ubiquitin modification in a first step and then went on to determine interplay between DNA binding and ubiquitination of the transcription factor (chapter 4). Lastly, I studied the non-proteolytic effect of ubiquitination on the activity of p53 and IRF-1 to gain insight into how these transcription factors are regulated by modification with ubiquitin (chapter 5).

Chapter 2: Materials and Methods

2.1 Reagents, plasmids and centrifuges

pET-15b-mod-CHIP and pGEx6MDM2-WT was a kind gift from Alicja Zylicz; pcDNA3-IRF-1 WT and mutants (W11R) were from Emmanuelle Pion and Kathryn Ball; pcDNA3-p53, pcDNA3-MDM2, His-ubiquitin were from Susanne Pettersson, Ted Hupp and Kathryn Ball, FLAG-IRF-1, FLAG-IRF-1 ΔMf2, FLAG-empty vector, pDEST15-IRF-1 WT and W11R (codon optimised) were from Vikram Narayan, Emmanuelle Pion and Kathryn Ball, pT7-7Hup53 was from Ted Hupp, ubiquitin-pHISTEV30a was a kind gift from Dr. Anna Plechanovova and Prof. Ron Hay (see Table 2-1 for details of plasmids).

Table 2-1 List of Vectors

Vector	Tag	Promoter	Antibiotic resistance	Use
pET-15b (Novagen)	His	T7	Ampicillin	Bacterial protein expression
pGEx6 (Amersham)	GST	tac	Ampicillin	Bacterial protein expression
pDEST15 (Life technologies)	GST	T7	Ampicillin	Bacterial protein expression
pT7-7Hup (Novagen)	none	T7	Ampicillin	Bacterial protein expression
pHISTEV30a (Hay group)	His	T7	Kanamycin	Bacterial protein expression
pcDNA3.1 (Invitrogen)	none	T7	Ampicillin	Expression in mammalian cells

Chemicals and reagents were purchased from Sigma or BDH, unless otherwise indicated. Sorvall RC-5C plus and Eppendorf 5415R were used for all centrifugations, unless otherwise indicated.

2.2 Microbiological techniques

2.2.1 Growth of bacterial cultures

2.2.1.1 Over-night cultures

For overnight cultures, 5-250 ml of LB broth media with the appropriate antibiotic was inoculated with colonies from either a glycerol stock or a bacterial culture dish. The culture was incubated over-night at 37°C in a shaking incubator.

Luria-Bertani (LB) broth

1% (w/v) Tryptone
1% (w/v) NaCl
0.5% (w/v) Yeast extract
The media was sterilised by autoclaving at 121°C for 20 minutes and 50 μg/ml kanamycin (Gibco) or 100 μg/ml ampicillin (SIGMA) was added after autoclaving.

2.2.1.2 Glycerol stocks

For long time storage of the bacteria cultures glycerol stocks were prepared. Therefore, 850 μl of a liquid over-night culture was mixed well with 150 μl sterile glycerol, snap frozen in liquid N_2 and stored at -80°C.

2.2.2 Preparation of competent cells

Bacterial cells from glycerol stock were inoculated into 2 ml of antibiotic free LB media and incubated overnight at 37°C in a shaking incubator.. The overnight culture was diluted 1:200 in 100 ml LB media and grown till the OD_{600nm} has reached 0.6. The culture was pelleted for 20 minutes at 4000 g, re-suspended in 16 ml ice-cold buffer I and incubated for 10 minutes on ice. Cells were centrifuged again as above and the pellet was re-suspended in 2 ml ice-cold buffer II. After a 10 minutes incubation time, cells were aliquoted (30 μl) and snap frozen using liquid nitrogen. Competent cells were stored at -80°C.

Buffer I

60 mM CH3COOK
10 mM CaCl2
40 mM MgCl2
100 mM RbCl
15% (v/v) glycerol
Adjusted to pH 5.8 with CH3COOH and sterilised by filtration

Buffer II

10 mM MOPS
75 mM CaCl2
10 mM RbCl
15% (v/v) glycerol
Adjusted to pH 6.5 with NaOH and sterilised by filtration

2.2.3 Heat shock transformation of *E.coli*

30 µl of competent cells (stored at -80°C) were thawed on ice. Next, 50-200 ng of plasmid DNA was added to the cells and incubated for 20 minutes on ice. The bacteria were incubated at 42°C (water bath) for 45 seconds and subsequently 500 µl of LB broth media (antibiotic free) was added and bacteria cells were incubated for 1 hour at 37°C while shaking. Cells (100 µl and 250 µl) were plated on agar plates and incubated at 37°C over-night.

LB agar plates

1% (w/v) tryptone
0.5% (w/v) yeast extract
1% (w/v) NaCl
1.5% (w/v) agar, granulated

Sterilised by autoclaving at 121°C for 20 minutes.

To prepare plates the agar was melted using a microwave, cooled down and 100 μg/ml ampicillin or 50 μg/ml kanamycin (SIGMA and Gibco) was added after the agar had reached around 45°C. Next, the agar was poured into 90 mm petri dishes (Sterilin), allowed to cool down and dried in a 37°C incubator.

2.2.4 Amplification, purification and quantification of plasmid DNA

One distinct colony from a LB agar plate was inoculated in 5 ml (Mini-prep) or 250 ml (Maxi-prep) of LB broth (with selective antibiotic) and incubated for 12-16 hours at 37°C shaking. Bacterial cells were collected by centrifugation at 4000 g and plasmid DNA was extracted using either the Qiagen HiSpeed Mini-prep or Maxi-prep kit following supplier's instructions. DNA was eluted using 30 or 500 μl H_2O respectively. DNA content was quantified using a NanoDrop ND-1000 spectrophotometer following manufacturer's instructions.

2.2.5 Agarose gel electrophoresis of DNA

DNA samples were analysed using agarose gel electrophoresis. Therefore, 1- 2% agarose (electrophoresis-grade - Invitrogen) was dissolved in 1X TAE by gentle heating in a microwave oven. After all the agarose had dissolved, the mixture was allowed to cool down slightly and ethidium bromide (0.5 μg/ml) was added to the gel prior to pouring into a gel chamber. DNA samples were mixed with 6X DNA loading dye and loaded onto the gel. Gels were run at 100 V for 45-60 minutes.

1X TAE Buffer

40 mM Tris-HCl

1 mM EDTA

Adjusted pH to 8 with glacial acetic acid

6X DNA Loading Dye

0.25% bromophenol blue
0.25% xylene cyanol
15% glycerol

2.2.6 Site-directed mutagenesis

Site-directed mutagenesis was carried out using the QuikChange Kit (Stratagene) according to the manufacturer's instructions. Primers used for site-directed mutagenesis are listed in Table 2-2.

PCR reaction mix for site-directed mutagenesis was prepared as follows:
12.5 µl Pfu Master Mix (2X)
2.5 µl Band Doctor
50 ng Plasmid DNA template
0.13 µl Forward Primer (100 µM stock)
0.13 µl Reverse Primer (100 µM stock)
Nuclease-free water to 25 µl

Thermal cycling conditions were:
95°C for 1 minute
95°C for 50 sec
55°C for 1 minute
68°C for 12 minutes
Repeat steps 2-4 for 15 cycles
68°C for 30 minutes
Hold at 4°C

To remove the template DNA the reactions were digested with 1 µl DpnI (5 U/µl, Invitrogen) at 37°C for 90 minutes, followed by heating at 65°C for 10 minutes to inactivate the enzyme. Of the digested product 5-15 µl was transformed into competent DH5α cells. Two to three single colonies were picked and DNA was

prepared using the Qiagen Mini-prep kit (2.2.3 and 2.2.4). The isolated DNA was sequenced to confirm that it contained the respective mutation (Source BioScience). PCR was performed using DNA Engine Dyad peltier thermal cycler (Bio Rad)

Table 2-2 Primer sets for site-directed mutagenesis (with sites of codon change indicated in red)

Mutation	Primer Sequence	Vector
p53 ubiquitination site K101R	F: 5'CCTTCCCAGAGAACCTACCAGGGCAGC'3 R: 5'GCTGCCCTGGTAGGTTCTCTGGGAAGG'3	pcDNA3.1-p53 and pT7-7Hup53
p53 ubiquitination site K164R	F: 5'GCCATCTACAGGCAGTCACAGC3' R: 5'GCTGTGACTGCCTGTAGATGGC'3	pcDNA3.1-p53 and pT7-7Hup53
p53 ubiquitination site K292R	F: 5'GAATCTCCGCAAGAGAGGGGAGCCTCAC'3 R: 5'GTGAGGCTCCCCTCTCTTGCGGAGATTC'3	pcDNA3.1-p53 and pT7-7Hup53
p53 ubiquitination site K305R	F: 5'CAGGGAGCACTAGGCGAGCACTGC'3 R: 5'GCAGTGCTCGCCTAGTGCTCCCTG'3	pcDNA3.1-p53 and pT7-7Hup53
IRF-1 ubiquitination site K39R	F: 5'ATTCCGTGGAGACATGCGGC'3 R: 5'GCCGCATGTCTCCACGGAAT'3	pDEST15-IRF-1 (codon optimised)
IRF-1 ubiquitination site K50R	F: 5'TATTAACAGAGATGCGTGCC'3 R: 5'GGCACGCATCTCTGTTAATA'3	pDEST15-IRF-1 (codon optimised)

IRF-1 ubiquitination site K78R	F: 5'AACCTGGAGAGCGAATTTTCG'3 R: 5'CGAAAATTCGCTCTCCAGGTT'3	pDEST15-IRF-1 (codon optimised)
IRF-1 ubiquitination site K95R	F: 5'ATTGAAGAAGTGAGAGATCAGAGCCG'3 R: 5'CGGCTCTGATCTCTCACTTCTTCAAT'3	pDEST15-IRF-1 (codon optimised)
IRF-1 ubiquitination site K117R	F: 5'CTGACCAGAAATCAGCGTAAAGAACG'3 R: 5'CGTTCTTTACGCTGATTTCTGGTCAG'3	pDEST15-IRF-1 (codon optimised)
Ubiquitin K6A	F: 5'GCAGATCTTCGTGGCGACCCTGACTGG'3 R: 5'CCAGTCAGGGTCGCCACGAAGATCTGC'3	ubiquitin-pHISTEV30a

2.3 Biochemical Techniques

2.3.1 Separation of proteins by SDS-PAGE

The Biorad System was used for gel preparation and running. First the separation gel was poured (70% of gel) and overlaid with H_2O to obtain an even surface and to exclude oxygen from the gel. After the separation gel had polymerised, the water was thoroughly removed and the stalking gel was poured on top. Immediately a comb (10 or 15 wells) was inserted and the gel was left to polymerise. After solidifying, the gel was placed in a tank with running buffer and the comb was removed. Samples were prepared by addition of sample buffer (2 x) and heating for 2-5 minutes at 95°C. In the first lane 5 µl of pre-stained protein standard (Bio-Rad) was loaded as a size marker. The gel was run at 120 V (constant) until the proteins left the stalking gel and then at 170-200 V (constant) until the bromophenol blue dye had reached the bottom of the gel.

Running Buffer

192 mM glycine
25 mM Tris-HCl (pH 6.8)
0.1% (w/v) SDS

2 x sample buffer

5% (w/v) SDS
125 mM Tris-HCl (pH 6.8)
25% (v/v) glycerol)
200 mM DTT
bromophenolblue (as required)

Separation Gel 0.75 mm

8-15% acrylamide mix
0.39 M Tris-HCl (pH 8.8)
0.1% (w/v) SDS
0.1% (w/v) APS
0.04% (v/v) TEMED

Stalking Gel 0.75 mm

5% acrylamide mix
0.13 M Tris-HCl (pH 6.8)
0.1% (w/v) SDS
0.1% (w/v) APS
0.04% (v/v) TEMED

SDS-PAGE was carried out using the Biorad Protean II mini-gel system.

2.3.2 Invitrogen precast gel system

All ubiquitination assay samples were run on gradient precast gels (4-12% Bis- Tris Gels, Invitrogen) with 1 x MOPS running buffer (Invitrogen). The gels were run at 175 V (constant) for around 60 minutes.

2.3.3 Colloidal Blue Staining

After the proteins were separated by SDS-PAGE the gel was transferred into 20 ml fix solution for 10 minutes and subsequently into 20 ml stain solution (Invitrogen). After 10 minutes in the stain solution 1 ml of Stainer B (Invitrogen) was added and the gel was stained for at least 3 hours or over-night. To destain, the gel was transferred into H_2O and a ball of tissue paper was added to the petri dish to absorb the dye and fasten destaining. Subsequently, gels were dried onto chromatography paper using a heated vacuum gel dryer (Gel Master Model 1426, Welch Rietschle Thomas).

Fix Stain

10 ml methanol 11 ml H_2O

2 ml acetic acid 4 ml methanol

8 ml H_2O 4 ml Stainer A (Invitrogen)

2.3.4 Coomoassie Blue Stain

For Coomassie blue staining polyacrylamide gels were incubated for 10 minutes in the Coomassie Stain and subsequently placed in destain until bands had reached the desired intensity (for 4-16 hours). Gels were dried as above (2.3.3).

Coomassie stain

5% Coomassie blue R-450 (Sigma)

10% (v/v) acetic acid

50% (v/v) methanol

Destain

7.5% (v/v) methanol

10% (v/v) acetic acid

2.3.5 Immuno blotting

After separation by SDS-PAGE, proteins were transferred electrophoretically from the gel onto a nitrocellulose membrane (Whatman) by western blotting. The gel was placed on the membrane (pre-wetted in transfer buffer) and filter paper and a sponge was placed on either side. The blot was placed in a tank and the transfer was carried out either for 1 hour at 100 V (with an ice block to control the temperature) or at 30 mA overnight. After the transfer, the membrane was ink stained (Pelikan; diluted 1:1000 in PBST) for 10 minutes and then washed 3 times for 5 minutes in PBST. To block any nonspecific binding sites for the antibody, the membrane was blocked in PBST + 5% (w/v) dried skimmed milk (PBST5M; Marvel) for 1 hour or over-night. The membrane was then incubated with the primary antibody in PBST5M for 1 hour at room temperature (24°C) or overnight at 4°C. The membrane was washed with PBST as previously and incubated with the secondary antibody diluted 1:2000 in PBST5M for 1 hour at room temperature (24°C), subsequently the membrane was washed again and incubated in 2 ml of a 1:1 mix of ECL solution 1 and 2. Then the membrane was dried with a tissue paper, exposed to X-Ray Film (SLS) or Hyperfilm ECL (Amersham) and the film was developed using a Konica Medical Film Processor (SRX-101A).

10x PBS	*Transfer Buffer*
1.37 M NaCl	192 mM glycine
0.1 M Na_2HPO4	25 mM Tris
27 mM KCl	20% (v/v) methanol
18 mM KH_2PO_4	

Table 2-3 Primary Antibodies

Target	Clonality	Name	Supplier	Dilution
IRF-1	mouse monoclonal	20/IRF-1	BD	1:1000
IRF-1	rabbit polyclonal	C20	Santa Cruz	1:1000
p53	mouse monoclonal	DO1	Moravian Biotechnology	1:5000
p53	rabbit polyclonal	CM1	Moravian Biotechnology	1:1000
CHIP	mouse monoclonal	v3.1	Gift from B.Vojtesek	1:30
CHIP	rabbit polyclonal	N-ter	SIGMA	1:1000
MDM2	mouse monoclonal	2A10	Moravian Biotechnology	1:1000
MDM2	mouse monoclonal	4B2	Moravian Biotechnology	1:1000
ubiquitin	mouse monoclonal	sc-8017	Santa Cruz	1:1000
ubiquitination	mouse monoclonal	FK2	Enzo Life Sciences	1:1000
polyubiquitination	mouse monoclonal	FK1	Enzo Life Sciences	1:0000
His tag	mouse monoclonal		Novagen	1:1000
FLAG M2	mouse monoclonal		SIGMA	1:1000
p21	mouse monoclonal	OP64	Calbiochem	1:1000
GAPDH	mouse monoclonal		Abcam	1:30000
b-actin	mouse monoclonal		SIGMA	1:5000
HP1	mouse monoclonal		Upstate	1:5000
Histone 3	rabbit polyclonal		Abcam	1:1000
GST	mouse monoclonal	GST-2	SIGMA	1:1000

PBST

1x PBS + 0.1% (v/v) Tween 20

ECL Solution 1	*ECL Solution 2*
100 mM Tris-HCl (pH 8.5)	100 mM Tris-HCl (pH 8.5)
2.5 mM luminol stock	0.02% (v/v) H_2O_2
0.4 mM p-coumaric acid	

ECL 1 and 2 were stored in the dark at 4°C.

2.4 Cell culture, cell lines and media

All tissue culture disposables such as culture plates, flasks and pipettes were from TPP or Greiner-Cellstar unless otherwise indicated. Media was obtained from Gibco.

Table 2-4 Cell lines and media

Cell line	**Media**	**$C0_2$**	**Origin**
A375	DMEM	10%	Human malignant melanoma
Mcf7	DMEM	5%	Human breast adenocarcinoma
HCT-116 (p53 wt)	McCoy's	5%	Human colon carcinoma
HCT-116 (p53 -/-)	McCoy's	5%	Human colon carcinoma
H1299	RPMI	5%	Human non-small cell lung carcinoma

2.4.1 Sub-culturing of cells

Cells were grown in 10 cm diameter culture dishes and sub-cultured when cells reached 100% confluency (depending on cell type 2-3 times a week). To sub-culture, cells were washed once with 10 ml of sterile PBS and then incubated with 2 ml of Trypsin-EDTA until the monolayer had detached from the plate. Then 8 ml of fresh media was added to the cells and mixed. From the cell suspension 1 ml was placed into a new dish containing 9 ml of fresh media (1:10 dilution), to use as stock plate to maintain the cell line. The remaining cells were used to seed cells in different dish sizes and cell dilutions to be used in experiments as required.

2.4.2 Freezing and recovery of cells

To freeze cells for storage a cell dish at 80-100% confluence was washed and trypsinised as above (2.4.1). Once fresh media had been added, the cell suspension was transferred into a 15 ml falcon tube and centrifuged for 3 minutes at 200 g. Subsequently cells were re-suspended in 3 ml of freezing media and divided in 1 ml aliquots in cryotubes (NunC). To freeze cells, the aliquots were stored in a Nalgene™ Cryo freezing container at -80°C overnight and then placed in liquid nitrogen for long term storage.

To recover cells the cryotubes were removed from liquid nitrogen and warmed up immediately. Once cells had thawed they were mixed with 10 ml warm full media and placed in the incubator overnight to allow cells to attach. Next, the media was exchanged to remove any residual DMSO.

Freezing media

10% DMSO
90% full growing media

2.4.3 Transient transfection of DNA

For transfection, cells were grown to approximately 70-80% confluency and transfected with the amounts of DNA indicated in the figure legends using Attractene (Qiagen) following the supplier's instructions. DNA levels were normalised using the corresponding empty vector and cells were harvested 16-24 hours post transfection.

2.4.4 Cell irradiation

Cells were irradiated in tissue culture dishes without a lid, with 5 Gray (Gy) using a Faxitron cabinet X-ray system, 43855D (Faxitron X-ray Corporation) at 2 Gy/min.

2.4.5 Drug treatment

In several experiments described in this thesis, cells were treated with various drugs prior to harvest and lysis. Table 2-5 summarizes drugs, concentration and times used for the treatments; details are indicated in the relevant figure legends.

Table 2-5 Drugs treatments

Drug	Supplier	Concentration	Time
Nutlin-3	Enzo Life Sciences	10 μM	2-24 hours
KU-55933 (ATM Inhibitor)	Merck	10 μM	4 hours
Cycloheximide	Suelco	30 μg/ml	20-150 minutes
MG-132	Calbiochem	10 μM	4 hours
Lactacystin	Calbiochem	10 μM	4 hours

2.4.6 Harvesting cells

Cell containingdishes were placed on ice and culture media was removed. The cell monolayer was washed with ice-cold PBS. Then 1 ml of ice-cold PBS was added to the cells and they were scraped off carefully using a cell scraper and transferred into an eppendorf tube. Cells were centrifuged for 5 minutes at 5000 g at 4°C and supernatants were discarded. The cell pellet was snap-frozen in liquid nitrogen and stored at -80°C until cell lysis.

2.4.7 Cell lysis

For cell lysis, approximately two volumes (with respect to the size of the cell pellet) of lysis buffer was and mixed thoroughly with the pellet by pipetting. Cells were incubated on ice for 20 minutes, followed by centrifugation at 15 000 g for 15 minutes at 4°C. The supernatant was transferred to a new eppendorf tube and total protein concentration was determined using the bradford protein quantification assay.

0.4% Triton X-100 Lysis Buffer	*Urea Lysis Buffer*
50 mM HEPES (pH 7.5)	8 M Urea
0.4% (v/v) Triton X-100	50 mM HEPES (pH 7.6)
150 mM NaCl	5 mM DTT
10 mM NaF	1 mM benzamidine
2 mM DTT	50 nM NaF
0.1 mM EDTA	120 nM okadaic acid
1X PIM (see below)	

PIM- Protease Inhibitor Mix (10X stock)
200 µg/ml leupeptin
10 µg/ml aprotinin
20 µg/ml pepstatin
10 mM benzamidine
100 µg/ml soybean trypsin inhibitor
20 mM pefabloc
10 mM EDTA

2.4.8 Protein quantification

Protein concentrations were estimated using Bradford's reagent (Bio-Rad), according to the manufacturer's instructions. Absorbance (595 nm) was determined using the Victor 3 plate reader (Perkin Elmer).

2.5 Protein Purification from *E.coli*

All proteins were expressed in *E.coli* BLR21-A1 cells (Invitrogen, genotype Genotype: F- ompT hsdSB(rB- mB-) gal dcm araB::T7RNAP-tetA). This *E.coli* strain contains a firmly regulated arabinose-inducible araBAD promoter upstream of a T7 RNA polymerase gene and can be used with all T7 promoter-based vectors.

2.5.1 Purification of His-tagged CHIP

25 ml of an overnight culture of BLR21-A1 cells containing the PET15b-CHIP plasmid were transferred into 500 ml LB broth with ampicillin (50 μg/ml). Bacteria cells were incubated at 37°C shaking until the OD_{600} had reached 0.4 (U-2800 Spectrophotometer, Digilab Hitachi), then protein expression was induced by the addition of 0.2% arabinose and the cells were incubated for another 3 hours at room temperature (24°C) with shaking. Subsequently, the bacteria were spun down at 6000 g for 15 minutes at 4°C and the supernatant were discarded. The cell pellet was re-suspended in 15 ml lysis buffer and kept on ice for 20 minutes. To help cell lysis the cells were snap frozen and thawed twice, then sonicated 3 times for 15 seconds on ice with 30 seconds cooling intervals. The lysate was next centrifuged at 10 000 g for 10 minutes at 4°C to remove cell debris. In the meantime, Ni^{2+} beads (Qiagen) were prepared, 1 ml of agarose (50% slurry) solution were transferred into a Falcon tube and washed 3 times with lysis buffer. To wash the beads 5 ml of lysis buffer was added, mixed well and removed again after separation from the beads by gentle centrifugation at 500 g. The lysate was added to the washed beads and incubated for 1 hour at 4 °C on a rotating table. Subsequently, the beads were washed to remove any unbound protein, the wash steps were performed as before, 2 x with wash buffer 1 and 3 x with wash buffer 2. Then the proteins were eluted for 30 minutes at 4°C on a rotating table using 5 ml elution buffer. The beads were separated from the proteins by gentle centrifugation at 500 g and the protein concentration was determined using the Bradford assay. His-tagged proteins were aliquoted, snap-frozen and stored at -80°C

Lysis buffer

20 mM Tris-HCl (pH 8)
150 mM NaCl
0.1% (v/v) IGEPAL
10 mM NaF
2 mM DTT
1x PIM
20 mM imidazole
10 mg/ml lysozyme

Wash buffer 1

20 mM imidazole
150 mM NaCl
20 mM Tris-HCl (pH 8)
2 mM benzamidine
0.1% (v/v) IGEPAL

Wash buffer 2

40 mM imidazole
150 mM NaCl
20 mM Tris-HCl (pH 8)
2 mM benzamidine
0.1% (v/v) IGEPAL

Elution buffer

20 mM Tris-HCl pH 8
150 mM NaCl
150 mM imidazole
1x PIM

2.5.2 Purification of GST-tagged proteins

25 ml of an over-night culture of BLR21-A1 cells containing pDEST15-GST- IRF-1 or pGEx6MDM2-WT plasmid were transferred into 1 l LB broth with ampicillin (50 μg/ml). The cells were incubated at 37°C shaking until the OD_{600} had reached 0.4, then protein expression was induced by the addition of 0.2% arabinose and the bacteria were incubated for another 3 hours at room temperature (24°C) in a shaker. Subsequently the bacteria were spun down at 6000 g for 15 minutes at 4°C and the supernatant was discarded. To lyse the cells, the pellet was re-suspended in 20 ml lysis buffer and sonicated 2 x for 10 seconds on ice with 30 seconds cooling intervals. To remove cell debris, the lysate was spun down at 6000 g for 10 minutes at 4°C. Glutathione-sepharose 4B (Amersham/GE) columns were prepared by transferring 1 ml of beads (50% slurry) to a falcon tube. The beads were washed three times with 10 ml PBS, therefore PBS was added to the beads and mixed well,

then the beads were separated from PBS by gentle centrifugation at 1000 g at 4 °C. In a final wash step beads were washed with TNEN in the same way as before and then re-suspended in TNEN. The entire lysate was added to the beads and incubated rotating for 60 minutes at 4°C. After incubation the beads were washed five times with TNEN as previously to remove any unbound protein. Then the GST tagged proteins were eluted with 5 ml elution buffer for 30 minutes at 4°C on a rotating table. The protein was separated from the beads by centrifugation at 1000 g, aliquoted, snap frozen and stored at -80°C. The protein concentration was determined using the Bradford assay.

Lysis Buffer

20 mM Tris-HCl (pH 8)
150 mM NaCl
1 mM EDTA
0.5% (v/v) IGEPAL
1x PIM
10mg/ml lysozyme
10 mM NaF
2mM DTT

TNEN

2 mM benzamidine
20 mM Tris-HCl (pH 8)
1 mM EDTA
0.5% (v/v) IGEPAL
10 mM NaF
2 mM DTT

Elution buffer

100 mM Tris-HCl (pH 8)
20 mM reduced glutathione
120 mM NaCl
1 x PIM

2.5.3 Removal of GST tag using Prescission Protease

To remove the GST-tag from GST-MDM2 protein, after the last wash step, instead of addition of elution buffer, beads were washed and then suspended in 1 ml Prescission buffer. Prescission protease (30 µl, GE Healthcare) was added to the beads and incubated over-night at 4°C on a rotating table. Beads were removed by 2 minutes centrifugation at 1000 at 4°C and the supernatant, which contained the purified and cleaved MDM2 protein was aliquoted, snap frozen in liquid nitrogen and stored at -80°C.

Precission buffer

50 mM Tris-HCl (pH 8)
1 mM EDTA
120 mM NaCl
1 mM DTT

2.5.4 p53 Purification

25 ml of an overnight culture of BLR21-A1 cells containing the pT7-7 Hup53 plasmid were transferred into 1 l LB broth with ampicillin (50 µg/ml). The cells were incubated at 37°C in a shaker until the OD_{600} had reached 0.6, then protein expression was induced by the addition of 0.2% arabinose and the bacteria were incubated for another 3 hours at room temperature (24°C) in a shaker. Next, cells were harvested by centrifugation at 6000 g for 15 minutes at 4°C, the supernatant was discarded and the cell pellet was re-suspended in 5 ml re-suspension buffer. For cell lysis, the cell suspension was snap-frozen and thawed on ice, then sonicated 4 times for 15 seconds with 30 seconds incubation periods on ice between pulses. The lysate was cleared by centrifugation at 10 000 g for 15 minutes at 4°C. Subsequently, the lysate was loaded onto a Heparin HiTrap 5 ml column (Amersham) and the column was attached to a FPLC (UPC_900/P-920, Amersham). The proteins were eluted with 15 x column volume (75 ml) using a salt gradient from 100% Buffer A

with 0 M KCl to 100% Buffer B with 1 M KCl. The eluent was collect in 1 ml fractions. Every second fraction collected (90 in total), was analysed by SDS-PAGE followed by either Coomassie Brilliant Blue staining or western blotting with an anti-p53 (DO1) antibody to identify fractions containing p53 protein.

The fractions containing the majority of p53 protein were identified (0.4-0.6 M KCl), pooled and further cleaned using p11 cellulose. Therefore, 2 g of p11 cellulose (Whatman) was incubated in 5 ml 0.5 M NaOH for 5 minutes. The cellulose was subsequently washed with water until the pH had reached 11, incubated in 5 ml 0.5 M HCl for another 5 minutes and washed again until the pH had reached 3. The equilibrated P11 cellulose was washed two times in 10x Buffer A, diluted 1:1 in Buffer A and incubated at 4°C over-night. To wash the cellulose, the respective washing solution was added, mixed well and then removed by gentle centrifugation at 500 g for 4 minutes at 4°C. 15 ml of pooled fractions from the heparin column purification (0.4-0.6 M KCl) were diluted in 135 ml Buffer C to give a final salt concentration of 50 mM KCl. Then, the samples were added to the equilibrated P11 cellulose, mixed at 4°C for 1 hour and loaded onto a column. The column was washed with 1 ml of Buffer A and then the proteins were eluted using 1 ml Buffer A with increasing salt concentrations (100 mM, 200mM … 1M KCl). The fractions were separated by SDS-PAGE and then visualised using Coomassie Brilliant Blue stain.

Re-suspension buffer	*Buffer A*
10% (w/v) sucrose	25 mM HEPES (pH 7.4)
10 mM HEPES (pH 7.4)	10% (v/v) glycerol
25mM NaCl	5 mM benzamidine
1 PIM tablet (Roche)	5 mM DTT
0.5 mg/ml lysozyme	0.1% (v/v) Triton X-100

Buffer B

25mM HEPES (pH 7.4)
10% (v/v) glycerol
5 mM benzamidine
5 mM DTT
0.1% (v/v) Triton X-100
1 M KCl

10 x Buffer A w/out glycerol

250 mM HEPES (pH 7.4)
50 mM benzamidine
50 mM DTT
1% (v/v) Triton X-100

Buffer C

25 mM HEPES (pH 7.4)
1 mM benzamidine
1mM DTT

2.6 Assays

2.6.1 *In vitro* protein-protein binding assay (ELISA)

A white 96 well microtiter plate (Fisher) was coated with 100 ng of protein 1 (His-CHIP, MDM2, p53, GST-IRF-1, His-UbcH5 or His UbcH13/Mms2 (Boston Biochem) per well in 50 µl 0.1 M $NaHCO_3$ and incubated over-night at 4°C. Then, the plate was washed three times with 200 µl PBST and any free binding sites on the plate were blocked using 3% BSA in PBS for 1 hour at room temperature (24°C). The plate was washed as previously and 50 µl ELISA buffer with a titration (0-100 ng) of protein 2 (His-CHIP, MDM2, p53 or GST-IRF-1) was added to each well and again incubated for 1 hour at room temperature (24°C). The plate was washed as previously and 50 µl anti-protein 2 mAb diluted 1:1000 in 3% BSA in PBS was added to the wells and incubated for 1 hour at room temperature (24°C). The plate was washed again and a secondary anti-mouse antibody was added diluted 1:1000 in 3% BSA (w/v) in PBS and incubated for 1 hour. Subsequently the wells were washed again and 50 µl of a mixture of ECL1/ECL2 (1:1) was added to the wells and incubated for 1 minute. Then electrochemical luminescence was measured using a luminometer (Labsystems; Flousoskan Ascent FL).

ELISA buffer

25 mM HEPES (pH7.5)

50 mM KCl

10 mM $MgCl_2$

5% (v/v) glycerol

0.1% (v/v) Tween-20

2 mg/ml BSA

2.6.2 Competition ELISA

Competition assays were carried out similar to *in vitro* protein-protein binding assays (2.6.1), with His-CHIP, NPM, Kap-1, MDM2 or His-Set as protein 1 (NPM, His-SET and Kap-1 was a kind gift from Vikram Narayan). Instead of a titration, 100 ng of protein 2 with a titration of peptides or oligonucleotides (as detailed in figure legends) was added to the plate in PBS. Washing and detection was carried out as detailed in 2.6.1.

2.6.3 *In vitro* peptide binding assay (peptide ELISA)

A white 96 microtiter well plate was coated with 50 µl Streptavidin (1 µg per well in PBS) and dried in a 37°C incubator over-night. Next, wells were washed three times with 200 µl PBST and incubated with saturating amounts of biotin tagged peptides (~60 pmol; 0.25 µl of 5 mg/ml stock) in 50 µl PBS for 1 hour at room temperature (24°C). Peptides were obtained from Chiron Mimotopes and contain a Ser-Gly-Ser-Gly spacer between peptide and N-terminal Biotin tag. Plates were washed again as above and incubated with 3% BSA (w/v) in PBS for 1 hour at room temperature (24°C), to block any free binding sites on the plate. After another wash step a titration of protein was added to the plate (0-100 ng or as indicated in the figure legends) and bound protein was detected as detailed in 2.6.4.

Table 2-6 IRF-1 peptides

1.	WLEMQINSNQMPITRMRMRP	12.	PALSPTQDLEVEQALVPGYM
2.	EMIFQINSNQIPGLIWINKE	13.	TLPDWHIPVEPALSPCAVSS
3.	AAKHGWDINKEMIFQIPWKH	14.	QVSNFSDLYVVPDSTHIPVE
4.	YTGRHIDACLFRSWAWDINK	15.	DEDEETTAESNFQVSPMPST
5.	EPDPKTWKANHTGRYKAGEK	16.	LEQSELGKLPEDIMKDEDEE
6.	IEEVKFRCAMNSLPDTWKAN	17.	VDGKGYLLNELEQSEWQPTN
7.	GSSAVRVYRKIEEVKDQSRN	18.	DFSCKPGVQPTSVYGYLLNE
8.	SERKKRMLPPLTKNQVRVYR	19.	DSPGGDIGLSEEPEIKCSFD
9.	CKRKSAAKSKERKSKSSRDK	20.	MDATWNLQRVFTDLKDIGLS
10.	GLSSSGDSSPDTFSDKRKSC	21.	AQISPLRVPTMDATWLDSLL
11.	HSSYTVPGYMGLSSSTLPDD	22.	PIPCALDSLLTPVRLPSIQA

2.6.4 Immunoprecipitation (IP)

A375 cells were treated with 10 μM Nutlin-3 or an equivalent volume of DMSO for 8 hours. Then cells were scraped into 1 ml IP lysis buffers, incubated for 20 minutes and lysate was collected by centrifugation at 4°C for 20 minutes at 500 g. Lysates were pre-cleared by 40 minutes incubation with 100 μl of sepharose CL 4B (Sigma-Aldrich, washed 4 times in PBS) at 4°C with rotation. Pre-cleared lysate was collected by centrifugation at 1000 g for 2 minutes and concentration of total protein was quantified using Bradford. Subsequently, 1 μg of CM1 (p53 pAb) was added to 2 mg of total protein in the pre-cleared lysate and, in a final volume of 1 ml, incubated for 1 hour at 4°C with gentle rotation. Then, 15 μl of protein G-SepharoseTM 4 FastFlow (GE Healthcare; washed 4 times in PBS) was added to the above samples and incubated over-night at 4°C with gentle rotation. Beads were washed four times with 500 μl of IP buffer. Samples were then eluted by addition of 50 μl of SDS sample buffer and incubation at 95°C for 5 minutes. The eluate was collected by centrifugation and analyzed by SDS-PAGE/Immunoblot.

IP buffer 5

0.3 M NaCl
1% (v/v) Triton X-100
50 mM HEPES pH 7.6

2.6.5 Flag -IP

A375 were transfected with either 2 μg FLAG-IRF-1 WT, FLAG-IRF-1 ΔMf2 or FLAG empty vector. 24 hours post transfections, cells were scarped into 0.5% Triton lysis buffer and lysate was prepared and pre-cleared as in 2.6.3. Then, 2.5 mg of pre-cleared lysate was mixed with 35 μl (50% slurry) FLAG-M2-agarose beads (SIGMA, washed 4 times in PBS) and incubated for 1 hour at 4°C. Next, beads were washed 4 times with 500 μl wash buffer and 2 times with PBS and then samples were eluted by incubation with 15 μg 3X FLAG peptide in 70 μl PBS for 30 minutes at 4°C on a rotating table. Samples were collected by centrifugation at 1000 g for 2 minutes and eluate and lysate were analysed by SDS-PAGE/Immunoblot.

Wash buffer

PBS
0.4% (v/v) Triton X-100

2.6.6 *In vitro* ubiquitination assay

First the ubiquitination mix for 16 reactions was prepared as follows:

366 µl H_2O

10 µl HEPES (pH 8)

2.4 µl $MgCl_2$

2 µl 10% Triton X-100

6 µl 0.2 M ATP

0.2 µl 1M DTT

0.4 µl benzamidine

3.2 µl 10 mg/ml ubiquitin (Boston Biochem)

0.7 µl E1 (UBE1, Boston Biochem)

0.4 µl E2 (His-UbcH5a)

The mix was aliquoted into 22 µl reactions. Next, 25 ng (unless otherwise indicates) substrate (p53, GST- IRF-1 or Bag-1s) and 50 ng CHIP or MDM2 (unless otherwise indicated) was added to each reaction. Where specified peptides or other proteins were added, the reactions were normalised by either DMSO or the respective protein buffer. The reactions were carried out at 30°C for 15 minutes, unless otherwise indicated. To stop the reaction 22 µl of 2x sample buffer was added and the samples were analysed by 4-12% NuPAGE Gels followed by immunoblotting.

2.6.7 Discharge Assay

First the mix for 16 reactions was prepared as follows:

Mix (for 16 tubes)

366 µl H_2O

10 µl HEPES (pH 8)

2.4 µl $MgCl_2$

2 µl 10% Triton X-100

5 µl 20 µM ATP

0.2 µl 1M DTT

0.4 µl benzamidine

3.2 µl 10 mg/ml ubiquitin (Boston Biochem)

0.7 µl E1 (UBE1, Boston Biochem)

0.4 µl E2 (His-UBch5a)

The mix was aliquoted to 22 µl and incubated at 30°C for 5 minutes to allow the E2 to be charged by the E1. Then, the reaction was incubated on ice for 30 minutes and an E3 ligase was added to the reactions (amounts indicated in figure legends). E2 discharge was either monitored over time and aliquots were taken after 5, 10, 15 and 20 minutes, or a titration of the E3 ligase (as indicated in figure legends) was added and all reactions were terminated after 15 minutes. To stop the reaction 22 µl of 2x non-reducing sample buffer was added.

2.6.8 *In vivo* ubiquitination assay

H1299 or A375 cells were seeded onto a 6-well plate and transfected with His-tagged ubiquitin, IRF-1 (WT or W11R), MDM2 and CHIP as indicated in the figure legends. Cells were treated as indicated in figure legends and harvested 24 hours post transfection into 1 ml of ice cold PBS. 20% cell suspension was removed for direct lysis and the remaining 80% were used to for a His-pull down. Both samples were pelleted by centrifugation at 2000 g for 5 minutes at 4°C, the supernatant was discarded and the samples were lysed. For the His-pull down samples were lysed in 1 ml lysis buffer by mixing and passing the cells through a needle and syringe, to break up the cells, 10-15 times. The lysate was mixed with further 4 ml of lysis buffer and 75 µl Ni^{2+}-NTA agarose beads (Qiagen, washed in PBS) and incubated on a rotating table over-night in a 15 ml falcon tube. Subsequently, beads were collected by centrifugation at 1000 g, for 5 minutes at 4°C. To wash, cells were re-suspended in 750 µl buffer A and transferred to a 1.5 ml eppendorf tube, incubated for 5-15 minutes on a rotating table at room temperature (24°C) and pelleted by centrifugation as above. Beads were washed in the same way 4 more times using buffer B-D. Then, 75 µl elution buffer was added to the beads and incubated for 30 minutes at room temperature (24°C) on a rotating table. Beads were pelleted by centrifugation as before, the supernatant was transferred to a new tube, mixed with an equal volume of SDS sample buffer and analysed using a 4-12% NuPAGE gel (Invitrogen). Ubiquitinated protein was detected using anti-IRF-1, anti-p53 or anti –CHIP mAb. For direct lysis, the second aliquots (20%) were lysed in 25 µl of triton X-100 lysis buffer. Samples were analysed on a 10% SDS-polyacrylamide gel using the indicated antibodies.

Buffer A	*Lysis buffer*
6 M Guanidinium-HCl	Buffer A + 5 mM imidazole
95 mM Na2HPO4	
5.3 mM NaH_2PO_4	
10 mM Tris-HCl, pH 8.0	
10 mM β-mercaptoethanol	
Adjusted to pH 8.0	

Buffer B

8 M Urea
95 mM Na_2HPO_4
5.3 mM NaH_2PO_4
10 mM Tris-HCl, pH 8.0
10 mM β-mercaptoethanol
Adjusted to pH 8.0

Buffer C

8 M Urea
22.5 mM Na2HPO4
77.5 mM NaH2PO4
10 mM Tris-HCl, pH 6.3
10 mM β-mercaptoethanol
Adjusted to pH 6.3

Buffer D

Buffer C + 0.2% Triton X-100

Buffer E

Buffer C + 0.1% Triton X-100

Elution buffer

0.2 M Imidazole
5% SDS
150 mM Tris-HCl (pH 6.8)
10% glycerol
0.72 M β-mercaptoethanol

2.6.9 Dual Luciferase reporter assay

Cells, either H1299 or HeLa, were seeded in 24 well plates and transfected with pCMVRenillaLuc (60 ng per well) and the indicated reporter constructs (120 ng per well). Cells were harvested 16-24 hours post-transfection and the Dual Luciferase Reporter Assay System (Promega) was carried out according to manufacturers instructions.

2.6.10 Electrophoretic mobility shift assay (EMSA)

The ability of p53 and IRF-1 to bind to specific promoter sequences from their target genes was determined using EMSAs. In a first step the oligonucleotides containing the binding sequence of either IRF-1 or p53 was labelled using γ-32P ATP.

Therefore, the following reaction was assembled:

0.6 µl Forward Primer (stock: 1 mg/ml, SIGMA)

0.6 µl Reverse Primer (stock: 1 mg/ml, SIGMA)

1 µl of T4 DNA kinase buffer (New England Biolabs)

0.4 µl of T4 DNA kinase (New England Biolabs)

0.4 µl of 10 mCi/ml γ-^{32}P ATP (Perkin Elmer)

The mixture was incubated for 2 hours at 37°C. Then, 15.5 µl TE and 4.5 µl KCl was added and the reaction was heated to 95°C for 2 minutes and cooled down slowly inside the metal heat block to assist proper annealing of the oligonucleotides. To remove any γ-^{32}P ATP that was not incorporated into the oligonucleotide, the sample was purified using a 1.5 ml micro-spin column (Biorad), following supplier's instructions. The labelled probe was stored at 4°C.

Table 2-7 Oligonucleotides used in DNA binding assays

Oligo-nucleotide	Sequence	Reference
p21	F: 5'TTTAAAAGCAAAACTGCAAATGTTTCAGGCACA3'	Hupp and Lane, 1994 [290]
	R: 5'TGTGCCTGAAACATTTGCAGTTTTGCTTTTAAA3'	
Bax	F: 5'GGGCTCACAAGTTAGAGACAAGCCTGGGCG3'	Patel *et al*., 2008 [291]
	R: 5'CGCCCAGGCTTGTCTCTAACTTGTGAGCCC3'	
MDM2	F: 5'GGTCAAGTTGGGACACGTCCGGCGTCGGCTGTC GGAGGAGCTAAGTCCTGACATGTCT3'	Kaku *et al*., 2001 [292]
	R: 5'AGACATGTCAGGACTTAGCTCCTCCGACAGC CGACGCCGGACGTGTCCCAACTTGACC3'	
PUMA	F: 5'CGCGCCTGCAAGTCCTGACTTGTCCGCGGC3'	Patel *et al*., 2008 [291]
	R: 5'GCCGCGGACAAGTCAGGACTT GCAGGCGCG3'	
C1	F: 5'GGGCATCGGTCGAAGTGAAAGTGAAAGTGAAA GTGAG ACTCTAGAGGATCCGCT3'	Fujita *et al*., 1989 [144]
	R: 5'AGCGGATCCTCTAGAGTCTCACTTTCACTTTCAC TTTCACTTCGACCGATGCCC3'	
TRAIL	F: 5'TCAGTGAGGAAATGAAAGCGAATGAGTTGT3'	Clarke *et al*., 2004 [293]
	R: 5'ACAACTCATTCGCTTTCATTTCCTCACTGA3'	
ISG15	F: 5'GATCCTCGGGAAAGGGAAACCGAAACTGAAGCC3'	Lace *et al*., 2009 [294]
	R: 5'GGCTTCAGTTTCGGTTTCCCTTTCCCGAGGATC3'	
ISG20	F: 5'TTGATAACAAACTAGAAACTGAAACAGGGTCG3'	Gongora *et al*., 2000 [295]
	R: 5'CGACCCTGTTTCAGTTTCTAGTTTGTTATCAA3'	
Caspase 8	F: 5'CACAAGGTGAAACAGAAACCGGGGCGATC3'	Ruiz-Ruiz *et al*., 2004 [296]
	R: 5'GATCGCCCCGGTTTCTGTTTCACCTTGTG3'	

Separating gel %

5% acrylamide mix
1 x TBE
0.1% (w/v) APS
0.1% (v/v) Triton- X100
44.2 ml H_20
Volume for one gel: 70 ml

TBE

90 mM Tris-HCl (pH 8.3)
80 mM Boric Acid,
2.6 mM EDTA.

The gel mixture was prepared as described above. Then 2 ml was removed, 3% (v/v) TEMED was added and it was quickly poured into the sides of the gel chamber to form a seal. Then 0.1% (v/v) TEMED was added to the remaining mixture, the gel was poured and a comb was inserted. Prior to loading the samples, gels were pre-run at 35 mA for 30 minutes at 4 ºC.

The reaction was prepared as a multiple of the following (1,2 or 3 x):

2 μl of 6x reaction buffer
p53 or IRF-1 (as indicated in figure legend)
0.5 μl (10 mg/ml) Salmon Sperm DNA (Invitrogen)
1 μl (1 mg/ml) poly DI/DC (SIGMA)
1 μl probe (γ-32P labelled)
1 μl anti-IRF-1 or anti-p53 mAb (as indicated in figure legend)
Adjusted to 12 μl with water

6x reaction buffer

120 mM HEPES pH 7.5
300 mM KCl
30% Glycerol
2.4 mM DTT
0.6 mg/ml BSA
0.03% TritonX-100

The reactions were incubated for 30 minutes at room temperature (24°C), mixed with 6X DNA loading buffer (2.2.5) and loaded onto the pre-run 5% polyacrylamide gel. The gel was run at 35 mA for 150 minutes at 4°C and then transferred onto 3 mm chromatography paper (Whatman), dried in a vacuum gel dryer and covered with a phosphoimager screen over-night. Radiolabelled bands were detected using a Storm840 phosphoimager (GE Healthcare).

2.6.11 *In vitro* DNA binding assay

A white 96 microtiter well plate was coated with 50 µl Streptavidin (1 µg per well in PBS) and dried in a 37°C incubator over-night. Next, wells were washed 3 times with 200 µl PBST and incubated with saturating amounts of biotin tagged C1 oligonucleotides (25 ng/well, SIGMA) in 50 µl PBS for 1 hour at room temperature (24°C). Only the forward primer contained a biotin tag and was annealed with the reverse primer prior to addition to the well by heating to 95°C and then allowing to cool down to room temperature (24°C) slowly. Plates were washed again as above and incubated with 3% BSA (w/v) in PBS for 1 hour at room temperature (24°C) to block any free binding sites on the plate. After another wash step a titration of ubiquitinated IRF-1 protein (in ubiquitin reaction mix, 2.6.6) was added to the plate and bound protein was detected as detailed in 2.6.4.

2.6.12 Cell Fractionation

To fractionate cells into soluble and insoluble fractions, cells were washed in ice-cold PBS, and then lysed on the plate in gentle lysis buffer (PBS + 0.5% Triton-X 100, 5 mM EDTA, 20 mM DTT, 0.05 mM Pefabloc) for 20 minutes with shaking. Cells were scraped and centrifuged at 6000 g for 5 minutes. Pellet and supernatant was taken and re-suspended in 2x SDS sample buffer, sonicated and heated (95°C). Subcellular Fractionations was carried out using the Proteo Extract Kit (Calbiochem), following supplier's instructions.

2.6.13 Nuclei Fractionation

A375 cells were grown in 15 cm dishes and treated as indicated in the figure legend. Cells were harvested using 2 ml Trypsin-EDTA and taken up in further 10 ml 10% FBS in PBS plus 20 mM DTT, pelleted by centrifugation at 500 g for 4 minutes and re-suspended in 3 ml NBA. Then 3 ml of NBB was added, cells were incubated for 3 minutes on ice and centrifuged for 4 minutes at 1000 g. The supernatant was discarded and nuclei were washed in 10 ml NBR and then re-suspended in 500 µl NBR. In order to prepare soluble chromatin, nuclei were digested using 10 units of micrococcal nuclease for 10 minutes at room temperature (24°C) in the presence of 5 µl per ml RNaseA/T1 (Ambion). The reaction was stopped by addition of EDTA to a final concentration of 10 mM. Then samples were pelleted for 30 seconds at 2000 g, re-suspended in 500 µl Teep80 and incubated on ice over-night for cells lysis. To remove cell debris samples were centrifuged for 5 minutes at 5000 g at 4°C and soluble chromatin was fractionated using 10-50% (w/v) isokinetic sucrose gradients in TEEP80 by centrifugation for 110 minutes at 50 000 rpm in a MLS 50 Beckman rotor at 4°C. Gradients were fractionated in 500 µl fractions by upward displacement with continuous monitoring of the absorbance profile. Half the fractions were used to analyse the protein content by ethanol precipitation, followed by intense washing to remove all sucrose and then re-suspension in SDS-sample buffer. DNA was extracted from the other half of the fractions using phenol/chloroform and enriched by ethanol precipitation. DNA pellets were washed, re-suspended in H_2O and analysed on a 1% agarose gel.

NBA	*NBB*
85 mM KCl	NBA + 0.1% (v/v) IGEPAL
10 mM Tris-HCl (pH 7.6)	
5.5% (w/v) sucrose	
0.5 mM spermidine	
0.2 mM EDTA	
0.05 mM Pefabloc	
20 mM DTT	

NBR

85 mM KCl
5.5% (w/v) sucrose
10 mM Tris-HCl (pH 7.6)
1 mM $CaCl_2$
1 mM $MgCl_2$
0.1 mM pefabloc

Teep 80

10 mM Tris-HCl (pH 7.6)
1 mM EDTA
1 mM EGTA
0.1 mM pefabloc
80 mM NaCl

2.6.14 Mass Spectrometry

2.6.14.1 Sample preparation for mass-spectrometry

When handling samples for mass spectrometry analysis the utmost care was taken to avoid contamination of the samples by keratin. The solutions used for the reactions were filtered before use where possible, gloves and a lab coat were worn at all times and most of the work was preformed in a fume hood. Five *in vitro* ubiquitination reactions with 1 μg substrate (GST-IRF-1, GST-MDM2, or His-CHIP) and 1.6 μg E3-ligase (for IRF-1) were pooled and a GST- or His- pulldown was preformed to remove reaction partners. The samples were separated on a 4-12% NuPAGE and protein-peptides were isolated from the gel by in gel trypsin digestion.

2.6.14.2 GST- and His-pulldown

To isolate GST-IRF-1, GST-MDM2 or His-CHIP from the other components in the reaction a GST or His- pulldown was performed. First the glutathione sepharose beads 4B (Amersham, GE) or Ni^{2+} beads (Qiagen) were prepared by washing 3 times with sterile PBS. Next, five *in vitro* ubiquitination reactions were pooled, added to 75 μl beads (50% slurry) and rotated at 4°C for 1 hour. To remove any unbound proteins the beads were washed 5 times with TNEN (2.5.1) or 2 times with His-

washing buffer I and 3 times with His-washing buffer 2 (2.5.2). Then 40 µl of sterile 4x LDS sample buffer (NuPage, Invitrogen) was added to the beads and heated for 4 minutes at 85°C. The beads were separated from the solution by centrifugation and the samples were loaded onto a gel. The gel was stained using colloidal blue and sealed well.

2.6.14.3 Microwave-assisted in gel trypsin digestions for mass spectrometry

Destaining

Bands to be analysed by mass spectrometry were cut out of the gel and transferred to a separate petri-dish. The bands were cut further in pieces of around 1 mm^2 and transferred to LoBind Eppendorf tubes. 1 ml of H_20 was added to the gel pieces, which were then vortexed for 15 minutes, spun down at 1000 g for one minute (as all following centrifugation steps) and the water was carefully removed by pipetting. To destain, 750 µl 50 mM ammonium bicarbonate (ABC) in 50% ammonium bicarbonate (ACN) was added and the samples were microwaved in a water bath for ten minutes on full power (700 W). The temperature of the water bath was not allowed to exceed 80°C in this step. The tubes were inverted, spun down and the liquid was removed. Then the gel pieces were dehydrated by addition of 200 µl 100% ACN and vortexed for 5 minutes (gel pieces shrunk and turned white). The liquid was removed and samples were left open in the fume hood to dry for 20 minutes.

Reduction and alkylation

For reduction, 200 µl of 10 mM DTT in 100 mM ABC was added to the samples and microwaved for 10 minutes on half power (350 W). The temperature of the water bath was not allowed to exceed 55°C. Samples were spun down and all liquid was removed. Next, the gel pieces were washed by addition of 750 µl ABC, mixed well, spun down and all liquid was removed. To alkylate the samples and thereby inhibit interactions of the peptide's cysteine residues, 200 µl of iodoacetamide was added to the samples and incubated for 30 minutes vortexing in the dark. Then the samples

were washed twice, first with 750 µl 100 mM ABC and next with 750 µl 20 mM ABC in 50% ACN. Therefore, the washing solution was added, the samples were vortexed for 15 minutes, spun down and the solution was carefully removed. The gel pieces were dehydrated by addition of 200 µl of 100% ACN and vortexed for 5 minutes. The gel pieces shrank and turned white. The liquid was removed and samples were left open in the fume hood to dry for 20 minutes.

Trypsin digestion

The gel pieces were rehydrated in 45-60 µl of 12.5 mg/mL trypsin in 20 mM ABC in 9% ACN, further 10-50 µl 20 mM ABC in 9% ACN was added until the gel pieces were just covered with liquid. The pieces were left for 10 minutes to fully dehydrate. The total amount of liquid added to each sample was written on the lid of the tube. The samples were digested by microwaving twice for 10 minutes on half power (350 W) while the temperature in the water bath did not exceed 55 °C. The samples were incubated at room temperature (24°C) over-night in the dark.

Peptide extraction

An equivalent of the amount written on the lid of 100% ACN was added to each sample and incubated for 30 minutes while vortexing. The pieces were spun down and the liquid containing peptides was transferred to new LoBind eppendorf tubes. Another equivalent of the amount written on the lid of 5% formic acid (FA) in 50% ACN was added to the samples and vortexed for 10 minutes. The gel pieces were spun down and the liquid was transferred to the new LoBind eppendorf tubes. This step was repeated. Next, the gel pieces were dehydrated by addition of 50-100 µl 100% ACN, incubated for ten minutes, then spun down and the liquid was again transferred to the new eppendorf tubes. The liquid was evaporated in a gyrovap (Eppendorf) at 60°C for 2.5 hours. Subsequently, the peptides were re-suspended in 35 µl of 1% FA by vortexing for 10 minutes. Then the samples were spun down for 10 minutes at 10 000 g at room temperature (24°C) and 17 µl of the samples was analysed by mass-spectrometry (FingerPrints Proteomics Facility, College of Life Sciences, University of Dundee).

2.7 Microscopy

2.7.1 Dual-Link

Cells were grown onto glass coverslips in a 6 well dish until they reached around 50% confluency. After treatment (as indicated in the figure legends), cells were fixed by addition of 4% formaldehyde solution for 10 minutes and then permeabilised using 1% Triton X-100 in PBS. Next Duolink® II (red) assay from Olink® Bioscience was carried out following suppliers instructions. Briefly, any unspecific antibody binding sites were blocked using 3% BSA (w/v) in PBS for 1 hour at room temperature (24°C), next primary antibodies, anti-ubiquitin (mouse, 1:50, Santa Cruz) and anti-p53 (CM1, rabbit, 1:100) were diluted in the supplied antibody diluent and added to cells and incubated over-night at 4°C. As a control one slide was incubated with only anti-ubiquitin mAb and no second primary antibody. Next PLA probes conjugated to secondary antibodies anti- mouse and anti-rabbit respectively were added to the cells for 1 hour at 37 °C and ligation and amplification was carried out as detailed by the supplier. In the last step an amplification reaction produces a fluorescent signal that can be detected using a fluorescent microscope with a Texas Red filter (Ex 644 nm, Em 669nm). Results were visualised using an Axioplan2 (Zeiss) fluorescent microscope with Plan-neofluar objectives, a 100W Hg source (Carl Zeiss, Welwyn Garden City, UK) and Chroma #89014ET single emission filters (Chroma Technology Corp., Rockingham, VT) using a 100x magnification Zeiss lense and a Hamamatsu Orca AG CCD camera (Hamamatsu Photonics (UK) Ltd, Welwyn Garden City, UK).The single excitation and emission filters are installed in motorised filter wheels (Prior Scientific Instruments, Cambridge, UK). Image capture and analysis were performed using in-house scripts written for IPLab Spectrum (Scanalytics Corp, Fairfax, VA).

4% formaldehyde solution

4% (v/v) formaldehyde
100 mM PIPES (pH)
10 mM EDTA
1 mM $MgCl_2$

2.8 Modelling Techniques

2.8.1 Generation of IRF-1/p53 - ubiquitin models

The 'Easy Interface' of the HADDOCK web server [271, 297] was used to generate models of the IRF-1 and p53 DBD conjugated to ubiquitin. For p53, the C-terminus of the p53 DBD crystal structure (PDB:1TUP, resolved at 2.2 Å; [182]) was extended from residue 291 by grafting residue 292 from 2AHI (resolved at 1.85 Å;[187]) onto 1TUP. For the model, the C-terminal glycine residue of ubiquitin (Gly^{76}) was selected as the active residue on ubiquitin (PDB :1UBQ, resolved at 1.8 Å;[36]) and Lys ^{292} on p53 or Lys^{39}, Lys^{50} and Lys^{78} on IRF-1 (PDB:1IF1, resolved at 3 Å;[124]), were chosen as the active residue in the p53 or IRF-1 crystal structure, respectively. No passive residues were selected. The best four structures in the three clusters with the best HADDOCK score were analysed. After the models were generated the DBD:ubiquitin complex was superimposed back onto the respective crystal structure to obtain a model of the DBD:ubiquitin:DNA complex. Electrostatic surface analysis of the IRF-1/p53 DBD:monoubiquitin complex were carried out using APBS (Adaptive Poisson-Boltzmann Solver;[298] in PyMOL v1.4.1 (http://www.pymol.org).

2.8.2 Molecular Simulations

To model the interactions of DNA with p53 or IRF-1 in its ubiquitinated or unmodified forms, the (extended) crystal structures of the p53 DBD (PDB: 1TUP, 2AHI) or IRF-1 DBD (PDB: 1IF1) and the model of monoubiquitinated p53 or IRF-1 DBD in complex with DNA as generated above were used. The N- and C- termini of the p53 DBD were capped with acetyl (ACE) and N-methyl (NME) respectively to keep them neutral. Molecular dynamics simulations were performed with the SANDER module of the AMBER (Assisted Model Building Refinement) 9 package (http://ambermd.org/) together with the ff99SB forcefield. The antechamber and LEaP modules were used to set up the simulation. Systems were solvated in a TIP3P water box with walls at least 8 Å away from any protein atom and net charges on the protein were neutralized using counter ions as required (20-26 Na^+). To simulate a

covalent linkage, a distance restraint between Gly^{76} of ubiquitin and Lys^{292} of p53 or Lys^{78} of IRF-1 (between 1.2 and 2Å) was created using a DISANG file in AMBER. A brief energy minimization was carried out followed by heating of the systems to 300 K and subsequent MD simulations were performed under constant pressure (1 atm) and temperature (300 K) using the Sander module. Structures were stored every 2 ps a. The free energies of binding (ΔG_{bind}) of the p53 DBD +/- ubiquitin to DNA were computed and visualizations were carried out using the ptraj modules in AmberTools1.5. Figures were prepared using PyMOL

Chapter 3: Modulation of CHIP and MDM2 E3 ligase activity by ligand binding: using MD simulations to inform experimental approaches

3.1 Introduction

3.1.1 Molecular Dynamic Simulations

Very limited options are available to study dynamics of proteins in solutions. Most studies are based on the rigid crystal structure and neglect the dynamic nature of proteins, which are in a constantly changing conformation and can adjust particularly upon ligand binding. Molecular Dynamics simulations is an in silico technique that utilises the crystal structure of a protein as a starting point and then calculates the predicted motions of the protein over a given period of time using physical approximations. The crystal structure of specific protein serves as the starting structure, next the forces that act on each atom are calculated using an energy function. With the help of the position and force that acts on an atom at a given temperature and pressure, the velocity and direction of the movement of this atom can be predicted [299]. In the simulation the structure moves forward in 2 fs steps and then the energy function and forces are recalculated. Along with many other applications the technique can be used to compute binding energies between small molecules and receptor proteins; and additionally the effect of ligands or single point mutation of the overall structure and flexibility of a protein can be predicted [300].

3.1.2 CHIP and MDM2 autoubiquitination

As discussed in detail in Chapter 1, protein ubiquitination is involved in the regulation of a vast variety of cellular processes, affecting both proteins stability and function. It is thus not surprising that components of the ubiquitin machinery themselves are regulated by ubiquitination. The majority of E3 ligases exhibit autoubiquitination activity *in vitro,* and this can be utilised to study the activity of a ligase in a substrate independent manner. *In vivo* ubiquitination of E3 ligases was shown to lead to E3 degradation, resulting in a decrease of their E3 ligase activity on heterologous substrates. Additionally, autoubiquitination can modulate the activity of

E3 ligases without leading to their degradation. Further, DUBs and E2 enzymes can also be regulated by ubiquitination, and there is at least one example of an E2 that can undergo autoubiquitination independent of any E3, leading to its destruction by the proteasome [301].

Both MDM2 and CHIP were previously shown to autoubiquitinate *in vitro* and *in vivo* [302-305]. Whether ubiquitination occurs *in cis* or *in trans* or in a combination of both remains to be investigated. Autoubiquitination of MDM2, which is dependent on its RING finger activity leads to its degradation and is therefore one mechanism by which its activity can be controlled [304]. It is not known whether MDM2 autoubiquitination has any non-proteolytic functions.

In contrast to MDM2, autoubiquitination of CHIP has not been implicated in its degradation, but increased CHIP ubiquitination correlates with an increase of its E3 ligase activity [244, 303]. The ubiquitin conjugating enzyme Ube2w leads to autoubiquitination of CHIP at Lys^2 and this in turns activates CHIP dependent ubiquitination and degradation of its target substrate INOS [306]. Furthermore, ubiquitination of Lys^2 initiates the recruitment of ataxin-3, a DUB enzyme with three UIMs that bind ubiquitin chains, ataxin-3 binding to CHIP restricts the length of its substrate's polyubiquitin chains and additionally, ataxin-3 deubiquitinates CHIP in response to substrate polyubiquitination [306]. CHIP autoubiquitination has also been implicated in recruitment of other cofactors that contain a UBDs like the Ubiquitin Interacting Motif (UIM)-containing proteasomal subunit S5a for instance. Association of S51 with CHIP inhibits the formation of forked ubiquitin chains and thus favours turnover of CHIP substrates (as forked ubiquitin chains do not lead to degradation by the proteasome [307]). Moreover, other E2 enzymes, e.g. are involved in CHIP autoubiquitination, however, the target lysines and the mechanism by which this modulates CHIP activity remain elusive.

3.2 Results

3.2.1 TPR-domain can modulate CHIP E3-ligase activity

3.2.1.1 CHIP activity is modulated by Hsp70 binding

The best-understood role of the E3 ligase CHIP, is its function in the triage system of cells where it works in synergy with Hsp70 to target chaperone client proteins for degradation. In this pathway, Hsp70 is required to 'deliver' substrates to CHIP for ubiquitination. However, the Ball group has recently identified the tumour suppressor protein IRF-1 as an Hsp70 independent substrate for CHIP. CHIP facilitates IRF-1 ubiquitination under specific stress conditions (see 1.3.4). Interestingly, IRF-1 ubiquitination by CHIP is not only independent of Hsp70 *in vitro* and in cells, but furthermore Hsp70 protein (Fig 3-1a) or an Hsp70 peptide from the CHIP binding interface that is sufficient to mimic Hsp70 (data not shown, Narayan, Landré *et al.,* submitted manuscript [368]), inhibit ubiquitination of IRF-1 by CHIP. This is an intriguing observation, as CHIP 's E3 ligase activity is generally believed to be dependent on interactions with Hsp70. To test if this inhibitory effect of Hsp70 was specific for IRF-1 ubiquitination, *in vitro* CHIP assays were performed; using p53 as the substrate, in the presence of Hsp70/40. Strikingly, the ubiquitination of p53, like that of IRF-1, was inhibited in the presence of Hsp70 (Fig 3-1b). Furthermore, autoubiquitination of CHIP was reduced by the addition of Hsp70, both in the presence of IRF-1 or p53 and in the absence of any added substrate (3.1a, b (lower panel), c). This is in contrast to the observation made by others, where Hsp70 has an activating effect on CHIP activity, most strikingly on CHIP dependent ubiquitination of Bag-1s [308]. In order to investigate this discrepancy further I asked, if the inhibition of CHIP activity by Hsp70 observed in the Ball laboratory was due to technical differences in the way the ubiquitination assay was performed. Thus, I expressed and purified Bag-1s and examined the effect of Hsp70/40 on Bag-1s ubiquitination. As shown in Figure 3-1d, ubiquitination of Bag-1s was indeed strikingly increased in the presence of Hsp70, while CHIP alone led to a faint monoubiquitination band. Thus, in the presence of Hsp70 CHIP can facilitate Bag-1s polyubiquitination under conditions were it inhibits IRF-1 and p53 modification. Additionally, no inhibition of CHIP autoubiquitination can be seen in the presence of Bag-1s. Taken together these results suggest that CHIP can mediate

substrate ubiquitination through two distinct pathways, in one, which is dependent on Hsp70, CHIP does not directly bind to its substrate but forms a complex through binding to Hsp70. In the other pathway, CHIP binds directly to its substrate and mediates ubiquitination, which is inhibited by binding of Hsp70 to CHIP.

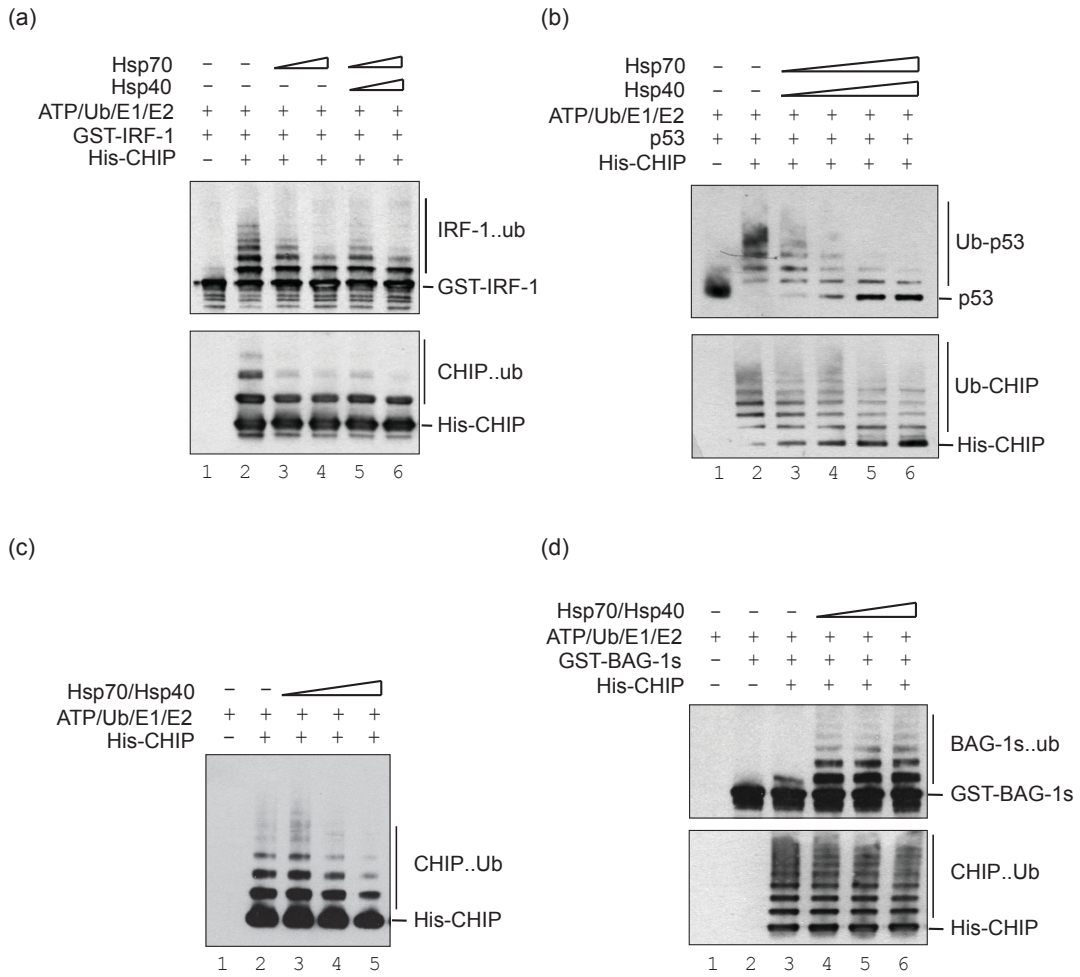

Figure 3-1 Hsp70/40 modulates the E3 ligase activity of CHIP

In vitro ubiquitination assays with all components of the ubiquitination cascade as purified components (10 µM ubiquitin, 100 nM UBE1, 1 µM UbcH5a and 4.5 mM ATP) using CHIP as the E3 ligase with a titration of Hsp70/40 (3, 6, 15 µM Hsp70 and 0.3, 0.6, 1.5 µM Hsp40). The highest Hsp70 concentration of 15 µM relates to a 1:10 ratio of CHIP:Hsp70 in the reaction and is the same ratio found in human cells [309] (the same concentration of ubiquitin, UBE1, UbcH5a and ATP was used in all *in vitro* ubiquitination assays in this chapter). The activity of CHIP as an E3-ligase using (a) GST-IRF-1, (b) p53, (d) GST-BAG-1s as the substrate plus (c) CHIP autoubiquitination in the presence of Hsp70/40 was determined. Reactions were carried out for 15 (a,b,d) or 5 (c) minutes and analysed using western blot with mAb against the indicated proteins. (a+b were carried out in collaboration with Vikram Narayan).

3.2.1.2 The flexibility and conformation of CHIP is regulated through its TPR domain

As part of a collaborative study with Vikram Narayan (Narayan, Landré *et al*., submitted manuscript, [368]), I revealed that a CHIP mutant with a single mutation from Lys to Ala in the TPR domain (K30A), which is unable to interact with the Hsp70 protein, renders the protein intrinsically less active for substrate and autoubiquitination *in vitro* (Fig 3-2a). This is a surprising observation as this mutant has in the past been extensively used to demonstrate the effects of Hsp70 binding on CHIP activity in a cellular environment even though it has not previously been characterised *in* vitro or in cells. Any loss of CHIP mediated substrate ubiquitination using the K30A mutant in cells has been explained by its inability to interact with Hsp70, however as shown here the mutant is intrinsically inactive when compared to wild-type CHIP in the absence of any Hsp70 protein. In a cell based ubiquitination assay, the TPR mutant is not only defective in IRF-1 ubiquitination, but also in autoubiquitination (Fig 3-2b). Further, both biochemical and biophysical characterisation of the mutant showed that it, in fact, has similar characteristics to Hsp70 bound CHIP and is very different from wild type CHIP. (i) CHIP K30A has a similar melting temperature (46°C) to Hsp70 peptide bound CHIP (45.5°C), which is different from $CHIP^{WT}$ (43.5°C) (data not shown). (ii) Limited proteolysis of ligand bound, K30A mutant and wild-type CHIP proteins show a striking similarity of the banding pattern observed in a time course for mutant and liganded CHIP, which appeared more resistant to cleavage and thus less flexible than the $CHIP^{WT}$ protein (data not shown). (iii) SAXS analysis suggested a similar conformation of CHIP K30A protein and CHIP that is in complex with an Hsp70 peptide, which is significantly different from the CHIP apo-protein (data not shown, see Appendix 1.2 for manuscript). Taken together these observations suggest that the K30A CHIP mutant mimics its Hsp70 bound form and exhibits reduced E3 ligase activity. As both the site of mutation (K30) and the Hsp70 binding site are located in the TRP domain of CHIP, these results indicate that mutation or ligand binding to the N-terminal TPR domain affects the C-terminal catalytic U-Box domain of CHIP.

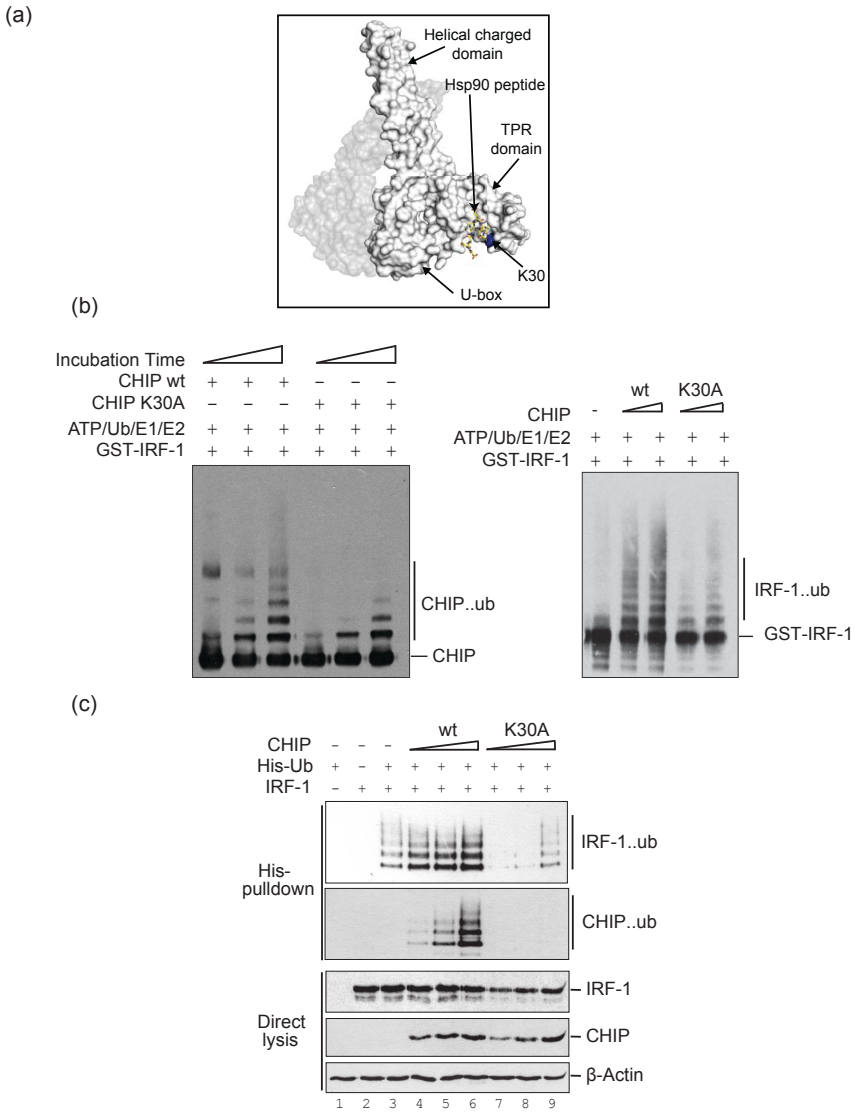

Figure 3-2 CHIP^{K30A} mimics Hsp70 bound CHIP and reduces CHIP mediated ubiquitination

(a) CHIP structure (mouse) (b) *In vitro* ubiquitination assay comparing the activity of CHIP^{WT} and CHIP^{K30A} autoubiquitination (left panel) and GST-IRF-1 ubiquitination (right panel) in a time course. Reactions determining CHIP autoubiquitination were incubated for 0, 2 and 5 minutes and reactions with GST-IRF-1 for 5 and 15 minutes. Reactions were analysed by SDS-PAGE/immunoblot. (c) H1299 cells were co-transfected with IRF-1, His–ubiquitin (0.5 µg) and CHIP or CHIP K30A (0.5-2 µg) as shown. At 20 hours post-transfection cells were treated with MG132 (50 µM) for 4 hours and histidine-labelled ubiquitinated protein was isolated using Ni-NTA chromatography and analysed by SDS/PAGE and immunoblot. Total amounts of IRF-1, CHIP and β-actin (bottom panel) and modified IRF-1 (top panel) are shown (c, data courtesy Vikram Narayan).

3.2.1.3 CHIP^{K30A} and Hsp70-bound CHIP exhibit similar dynamics in MD simulations

To gain insight into the mechanism by which TPR modulation can change the activity of the CHIP U-box, I set up and carried out molecular dynamic simulations of wild-type, mutant and ligand bound CHIP structures. As a basis for the simulation, the crystal structure of mouse CHIP (aa 25-304) bound to an Hsp90 peptide was used (PDB code: 2C2L [254]). Using Pymol, five mutations were introduced into the crystal structure, prior to the simulation, to obtain human CHIP. This was done to better relate the modelling to experimental data, where human CHIP was used.

Simulations were run on five different systems: dimeric CHIP wild-type protein with an Hsp90 or Hsp70 peptide bound to each TPR domain, with one CHIP protomer Hsp90 peptide bound and the other unbound, with unbound CHIP and on the Lys^{30} mutant (Fig 3-3). The simulations were run in an explicit water system in a tip3p water box. Prior to the simulations, the systems were minimized, followed by a heating and equalisation step. The results of the simulation show that, similar to the experimental data obtained, liganded or mutant CHIP behave in a similar manner to each other, but are different to wild type CHIP. Unliganded CHIP undergoes big conformational changes in the simulation, resulting in a more linear and extended conformation while peptide bound or mutant CHIP appears less flexible and retains the closed conformation seen in the crystal structure. See Fig 3-3b for changes in the conformation of wild-type, mutant and ligand bound CHIP, compared to the starting structure and Fig 3-3c for comparison of the structure after 20 ns simulation between each other. It should be noted that the crystal structure was solved in a peptide bound form, and it is consequently not surprising that the liganded structure undergoes fewer changes in the simulation than the unbound form.

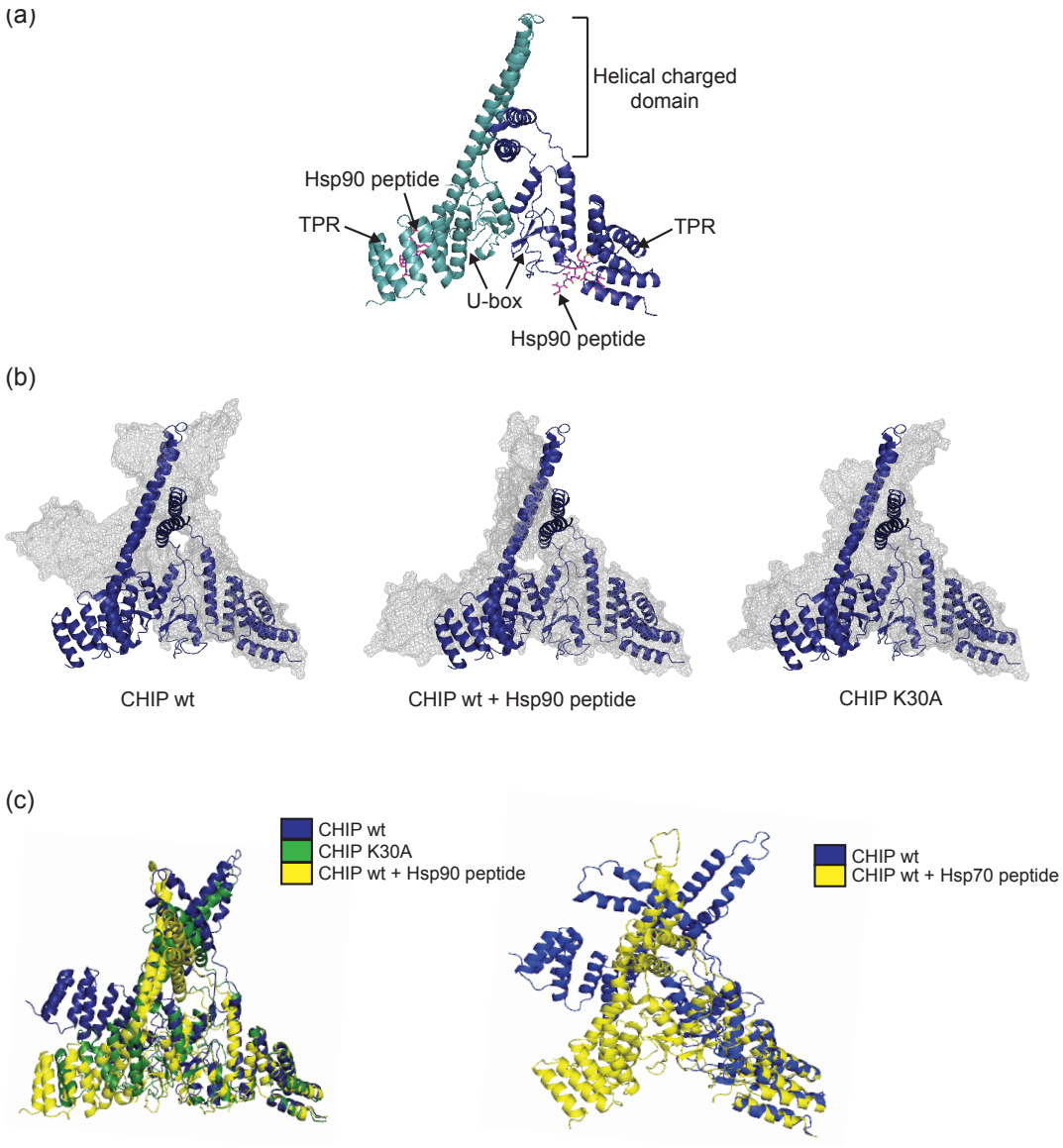

Figure 3-3 CHIP^{K30A} and Hsp70-bound CHIP exhibit similar dynamics in MD simulations

(A) Crystal structure of murine CHIP dimer (monomers in shades of blue) in complex with Hsp90 peptide (pink sticks; adapted from PDB 2C2L). (B) Overlay of the CHIP dimer before (blue ribbon) and after (grey mesh) 20 ns MD simulations for unliganded CHIP^{WT} (left), CHIP^{WT} in complex with Hsp90 peptide (centre) and CHIP (right). (C) Overlaid snapshots of the CHIP dimer in apo and liganded forms and with Lys^{30} mutated to Ala after 20 ns MD simulations. All images were generated using PyMOL v.1.4.1.

In order to determine the overall dynamics and flexibility of CHIP in the different states, the root mean square fluctuation (RMSF) of each amino acid was computed and averaged over a stable period of the simulation (5 ns frames). The results of the analysis were colour coded and are presented on the crystal structure in Fig 3-4. To access if the obtained results are in agreement with the b-factor of the crystal structure, which is a readout of the fluctuation of the different atoms in the crystal, the b-factor of the mouse structure (2C2L) in complex with Hsp90 and the RMSF in the MD simulation of the same structure were compared (Fig 3-4a). The results of the analysis showed that the relative values for fluctuation in the simulation and the b-factor are comparable in the different domains of the protein, e.g. the tip of the charged domain showed high amount of fluctuation and has a high b-factor while the 6th and 7th helix of the TPR domain had low values for both. This indicates that the calculation of the RMSF from the MD simulation gives relatively accurate information about the fluctuation of the protein, I next went on to compare the RMSF of CHIP in its wild-type, ligand bound and mutant form. This showed that wild type CHIP displayed larger and more widespread fluctuations than the ligand bound or mutant form. Interestingly, ligand binding or mutation of the TPR domain resulted in a loss of flexibility, not only in the TPR domain, but in all three domains of CHIP. In a simulation where only one protomer is bound to Hsp90 peptide, while the other one is in an unbound conformation, the unbound protomer exhibits more flexibility than the bound protomer, further confirming the stabilising effect of ligand binding to CHIP's TPR domain. This is in good agreement with a HX-MS study on CHIP, which showed that the apo-CHIP protein is more flexible than the Hsp70 or Hsp90 peptide-bound forms [256].

Taken together, the MD data are in agreement with the Ball groups experimental observation, which shows that CHIP with a mutation at K30A or in a peptide bound conformation is less thermostable and more susceptible to limited proteolytic cleavage than wild type CHIP (Narayan, Landré *et al.,* submitted manuscript, [368], Appendix 1.2). This shows that $CHIP^{K30A}$, even though unable to interact with Hsp70, displays properties of an Hsp70 bound state of CHIP. A close look at the dynamic simulations, together with analysis of salt bridges formed during the

simulation using VMD, revealed that the side-chain of Lys^{30} does not form any hydrogen bonds with atoms of other CHIP residues during the MD simulations and is instead well hydrated. We can therefore speculate that, consistent with studies showing alanine residues favour the formation of ordered helical structures [310], mutation of Lys^{30} to the much smaller and hydrophobic Ala, will make this region less hydrated and more likely to fold into an ordered structure which is more similar to the peptide bound structure than to the flexible, less ordered structure described for the apo-TPR [256].

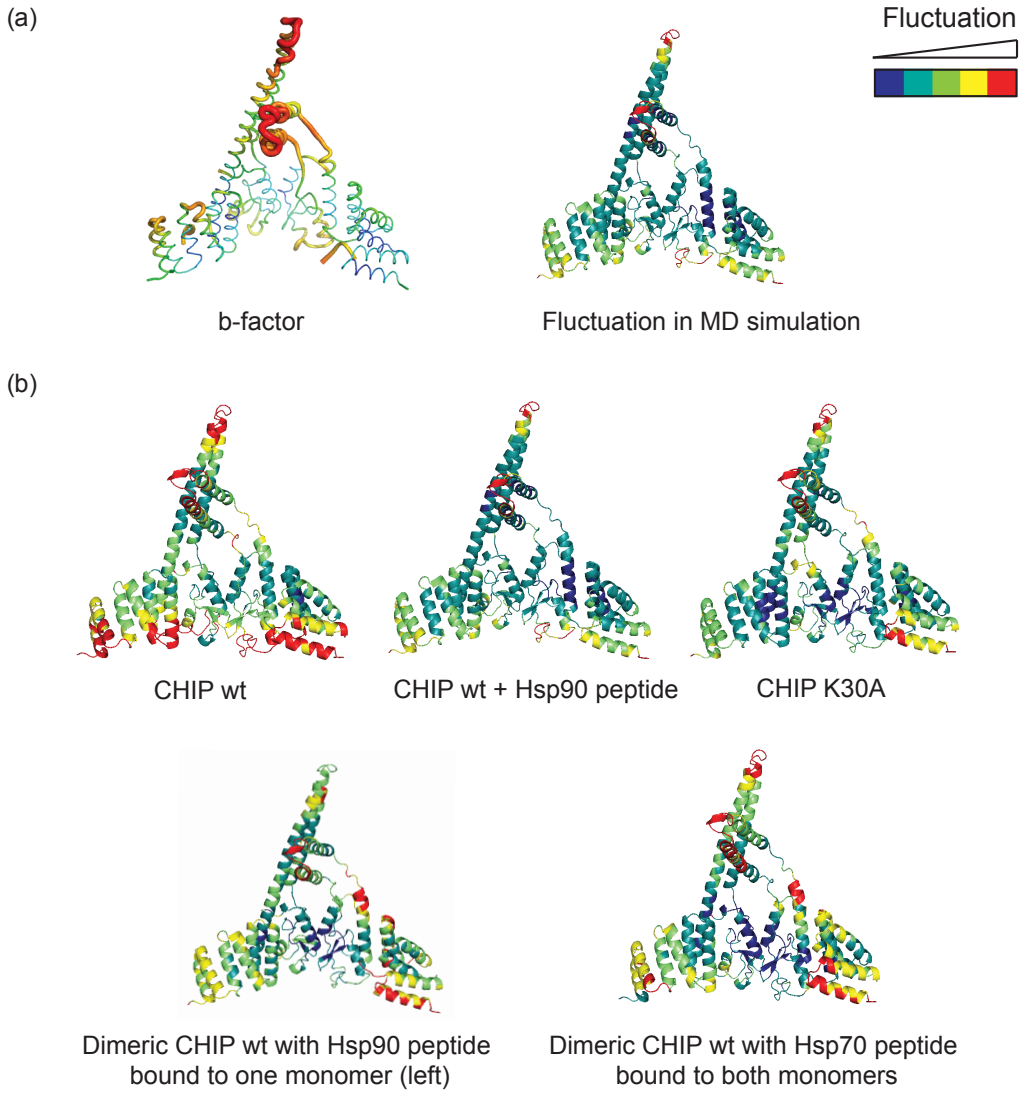

Figure 3-4 CHIP^{K30A} and Hsp70-bound CHIP exhibit similar flexibility in MD simulations

(a) Comparison between b-factor putty of the CHIP structure in complex with Hsp90 and the calculated fluctuation (root mean square fluctuation RMSF) using the MD simulation and AMBER tools. The score of the positional fluctuation analysis averaged over a 5 ns time frame were colour coded and indicated on the crystal structure, the b factor was also colours coded and is shown in the crystal structure, additionally the cartoon of CHIP is thicker in areas that has been assigned a high b-factor and thinner in areas with a low b-factor. Both b-factor and RMSF are in Å^2. (b) RMSF of Cα obtained from trajectories of 20 ns simulations of CHIP^{WT} ± peptide and the K30A mutant. The score of the positional fluctuation analysis averaged over a 5 ns time frame were colour coded and indicated on the crystal structure.

3.2.1.4 The TPR-domain is an allosteric modulatory site which affects U-box activity

The results presented above indicate that modulation of the TPR, either by mutation or peptide binding, has an effect on the overall structure of CHIP and thus affects not only the TPR, but also the middle charged and catalytic U-box domain. To investigate if there are any correlated movements between different domains of CHIP, the distribution of cross correlation between the Cα atoms of each amino acid was plotted as a function of the distances between the atoms (Fig 3-5). A striking anti-correlated motion (motion occurring in the opposite phase) was seen between the TPR-domain of one CHIP wild-type protomer with the U-boxes of both dimer components (Fig 3-5; movement A). This motion was strongly suppressed upon peptide binding and almost completely lost in the Lys^{30} mutant. Additionally, correlated motions (motion occurring with the same phase) were observed between the two U-box domains of the dimer in the wild-type conformation and again these were lost upon peptide binding or substitution of Lys^{30} (Fig 3-5; movement B).

These results implicate a mechanism in which the flexibility of the TPR is passed on to the U-Box domain and where when the TPR domain is stabilised by peptide binding or mutation this inter-domain communication is blocked, resulting in a loss of flexibility in the U-Box domain. As K30A mutation and Hsp70 binding modulate the U-box activity of CHIP, we believe that this loss in flexibility may directly affect its E3 ligase function. Consequently, we conclude that the loss of anti-correlated motions upon peptide binding or mutation of Lys^{30} is evidence that the TPR-domain is acting as a binding site for allosteric effectors, which regulate CHIP activity. To explore this experimentally, I next set-up assays to determine the effect of TPR modulation on U-Box function.

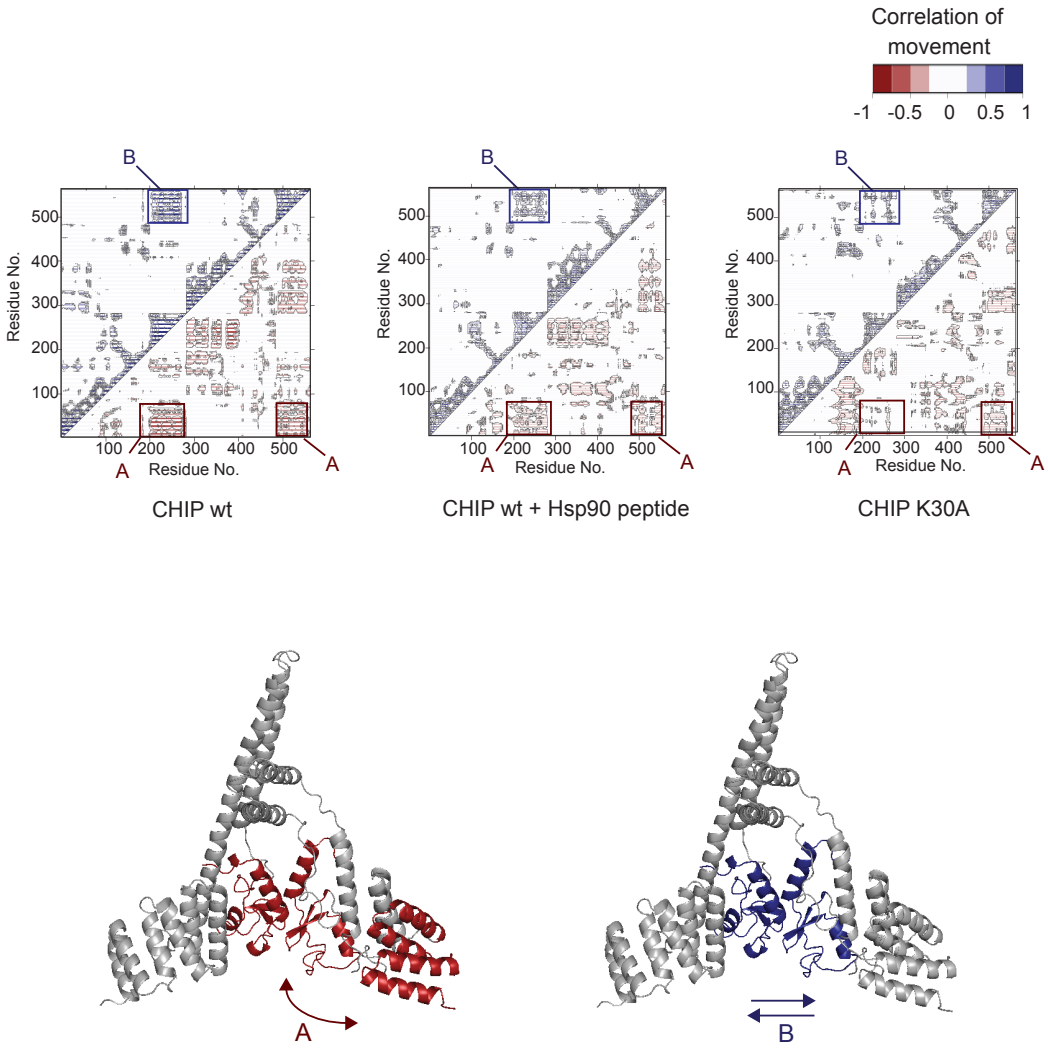

Figure 3-5 Correlated motions between the TPR and U-box domains of CHIP

Dynamic cross-correlation maps of Cα atoms for the CHIP dimer in the presence or absence of Hsp90 peptide and with a K30A point mutation (upper panels). Anti-correlated movements of the TPR domain with both U-boxes (A) and correlated movements of the two U-boxes with each other (B) can be seen for the wild-type CHIP protein, but are strongly decreased upon Hsp90 peptide binding and in the Lys^{30} mutant. Sections of $CHIP^{WT}$ dimer coloured in red or blue (lower panels) correspond to the respective regions that are highlighted in the correlation maps.

3.2.1.5 CHIP interacts with different E2 enzymes

Previous studies have concluded that the CHIP dimer is asymmetric and that as a consequence, the U-box of one of the protomers is unavailable for E2 binding due to the location of its associated TPR-domain, whereas the U-box from the other protomer remains accessible to the E2 [254]. The MD simulations suggest that changes in TPR-domain and U-box motion would not affect the ratio of E2-binding as access of UbcH5 to the U-box of one CHIP protomer remains unaltered. Thus, in our model loss of anti-correlated motion would impact on the dynamic structure of the U-box rather than altering the accessibility of one, or the other, U-box at any given time.

We were, therefore, interested to find out how changes in CHIP dynamics affect interactions of the U-Box with E2 enzymes. In a first step, an E2 library for enzymes that would interact with CHIP to result in IRF-1 ubiquitination and or the formation of free ubiquitin chains was screened (Fig 3-6). Results of the assays show that of the E2s screened, CHIP can interact with UbcH5 enzymes (a,b and c) and UbcH6 resulting in IRF-1 ubiquitination (Fig 3-6a). When the assay was carried out in the absence of any substrate and probed with an anti-ubiquitin antibody to detect any complexes of higher molecular mass, corresponding to free ubiquitin chains or ubiquitin linked to CHIP itself, CHIP was seen to additionally interact with the UbcH13/Mms2 heterodimer resulting in abundant amounts of free ubiquitin chains (Fig 3-6b).

Thus, interaction of CHIP with UbcH13/Mms2 does not lead to substrate ubiquitination *in vitro*, however, it efficiently catalyse the formation of free ubiquitin chains. In order to determine if interplay between UbcH13/Mms2 and CHIP can catalyse the elongation of monoubiquitin added to a substrate by CHIP in combination with UbcH5, I assembled *in vitro* ubiquitination assays, with limiting amounts of UbcH5 and a titration of UbcH13/Mms2. Results show that, while UbcH13/Mms2 on its own does not mediate CHIP autoubiquitination (Fig 3-7, lane 2), in the presence of a low concentration of UbcH5, UbcH13/Mms2 leads to a striking increase in polyubiquitinated forms of CHIP (lane 3-8). This indicates that even though a CHIP-UbcH13/Mms2 complex cannot catalyse attachment of the first

ubiquitin to a substrate, it can lead to ubiquitin chain elongation following UbcH5 priming. The UbcH13/Mms2 heterodimer is believed to result in the formation of chains solely linked via K63, indicating a role of this complex in specific substrate ubiquitination that serve as a molecular signal in pathways distinct from proteasome mediated degradation.

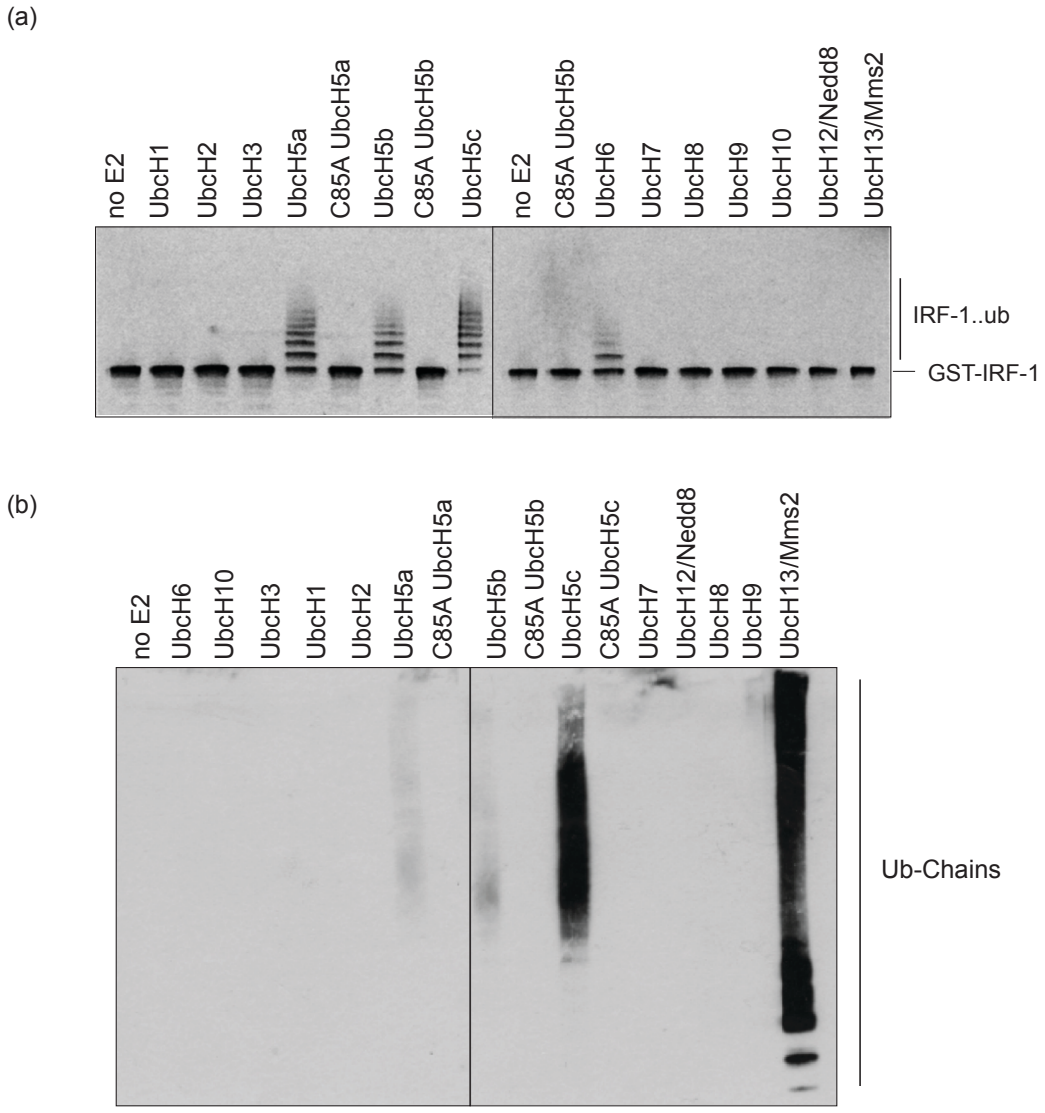

Figure 3-6 CHIP can interact with a specific set of E2 enzymes

In vitro ubiquitination assays were assembled with E1, His-CHIP, ubiquitin, ATP and various E2 enzymes as indicated and either with (a) GST-IRF-1 or (b) in the absence of any substrate. Reactions were incubated for 15 minutes and ubiquitinated protein was analysed by SDS-PAGE/immunoblot, using anti-IRF-1or anti-ubiquitin antibody as indicated (a was carried out in collaboration with Vikram Narayan).

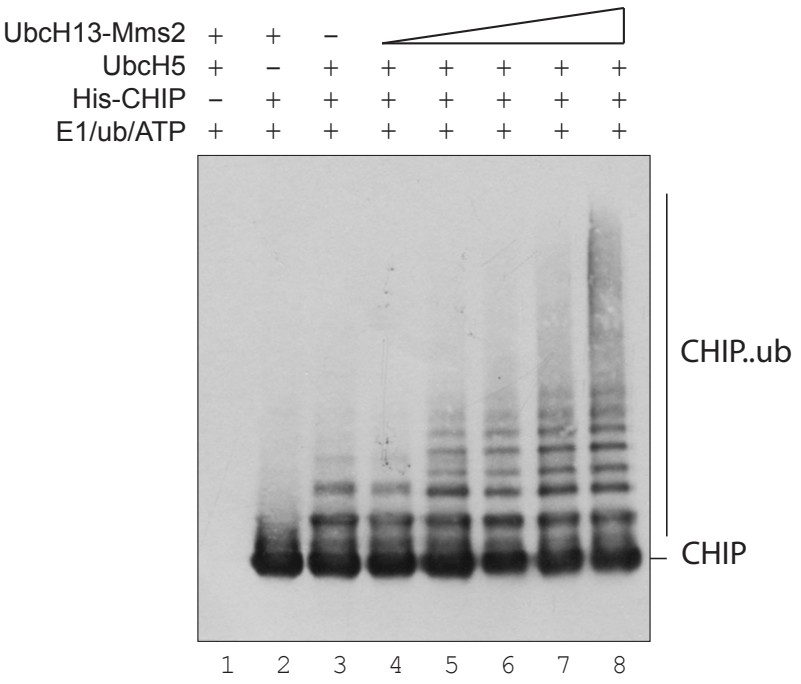

Figure 3-7 UbcH13/Mms2 can enhance CHIPs polyubiquitination in the presence of UbcH5

In vitro ubiquitination assays with constant amounts of CHIP (50 ng) and UbcH5 (25 ng) and a titration of UbcH13/Mms2 (6-100 ng). Samples were analysed by SDS-PAGE/Immunoblot using an anti-CHIP mAB,

3.2.1.6 The TPR-domain regulates CHIP's ability to interact with ubiquitin conjugating enzymes

To determine if loss of U-box flexibility seen by modulation of the TRP domain affects the ability of CHIP to interact with the two E2s UbcH5 and UbcH13/Mms2, protein-protein interaction assays were utilised. First, the amounts of purified CHIP wild type and $CHIP^{K30A}$ were normalised to ensure that any differences observed in binding to the E2 were due to the protein's ability to interact with each other and not to the amounts of CHIP used or the ability of the antibody to detect the different forms of CHIP. Increasing amounts of $CHIP^{WT}$ or $CHIP^{K30A}$ were therefore coated onto a microtiter plate and detected with a CHIP mAb (Fig 3-8, upper panel). Following normalisation, binding of CHIP to UbcH5 and UbcH13/Mms2 was determined. The E2 enzymes were immobilised on a microtiter plate and incubated with a titration of either $CHIP^{WT}$ or $CHIP^{K30A}$. Results of the assay show a significant reduction in the ability of the mutant protein to bind both E2s, when compared to wild-type CHIP (Fig 3-8, middle and lower panel). This shows that the conformational changes initiated by TPR domain mutation reduce the ability of the U-Box to interact with these two E2 enzymes. To determine if this directly affects the ability of CHIP to mediate ubiquitin discharge from the E2, I set up an assay that measures the ability of an E3 ligase to stimulate E2~Ub discharge. The assay consists of two steps, in the first 'Charge Step' the E1 and E2 are incubated in the presence of ubiquitin and ATP, but without an E3 (Fig 3-9a; step 1). In this step, the E2 is loaded with ubiquitin by the E1 forming an active thioester bond between ubiquitin's C-terminal glycine and a cysteine in the E2's catalytic centre, in an ATP dependent manner. The charge of the E2 can be monitored over time using SDS-PAGE/immunoblot analysis under non-reducing conditions (Fig 3-9b). In order to limit the E2 charge to approximately one round per molecule, the amount of ATP in the assay was titrated to the minimal amount needed for maximum charge of the E2 (Fig 3-9c). In this way, once the E2 is discharged by an E3, it will not be recharged, and the discharge can be monitored under different conditions. Accordingly, the second step is the 'Discharge Step' (Fig 3-9a; step 2), where an E3 ligase is added to the reaction. The E3 catalyses the transfer of the E2 bound ubiquitin to a substrate or a free ubiquitin molecule in the reaction. This discharge can be monitored over time.

Because ubiquitin is attached to the E2 via a thioester bond, the charged E2 species is sensitive to reducing agents such as DTT, while if ubiquitin was attached to an E2 residue via an isopeptide bond (E2 ubiquitination), the complex would be stable under reducing conditions. Thus, addition of DTT to the sample prior to analysis by SDS-Page can confirm that the double band detected with the antibody specific for the E2 is indeed a charged E2~conjugate and not ubiquitinated E2 (Fig 3-9c).

To investigate the effect of Hsp70 binding and K30A mutation on CHIP's ability to discharge UbcH5, E2-discharge assays were assembled to follow the loss of ubiquitin from thioester-linked UbcH5-ubiquitin complexes in response to the addition of CHIP in the absence of added substrates (Fig 3-10). Whereas increasing amounts of wild-type CHIP stimulated ubiquitin discharge from UbcH5, the addition of Hsp70 peptide strongly suppresses the ability of CHIP to stimulate ubiquitin loss from the E2~Ub complex (Fig 3-10a). Similarly, when the ability of $CHIP^{WT}$ to discharge UbcH5 is compared to that of $CHIP^{K30A}$, the mutant protein had a significantly reduced ability to discharge ubiquitin from UbcH5. In fact, the activity of the K30A mutant was intermediate between that of $CHIP^{WT}$ and a U-box mutant (H260Q) that can no longer interact with the E2. The experimental data on E2-discharge and CHIP-UbcH5 binding thereby support a role for the TPR-domain of CHIP as an allosteric modulator site, and shows that its occupation can generate long range inter-domain changes in the affinity and activity of the U-box resulting in an inhibition of CHIP E3-ligase activity.

To determine if discharge of UbcH13/Mms2 by CHIP was also impaired by mutation of the TPR domain, discharge assays using UbcH13/Mms2 were carried out. Surprisingly, even though binding of $CHIP^{K30A}$ to the E2 dimer was reduced (Fig 3-8), its ability to catalyse discharge of ubiquitin from the UbcH13/Mms2 heterodimer was increased when compared to $CHIP^{WT}$ (Fig 3-10a). I therefore wanted to know, if the K30A mutant was able to facilitate the formation of free ubiquitin chains in the presence of UbcH13/Mms2 and how its activity compared to that of the wild type protein. Ubiquitination assays with either $CHIP^{WT}$ or $CHIP^{K30A}$ as the E3 and either UbcH13/Mms2 or UbcH5 as the E2 component were assembled. As shown in Figure

3-11b, while CHIP^{K30A}'s ability to form ubiquitin chains is reduced when UbcH5 is present in the reaction (compare lane 2,3 to 7,8), in the presence of UbcH13/Mms2 the mutant's ability to form ubiquitin-chains is increased compared to wild-type CHIP (compare lane 4,5 to 9,10). This suggest that the TPR domain can generate conformational changes in the U-box that inhibit its activity in combination with specific E2s, while its E3 ligase activity in combination with another subset of E2s is stimulated. Protein-protein interaction assays showed that binding of mutant CHIP to UbcH13/Mms2 is reduced when compared to wild type (Fig 3-8), it has to be investigated if this is because transient interactions between CHIP and UbcH13/Mms2 are sufficient for transfer of ubiquitin, or if CHIP^{K30A} would bind more stably to the ubiquitin charged form of UbcH13/Mms2 and only its ability to interact with the uncharged E2 is impaired compared to wild-type CHIP. As a study from Plechanovova *et al.* (2012) [46] demonstrated, the E3 enzymes form interactions with residues from both the E2 and ubiquitin molecule. The E3 protein therefore exhibits a higher binding affinity for the E2~ubiquitin conjugate than for the E2 alone, thus once ubiquitin has been discharged from the E2, the complex is less stable and E2-E3 dissociate.

Taken together the data presented in this section support a mechanism where ligand binding to the TPR domain of CHIP leads to conformational changes within the protein that alters its catalytic activity. Hence, we propose that the TPR domain can function as an allosteric regulator of CHIP activity.

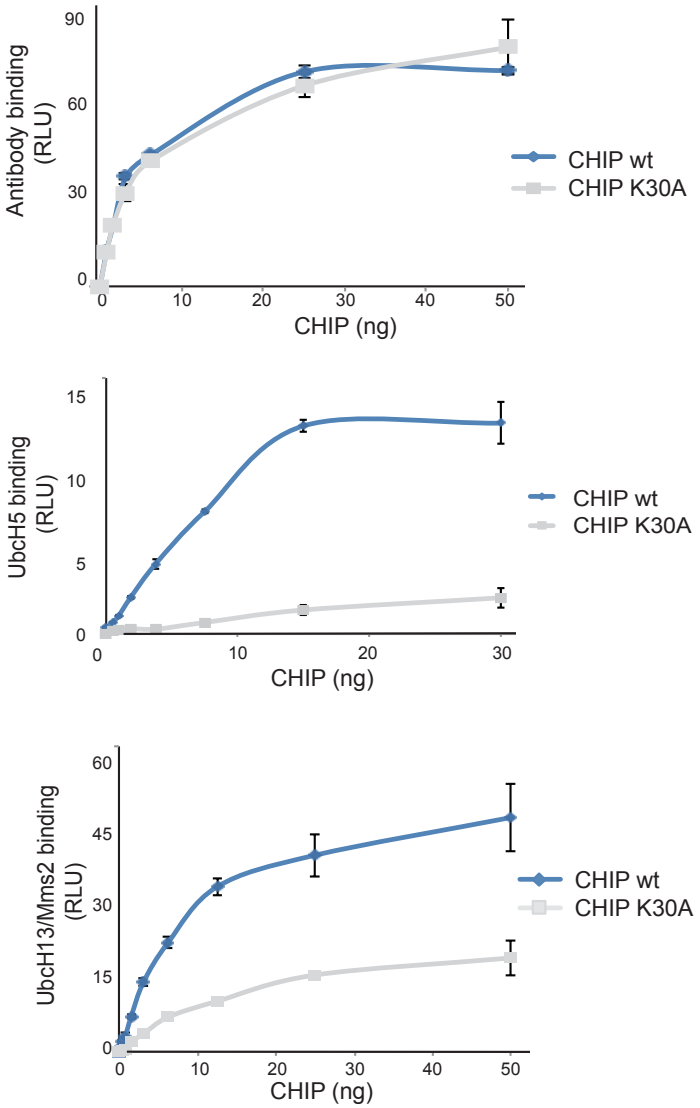

Figure 3-8 CHIP^{K30A} binds the two E2 enzymes UbcH5 and UbcH13/Mms2 with lower affinity when compared to CHIP^{WT}

First amounts of CHIP^{WT} and CHIP^{K30A} recombinant protein were normalised using an anti-CHIP mAb, a titration (0-50 ng) of CHIP protein was coated onto a micotiter plate and detected using a CHIP mAb (upper panel). Binding was detected using chemiluminescence and is expressed as relative light units (RLU). Binding of the wild-type and mutant CHIP to UbcH5 (middle panel) and UbcH13/Mms2 (lower panel) was determined, E2 (100 ng) were coated onto a micotiter well and incubated with increasing amounts of CHIP^{WT} or CHIP^{K30A} (0-30 ng or 0-50 ng as indicated) in the mobile phase. CHIP binding was analysed using a CHIP pAb (N-ter) and detected as above. The data represents the mean of technical duplicate binding assays, additionally the assay was carried out at least twice in biological replicates.

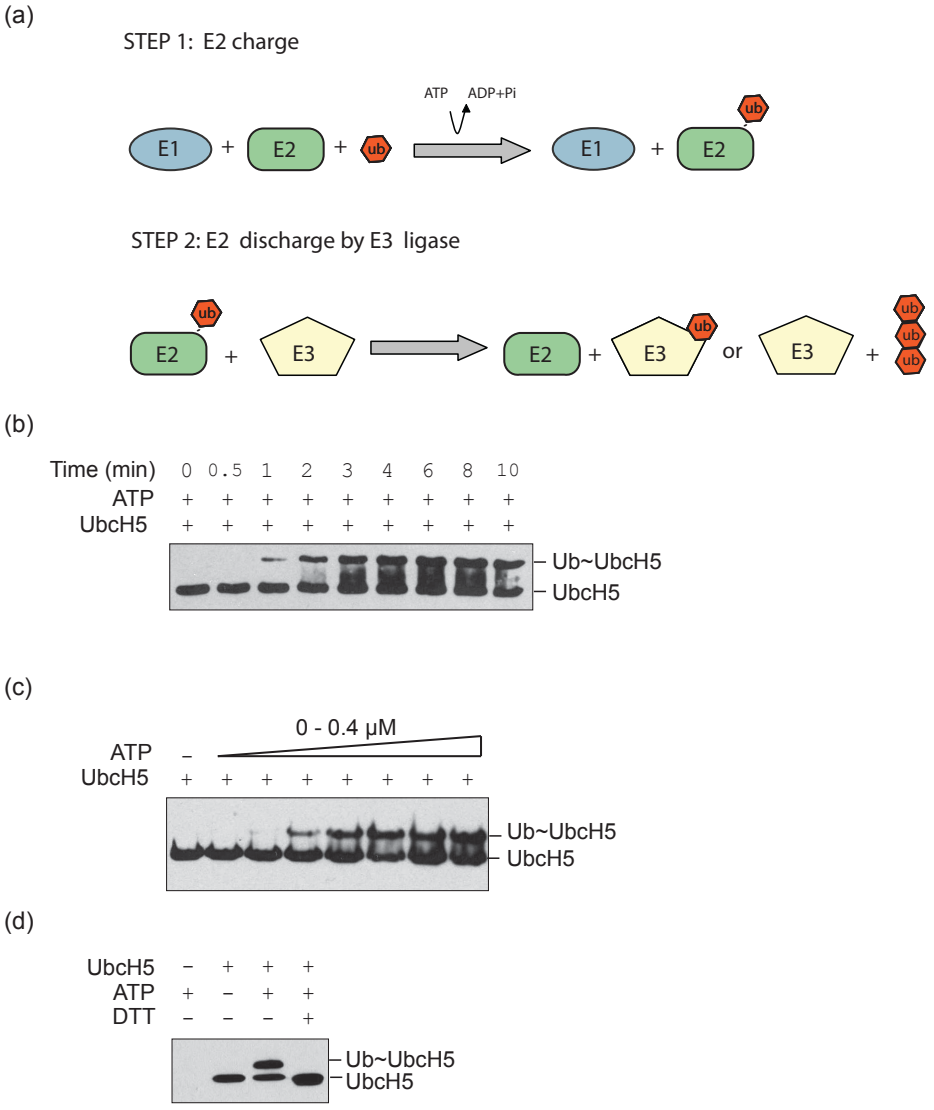

Figure 3-9 Schematic illustration of the discharge assay

(a) Step 1: the E2 is charged by the E1 in an ATP dependent reaction using purified components. The charge can be monitored over time using western blot analysis and an anti-His antibody detecting His-UbcH5 (b and c). Importantly, this first charge step is limited by the amounts of ATP present in the reaction. The amount of ATP was titrated to a concentration, which only allows each E2 molecule to be charged with ubiquitin roughly one time (c). (a) Step 2: After the E2 is charged an E3 is added to the reaction, the E3 binds to the charged E2 and catalyzes ubiquitin transfer to either itself resulting in autoubiquitination, to free ubiquitin forming free ubiquitin chains or to a substrate. (d) UbcH5 was charged with ubiquitin in an *in vitro* reaction and subsequently analysed under reducing (abolishing the thioester linkage between ubiquitin (Gly^{76}) and UbcH5 (Cys^{85})) and non reducing-conditions (leaving the thioester linkage intact) on SDS-Page/immunoblot.

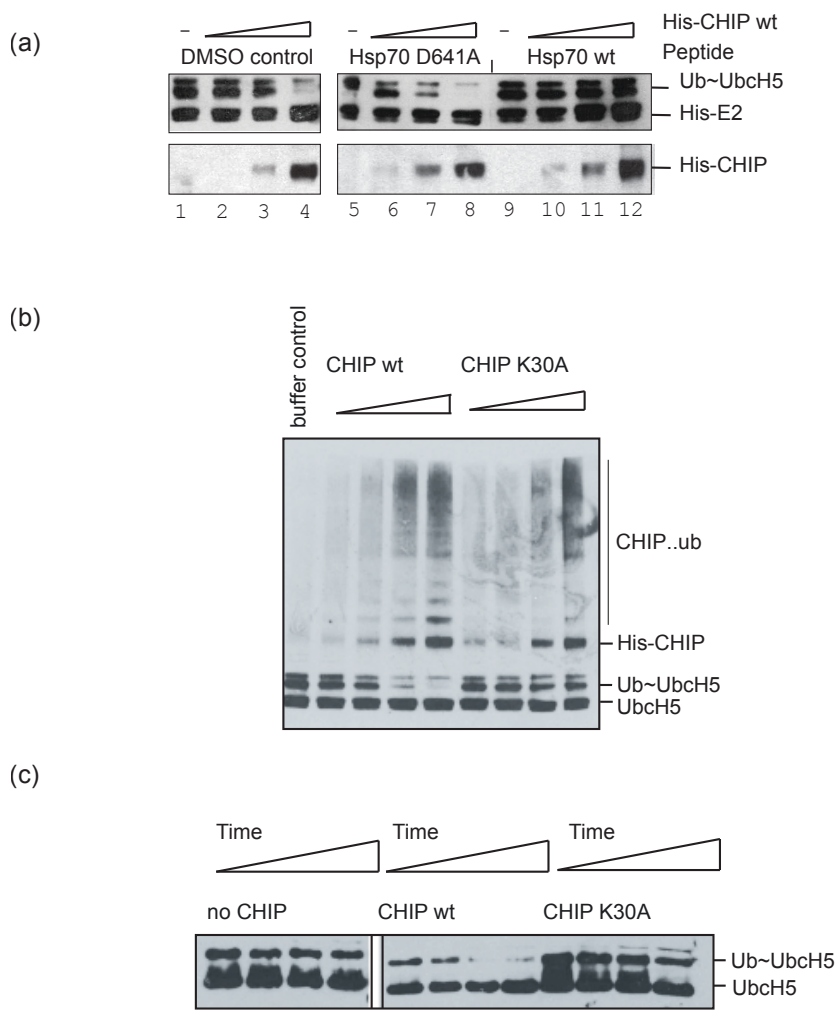

Figure 3-10 Hsp70 peptide binding or TPR mutation reduces CHIPs ability to discharge UbcH5

Discharge assays with UbcH5 and CHIP, E1, ubiquitin, E2 and ATP were incubated for 10 minutes to charge the E2. Then discharge of the E2 by CHIP was monitored with either (a, b) a titration of CHIP (6-50 ng) or (c) over a time (5-20 minutes), in (a) the presence of Hsp70 wt peptide, D641A mutant peptide (3 mM) or DMSO control; or (b, c) with $CHIP^{WT}$, $CHIP^{K30A}$ or the E2-binding-defective mutant H260Q. The reactions were analysed by SDS-Page/western blot under non-reducing conditions with an anti-His antibody that detects His-UbcH5 and His-CHIP

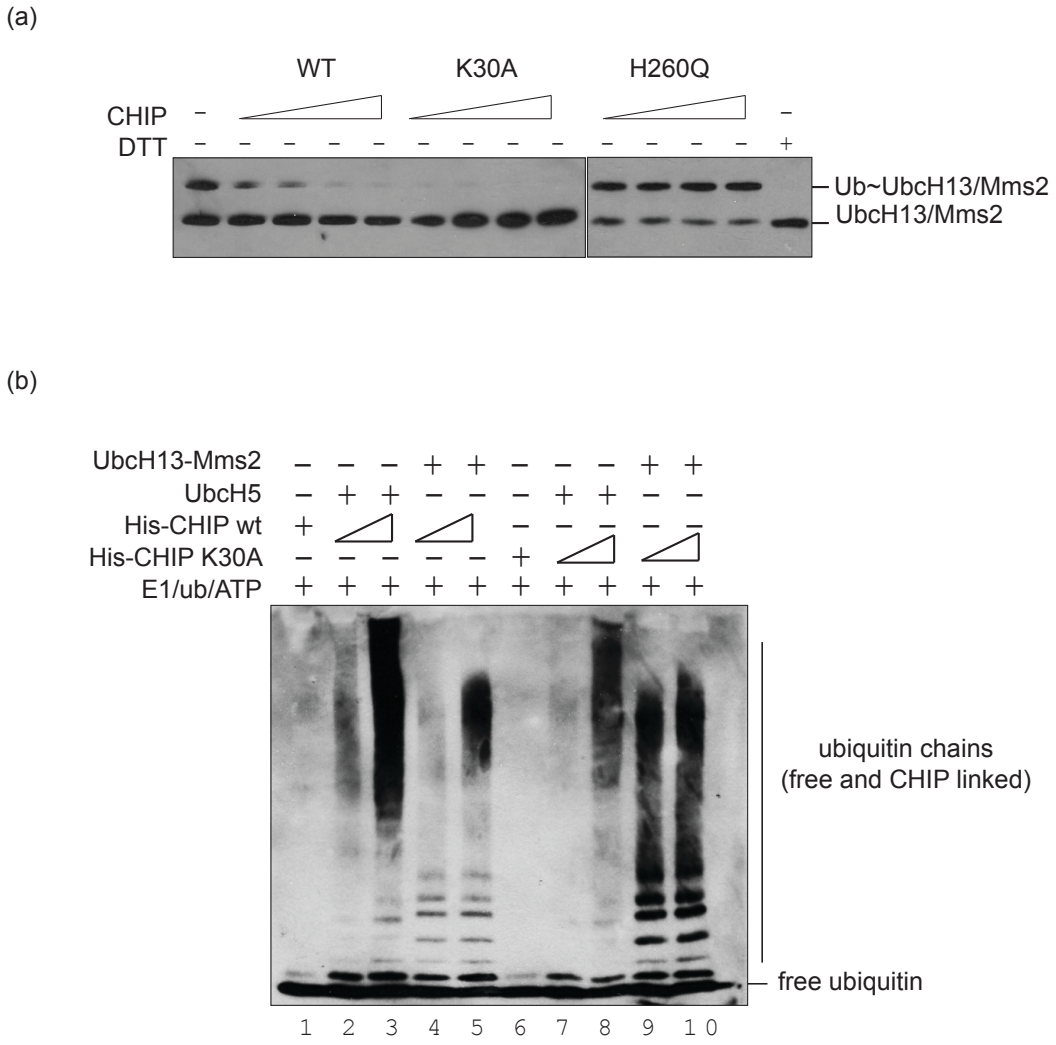

Figure 3-11 CHIP K30A exhibits increased E3 ligase activity compared to CHIP^{WT} when interacting with UbcH13/Mms2

(a) Discharge assays with UbcH13/Mms2 and CHIP, E1, ubiquitin, E2 and ATP were incubated for 10 minutes to charge the E2. Then discharge of the E2 by a titration of CHIP^{WT} or CHIP^{K30A} (6-50 ng) was monitored. The reactions were analysed by SDS-Page/western blot under non-reducing conditions with an anti-His antibody that detects His-UbcH5 and His-CHIP. (b) *In vitro* ubiquitination assay with a titration of CHIP^{WT} or CHIP^{K30A} (25 or 50 ng) and UbcH5 or UbcH13/Mms2 as indicated. The reactions were incubated for 15 minutes and analysed by immunoblot using an anti-ubiquitin antibody.

3.2.2 CHIP is autoubiquitinated at multiple residues in its functional domains

Data presented in this chapter demonstrates how CHIP E3 ligase activity can be modulated by its TPR domain. Additionally, CHIP activity has previously been shown to be controlled by autoubiquitination. Interaction of CHIP with Ube2w leads to CHIP autoubiquitination at Lys^2, and this activates its E3 ligase function [306]. To further our understanding of the regulation of CHIP activity by autoubiquitination, I was interested to investigate, if there are any additional lysine residues within CHIP that are targeted by its autoubiquitination activity when interacting with the E2 enzyme UbcH5. In particular, I asked if any sites within the TPR are modified, and how this modification could affect its dynamics and activity.

To identify lysine residues in CHIP that are subject to modification by ubiquitin as a result of its interaction with UbcH5, the ubiquitination sites on CHIP were mapped using mass spectrometry. Recombinant His-CHIP protein was allowed to autoubiquitinate in an *in vitro* ubiquitination reaction with UbcH5, E1, ubiquitin and ATP, then the samples were analysed by SDS-PAGE and Colloidal Blue Stain. The ubiquitinated forms of CHIP were identified, bands excised, and the samples were prepared for mass spectrometry analysis. Briefly, gel slices were first destained, followed by reduction, alkylation and digestion using the endopeptidase trypsin, subsequently peptides were extracted and analysed by mass spectrometry. Ubiquitin-modified lysine residues are protected from trypsin cleavage, resulting in a distinct cleavage pattern for the ubiquitinated protein. Furthermore, ubiquitin that is attached to the protein is cleaved off at its C-terminal arginine residue leaving a di-glycine peptide remnant that adds 114.043 Da to the ubiquitinated peptide. The modified cleavage pattern, together with the mass additions, facilitates identification, by MS, of peptides that have been ubiquitinated (Fig 3-12).

The results of the mass spectrometry analysis identified seven lysines within CHIP that were linked to ubiquitin (Fig 3-13). Two of these are located in or adjusted to the U-box domain, while the other five lie in or around CHIP's TPR domain. None of the lysines in the extreme N-terminus or its charged middle domain were subject to ubiquitination. Stable forms of ubiquitinated CHIP have been observed in cells [306]

(unpublished observation by the Ball group), suggesting that at least under some conditions CHIP ubiquitination does not signal its degradation but serves a different function. The observation that CHIP autoubiquitination is concentrated on its catalytic U-box and regulatory TPR domain, indicates that ubiquitination of these residues could affect its function. Addition of the 8-kDa protein ubiquitin to a molecule of CHIP could have an effect on the accessibility of surface residues that are involved in interaction with other proteins, e.g. E2 enzymes binding to its U-box or chaperones and other substrates that interact with its TPR domain. In fact, two of the lysine residues within the TPR, Lys^{30} and Lys^{72}, which are involved in the interaction with Hsp90, are subject to autoubiquitination by CHIP (as shown in the crystal structure, Fig 3-14). This is an interesting observation and raises two questions (i) would ubiquitination of residues in the chaperones binding cleft sterically inhibit binding of proteins to this site and (ii) as the data in this chapter demonstrate that modulation of the TPR domain affects the overall dynamics of CHIP, how would ubiquitination of lysines in the TPR, especially Lys^{30}, affect the flexibility and structure of this domain and could this possibly alter the activity of CHIP's U-box? Further studies are necessary to address these questions and to fully evaluate the physiological relevance of CHIP TPR and U-box ubiquitination.

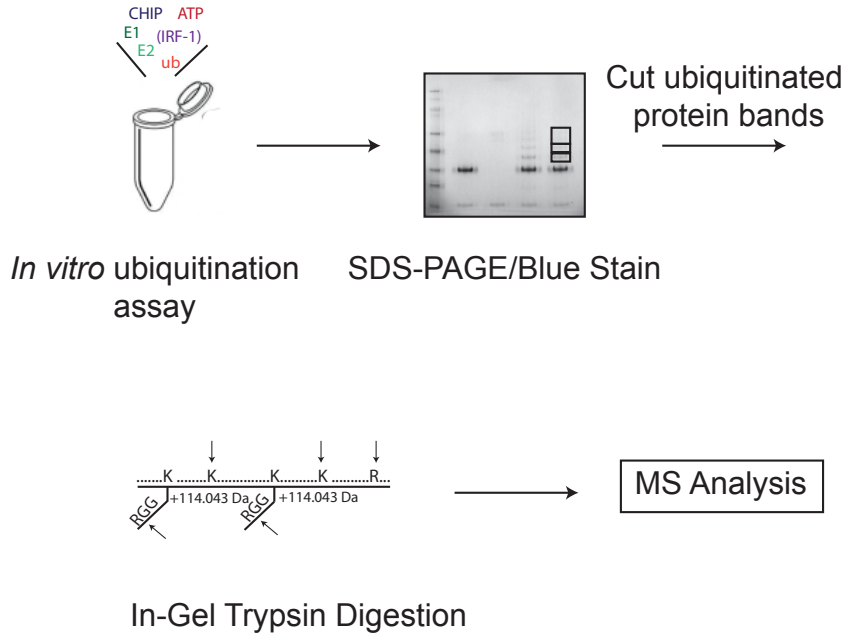

Figure 3-12 Schematic illustration of the procedure used to map ubiquitination sites. First the protein of interest is ubiquitinated in an *in vitro* ubiquitination reaction including all the components of the reaction as purified recombinant proteins. The ubiquitinated protein is then isolated using a tag-system and separated by SDS-PAGE. Bands corresponding to ubiquitinated proteins are excised and digested with the endopeptidase Trypsin. Trypsin cleaves proteins after either lysine or arginine residues, however, ubiquitinated lysine residues are protected from cleavage. Ubiquitin is also cleaved, and only a glycine dipeptide remains on the ubiquitinated peptide. This glycine dipeptide leads to a mass addition of 114.043 Da. Peptides are analysed using mass spectrometry and ubiquitinated peptides are identified due to the mass addition and modified cleavage pattern.

(a)

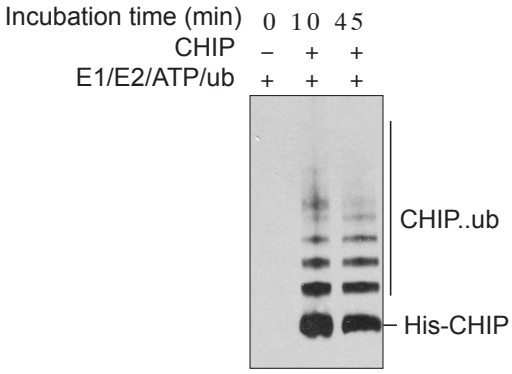

(b)

Peptide Sequence	*Modified Lysine*	*Mascot Score*	Domain
GGGSPEKSPSAQE	K22	54.71	-
PSAQELKEQGNRL	K30	69.62	TPR
RLFVGRKYPEAAA	K41	43.82	TPR
RALCYLKMQQHEQ	K72	22.78	TPR
RAYSLAKEQRLNF	K125	31.52	-
FSQVDEKRKKRDI	K221,223,224	26.25	U-Box
GITYDRKDIEEHL	K255	7.73	U-Box

(c)

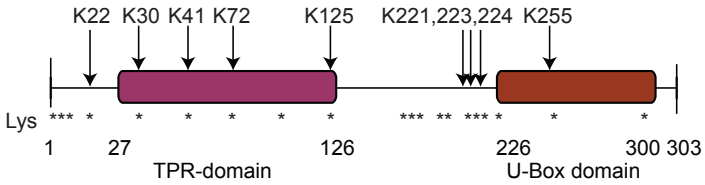

Figure 3-13 Auto-ubiquitination sites on CHIP mapped by MS analysis

(a) Western blot of *in vitro* ubiquitinated His-CHIP (0.5 μg), after isolation of CHIP from the reaction using Ni-NTA chromatography. The *in vitro* ubiquitination reaction was incubated for 0, 10 or 45 minutes. (b) Results of MS analysis, showing modified peptides in CHIP. Lysine residues that were shown to be modified by ubiquitin are highlighted in red. (c) Modified lysine residues indicated above and total CHIP lysine residues indicated underneath a schematic CHIP domain structure. (Unfortunately, data on peptide coverage of the analysis could not be obtained).

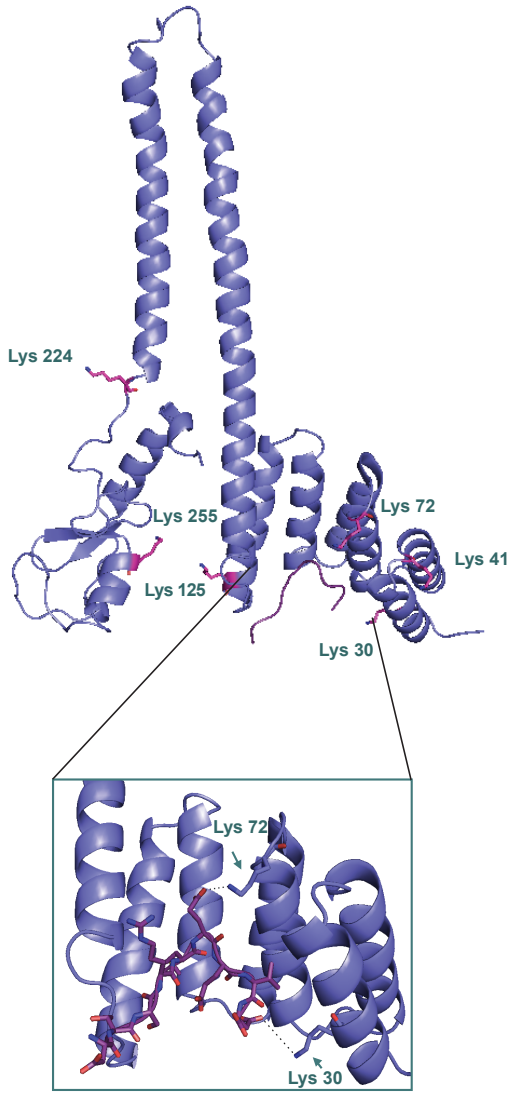

Figure 3-14 The two ubiquitination sites Lys^{30} and Lys^{72} are involved in interactions with Hsp90

Structure of CHIP TPR (cartoon) in association with Hsp90 peptide (highlighted). Autoubiquitination sites Lys^{30} and Lys^{72} are indicated as purple sticks and interactions between these residues and the Hsp90 peptide are highlighted.

3.2.3 Inhibition of MDM2 activity by aptamer binding

3.2.3.1 Identification of a MDM4 C-terminal peptide that inhibits MDM2 E3-ligase activity

The E3 ligase MDM2 is the main regulator of p53 activity and a significant amount of research is being invested to identify drugs that could inhibit its suppressive activity on p53 function. The Ball group has previously identified a peptide from the N-terminal RING domain of MDM4, T-apt, that binds to the MDM2 RING domain and inhibits its E3 ligase activity *in vitro* and in cells (Fig 3-15, data courtesy Susanne Pettersson). The MDM2 RING domain forms homodimers, and heterodimers with the MDM4 RING. When the T-apt peptide on MDM4 was mapped onto the available crystal structure of the MDM2/MDM4 dimer (PDB: 2VJF [268]), we found that the peptide lies within the dimer interface of the two proteins, indicating that T-apt binding could disrupt MDM2 dimer formation with either another MDM2 protomer or a MDM4 molecule. The MDM2 RING domain interacts with E2 enzymes leading to substrate ubiquitination. We were interested to establish, if MDM2's inability to ubiquitinate p53 in the presence of T-apt is due to a failure to discharge ubiquitin from the E2 or whether E2 discharge is unaffected. An UbcH5 discharge assay was therefore assembled that tested the ability of MDM2 to discharge this E2 in the presence of either T-apt or a control peptide with a C-terminal truncation that renders it less active. As shown in Figure 3-16, in the absence of any E3 ligase the UbcH5~ubiquitin complex is stable over the time of the assay, upon addition of MDM2 however, ubiquitin is quickly discharged (Fig 3-16a, compare lane 1 with 2-4, b compare lanes 1-3 to 4-9). If MDM2 was pre-incubated with T-apt, MDM2 mediated E2 discharge was completely abolished, while a control peptide did not have any effect on the ability of MDM2 to facilitate E2 discharge (a, compare lanes 5-7 with 8-10 and b, lanes 10-12 and 13-15). This shows that T-apt binding inhibits MDM2's ability to discharge UbcH5 and therefore, its catalytic activity, this implies that T-apt does not specifically inhibit p53 ubiquitination, but abolishes MDM2 mediate ubiquitination of any substrate, including autoubiquitination.

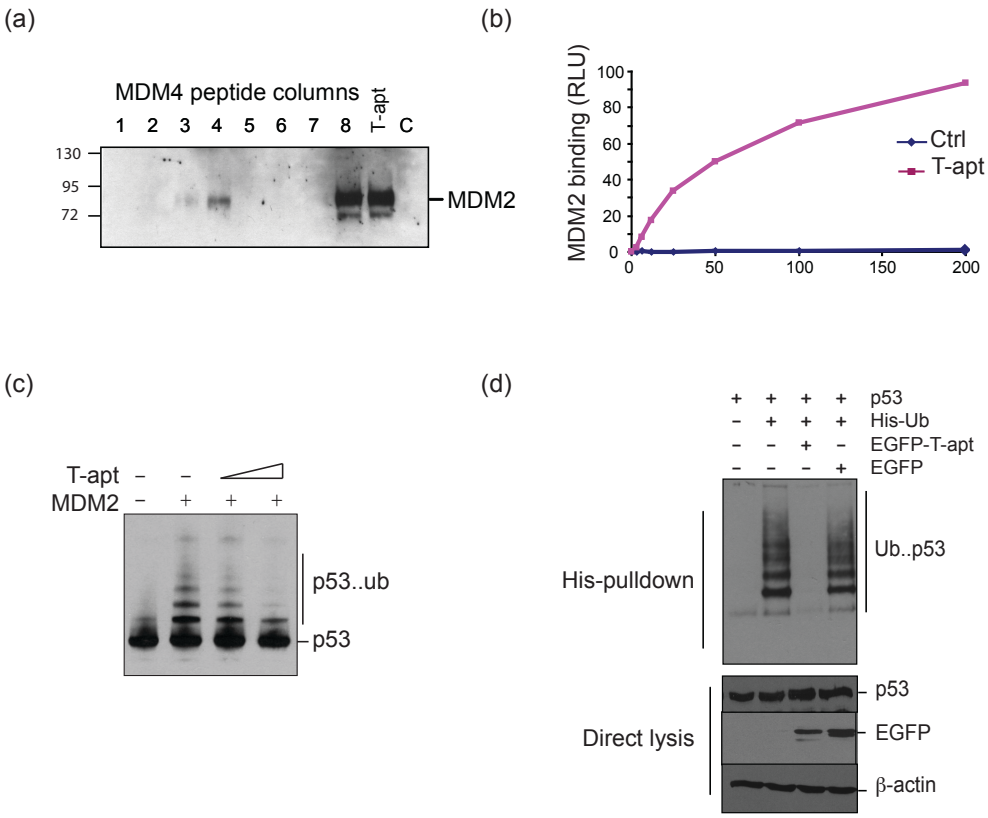

Figure 3-15 T-apt binds to the MDM2 and inhibits its E3 ligase activity *in vitro* and in cells

(a) Biotin tagged, overlapping peptides of the C-terminus of MDM4 were used to generate peptide aptamer affinity columns, which were incubated with cell lysate from H1299 cells. Eluates from the peptide aptamer affinity chromatography columns were analyzed by SDS-PAGE/immunoblot and probed with an anti-MDM2 mAb. (b) T-apt-biotin (KEIQLVIKVFIA) or a control peptide (KEIQLVIKVF) were immobilized on a microtitre plate and incubated with a titration (0–100 ng) of MDM2. Protein binding was detected using an anti-MDM2 mAb and the protein amount against binding is expressed as relative light units (RLU). (c) *In vitro* ubiquitination assay with MDM2 as the E3 ligase, p53 as substrate and a titration of T-apt (1.5 and 10 µM). (d) H1299 cells were transfected with p53 (0.5 µg), His- ubiquitin (0.5 µg) and EGFP-T-apt or EGFP alone as detailed. Post transfection (24 hours) cells were treated with MG132 (50 µM) for 4 hours. Ubiquitinated protein was isolated using affinity chromatography and immunoblots show total p53, EGFP and β-actin (lower panel) and His-ubiquitinated p53 (upper panel). (a,b,d data courtesy Susanne Pettersson)

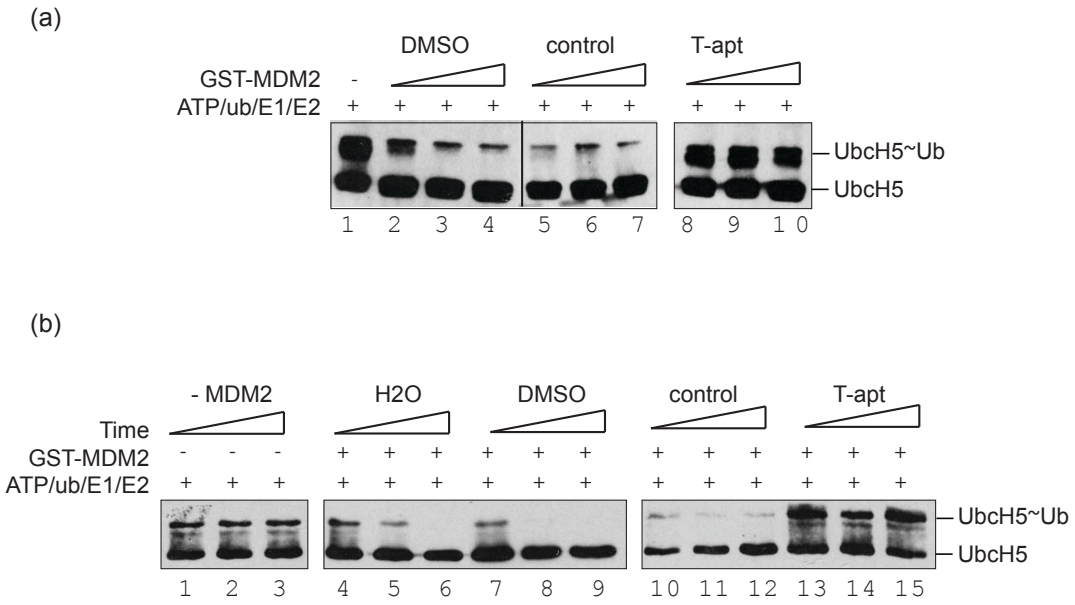

Figure 3-16 T-apt inhibits E2 discharge by MDM2

(a) E2 (His-UbcH5) discharge assays with a titration of MDM2 and constant amounts of T-apt, a control peptide with a C-terminal truncation or DMSO. The discharge reaction was incubated for 10 minutes and analysed by SDS-PAGE under non-reducing conditions followed by immunoblot with an anti-His antibody that detected His-UbcH5. (b) E2 discharge assay carried out as in (a), but with constant amounts of MDM2 and the discharge of UbcH5 was monitored over time (5, 10, 15 minutes).

3.2.3.2 Dynamics of the MDM2 RING-domain in association with T-apt

In order to get an insight into the binding dynamics and the residues involved in the interaction between T-apt and the MDM2 RING, I carried out molecular dynamic simulations on the MDM2 RING in complex with T-apt. The starting structure of the simulation was obtained from the MDM2/MDM4 heterodimer (PDB:2VJF [268]), with only the residues of the MDM4 molecule, which resemble T-apt, retained in the structure (Fig 3-17). After a 50 ns simulation, residues involved in contacts between the two molecules were computed using ptraj modules. Results from the analysis showed that the C-terminal residues (Phe-Ile-Ala) of the peptide form the most stable and energetically favourable interactions with the MDM2 molecule, this is supported experimentally by Dr. Pettersson using alanine scans of the peptide (data not shown). Strikingly, all interactions were hydrophobic and no salt bridges between the peptide and the RING were formed. Figure 3-18a (left panel) illustrates contacts between these three residues and the RING surface. The T-apt peptide contains a C-terminal cap, which neutralises its otherwise negative charged terminus; simulations show that this cap itself is involved in hydrophobic interaction with the MDM2 residues Val^{439} and Met^{459}. Modelling results are confirmed by experimental data, which show a reduction in binding between MDM2 and T-apt/OH (uncapped with a natively charged C-terminus) when compared to T-apt (Fig 3-18b, left panel). Furthermore, T-apt/OH displays a lower ability to inhibit MDM2 E3 ligase activity in an *in vitro* ubiquitination assay (right panel). These results suggest that the hydrophobic interactions between the cap and the MDM2 RING stabilise binding of the peptide, and additionally, the de-solvation energy of the free terminus is higher than that of the neutralised peptide and it is therefore less prone to form a complex with MDM2.

A snapshot of the simulation, after the structure has stabilised (7 ns), revealed that in addition to the interface between the C-terminal region of the peptide, which also forms part of the interface between MDM2 and MDM4 in the crystal structure, the N-terminal part of the peptides folds onto the surface of MDM2 forming additional interactions (Fig 3-19a, compare position of orange to green peptide; b compare left to right panel). As these do not form part of the natural interface, we reasoned that substitution of residues of this part of the peptide could increase its affinity for

MDM2. For example, the N-terminal lysine is in proximity to a positively charged surface area on MDM2 (Fig 3-20a), and we predicted that substitution with either a hydrophobic or negatively charged residue could increase the peptides binding affinity for MDM2. In a first step, the three N-terminal residues Lys-Glu-Ile were mutated in silico and short simulations (4 ns) were run on a complex between the MDM2 RING and the amended peptides. The binding energy between MDM2 and the different peptides was computed and compared to T-apt wild-type (Fig 3-20b). Several peptides exhibited higher negative binding energies than the wild type T-apt peptide, suggesting that these peptides might bind to MDM2 with a higher affinity. To exam the modelling results experimentally, synthetic peptides were obtained and binding between MDM2 and the peptide series was tested using a protein-peptide interaction assays. Specifically, biotin labelled peptides were immobilised by capture onto a streptavidin coated on a microtiter plate and incubated with MDM2 in the mobile phase. Results show that one of the novel peptides, T-apt 4, with a single mutation from the N-terminal Lys to Trp, showed a strong increase in affinity for MDM2 (Fig 3-20b). Further binding assays with titrations of MDM2 confirmed that the amended peptide interacts with MDM2 more stably than the T-apt peptide. A snapshot of the simulation with the T-apt 4 peptide after 4 ns demonstrates that the substituted tryptophan fits well onto the MDM2 surface (Fig. 3.20e).

Taken together, we have identified and optimised a small peptide derived from the interface of the MDM2/MDM4 dimer, which binds to MDM2 with a high affinity and inhibits its ability to discharge ubiquitin loaded E2 and thus MDM2 mediated ubiquitination.

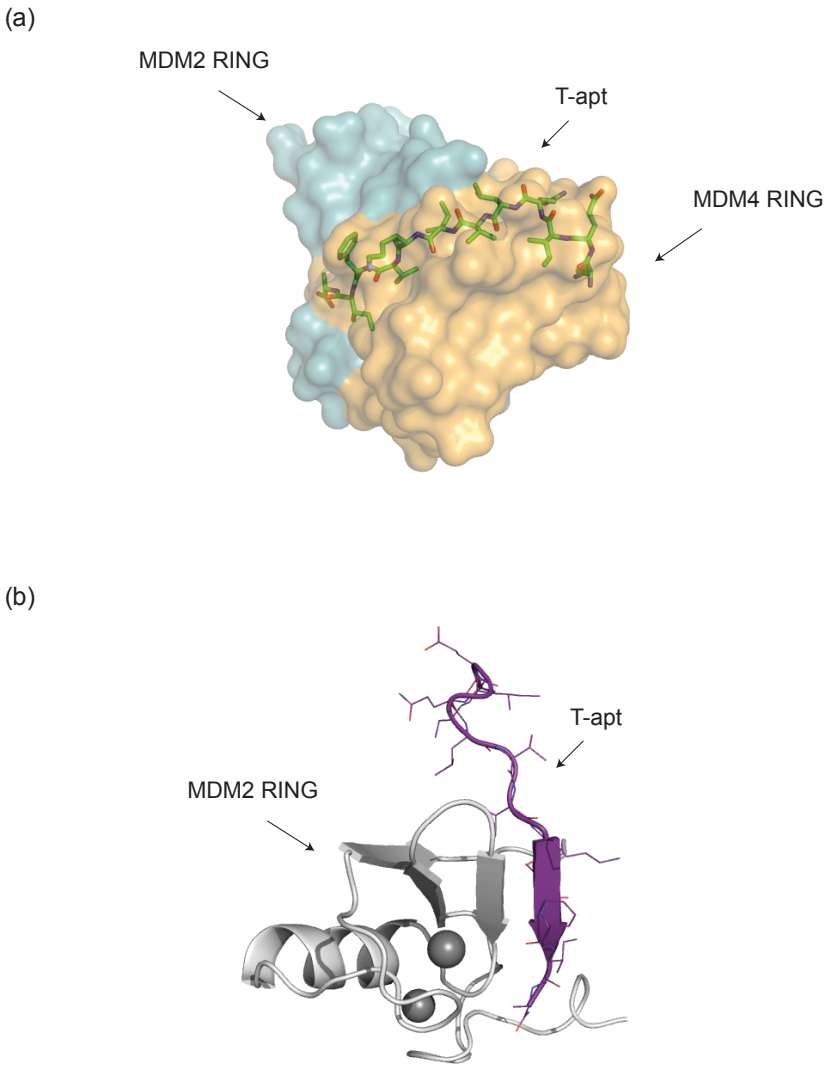

Figure 3-17 Structure of MDM2 in complex with MDM2/T-apt

(a) MDM2/MDM4 heterodimer shown as surface with the position of the T-apt peptide indicated by sticks (PDB:2VJF). (b) MDM2 RING domain associated with T-apt. The structure of T-apt was adapted from the conformation of the peptide in the MDM2/MDM4 heterodimer (a).

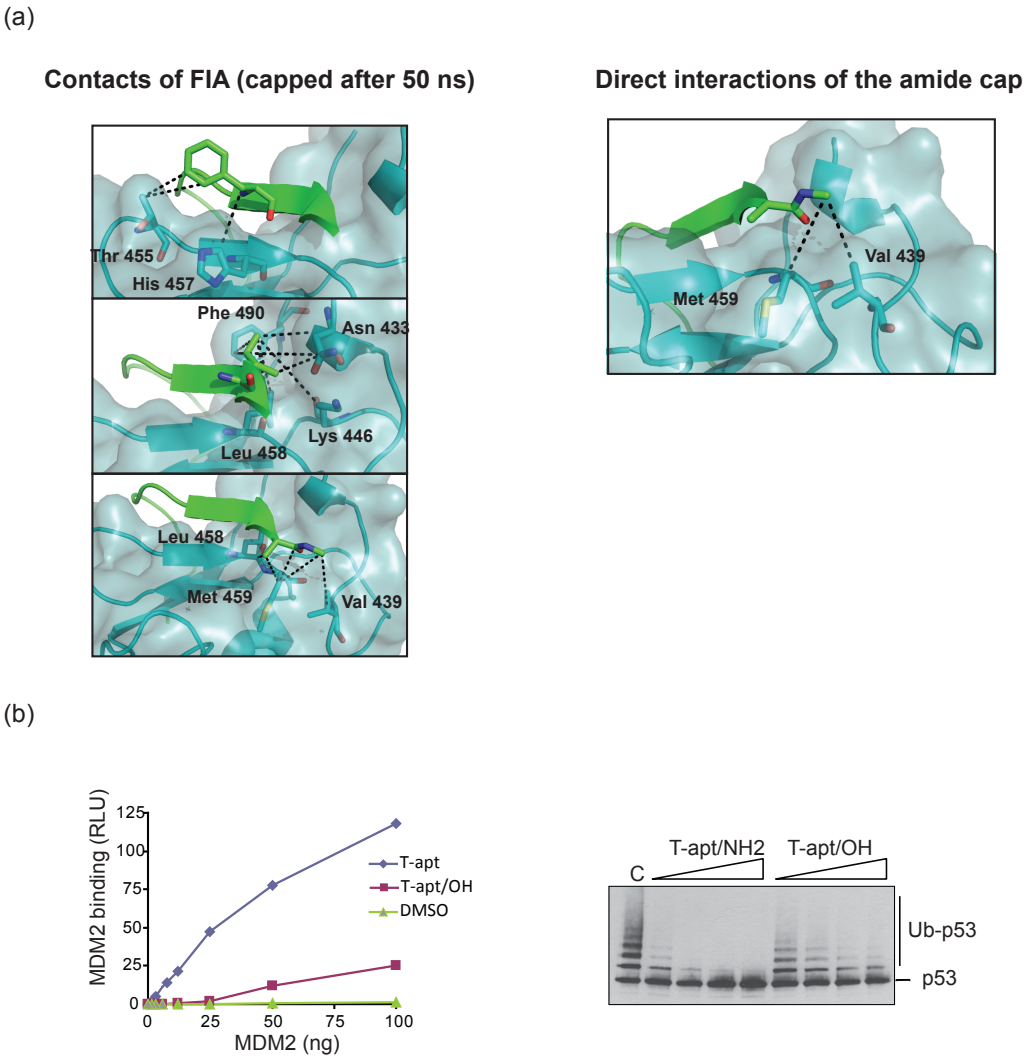

Figure 3-18 Hydrophobic interactions between the T-apt peptide cap and the RING surface stabilise binding of the two molecules.

(a) Contact analysis of the T-apt residues with the MDM2 RING domain in 50 ns molecular dynamic simulation was carried out using ptraj modules. Contacts identified by the analysis are indicated as dotted lines between atoms of RING and peptide residues. (b) Biotin-tagged T-apt wt or T-apt/OH (without a C-terminal cap) were immobilized on a microtiter plate and incubated with 100 ng of MDM2. MDM2 binding to the peptides was detected using an anti-MDM2 mAb (left panel). An *in vitro* ubiquitination assay was carried out using p53 as the substrate, MDM2 as the E3 ligase and a titration of either T-apt wt or T-apt/OH and incubated for 15 minutes. The samples were analysed using SDS-PAGE/immunoblot with an anti-p53mAb.

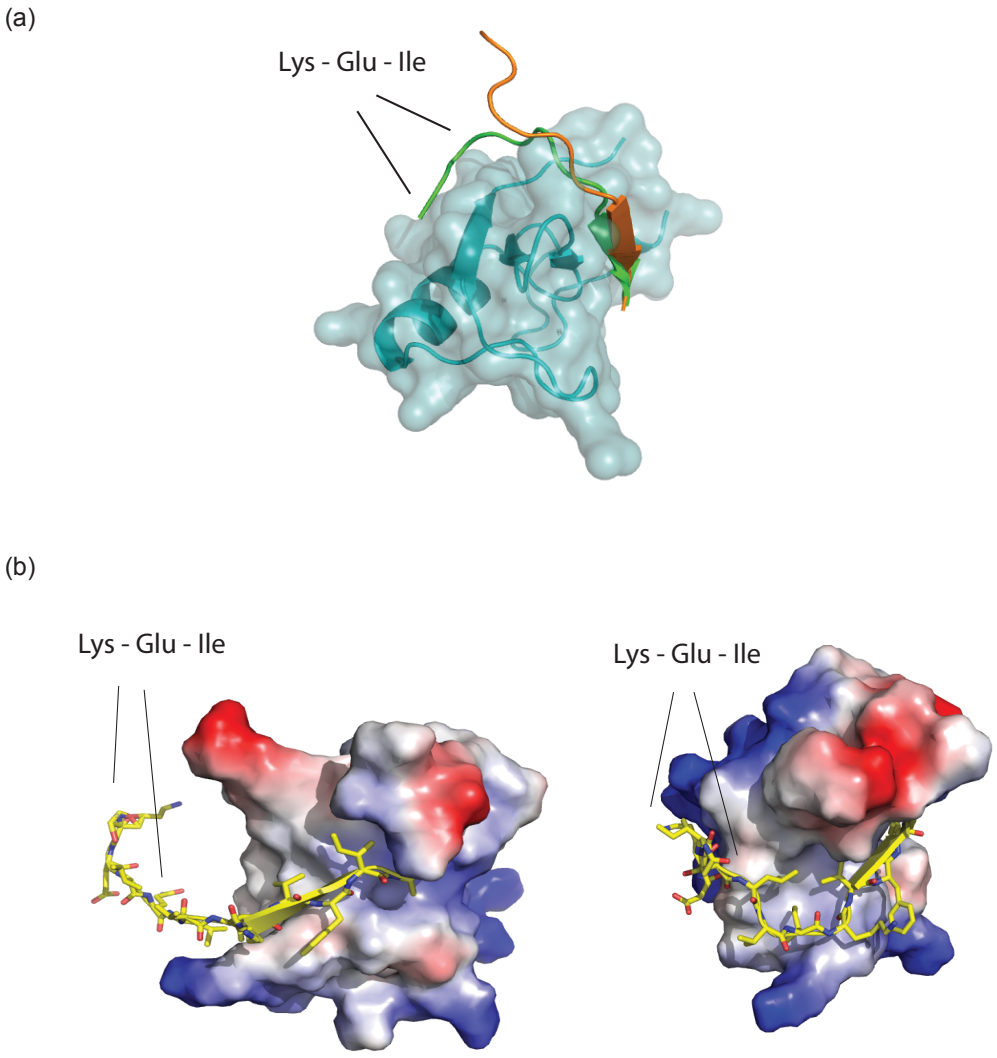

Figure 3-19 Molecular Dynamic simulations reveal a second binding of T-apt on the MDM2 RING

(a) Overlay of the starting structure of T-apt bound to the RING domain of MDM2, which was derived from the crystal structure of the MDM2/MDM4 heterodimer (orange) and a snapshot of the simulation after stabilisation (7 ns) (green). (b) The position of T-apt in the starting structure (left panel, as in a) and after 7 ns simulation (right panel) are shown with the MDM2 RING presented as surface with vacuum electrostatics and T-apt as yellow sticks.

(a)

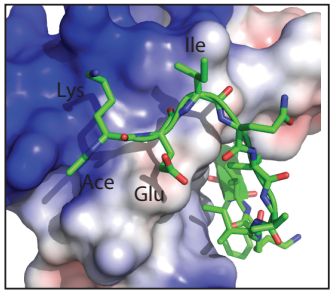

(b)

	Sequence	ΔGB
T-apt	KEIQLVIKVFIA	-38.45
T-apt/1	EWIQLVIKVFIA	-64.66
T-apt/2	EESQLVIKVFIA	-66.95
T-apt/3	EEIQLVIKVFIA	-58.54
T-apt/4	KWIQLVIKVFIA	-57.12
T-apt/5	KESQLVIKVFIA	-56.42

(c)

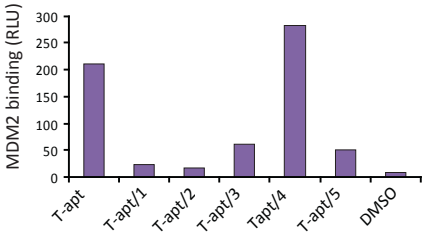

(d)

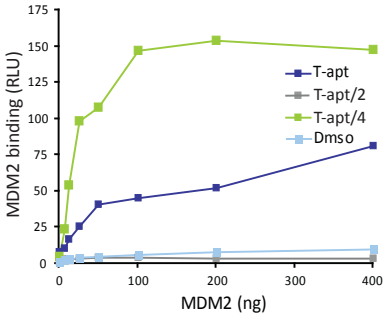

(e)

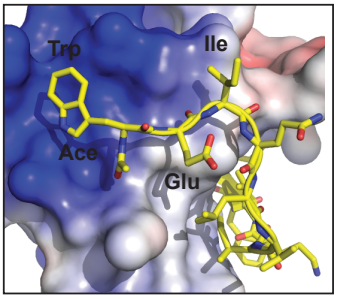

Figure 3-20 Optimisation of T-apt by molecular modelling

(a) Position of T-apt N-terminal (green sticks) on the surface of the MDM2 RING after 7 ns MD simulation. (b) T-apt residues were substituted in silico with the aim to obtain a peptide with higher affinity for MDM2. Short simulation of the amended peptide (4 ns) in complex with MDM2 were carried out and the free binding energy binding energies (ΔG_{bind}) of T-apt 1-5 was were computed using MM-GBSA (molecular mechanics/Generalized Born surface area) method using the GB module in Amber and are shown in in kcal/mol [311]. (c+d) Biotin-tagged T-apt like peptides (either wt or with N-terminal substitutions) were immobilized on a microtiter plate and incubated with (c) constant amounts (100 ng) or (d) a titration of MDM2 protein (0-400 ng). MDM2 binding to the peptides was detected using an anti-MDM2 mAb. (e) Position of T-apt 4's (K1W) N-terminal (yellow sticks) on the surface of the MDM2 RING after 4 ns MD simulation. Electrostatic surface was generated using the APBS pymol plug in.

3.2.4 Several lysine residues in MDM2 are subject to autoubiquitination

MDM2 has been reported to autoubiquitinate, which leads to its proteasomal degradation [304]. No additional functions of MDM2 autoubiquitination have been identified so far. To start investigating if there might be additional roles of MDM2 ubiquitination, we set out to map lysine residues that are targeted by autoubiquitination using mass spectrometry (see Fig 3-14 for an outline of the experiment). Ubiquitinated forms of MDM2 were generated using an *in vitro* ubiquitination assay with UbcH5 as the E2 enzyme, samples were separated on a SDS-PAGE followed by Colloidal blue staining (3.23 a) and bands corresponding to ubiquitinated MDM2 were excised and prepared for MS evaluation. Analysis of the samples identified several lysine residues within the protein to be subject to autoubiquitination (Fig 3-23b and c). Several of these are located within or adjacent to the p53-binding interface and additionally several lysine residues in its catalytic RING domain were shown to be subject to ubiquitination (c). It would be interesting to determine how ubiquitination of these residues could affect binding of p53, E2 and other binding partner, dimer formation and MDM2 activity.

(a)

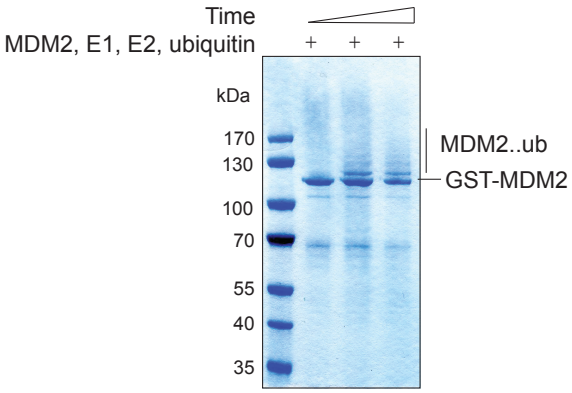

(b)

Peptide Sequence	*Modified Lysine*	*Mascot Score*	Domain
PKPLLLKLLKSVG	K 31, 36, 39	11.98	Hydrophobic pocket
EGGSDQKDLVQEL	K136	14.82	
QELQEEKPSSSHL	K146	32.02	
EISEKAKLENSTQ	K334,336	43.68	(zinc finger)
NWLPEDKGKDKGE	K 334,336,338	20.03	
FDVPDCKKTIVND	K 363,364	31.85	
CFTCAKKLKKRNK	K466,467,469,470	16.46	RING
KLKKRNKPCPVCR	K467,469,470, 473	27.84	RING

(c)

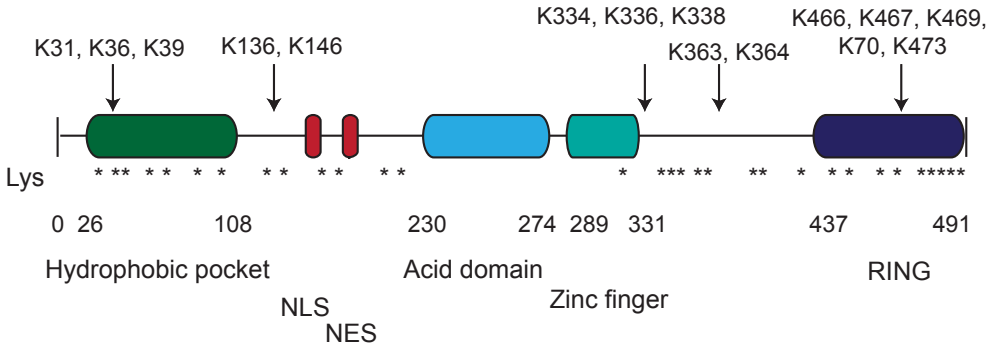

Figure 3-21 MDM2 autoubiquitinates at multiple sites

(a) Blue stained gel of *in vitro* ubiquitinated GST-MDM2 (0.5 µg), after isolation of MDM2 from the reaction using gluthathione beads. The *in vitro* ubiquitination reaction was incubated for 0, 10 or 45 minutes. (b) Results of MS analysis showing modified peptides in MDM2. Lysine residues that were shown to be modified by ubiquitin are highlighted in red. (c) Modified lysine residues are indicated above and total MDM2 lysine residues indicated underneath a schematic MDM2 domain structure. (Unfortunately, data on peptide coverage of the analysis could not be obtained).

3.3 Discussion

Several E3 ligases, including CHIP and MDM2, were shown to target a range of different substrates for ubiquitination, and furthermore to interact with more than one E2 enzymes resulting in ubiquitin chains of different length and linkages. However, only limited information is available on how the E3 is able to select different E2 enzymes and substrates under specific cellular condition. Studying the regulation of E3 ligase activity by ligand binding can (i) give insight into regulation of E3 ligases by physiological binding partners, (ii) be used as a tool to study the effect of ubiquitination on specific substrates, (iii) can provide tools to study the molecular mechanism of cellular function of E3s relevant to disease, and, (iv) can identify potential biologic drugs or drugable pathways, if the E3 ligase and/or its substrate has been implicated in the development of diseases. In this chapter, I have presented data on how the function of the E3 ligase CHIP can be modulated by allosteric regulation of its catalytic domain by mutation or ligand binding to the TPR domain. Furthermore, I characterised the binding dynamics of a novel MDM2 inhibitor and used this information to optimise the aptamer's binding affinity for the MDM2 RING domain.

The E3 ligase CHIP was identified as an Hsp70/Hsp90 interacting protein and was later shown to facilitate ubiquitination of Hsp bound client proteins through its catalytic U-box domain [312]. CHIP thereby connects the chaperone mediated refolding pathway to the proteasomal degradation of misfolded proteins [29, 312, 313]. In addition to this well-established role of CHIP, recently, another function of CHIP as an Hsp70 independent E3 ligase has emerged. Several proteins were identified that interact with CHIP in the absence of Hsp70. This suggests that, under some conditions, CHIP can act as direct E3 ligase, bypassing the need for chaperones to deliver their client proteins as substrates. Two CHIP substrates, death domain-associated protein (Daxx) and Runx1 bind to CHIP independently of Hsp70 [244, 314]. Furthermore, the Ball group has shown that binding and ubiquitination of IRF-1 is not dependent on the presence of Hsp and that CHIP directly binds to and ubiquitinates folded substrates [130]. These observations, however, do not exclude, that in the Hsp70 dependent pathway, CHIP can mediate ubiquitination of these

proteins, if they are misfolded and presented by a chaperone. Here, we expand on previous observation from the Ball group, which showed that CHIP could facilitate IRF-1 ubiquitination in an Hsp70 independent manner, and demonstrate an additional role of Hsp70 in the regulation of CHIP activity. We show that Hsp70, in contrast to the classical model, inhibits CHIP as an E3 ligase for IRF-1 and p53 *in vitro*. Furthermore, Hsp70 binding reduced CHIP autoubiquitination in both the presence of p53 or IRF-1 and the absence of any substrate. Biophysical analysis of CHIP bound to an Hsp70 peptide revealed that ligand binding reduces overall flexibility of CHIP protein and further demonstrated that a CHIP mutant, which carries a single mutation from Arg to Ala in its TPR domain, structurally mimics the Hsp70 bound form of CHIP. This observation was unexpected as this mutant, which is unable to interact with Hsp70/90, is commonly used to study dependence of Hsp70/Hsp90 on CHIP [315]. As the mutant is unable to bind to Hsp proteins and at the same time shows reduced activity towards its substrate, it was concluded that CHIP activity is inevitably dependent on Hsp70 binding. Results from the Ball group presented here, however, demonstrate that this CHIP mutant is not only unable to bind to Hsp70 (Narayan, Landré *et al*., submitted manuscript, [368], appendix 1.2), but also shows greatly reduced intrinsic E3 ligase activity when compared to the wild-type protein in the absence of any Hsp70 protein. Taken together the data suggest that, even though the mutant does not bind Hsp70, it adopts a conformation that is very similar to that of Hsp70 bound CHIP protein. The mutant is, therefore a structural mimic of ligand bound CHIP.

Using molecular dynamic (MD) simulations, I confirmed the biophysical data; fluctuation measurements for individual residues in MD simulations of CHIP show a high degree of flexibility, which is significantly reduced upon ligand binding or the introduction of a structure stabilizing amino acid providing evidence for a model where the CHIP structure 'tightens' in response to TPR modulation by either Hsp70 binding of mutation of K30A. This data is consistent with hydrogen exchange study on CHIP by Graf *et al.* [256], which suggest that the CHIP TPR and charged domain are highly flexible and that binding of Hsp70/90 to the TPR domain induces more stability to the TPR domain. And with SAXS data that suggested a similar

conformation of CHIP K30A protein and CHIP that is bound to an Hsp70 peptide, which is significantly different from the CHIP apo-protein (Ball/Walkinshaw groups, unpublished observation). Analysis of the MD simulations further demonstrated correlated and anti-correlated motions between one TPR and the U-box domains of the CHIP dimer and anti-correlated motion (motion occurring in a opposite phase) between the two U-box domains. Correlated and anti-correlated motions are linked to mechanisms of enzyme catalysis and protein allostery. It is striking therefore that these motions in the CHIP TPR and U-box can be suppressed upon TPR-domain binding or mutation, and this indicates a key role of loss of coordinated motion and intrinsic flexibility in the allosteric regulation of CHIP by TPR-binding ligands such as Hsp70.

Flexibility was shown to be essential for the function of several E3 ligases. As mentioned earlier, some E3s can function as both mono- and polyubiquitin ligases and target several lysine residues on one substrate. To achieve this range of outcomes, E3 ligases were shown to exhibit a high degree of flexibility. Cullin-RING E3 ligases complexes, for example, were shown to include flexible components that function by adapting the distance between E2 and substrate in order for the complex to initiate and then elongate ubiquitin chain formation [316]. In fact, flexibility in both substrate-binding proteins and Rbx subunits is required for efficient substrate polyubiquitination by cullin-RING E3-ligases. Similarly, we show here, that flexibility of CHIP is required for its activity as a direct E3 ligase. As described above, modulation of the CHIP TPR leads to a loss of inter domain communications and protein flexibility, resulting in tightening of the U-box domain. The U-box of CHIP interacts with different E2 enzymes to facilitate substrate ubiquitination. We demonstrate that TPR mediated allosteric regulation of CHIP's U-box affects its ability to interact with and discharge E2 enzymes. Strikingly, CHIP mediated substrate ubiquitination and E2 discharge is inhibited by mutation or ligand binding of CHIP's TPR in the presence of UbcH5. When interacting with UbcH13/Mms2, on the other hand, the ability of mutant CHIP to facilitate the formation of free ubiquitin chains and discharge the E2 is increased. Thus, demonstrating that modulation of CHIP's TPR can act as a 'molecular switch' favouring interactions with one E2 over

another. The E2 heterodimer UbcH13/Mms2 is mainly involved in the formation of K63 linked polyubiquitin chains when in complex with CHIP, however, it cannot facilitate transfer of the initial ubiquitin onto a substrate [254]. The observation that TPR modulation can favour E2 discharge from one E2 over an other provides an elaborate mechanism by which activity of an E3 ligase can be modulated to acting predominantly as an E4. We speculate that CHIP bound to Hsp70 prefers to interact with a specific set of E2s, while unbound CHIP interacts with other E2s, resulting in two distinct functions of the E3 ligase. The reduced flexibility of CHIP that is mediated by ligand binding to its TPR domain, could furthermore, narrow its interaction range and thus only allow ubiquitination of specific lysine residues on a substrate or ubiquitin, which are in proximity to the E2-CHIP complex. This can also explain why, in its rigid conformation, Hsp70 is required to deliver substrates to CHIP, as Hsp70 might be able to position the substrates closer to the E2/ubiquitin/U-Box complex, thereby allowing ubiquitin transfer to the Hsp70 bound protein. While wild type CHIP exhibits higher flexibility and it consequently able to adopt different conformations allowing ubiquitination of different lysine residues in a single substrate or ubiquitin. Thus, the TPR-domain in CHIP appears to provide the plasticity it requires to act as a direct E3-ligase, but can also act as an 'allosteric switch' where the introduction of a more ordered, stable structure can modulate the ability of its U-box domain to discharge specific E2 enzymes.

Interestingly, this study, in addition to giving insight into the control of CHIP function, demonstrates how a TPR domain can act as an allosteric modulator of a separate catalytic domain. This is in an intriguing observation and could shed light on an additional role of TPR structures, which have mainly been studied as protein binding domains that provide a scaffold for the assembly of multi-protein complexes. In fact, when studying effects of mutation or Hsp90 binding to the TPR domain of Cyclophilin 40 (Cyp40), an immunophilin cochaperone discovered in steroid receptor-Hsp90 complexes [317, 318], we found, that as for CHIP, ligand binding or mutation of the K^{30} equivalent K^{227} leads to a loss of protein flexibility and inter-domain correlated motions (Appendix 1.1). This loss in protein dynamics correlates with an increase of the Cyp40 PPIase activity *in vitro*, suggesting that TPR mediated

changes in the structure of the Cyp40 catalytic domain can assist the formation of a more structured and hence active conformation. On the basis of our observations on the control of CHIP and PPIase activity by modulators of their TPR domain, we suggest a role of this domain in the regulation of protein activity by allosteric control of other discrete domains. Whilst writing this thesis a paper was published demonstrating that the TRP domain containing Rap protein from *Bacillus subtilis* undergoes gross conformational changes in response to ligand binding to its TPR domain, locking the protein in an inactive state [319]. This study gives further evidence for TPR domain mediated allosteric control of protein conformation and activity. As TPR-domains are involved in pathways, like proteostasis, that are fundamental to health and to healthy aging, improving our understanding of TPR function and regulation could lead to the development of allosteric regulators that modulate the activity of rate-limiting steps in different cellular pathways.

The second part of this chapter addressed the characterisation and optimisation of an aptamer that binds to and inhibits MDM2's RING activity. Two main strategies are employed to identify drugs that lead to p53 (re-)activation in cancer cells. One is the reactivation of mutant p53 by peptides or small molecules that stabilise its active conformation and thus restore p53 DNA binding ability, potentially rescuing its wild-type activity [224, 229]. The other is inhibition of MDM2's repressive function on p53. MDM2 function towards p53 is targeted either by disruption of the MDM2-p53 interaction or by inhibition of MDM2's E3 ligase activity in order to block p53 degradation. A number of drug molecules that bind to MDM2 have been identified and are currently explored (reviewed by Wade et al., 2012 [289]). The Ball group has identified a C-terminal peptide of the MDM4 RING that inhibits MDM2 E3 ligase activity. The peptide was mapped to the MDM2/MDM4 dimer interface and is, consequently, likely to inhibit MDM2's dimerization ability. As MDM2 is only active as a homo- or heterodimer in complex with MDM4, dimer disruption results in decreased activity. The binding affinity and thus inhibitory potential of the natural occurring MDM4 peptide was increased through two modifications of the peptide. First the negative C-terminal charge was neutralised by the addition of a cap. Modelling data indicated that this favours hydrophobic interactions between the

peptide and RING surface and, additionally, decreases the de-solvation energy required for peptide binding. Second, on the basis of modelling results that suggested additional interactions between the N-terminus of T-apt and the MDM2 RING to those present in the MDM2/MDM4 crystal structure, the N-terminal lysine of the peptide was substituted with a tryptophan residue. The amended peptide displayed a strong increase in binding affinity for the MDM2 RING. This demonstrates how a peptide from a protein interaction partner can be utilised as a starting molecule for a regulatory aptamer and then optimised using modelling approaches combined with experimental testing. Further studies are necessary to reveal if the peptide could be translated into a potential drug that activates p53. Regardless of its therapeutic potential T-apt can be used as a tool to study MDM2 mechanism *in vitro* and the effects of E3 ligase inhibition *in vitro* and in cells.

I have shown how E3 ligase activity could be modulated or inhibited by ligand binding to their functional domains. For the physiological regulation of E3 ligases, this implies that their activity could be altered by either binding of an interacting protein, as in the case of Hsp70 binding to CHIP, or by a post translational modification, which could either interfere with binding of interaction partners or affect protein conformation. For example, acetylation and phosphorylation neutralise or create a charge on a side-chain, and this could affect the conformation of a protein. Protein modification by ubiquitin can be described as an intermediate of the two. Ubiquitin is directly attached to a receptor residue in the target protein but is an 8-kDa protein in itself. It can therefore be seen as a binding partner on its own that would be able to affect an E3 ligase in a similar way as binding of a peptide or protein. Interestingly, residues within the CHIP TPR domain, which we showed allosterically regulate the catalytic activity of its U-box domain, are subject to autoubiquitination. It would be interesting to determine how TPR ubiquitination affects the overall flexibly and activity of CHIP, and if TPR or U-box ubiquitination affect its ability to interact with specific E2 enzymes. Autoubiquitination site mapping on MDM2 shows that similar to CHIP, several functional domains in MDM2 are subject to ubiquitination. In addition to E2 interactions, autoubiquitination of substrate binding sites, i.e. the p53 binding site in MDM2s

hydrophobic pocket and the TPR domain of CHIP, could affect interactions with substrates, either blocking the binding site or changing the conformation of the E3:E2:ubiquitin:substrate complex. In this way, ubiquitin could amend the scaffold provided by the E3 and thereby change the conformation of the E3-E2-ubiquitin complex allowing ubiquitin transfer to specific residues on the substrate.

The physiological relevance of the ubiquitination sites mapped by MS still require full validation, however, they indicate that ubiquitination could play a principal role in the regulation of E3 ligase activity and its ability to interact with substrates and E2 enzymes. However, more work is necessary to investigate how and if E3 ligase self-ubiquitination affects chain and substrate specificity.

Chapter 4: Interplay between IRF-1 ubiquitination and DNA binding

4.1 Introduction

4.1.1 IRF-1 Interactome

IRF-1 has been shown to be involved in numerous cellular pathways, yet information about its interactome is limited. Several proteins that are involved in posttranslational modifications of IRF-1 have been identified. The SUMO-E3 ligase PIAS3 binds to IRF-1 and, together with the SUMO E2 Ubc9, leads to SUMOylation of lysine residues 275 and 299 [320, 321]. IRF-1 is phosphorylated by CK2 at cluster sites between aa138-150 and 219-231 [322]. Further, a study in HEK cells showed that MyD88 (myelod differentiation primary response gene 88) binding induces IRF-1 phosphorylytion and translocation, ultimately enhancing its transcriptional activity [323]. Additionally, IRF-1 was shown to be bound and acetylated by p300/CBP and, furthermore, IRF-1 binding to p300 leads to p53 acetylation and activation [134, 324, 325]. Both PCAF (p300/CBP associated factor) and GCN5 (general control of amino acid synthesis 5) were suggested to enhance acetylation of IRF-1 and thereby be involved in its activation [326]. IRF-1 associates with the E3 ligase CHIP, which leads to its ubiquitination and degradation under specific stress conditions (see 1.3.4). Moreover, a number of proteins were shown to bind to IRF-1 and either work synergistically to activate transcription e.g. NF-κB [327], HIV-Tat [328] and HPV E7 [329], or to repress its function like IRF-8/ICSBP [129] and NPM [330].

The C-terminal domain of IRF-1 (Mf1 domain, Fig 1-8) directly binds to Hsp70 and, furthermore, inhibition of Hsp90 leads to loss of IRF-1 protein while Hsp90 over expression decreases IRF-1's rate of degradation [112]. Taken together these results indicate that IRF-1 is a client of the Hsp70/Hsp90 chaperone machinery and that this is involved in IRF-1 stability and turnover [112].

A recent study by the Ball group, utilising affinity chromatography using overlapping IRF-1 peptides and subsequent mass spectrometry analysis, has identified a region adjacent to the DBD, which was named the Mf2 domain (aa 106-140, see 1.3.1.2) and this region is involved in interactions with a large number of proteins [127]. Several of the known IRF-1 binding partners interact with this region e.g. NPM and CK2 and a great number of additional proteins were identified in the study, with most still awaiting validation as direct interaction partners of IRF-1. YB-1 and TRIM28, which have been implicated in transcriptional regulation and cancer development, and SET were pulled out by the Mf2 peptides and have been validated as direct IRF-1 binding partners. The exact role of these interactions remains to be investigated.

4.2 Results

4.2.1 MDM2 can act as an E3 ligase for IRF-1 *in vitro* and in cells

Even though, IRF-1 was shown to be regulated by the ubiquitin/proteasome system, many details of the mechanism and outcome of IRF-1 ubiquitination remain unknown. Results by the Ball group showed that ubiquitination and degradation of IRF-1 are signalled by two distinct motifs in the C-terminus of the transcription factor and that these two events can be uncoupled, indicating that there might be a function of IRF-1 ubiquitination that is separate from its degradation [135]. IRF-1 was shown to be SUMOylated at residues Lys^{275} and Lys^{299} [331], and it was suggested that these lysine residues might also function as ubiquitin acceptor sites, a mutational study by the Ball group [135], however, found no evidence for an involvement of these residues in IRF-1 ubiquitination or degradation. I therefore, set out to identify the lysine residues on IRF-1 that are modified by ubiquitin in order to gain better insight into the mechanism and outcome of IRF-1 ubiquitination. We previously identified CHIP as an E3 ligase for IRF-1 under stress conditions [130]; however, an E3 for basal IRF-1 turnover remains elusive. The ball group published that the IRF family member IRF-2 is a substrate for MDM2 *in vitro* and in cells. However, IRF-2 is not subject to MDM2-mediated degradation leading us to speculate that MDM2 may be involved in the regulation of IRF-2 activity, rather than its turnover. Interestingly, the MDM2 binding sites in IRF-2 are conserved in IRF-1 (Fig 4-1a) and binding site I overlaps with the binding site for CHIP, suggesting that the Mf2 domain may comprise a general E3 docking site. As a first step, I set out to determine if MDM2 was an E3 ligase that binds and ubiquitinates IRF-1, in order to use MDM2 as a tool to study IRF-1 ubiquitination. Therefore *in vitro* binding and ubiquitination assays were performed. When GST–IRF-1 was immobilized on a microtiter plate and incubated with a titration of MDM2 in the mobile phase, the results showed that MDM2 bound to IRF-1 in a dose-dependent manner (Fig 4-1b, left panel). To identify the binding interface between MDM2 and IRF-1, a peptide–protein interaction assay was used. An overlapping IRF-1 peptide library (Table 2-6) was immobilized and incubated with a constant amount of MDM2 in the mobile phase; binding was then detected using an anti-MDM2 antibody. MDM2 bound to an

IRF-1 peptide from within the Mf2 domain (peptide 8, VRVYRMLPPLTKNQRKERKS; Fig 4-1b right panel) with homology to the MDM2-binding site-I of IRF- 2 (Fig 4-1a). This is the same interface where CHIP has been shown to interact with IRF-1, indicating that this could be a common docking site for multiple E3 ligases on IRF-1. To establish that IRF-1 can act as a direct substrate for MDM2 *in vitro*, I employed a minimal ubiquitination assay using only purified components, results of the assay showed that there was a positive correlation between the efficiency of IRF-1 ubiquitination and the concentration of MDM2 added to the assay (Fig 4-1c). To verify that the results obtained in the *in vitro* experiments are relevant in cells, I determined the interaction between IRF-1 and MDM2 in HCT-116 cells. I asked whether MDM2 was detectable after isolation of IRF-1 complexes using a FLAG pull-down, and whether the loss of the Mf2 domain affected binding. The results show that IRF-1 WT forms a complex containing MDM2 in cells (Fig 2a, lanes 2 and 5), whereas an IRF-1 Mf2 deletion mutant (Δ106–140) is not associated with MDM2 (lanes 3 and 6). In order to investigate, whether MDM2 is able to ubiquitinate IRF-1 in unstressed cells, in-cell ubiquitination assays using His–ubiquitin, IRF-1 and MDM2 (Fig 4-2b) were assembled in HCT-116 cells. After isolation and analysis of His-ubiquitinated proteins, an increase in the amount of ubiquitinated IRF-1 was seen in the presence of MDM2 (Fig 4-2b; compare lane 7 with lane 8), showing that under these conditions MDM2 can mediate ubiquitination of IRF-1 in cells. Whether ubiquitination of IRF-1 by MDM2 leads to its degradation and thus affects its half-life was determined using HCT-116 cells transfected with MDM2 and treated with the protein synthesis inhibitor cycloheximide. The loss of endogenous IRF-1 protein was then monitored over time by immunoblot analysis (Fig 4-2c). The results show that MDM2 overexpression did not lead to a decrease in the half-life of IRF-1; rather it gave a slight, but reproducible, increase in its half-life. This result shows that even though MDM2 facilitates IRF-1 ubiquitination, this is not sufficient to signal its degradation, suggesting that MDM2 may be involved in the regulation of IRF-1 activity rather than its rate of degradation as seen previously for IRF-2.

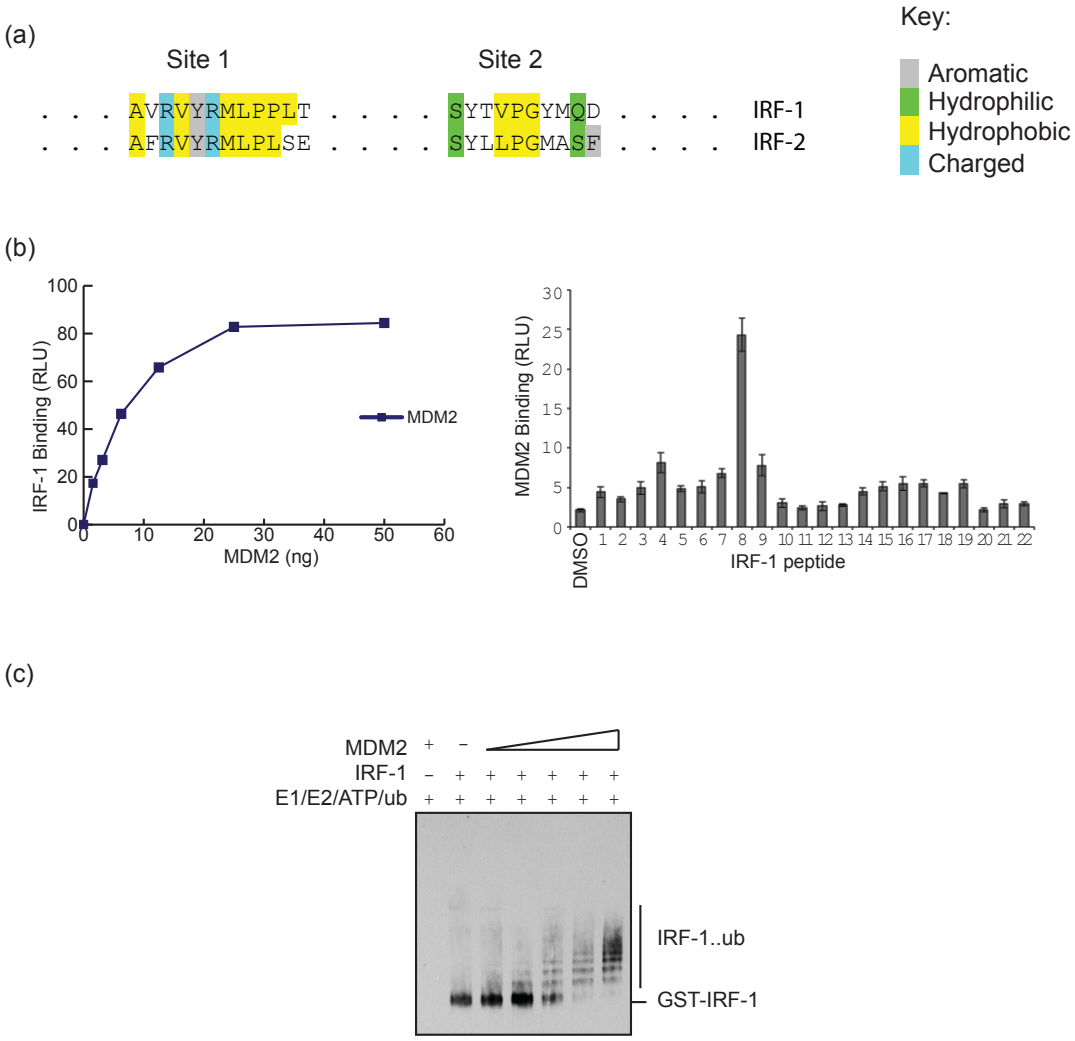

Figure 4-1 MDM2 binds and ubiquitinates IRF-1 *in vitro*

(a) Alignment of the two MDM2-binding motifs on IRF-2 with the homologous regions from IRF-1. (b) GST–IRF-1 (100 ng) was immobilized on a microtiter plate and incubated with a titration (0–100 ng) of MDM2. Protein binding was detected using an anti-MDM2 mAb and the protein amount against binding is expressed as relative light units (RLU). Biotin-tagged IRF-1 peptides (60 pmol/well, 20 amino acids with a five amino acid overlap) were immobilized on a microtiter plate and incubated with 100 ng of MDM2. MDM2 binding to the peptides was detected using an anti-MDM2 mAb and is expressed in RLU. (c) An ubiquitination assay was carried out using GST–IRF-1 as the substrate, increasing amounts of MDM2 as the E3 ligase (0–160 ng), 10 µM ubiquitin, 100 nM UBE1, 1 µM UbcH5a and 4.5 mM ATP and incubated for 15 minutes (the same concentration of ubiquitin, UBE1, UbcH5a and ATP was used in all *in vitro* ubiquitination assays in this chapter). The samples were analysed using SDS/PAGE and immunoblot with an anti-IRF-1mAb.

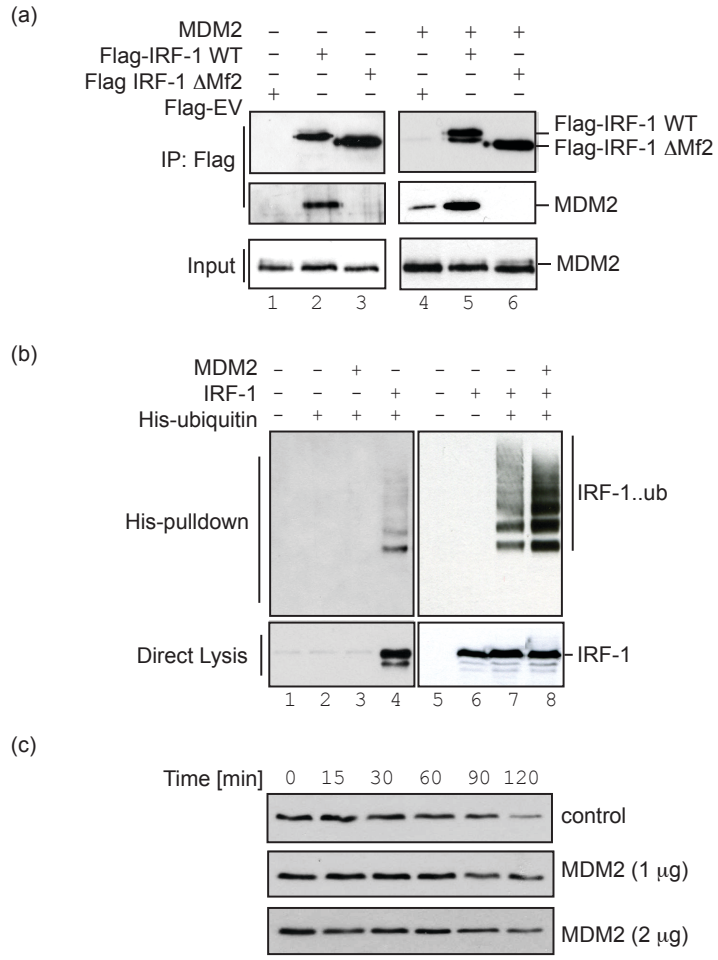

Figure 4-2 MDM2 can act as an E3 ligase for IRF-1 in cells

(a) HCT-116 cells were co-transfected with 2 μg of pcDNA3-MDM2 or pcDNA3-empty vector and 2 μg of FLAG–IRF-1WT, IRF-1ΔMf2 or empty vector. FLAG conjugates were immunoprecipitated using anti-FLAG-M2 agarose. After elution, samples and lysate (25 μg) were analysed by immunoblotting using an anti-MDM2 mAb and anti-FLAG mAb. (b) HCT-116 cells were co-transfected with pcDNA3-IRF-1 (0.5 μg), His–ubiquitin (0.5 μg) and pcDNA3-MDM2 (2 μg) as shown. Post-transfection (20 hours), cells were treated with MG132 (50 μM) for 4 hours and histidine-labelled ubiquitinated protein was isolated using Ni-NTA chromatography. Samples were analysed by SDS/PAGE and immunoblot using an anti-IRF-1 mAb. Total amounts of IRF-1 in the sample (bottom panel) and modified IRF-1 (top panel) are shown (right panel, data courtesy of Emmanuelle Pion). (c) Immunoblot analysis of HCT-116 cells transfected with the indicated amounts of pcDNA3-MDM2 following cycloheximide (30 μg/ml) treatment. Cells were harvested at the times shown and analysed (60 μg/lane) by SDS/PAGE (10% gel), followed by western blot using an anti-IRF-1 mAb.

4.2.2 MDM2 and CHIP mediate ubiquitination of IRF-1's DBD

To investigate the role of E3 ligase docking to the Mf2 domain, I first asked whether the Mf2 binding E3 ligases, CHIP and MDM2, ubiquitinate common or distinct lysine residues by mapping sites of modification using mass spectrometry (MS). First, *in vitro* ubiquitination of IRF-1 by CHIP and MDM2 was characterised by performing a time course of ubiquitination *in vitro*. Results show a time dependent increase of IRF-1 ubiquitination by both CHIP (Fig 4-3a, left-hand panel) and MDM2 (right-hand panel). To examine if ubiquitination of IRF-1, facilitated by the two enzymes leads to mono- or polyubiquitination, a time course of *in vitro* IRF-1 ubiquitination of up to 180 minutes was analysed using antibodies that detect only polyubiquitinated conjugates or both mono- and polyubiquitin conjugates (Fig 4-3b). This showed that CHIP generates both poly- and monoubiquitination of IRF-1; no signal at the size of IRF-1 was detected when MDM2 was used as the E3 ligase. Indicating that *in vitro* ubiquitination of IRF-1 by MDM2 was not as efficient as by CHIP under the utilised conditions. Both poly- and monoubiquitination can be observed at the top of the gel, at a size corresponding to MDM2 itself, indicating strong autoubiquitination of MDM2 in the assay.

For the identification of ubiquitination sites by mass spectrometry, IRF-1 was ubiquitinated for either 10 or 45 minutes and discrete ubiquitinated intermediates were excised and subjected to in-gel digestion using trypsin and subsequent analysis by MS (Fig 4-4a; for an outline of the experimental procedure see Fig 3-14).

Although there are a total of 23 lysine residues in the primary amino acid sequence of IRF-1, only a subset of those were detected by MS as being ubiquitin-acceptor sites for the Mf2-binding ligases CHIP or MDM2 (Fig 4-4b). Strikingly, IRF-1 was predominantly ubiquitinated in, or adjacent to, the DBD and no modified residues from within the C-terminal half of the protein were detected with either of the E3 ligases. Although both MDM2 and CHIP modified Lys^{39}, Lys^{50} and Lys^{117}, no modification of IRF-1 at Lys^{95} was detected by CHIP, whereas this residue was modified when MDM2 provided the E3 activity. Similarly, Lys^{78} was detected only in the CHIP-ubiquitinated samples. Although this difference in specificity remains to

be confirmed using a second analytical technique, the existing data suggest that although Mf2-directed ubiquitination of IRF-1 is specific for the DBD, there could be subtle differences in the exact residues targeted by MDM2 and CHIP and thus in the molecular signal of the modification.

4.2.3 Ubiquitination of IRF-1 residues Lys^{39}, Lys^{50} and Lys^{78} appears mutual exclusive

In order to gain a structural insight in the effect of IRF-1's DBD ubiquitination on the overall shape and surface of the domain, models of the DBD in its ubiquitinated state were computed using the HADDOCK web server [271, 297]. The model was generated using the C-terminal glycine on ubiquitin and either one of the ubiquitin acceptor residues present in the crystal structure as docking sites (active residues Lys^{39}, Lys^{50}, Lys^{78} and Lys^{95}) (Fig 4-5). Interestingly, modelling suggests that modification at three of the five ubiquitination sites (Lys^{39}, Lys^{50} and Lys^{78}) would result in ubiquitin occupying an overlapping three-dimensional space. Thus, ubiquitination at any one of these three sites could potentially block modification at the other two sites. To further investigate this model experimentally *in vitro* ubiquitination assays, using either WT ubiquitin or an ubiquitin mutant in which all of the lysine residues were mutated to arginine (NoK ubiquitin), were performed. For the majority of E3 ligases, NoK ubiquitin can only result in the formation of monoubiquitinated residues, as chain elongation is not possible (linear ubiquitin chain formation by M1 is an exception to this). I found that the ubiquitin mutant was, in general, a poor substrate for *in vitro* ubiquitination, with slower conversion of IRF-1 into its monoubiquitinated form, than was seen in the presence of WT ubiquitin. However, when assay conditions were adapted to facilitate ubiquitination I saw that monoubiquitination provided a maximum of three ubiquitins added per IRF-1 molecule, and in the case of MDM2 a single ubiquitinated form predominanted (Fig 4-6a; compare lanes 3 and 5 with lanes 2 and 4), suggesting that a maximum of three out of the five ubiquitin-acceptor sites identified could be modified at any one time. If the modelling was correct it would predict that mutation of Lys^{39}, Lys^{50} and Lys^{78} individually would not be sufficient to affect IRF-1 DBD monoubiquitination.

To complement the above approach a series of IRF-1 point mutant proteins were therefore generated in which Lys^{39}, Lys^{50} and Lys^{78} were individually mutated to arginine. When the mutant proteins were used as substrates for CHIP in the presence of NoK ubiquitin, loss of Lys^{39} and Lys^{78} did not produce qualitative or quantitative changes in monoubiquitination of IRF-1, consistent with the idea that ubiquitination at either one of these residues produces a similar outcome and that ubiquitination at these two sites is mutually exclusive. Although mutation of Lys^{50} did have an effect on monoubiquitination, with loss of the slowest migrating ubiquitinated form of IRF-1, this mutant was susceptible to cleavage during expression and the cleavage product was also a substrate for CHIP (Fig 4-6b faster migrating band in K50R sample), making these data difficult to interpret. When double or triple mutants were constructed to further study the role of specific residues, the resultant proteins were extremely susceptible to cleavage during expression and could consequently not be used in *in vitro* experiments. Taken as a whole, the data in this section support the modelling data and suggest that ubiquitination of Lys^{39} and Lys^{78}, and potentially Lys^{50}, are mutually exclusive and might, therefore, result in the generation of a very similar 'molecular signature'.

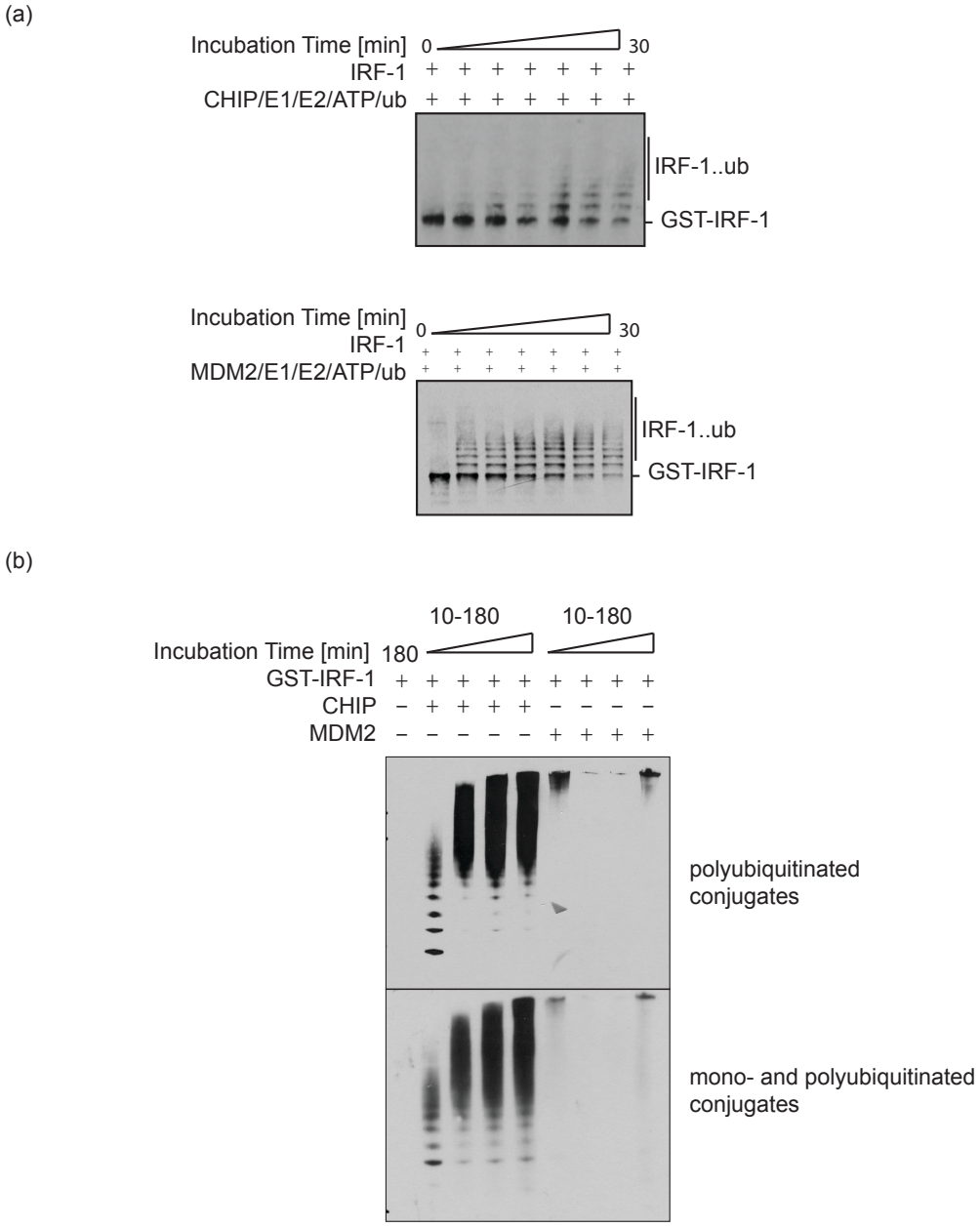

Figure 4-3 Ubiquitination of IRF-1 by CHIP and MDM2 *in vitro*

(a) Time course (0–30 min) of an *in vitro* ubiquitination assay of IRF-1 modified by His–CHIP (50 ng) (upper panel) and MDM2 (80 ng) (lower panel), analysed with an anti-IRF-1 mAb. (b) Time course (0–180 min) of an *in vitro* ubiquitination assay of IRF-1 modified by His–CHIP (50 ng) and MDM2 (80 ng), analysed with antibodies recognizing only poly- (upper panel; FK1 mAb) or poly- and monoubiquitination (lower panel; FK2 mAb).

(a)

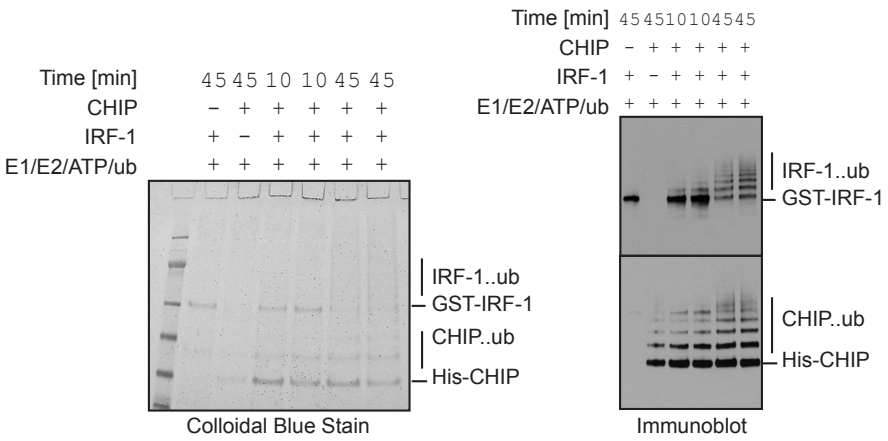

(b)

	IRF-1 peptide	Modified Lysine	Domain	Mascot Score
CHIP	HAAKHGWDINKDACLFR	K39	DBD	18.91
	HGWDINKDACLFR	K50	DBD	20.08
	YKAGEKEPDPK	K70	DBD	6.48
	YKAGEKEPDPKTWK	K78	DBD	12.75
	MLPPLTKNQR	K117	DBD/Mf2	23.96
	IRF-1 peptide	**Modified Lysine**	**Domain**	**Mascot Score**
MDM2	HAAKHGWDINK	K39	DBD	18.49
	HGWDINKDACLFR	K50	DBD	12.45
	YKAGEKEPDPK	K70	DBD	7.26
	CAMNSLPDIEEVKDQSR	K95	DBD	31.54
	MLPPLTKNQR	K117	DBD/Mf2	22.69

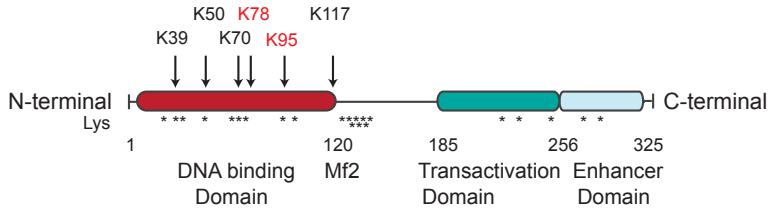

Figure 4-4 IRF-1 is exclusively ubiquitinated in its DNA-binding domain

(a) GST–IRF-1 was ubiquitinated using an *in vitro* ubiquitination assay with CHIP or MDM2 as the E3 ligase and isolated from the reaction mix using glutathione beads. A Colloidal-Blue-stained gel before band excision for MS analysis (left-hand panel) and immunoblot analysis of the samples blotted for IRF-1 and CHIP (right-hand panel) are shown. CHIP was co-purified from the reaction with IRF-1 as a result of IRF-1–CHIP protein interactions. (b) Results of MS analysis of modified peptides in IRF-1. Lysine residues that were shown to be modified by ubiquitin are highlighted in red. (c) Modified lysine residues are indicated on a schematic IRF-1 domain structure. Lysine residues that are modified by only MDM2 or CHIP are shown in red, whereas residues that are modified by both are shown in black.

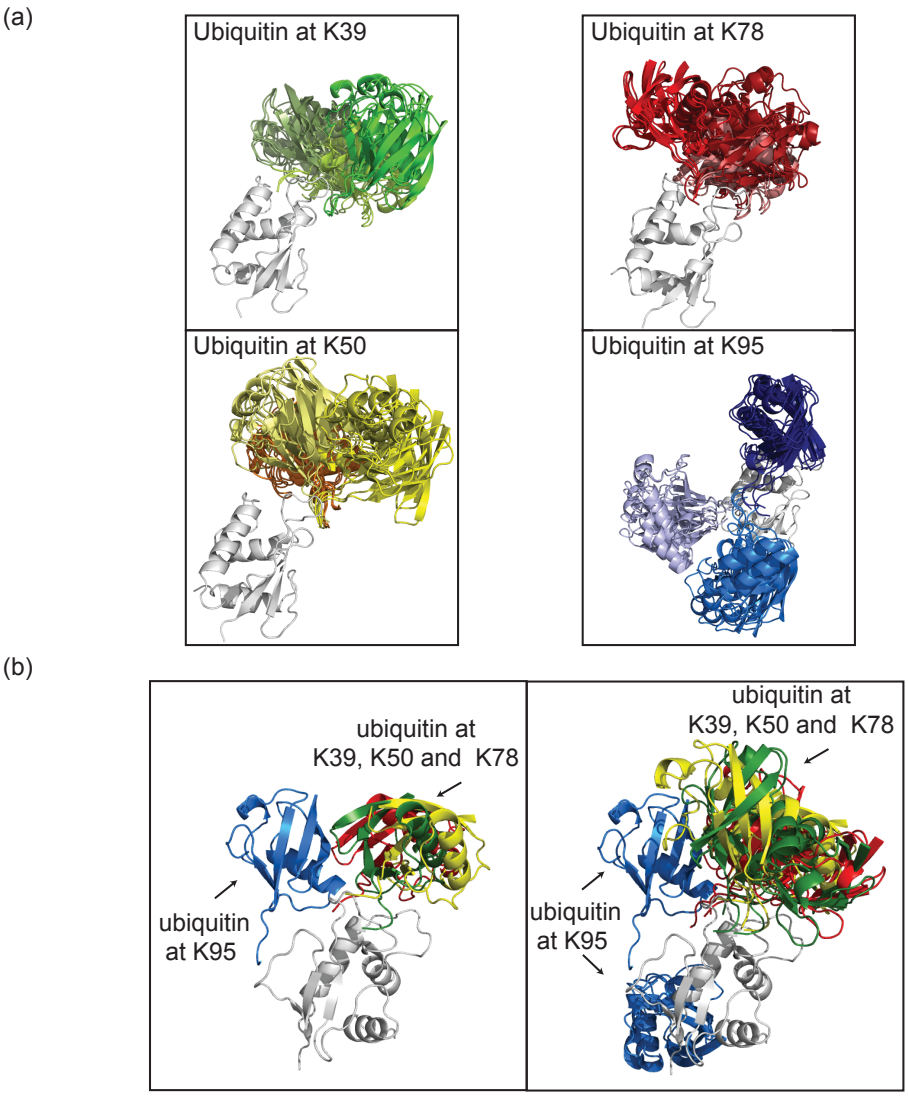

Figure 4-5 Model of monoubiquitinated IRF-1

(a) Ubiquitin was modelled on to the IRF-1 DBD at the ubiquitin receptor lysine residues present in the crystal structure (Lys^{39}, Lys^{50}, Lys^{78} and Lys^{95}) using the HADDOCK web server (detailed in section 2.8.1). From the results obtained the four best structures from the three best clusters were analysed. The overlay of the ubiquitin position in respect to IRF-1 for each lysine residue is shown, with ubiquitin in structures obtained from different clusters in different colours. (b) Model of ubiquitinated IRF-1. Ubiquitin was modelled on to the available crystal structure of the IRF-1 DBD (PDB:1IF1) (white) using the HADDOCK web server at Lys^{39} (green), Lys^{50} (yellow), Lys^{78} (red) and Lys^{95} (blue), the structure that obtained the highest score for each site (left-hand panel) and the three structures obtaining the highest score in one of the three best clusters for each site (right-hand panel) are shown.

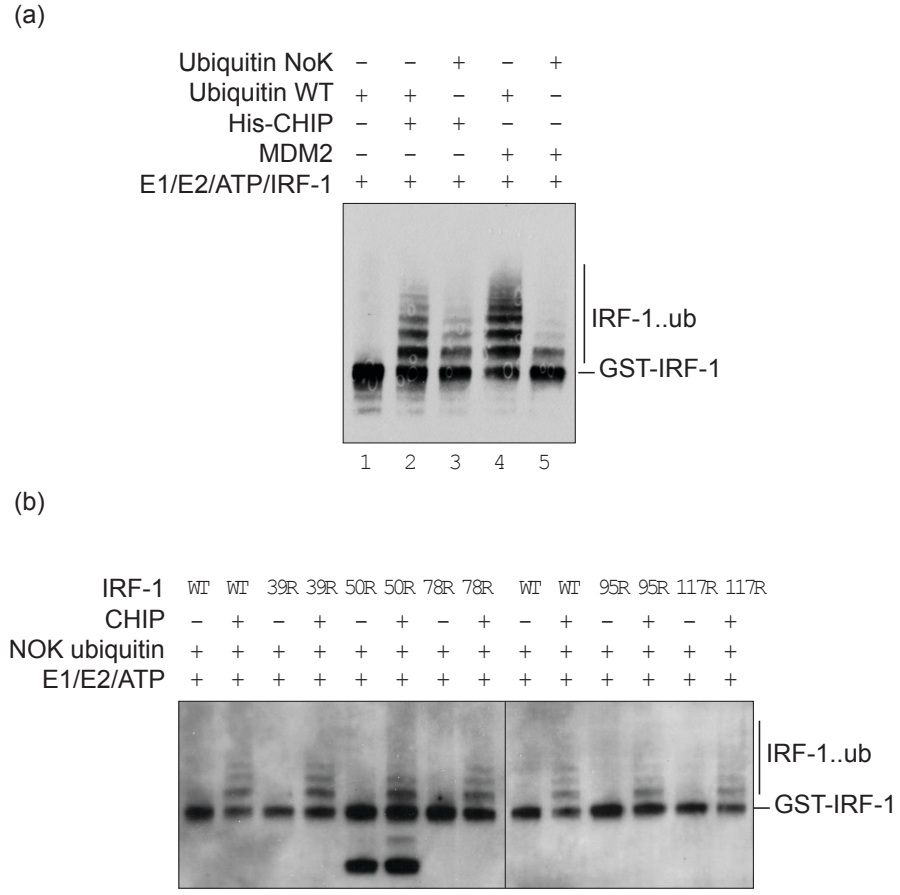

Figure 4-6 Ubiquitination of lysine residues K39, K50 and K78 appears mutual exclusive

(a) *In vitro* ubiquitination of IRF-1 with CHIP and MDM2 as E3 ligases and either WT or NoK ubiquitin (in which all lysine residues are mutated to arginine). Reactions with WT ubiquitin were incubated for 10 minutes, whereas the reactions with no E3 ligase and NoK ubiquitin were incubated for 60 minutes. (b) *In vitro* ubiquitination assay with GST-IRF-1 containing the indicated mutation at one of the ubiquitin-acceptor lysine residues, NoK ubiquitin and CHIP as the E3 ligase; the reactions were incubated for 45 minutes. Immunoblots were probed with an anti-IRF-1 pAb.

4.2.4 Ubiquitin receptor residues Lys^{78} and Lys^{95} are directly involved in DNA binding

When the ubiquitin-modified residues were mapped on to the available IRF-1 DBD crystal structure (PDB:1IF1), we found that Lys^{39}, Lys^{50} and Lys^{95} were located in exposed loops (L1, L2 and L3), whereas Lys^{78} was positioned within the α3-helix which forms the second helix of the HTH (helix–turn–helix) homologous motif (Fig 4-7, upper panel). Strikingly, residues Lys^{78} and Lys^{95} lay very close/within the DNA binding interface (Fig 4-7, lower panels). To determine if these residues are actively involved in DNA-interactions between IRF-1 and its consensus sequence at the promoters, molecular dynamic simulation of the IRF-1 DBD in association with DNA were carried out and the binding energy between the protein and DNA was computed. Decomposition analysis of the residues involved in the interaction using MMGBSA (Ambertools) shows that Lys^{78} is one of the most important residues mediating IRF- 1 DNA interactions and an additional involvement in Lys^{95} in the interaction (Fig 4-8).

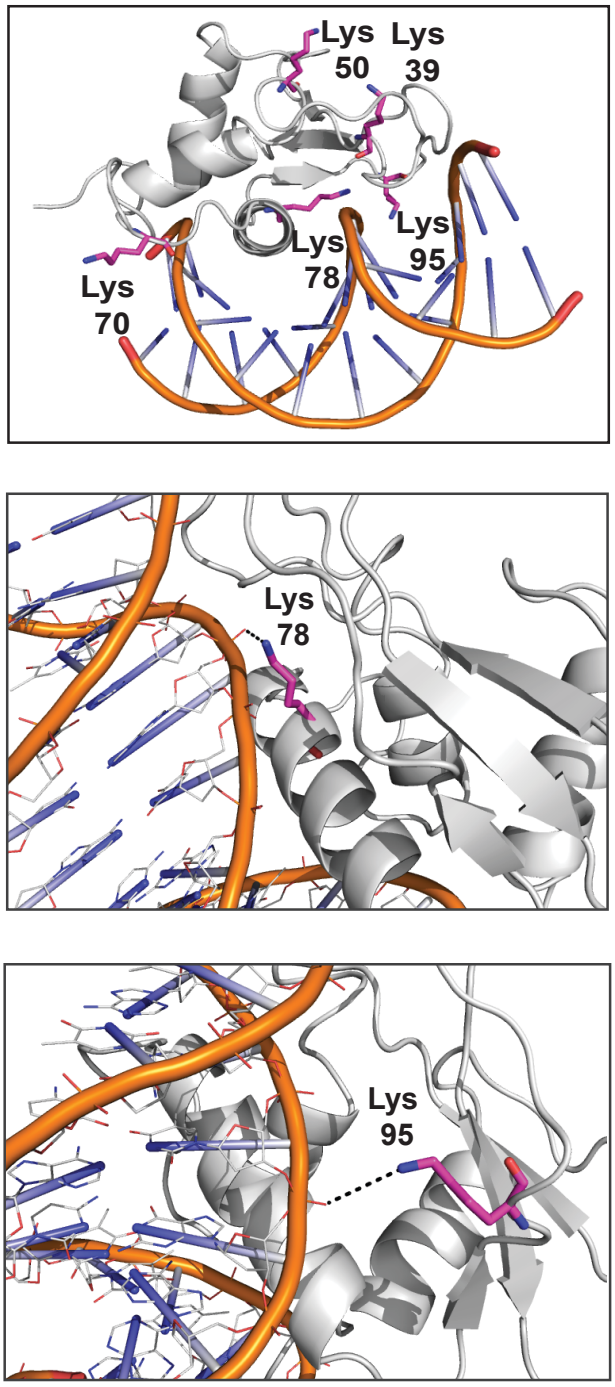

Figure 4-7 Position of ubiquitination sites on the IRF-1 DBD crystal structure

Crystal structure of the IRF-1 DBD (PDB code 1IF1) with lysine residues that were shown to be modified by ubiquitin highlighted by pink sticks.

(a)

Residue	DC Score	Structure
ARG 9	**- 8.52**	**N – terminal**
TRP 11	**- 6.34**	**α 1**
LEU 12	- 3.22	α 1
TRP 38	- 3.15	L 1
HIS 40	**- 5.8**	**L1**
ALA 41	- 3.59	L1
LYS 43	**- 7.55**	**L1**
ARG 64	**- 6.21**	**α 2**
LYS 75	- 3.19	α 3
LYS 78	**- 7.19**	**α 3**
ARG 82	**- 8.07**	**α 3**
LYS 95	- 4.9	L 3
ARG 99	**- 5.66**	**L 3**
ASN 100	- 3.81	L 3

(b)

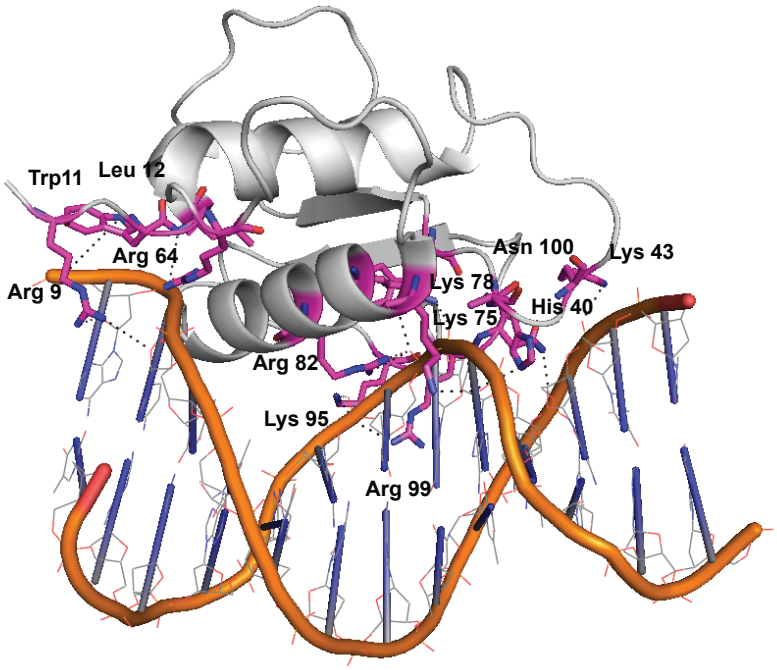

Figure 4-8 IRF-1 residues that are involved in DNA binding

(a) Molecular simulations were carried out on IRF-1 DBD (PDB:1IF1) and residues involved in DNA interactions were identified by decomposition analysis. (b) Crystal structure of IRF-1DBD shown as cartoon, with results identified as playing a major role in DNA interactions in the simulations indicated as sticks.

4.2.5 DNA-bound IRF-1 is protected from ubiquitination *in vitro*

As the ubiquitin-acceptor sites are all located within the DBD, with Lys^{78} and Lys^{95} being at the DNA-binding interface and directly involved in interaction, we reasoned that modification might be affected by the sequence-specific DNA-binding activity of IRF-1. To test this, a consensus site DNA oligonucleotide (C1) was utilised, which I show can bind to GST–IRF-1^{WT} (Fig 4-9, lanes 3–5) in an EMSA and is supershifted by an anti-IRF-1 mAb. To control for effects of DNA binding in subsequent experiments an IRF-1 DNA binding mutant with a single mutation from Trp to Arg was used (W11R). Analyses of the DNA binding ability of the mutant shows that binding to DNA is completely abolished (lanes 6–9), decomposition analysis of the binding energy between IRF-1 and DNA in molecular dynamic simulations shows that this residue is directly involved in and important for the interaction (Fig 4-8). To characterise this mutant further, molecular dynamic simulation of both IRF-1^{WT} and IRF-1^{W11R} were carried out in the absence of DNA. Results of the simulation, which are presented in Fig 4-10, suggest that a mutation at Trp^{11} to Arg has an effect on the overall shape of the IRF-1 DBD. The introduced arginine forms salt-bridges with side chains Glu^{13}, Asp^{90} and additionally interacts with the backbone of Ser^{87}. These interactions result in conformational changes, involving the positioning of loop 3 closer to the N-terminus of IRF-1 (Fig 4-10a). In turn, these changes lead to higher flexibility in loop 1, as shown by fluctuation analysis (Fig 4-10b), loop 1 is directly involved in DNA interactions, and it can be assumed that the changes in its dynamics, together with overall conformational changes in the DBD in the Arg mutant result in a strong decrease of its DNA binding ability.

To examine the effects of DNA binding on IRF-1 ubiquitination, IRF-1 was pre-incubated with C1 DNA or a control oligonucleotide that does not interact with IRF-1 (p21c) (Fig 4-9, lanes 7– 10). Whereas control DNA (p21c) had no significant effect on the ubiquitination of IRF-1 by CHIP (Fig 4-11a, left-hand panel) or MDM2 (right-hand panel), addition of IRF-1 consensus site DNA (C1) almost completely suppressed ubiquitination. To control for non-specific effects of DNA on IRF-1 the

non-DNA binding mutant IRF-1^{W11R} was used and determined whether this was refractive to the effects of DNA. Figure 4-11a shows that whereas C1 oligonucleotides inhibit the ubiquitination of wild-type IRF-1 (lanes 4 and 5) they had no significant effect on the ubiquitination of IRF-1^{W11R} (lanes 9 and 10). As an additional control we showed that C1 DNA did not affect CHIP activity directly as there was no effect on the ability of CHIP to mediate autoubiquitination (Fig 4-11a, bottom left panel). Ubiquitination of p53, a second well characterized substrate for both CHIP (Fig 4-11b, left-hand panel) and MDM2 (Fig 4-11b, right-hand panel), was not affected by p53 binding to DNA from the p21 promoter (p21c DNA), suggesting that protection of IRF-1 from ubiquitination by DNA is a specific property of this transcription factor (Fig 4-11b).

To expand on the observation described above, which used an optimized IRF-1 consensus DNA oligonucleotide, a range of oligonucleotide probes based on naturally occurring binding elements from IRF-1 target gene promoters was examined. Elements from all IRF-1 target genes tested were able to inhibit CHIP- and MDM2-mediated ubiquitination, and there was good agreement between the ability of IRF-1 to bind DNA in an EMSA (Fig 4-12, bottom panel) and the ability of the oligonucleotide to inhibit ubiquitination of IRF-1 in an *in vitro* ubiquitination assay (Fig 4-12, top panels). For example, IRF-1 binds only weakly to an oligonucleotide based on the TRAIL promoter and this probe is a weak inhibitor of IRF-1 ubiquitination (Fig 4-12, bottom panel, lane 5).

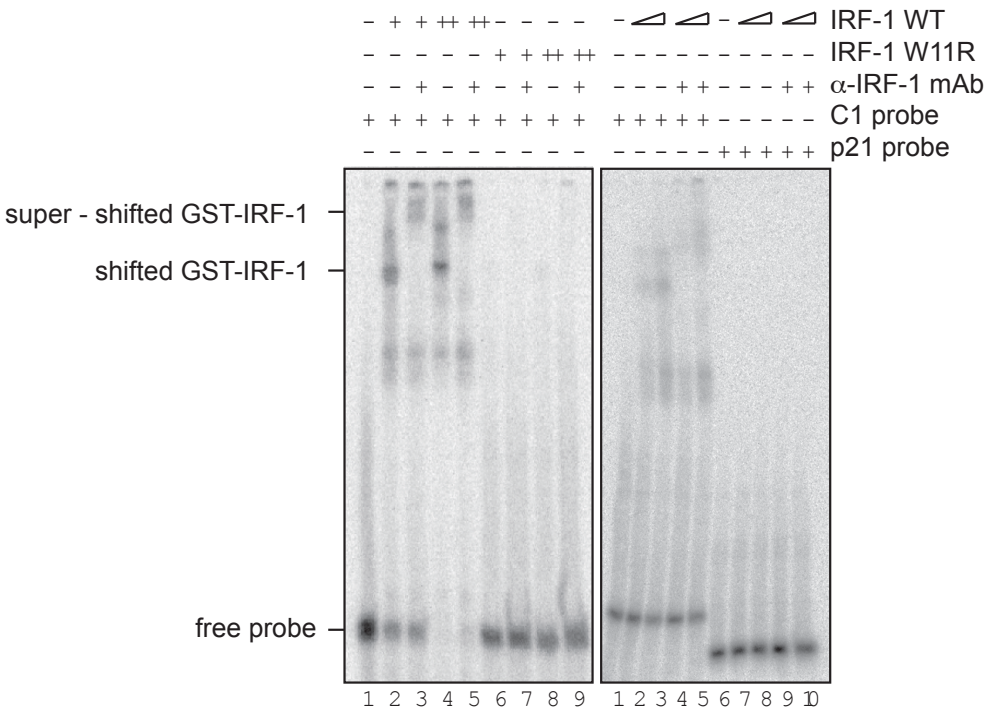

Figure 4-9 IRF-1^{WT} but not a W11R mutant specifically binds to the ISRE sequence *in vitro*

EMSA showing binding of a titration (100 and 300 ng) of purified GST–IRF-1^{WT} or of the DNA-binding mutant GST–IRF-1W11R to a 32P-labelled DNA probe of C1 DNA (left-hand panel) or binding of GST-IRF-1^{WT} to the C1 probe compared with the non-binding control probe (p21c) (right-hand panel). When indicated an anti-IRF-1 mAb was added to the reaction to supershift the protein–DNA complex.

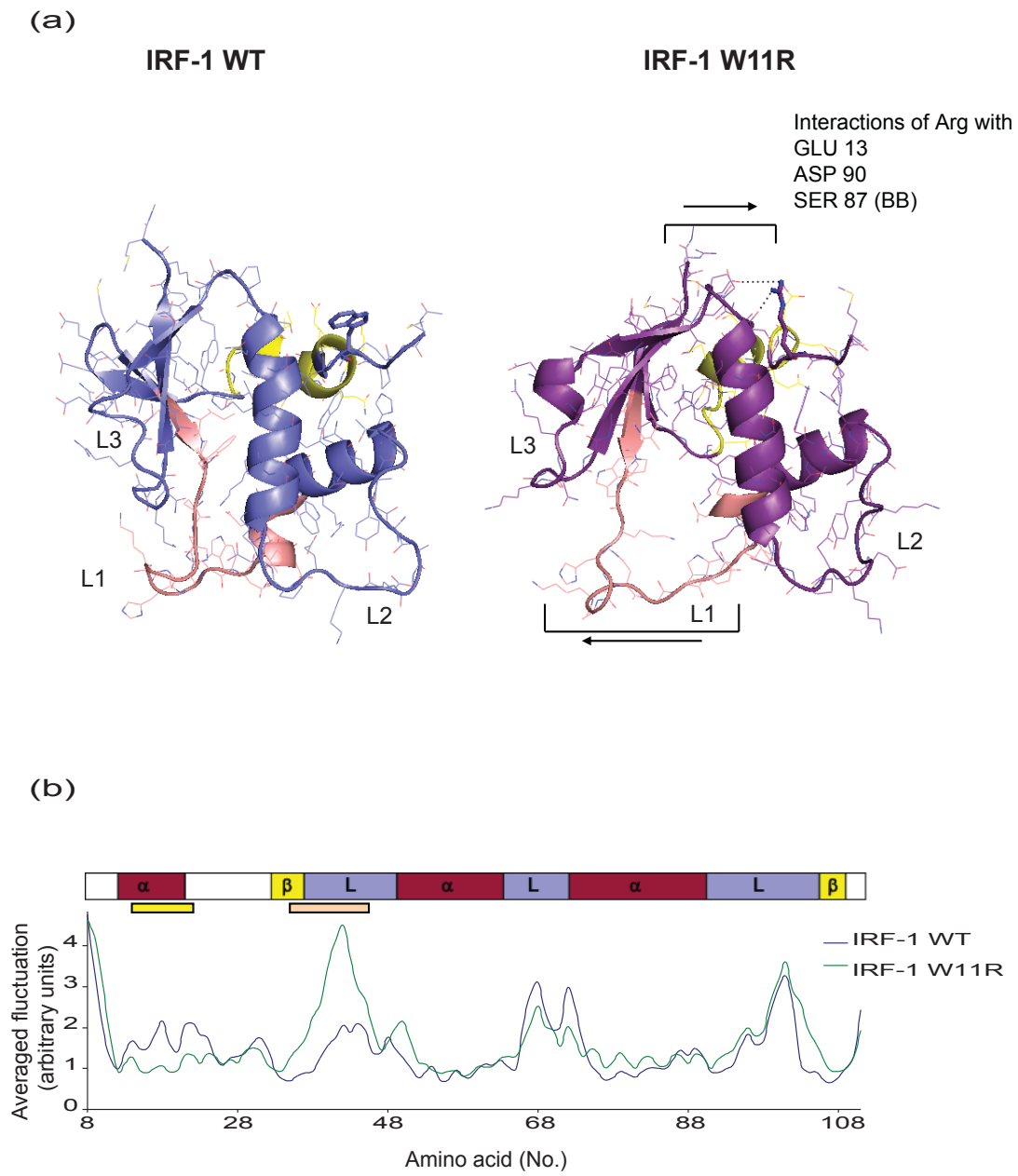

Figure 4-10 Effect of W11R mutation on IRF-1 structure

(a) Snapshot of molecular dynamic simulation of the IRF-1 DBD WT or W11R after 50 ns in the absence of DNA. Changes in the conformation of the DBD by substitution of Trp^{11} to Arg are indicated. (b) Averaged fluctuation of Cα atoms of all amino acids in the simulation after an initial stabilisation period. The corresponding three-dimensional is shown above the graph with α=α-helix, β=β-sheet and L=loop. Regions of higher flexibility in the mutant are indicated by yellow/orange bars.

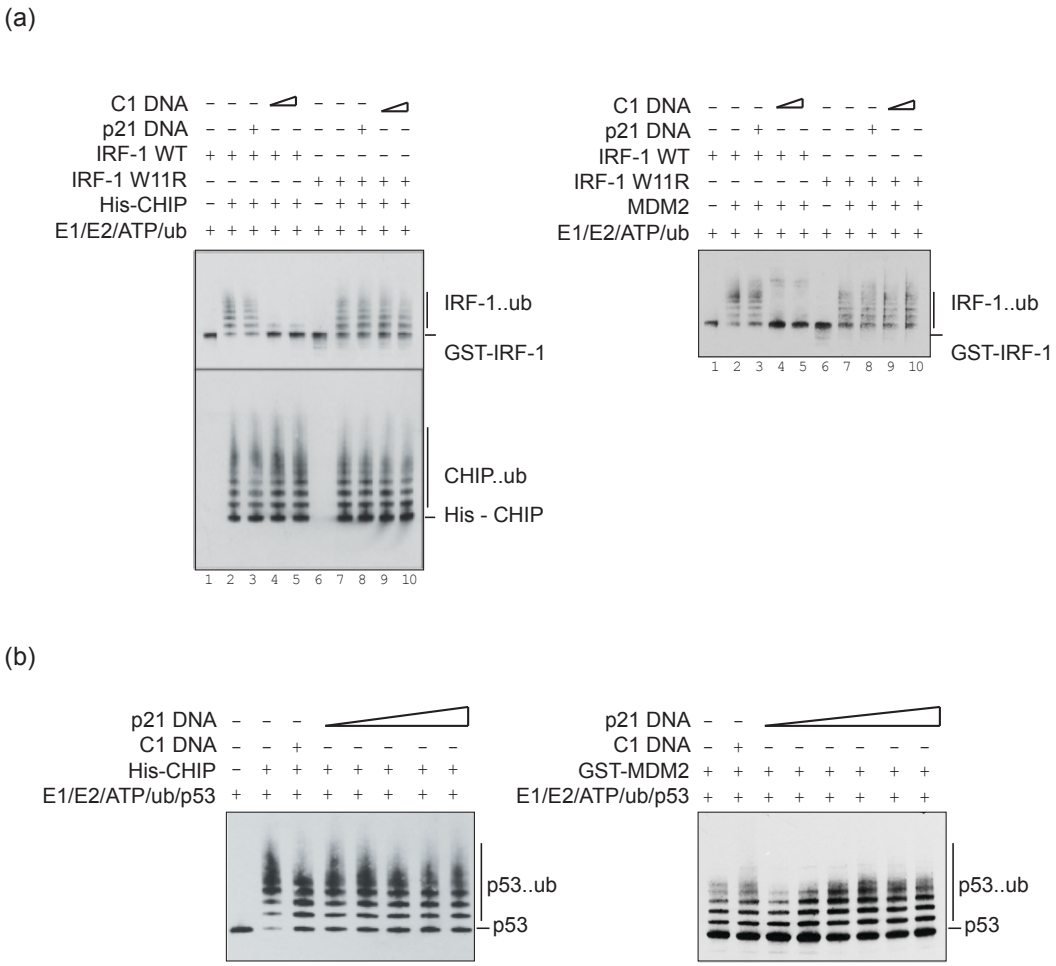

Figure 4-11 DNA bound IRF-1 is protected from ubiquitination *in vitro*

(a) *In vitro* ubiquitination assay using GST–IRF-1^{WT} and GST–IRF-1^{W11R} as substrate with a titration of either C1 oligonucleotides or p21c DNA (0.25 and 1 μM) using CHIP (left-hand panel) or MDM2 (right-hand panel) as the E3 ligase. (b) *In vitro* ubiquitination assay with p53 as the substrate and a titration of p21 promoter DNA (10 nm–1 μM) or C1 DNA (500 nM) with either CHIP (left-hand panel) or MDM2 (right-hand panel) as the E3 ligase**.**

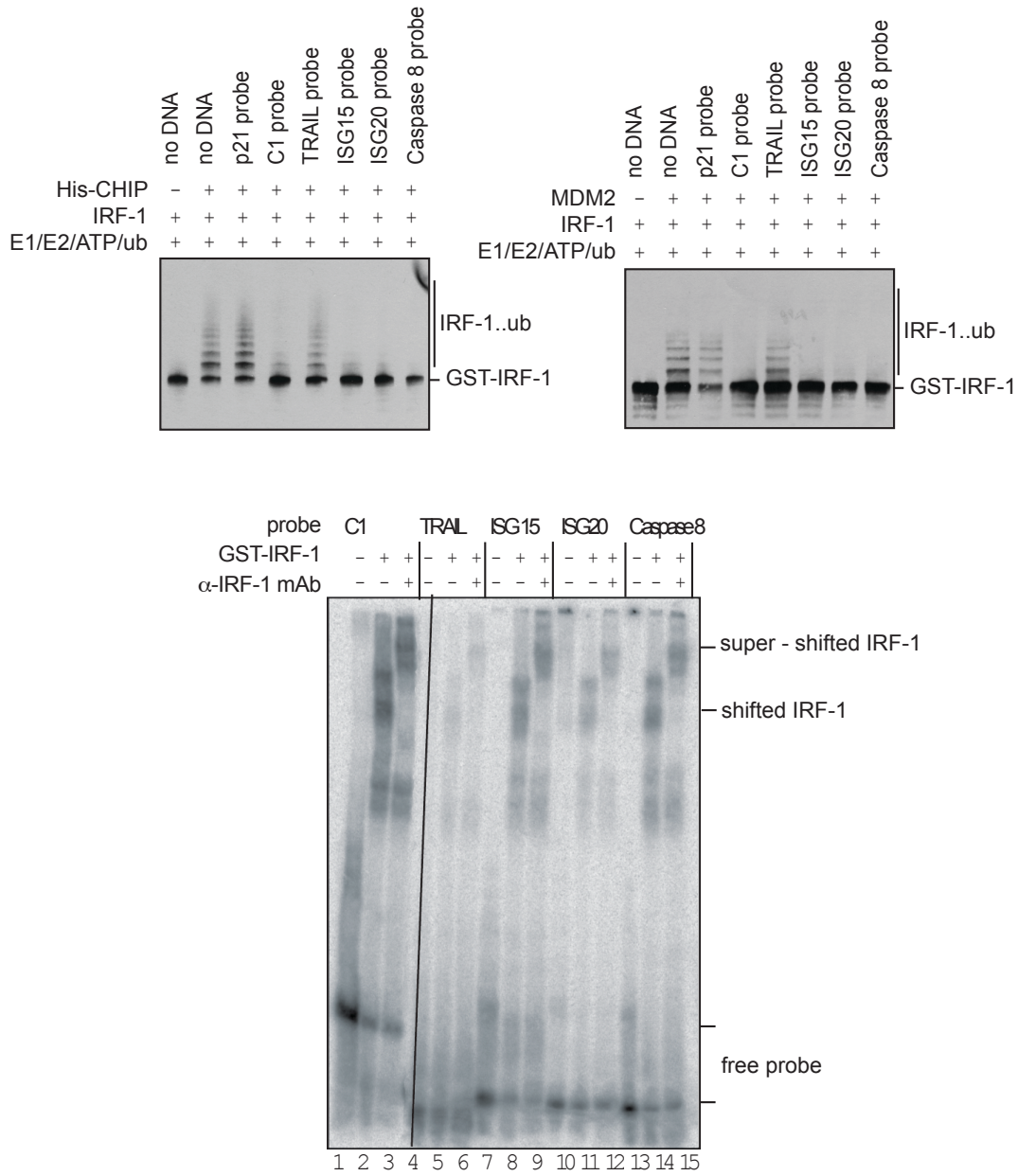

Figure 4-12 The ability of oligonucleotides to inhibit ubiquitination correlates to their binding affinity for IRF-1

The effects of oligonucleotides from promoters of different IRF-1-inducible genes (3 μM) were tested on the ubiquitination of IRF-1 by CHIP (top left-hand panel) and MDM2 (top right-hand panel) and compared with the ability of GST–IRF-1 (300 ng) to bind to the oligonucleotides in a band-shift assay (bottom panel). Where indicated, an anti-IRF-1 antibody was added to the reaction to supershift the complex.

4.2.6 IRF-1 bound to DNA is unable to associate with proteins that interact with its Mf2 domain

There are at least two possible mechanisms that could explain the loss of IRF-1 ubiquitination when in its DNA-bound form; first the targeted lysine residues may be 'cryptic' and consequently inaccessible to the ligases, or secondly, the ability of IRF-1 to bind to CHIP or to MDM2 may be impaired. As the available structural data for the DBD of IRF-1 bound to its consensus DNA sequence [124] suggests that at least some of the required lysine residues are still available for ubiquitination (Fig 4-7; for example Lys^{50}), I went on to investigate the second option, i.e. a change in the affinity of IRF-1 for Mf2-binding proteins. I therefore, studied the effects of IRF-1 DNA binding on its ability to interact with MDM2 and CHIP. Protein-interaction assays were used to measure CHIP binding to IRF-1 protein that had been pre-incubated with either C1 oligonucleotide or control DNA (p21c). Initial titrations demonstrated binding of native unliganded IRF- 1 in solution to immobilized CHIP in a dose-dependent manner (Fig 4-13a, left-hand panel). On the basis of this assay, a fixed amount of CHIP was immobilized and incubated with a constant amount of IRF-1 that had been pre-incubated with a titration of either C1 or p21c. Figure 4-13a (right-hand panel) shows that whereas IRF-1 binding to CHIP was largely unaffected by p21c, titration of C1 into the assay inhibited CHIP binding. The results of this assay suggest that stable binding of CHIP to IRF-1 is severely restricted when IRF-1 is in its DNA-bound form. Similarly, when I tested binding of MDM2 to IRF-1 in its DNA-bound and -unbound form, MDM2 bound preferentially to the unbound form of IRF-1 (Fig 4-13b). The docking site of MDM2 and CHIP on IRF-1, the Mf2 domain, is a multi-protein-binding site that interacts with a number of other IRF-1 regulators [127], I was thus interested to investigate whether DNA binding also affects the interactions of other Mf2 domain interactions proteins with IRF-1. The effects of DNA binding on the interaction between IRF-1 and Kap-1, SET and NPM were tested individually. Figure 4-13b shows reduced binding of IRF-1 to all Mf2 interacting proteins used in this assay when in its DNA-bound state. The crystal structure of the IRF-1 DBD in complex with its cognate promoter-binding element suggests that residues from within the Mf2 domain are not required for DNA binding; hence the results of the present study can be interpreted in two way's (i) that

access to the Mf2 interface is controlled through changes in the conformation of IRF-1 rather than through direct competition or (ii) that even though the E3 ligases do not bind directly to the DBD, binding of DNA would sterically inhibit access of the proteins to the binding site. To test whether CHIP and MDM2 binding had a reciprocal effect on DNA binding I examined whether the ligases could compete with DNA for binding to IRF-1 using an EMSA (Fig 4-14). Neither CHIP nor MDM2 had any effect on the ability of IRF-1 to bind to DNA, suggesting that IRF-1 has a higher affinity for DNA than for the Mf2-binding protein.

In summary, the experiments presented here suggest that Mf2-domain-binding partners are likely to function only on the unliganded form of IRF-1. Furthermore, the observation that neither MDM2 nor CHIP is able to ubiquitinate IRF-1 unless they are bound to the protein, lends strong support for a direct relationship between E3-ligase binding, ubiquitination and site specificity.

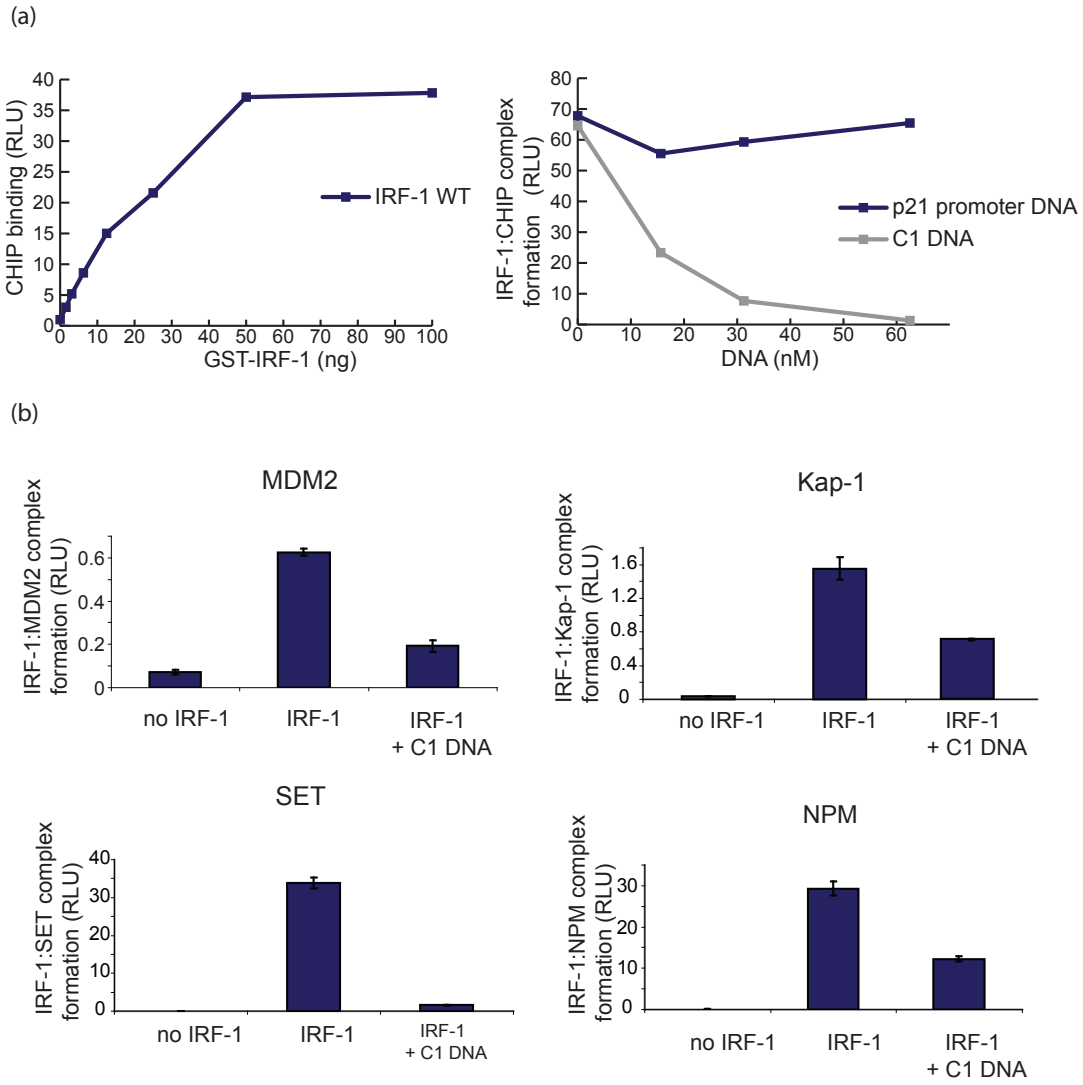

Figure 4-13 IRF-1 bound to DNA is unable to associate with proteins that interact with its Mf2 domain

(a) His–CHIP (100 ng) was immobilized on a microtiter plate and incubated with either a titration of purified GST–IRF-1 alone (0–100 ng) (left-hand panel) or with constant amounts of GST–IRF-1 (100 ng) and a titration of C1 DNA or p21c DNA (right-hand panel). (b) Different Mf2-domain-binding proteins, MDM2, SET, Kap-1 and NPM, were immobilized on a microtiter plate (100 ng) and incubated with GST–IRF-1 (100 ng) and C1 or p21c DNA (100 nM). Binding was detected using an anti-IRF-1 mAb.

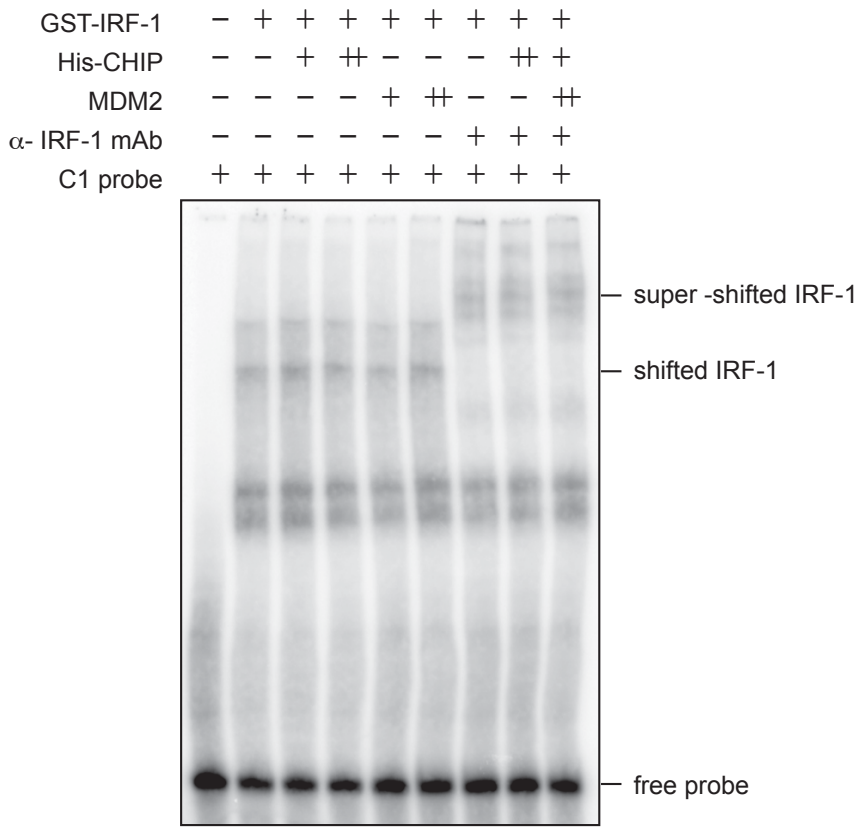

Figure 4-14 MDM2 or CHIP do not affect the ability of IRF-1 to interact with DNA *in vitro*

EMSA presenting binding of 300 ng of purified GST–IRF-1^{WT} to a 32P-labelled DNA probe of C1 DNA in the presence of 0.3 or 1.5 µg of purified His–CHIP or MDM2 as shown. When indicated an anti-IRF-1 mAb was added to the reaction to supershift the protein–DNA complex.

4.2.7 Ubiquitination of IRF-1 in cells is enhanced in a DNA-binding mutant

Taken together, the above observations led us to hypothesize that IRF-1 is protected from ubiquitination, and therefore presumably from degradation, when it is in its transcriptionally active DNA-bound conformation. To study this hypothesis, I determined whether the W11R non-DNA-binding mutant of IRF-1 was more or less prone to ubiquitination than the wild type protein. I first confirmed that specific DNA did not inhibit binding of CHIP to IRF-1^{W11R} *in vitro* using a protein– protein interaction assay. CHIP was coated onto a microtiter plate and incubated with IRF-1 plus a titration of C1 DNA (Fig 4-15a). As expected, C1 DNA inhibited binding of IRF-1^{WT} to CHIP, whereas binding of CHIP to IRF-1^{W11R} was not affected by the presence of DNA. To determine if there were any intrinsic differences in the ability of W11R to act as a CHIP substrate, I compared the ubiquitination profile of wild-type and W11R mutant IRF-1 *in vitro*. CHIP ubiquitinated both IRF-1^{WT} and IRF-1^{W11R} to a similar extent *in vitro* (Fig 4-15b). Next in cell ubiquitination assays were carried out in HCT-116 cells using IRF-1^{WT} and IRF-1^{W11R}. When histidine-labelled ubiquitinated proteins were isolated from cells that had been transfected with either IRF-1^{WT} or IRF-1^{W11R} together with His–ubiquitin we found that the IRF-1^{W11R} mutant was hyperubiquitinated when compared with the WT protein (Fig 4-15c, compare lanes 3 and 4). Thus all used experiments support the idea that IRF-1, which is not chromatin associated is more ‘available’ or susceptible to ubiquitination by endogenous Mf2-domain-interacting ligases. Thus, although CHIP ubiquitinates IRF–1^{WT} and IRF-1^{W11R} to a similar extent *in vitro*, in cells the Trp^{11} mutant is preferentially ubiquitinated, supporting the concept that free IRF-1 may be turned over more rapidly than the pool of IRF-1 that is bound, or able to bind, to DNA.

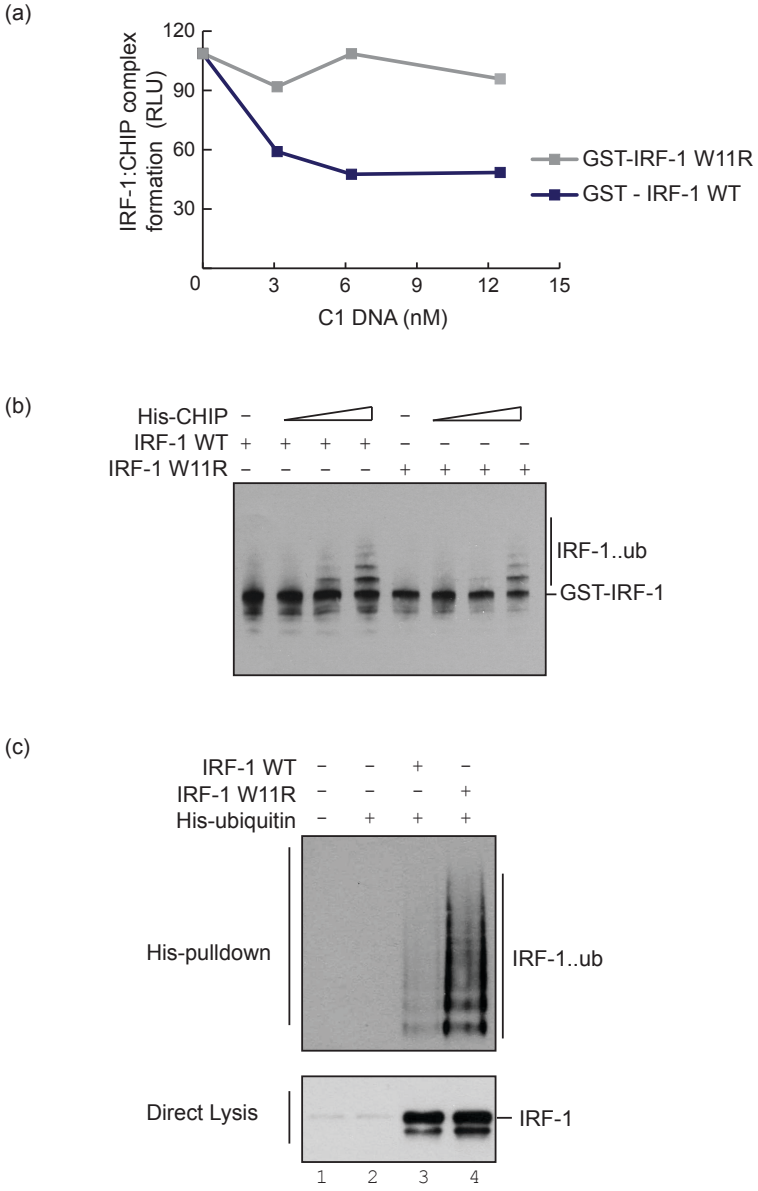

Figure 4-15 Ubiquitination of IRF-1 in cells is enhanced in a DNA-binding mutant
(A) His–CHIP (100 ng) was immobilized on a microtiter plate and incubated with constant amounts of either GST–IRF-1^{WT} or GST–IRF-1^{W11R} (100 ng) and a titration of C1 or p21c probe. (B) *In vitro* ubiquitination assay using GST–IRF-1^{WT} or GST–IRF-1^{W11R} as substrate with a titration of His–CHIP (0–60 ng). (C) HCT-116 cells were co-transfected with pcDNA3-IRF-1WT or pcDNA3-IRF-1W11R (0.5 µg) and His–ubiquitin (0.5 µg) as shown. At 20 hours post-transfection cells were treated with MG132 (50 µM) for 4 hours and histidine-labelled ubiquitinated protein was isolated using Ni-NTA chromatography and analysed by SDS/PAGE and immunoblotting. Total amounts of IRF-1 in the sample (bottom panel) and His-ubiquitin modified IRF-1 (top panel) are shown.

4.2.8 CHIP preferentially ubiquitinates folded substrates

As CHIP binding to IRF-1 is required to facilitate its ubiquitination and because DNA binding either sterically inhibits CHIP binding or leads to conformational changes that do not allow CHIP to bind, I was interested to determine whether the conformation of IRF-1 is an essential determinant for its ability to act as a substrate for CHIP. In a first step, I determined the thermostability of IRF-1. Specifically, FL GST-IRF-1 was incubated for 5 or 15 minutes at 30, 40, 50, 60, 70 or 80°C either in the presence or absence of C1 DNA and subsequently its ability to bind to C1 DNA was determined using an EMSA (Fig 4-16). The results of this assay show that IRF-1 in an unbound conformation is less thermostable than when associated with DNA and looses its DNA binding activity at temperatures over 40°C, with complete loss at a temperature over 50°C. IRF-1 bounds to its cognate DNA sequence, on the other hand, exhibits higher stability and remains active for DNA binding at temperatures up to 50°C. The tumour suppressor protein p53 is extremely thermo-unstable and looses DNA binding ability at a temperatures over 37°C *in vitro* [332].

Conventional wisdom would suggest that the unfolded, soluble protein should be an ideal substrate for CHIP due to its role in the protein triage pathway, where it targets misfolded proteins for degradation. In order to investigate how unfolding affects IRF-1's and p53's ability to act as a substrate for CHIP mediated ubiquitination, first the ability of CHIP to interact with heat inactivated, soluble IRF-1 or p53 was determined using a protein-protein interaction assay. CHIP was coated onto a microtiter plate and incubated with a titration of GST-IRF-1 or p53, which had been pre-incubated at either 4, 42 or 52°C (Fig 4-17a) and then centrifuged at high speed to ensure that the protein was soluble rather than denatured aggregates. Interestingly, CHIP preferentially binds to folded proteins, with a loss in binding correlated to heating temperature of IRF-1 or p53. To determine if this loss in binding is reflected in the ability of CHIP to act as E3 ligase, *in vitro* ubiquitination assays were assembled, using CHIP as the E3 ligase and GST-IRF-1 or p53, folded or heat inactivated, as substrates. Results of this assay (Fig 4-18) show a positive correlation between the decrease in CHIP's ability to facilitate ubiquitination of IRF-1 and p53 and the temperature at which the proteins had been incubated prior to the assay. It

has to be noted that strong ubiquitination can lead to the formation of high molecular mass adducts that can not be detected on the gel and therefore ubiquitination can results in loss of the protein signal on the gel (see Fig 4-18, lane 2+3 for IRF-1 and p53).

The above result are surprising, as CHIP has been described as a major player in the cell's triage decision, targeting proteins that are denatured, beyond the possibility to be refolded by chaperones, for degradation. We would, therefore, expect CHIP to be able to bind to and ubiquitinate substrates in their unfolded conformation. As CHIP works both as a direct binding ligase and as a chaperone associated E3 ligase (see Chapter 3), we were interested to find out if the Hsp70/Hsp40 chaperones had an effect on CHIP's ability to act as an E3 ligase for heat inactivated substrates. *In vitro* ubiquitination assays were assembled as above, with IRF-1 and p53 pre-incubated at 4 or 52°C, CHIP as the E3 ligase and a titration of Hsp70/Hsp40 (ratio 1:10). The results of the assay show that whereas Hsp70/40 inhibit ubiquitination of both IRF-1 and p53 by CHIP, when the substrates are in their native conformation (discussed in detail in Chapter 3), they had no inhibitory activity and in the case of p53 even increase ubiquitination, when the unfolded proteins were provided to CHIP as the substrate. This suggests two distinct roles of CHIP as an E3 ligase (i) it acts as a direct E3 ligase on folded substrates (as shown for IRF-1 by Narayan *et al*.[130]) and (ii) it ubiquitinates unfolded substrates in a Hsp70 dependent manner as part of the cells triage system.

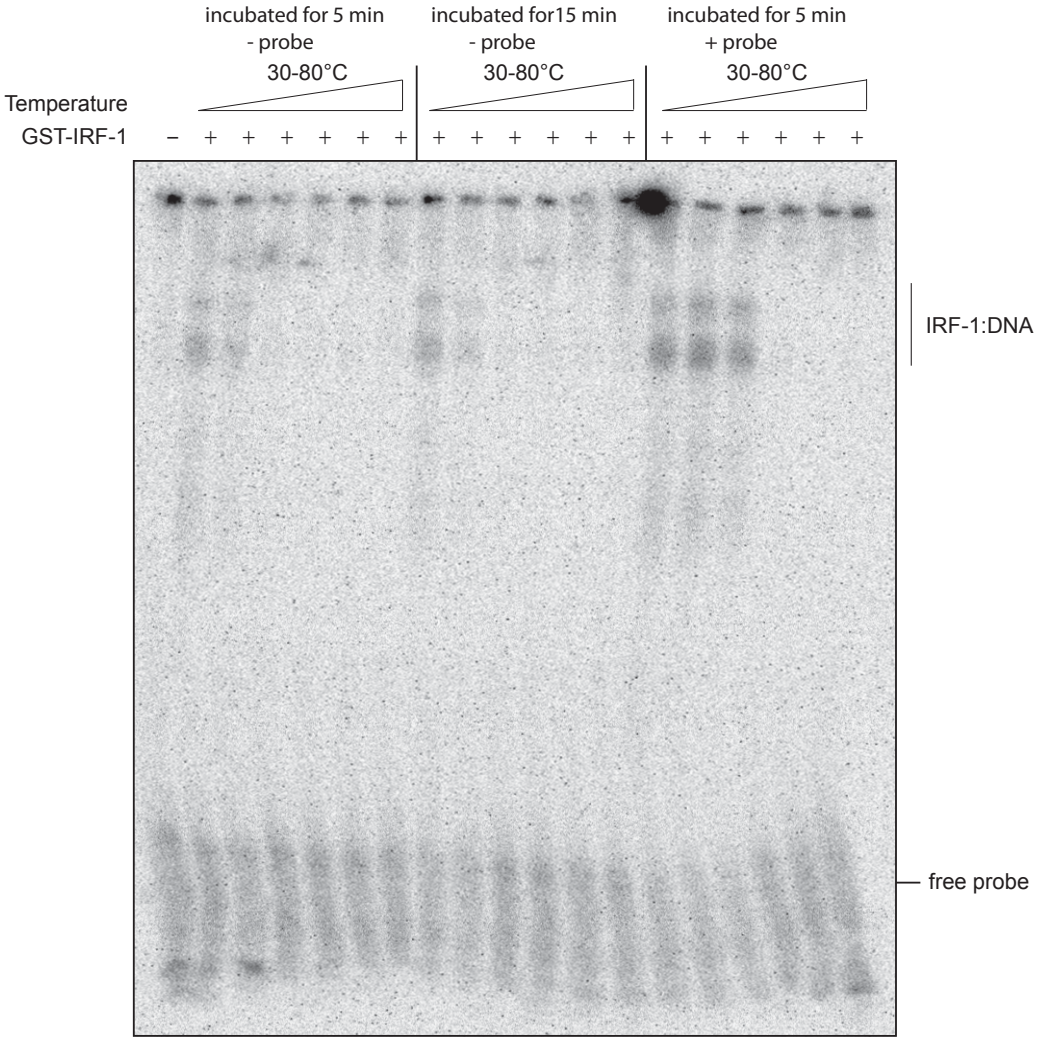

Figure 4-16 IRF-1 is more temperature sensitive in its free, DNA unbound conformation

GST-IRF-1 was incubated in the absence or presence of C1 done at increasing temperature (incubation time and temperature as indicated), subsequently the ability of 100 ng IRF-1 to bind a 32P-labelled DNA probe of C1 was determined using in an EMSA.

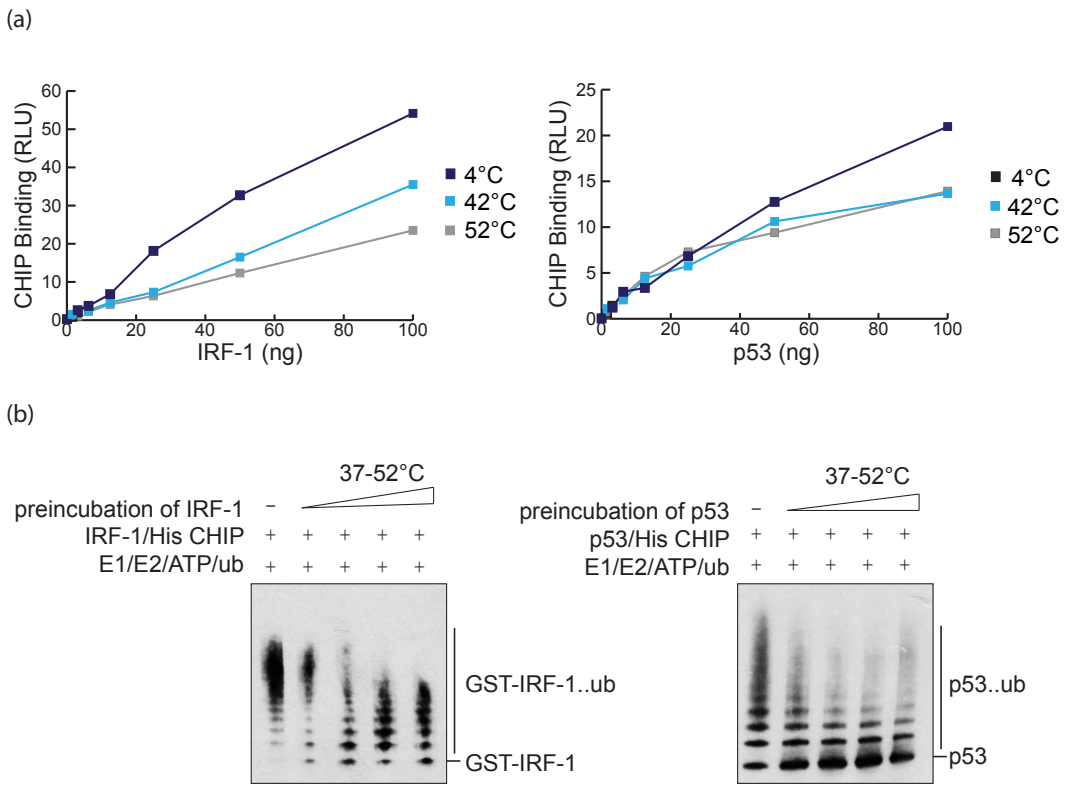

Figure 4-17 CHIP preferentially binds and ubiquitinates folded IRF-1 and p53 protein
(a) His-CHIP was immobilised on a microtiter plate and incubated with increasing amounts of GST-IRF-1 (left panel) or p53 (right panel) that had been pre-incubated at the indicated temperatures for 5 minutes. Binding of the two proteins was detected using an IRF-1 or p53 mAbs respectively. (b) *In vitro* ubiquitination assay with GST-IRF-1 (left panel) or p53 (right panel), that was pre-incubated for 5 minutes at the indicated temperatures, with CHIP as the E3 ligase. The reactions were incubated for 15 minutes and analysed using western blotting.

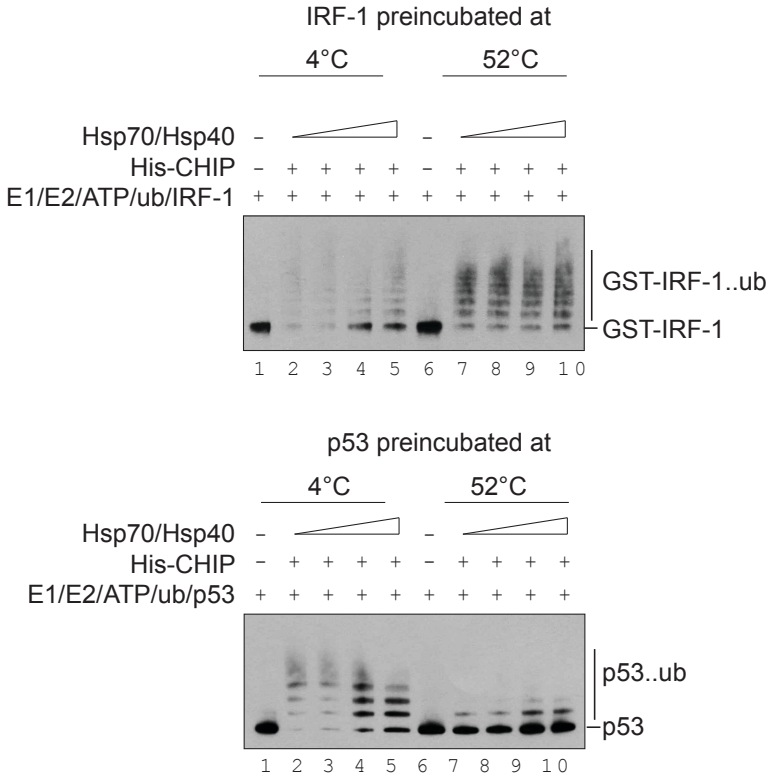

Figure 4-18 Hsp70 inhibits ubiquitination of folded, but not denatured CHIP substrates

In vitro ubiquitination assay with CHIP, a titration of Hsp70/40 (ratio 1:10) (3, 6, 15 μM Hsp70) and IRF-1 (upper panel) or p53 (lower panel) that were pre-incubated at 4 or 52°C for 5 minutes. p53 and IRF-1 were detected by immunoblot using mAbs.

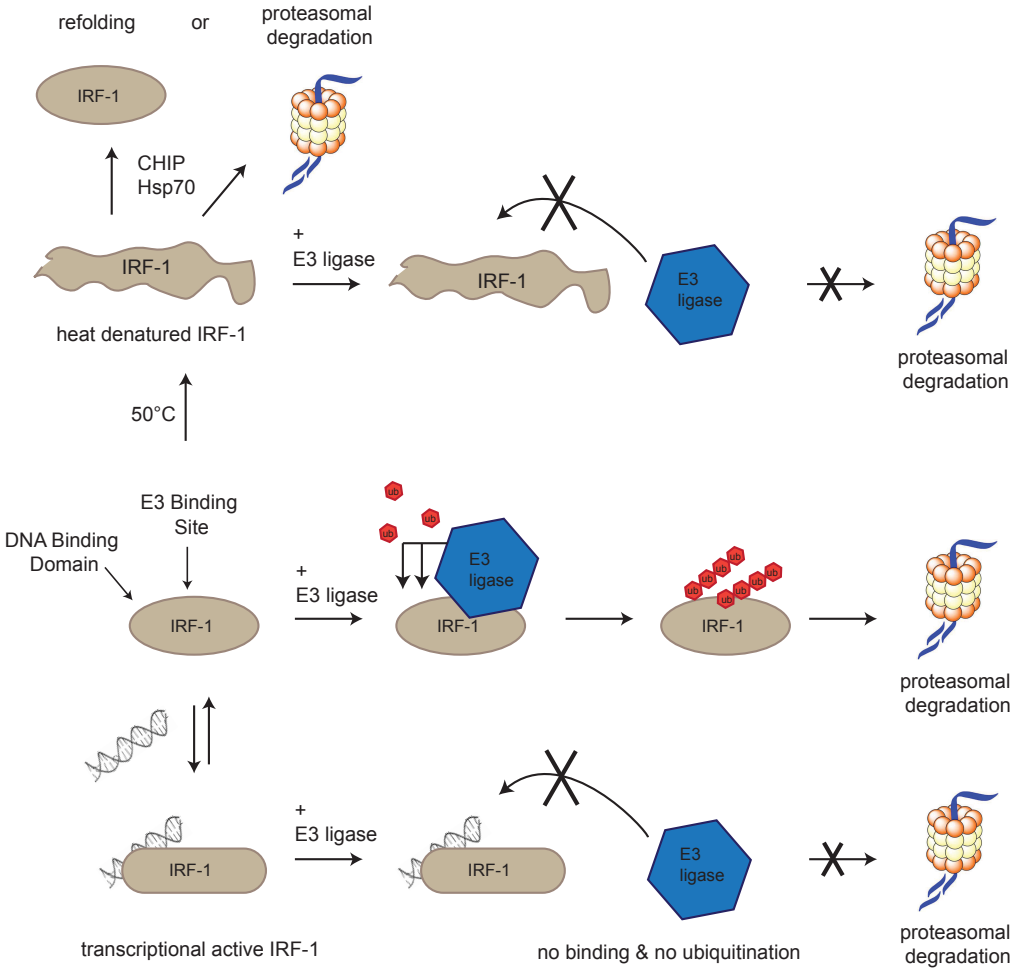

Figure 4-19 Model of interplay between DNA binding of IRF-1 and binding/ubiquitination by its E3 ligases

The Mf2 domain is a multi E3-ligase-docking site in close proximity to the DBD of IRF-1. Binding of E3 ligases to the Mf2 domain results in ubiquitination of the proximal DBD and this leads to the proteasomal degradation of IRF-1. In complex with DNA or in a denatured conformation, however, IRF-1 is unable to bind E3 ligases, is not ubiquitinated and thus protected from degradation.

4.3 Discussion

In recent years ubiquitination has been linked to a wide variety of cellular effects and it is now apparent that ubiquitin modification is involved in not only the proteasomal degradation system, but also serve as a molecular signal in a wide variety of cellular pathways [6, 8]. This raises the question of how the ubiquitin reaction is controlled to lead to different outcomes. Differences in the result of ubiquitination can be achieved by two factors, the linkage and length of the ubiquitination chain and the position of the target lysine in the acceptor protein [28]. However, how interplay between E3 and E2 leads to ubiquitination of specific residues remains largely unclear. One proposed mechanism is that the E3 positions the charged E2 in close proximity to the target lysine and thereby determines which residue is subject to modification [28]. Analysis of the UbcH5c - ubiquitin complex by both NMR and SAXS [333] has shown that the conjugate is very flexible and can exhibit a range of conformations in solution, explaining how one E3 ligase can result in ubiquitination of different lysine within one target protein. Here, the flexibility of the E2 enzyme could be restricted by binding of an E3 and thus result in targeting of specific lysines in the substrate. The data presented in this chapter is in good agreement with this mechanism, we propose that IRF-1 ubiquitination is specific to its DBD and that this is achieved through docking of E3 ligases to its Mf2 domain followed by ubiquitination of the lysine residues in close proximity. I can reason that the E3 ligase-docking site on the substrate defines which lysines are modified, and that this is achieved purely by steric determents. Lysines within the Mf2 itself and other DBD lysines are not subject to ubiquitination, suggesting that ubiquitination of these residues is sterically unfavourable or occluded by the E3 itself. It is interesting that binding of CHIP and MDM2 to the same site on IRF-1 can result in distinct Lys specificity with MDM2 able to ubiquitinate Lys^{95}, but not Lys^{78}, whereas no CHIP-dependent modification of Lys^{95} was detected. I can conclude that the E3 ligase-docking-site on the substrate defines the lysines that can be modified but that there must be additional determinants that are specific to the E3 rather than to the docking site or the E2~Ub complex.

We identified five residues in the IRF-1 DBD to be modified by either CHIP or MDM2, *in vitro* ubiquitination assay results utilising an ubiquitin mutant that exclusively leads to monoubiquitination, show that no more than three single ubiquitins are attached to IRF-1 at any one time. This, together with the fact that single point mutations at the IRF-1 ubiquitination sites to arginine do not change the efficiency of IRF-1 monoubiquitination, and molecular modelling results that predict ubiquitination of sites Lys^{39}, Lys^{50} and Lys^{78} resulting in the ubiquitin molecule occupying the same three dimensional space, suggest that not all target lysines can be ubiquitinated at any given time, but that ubiquitination of the sites is mutually exclusive. This suggests a mechanism where ubiquitination is specific to a certain protein domain, where several, but not all, lysine residues of this domain can be targeted resulting in the same molecular signal. We speculate that once the E3 ligase forms a complex with the charged E2 and the substrate, any lysine which lies in close proximity to the complex can be linked to the activated ubiquitin, this leads to specific modification of the lysines in a favourable position for the E3-E2 interaction site. This is in line with the fact that many substrates have been shown to be modified at several residues within a distinct domain [28].

Why and how, a specific lysine residue can be targeted or whether IRF-1 ubiquitination is purely domain specific remains unclear. One possibility is that through the involvement of other proteins in the ubiquitination enzyme complex ubiquitin could be sterically targeted towards one specific residue. The fact that MDM2 and CHIP ubiquitinate two different residues and that not all lysines in the DBD are subject to modification suggests that E3 ligases target specific residues in addition to protein domains. This could be controlled by the exact positioning of the E3 on the substrate only allowing access of certain target lysines to the ubiquitin loaded E2.

The observation that DNA binding protects IRF-1 from ubiquitination is intriguing as it suggests a mechanism by which turnover of this transcription factor might decrease when it is in an active state, i.e. when part of a pre-initiation complex. In recent years, it has become clear that the ubiquitin–proteasome system and the transcriptional machinery are intimately linked, and that ubiquitin-mediated

proteolysis can enhance the activity of TAs (transcriptional activators). This is known as the 'activation by destruction' mechanism [334] and was first indicated by the observation that the transactivation domain and the region required for degradation (degron) overlap in many TAs, including IRF-1 [335]. This led us to think it would be interesting to investigate the exact interplay between IRF-1 activation and ubiquitination (chapter 5).

The Mf2 domain is a multi protein binding interface on IRF-1, DNA binding abolishes interactions between IRF-1 and several of its Mf2 domain binding partner, resulting in a subset of IRF-1 interactions partner that can only take place when IRF-1 is ligand free, and inactive. We propose that the Mf2 domain is a docking site for multiple E3 ligases and that, since docking is required for ubiquitination, ligand bound IRF-1, is protected from ubiquitination and subsequent degradation (see model, 4-19). This suggests a mechanism by which ubiquitination of IRF-1 is regulated through its DNA binding state, in its active, DNA bound conformation IRF-1 is not recognised by its E3 ligases, however, as soon as it dissociates from the DNA, IRF-1 can be targeted for ubiquitination and degradation, resulting in fine regulation of the protein levels in the nucleus. In this way even though active DNA bound IRF-1 is not ubiquitinated, it could be turned over quickly once it dissociates from the promoter of target genes.

The most popular hypothesis to explain the connection between degradation and TA function in gene expression is based on a 'suicide' model where activator degradation is somehow required as part of the activation mechanism and potentially also to terminate the signal [91]. Implicit in this model is that the TA is not subject to degradation prior to completing its function or when part of an active DNA-bound complex [91]. Here I show that DNA-bound IRF-1 has an inaccessible E3-binding site, and that a non-DNA binding mutant of IRF-1 is hyperubiquitinated in comparison to the wild-type protein (see model, Fig 4-19). The data therefore support the idea that IRF-1 is protected from degradation when it is part of an active pre-initiation complex, but can be rapidly degraded when it is not functional or when it has completed its function.

We have previously shown that the E3 ligase CHIP has two distinct functions (see chapter 3 for details), as a chaperone depended ligase that targets Hsp70/90 client proteins for degradation and as a chaperone independent ligase that directly binds to and ubiquitinates its substrates. Here, I demonstrate the importance of CHIP substrate binding for ubiquitination, in its role as a "direct E3 ligase". If IRF-1 is in a DNA bound or heat denatured conformation, CHIP is unable to directly interact with the protein. As discussed in chapter 3 (Fig 3-1, 4-18), Hsp 70 inhibits ubiquitination of folded IRF-1 and p53 protein, however, in their unfolded conformation Hsp70 does not reduce CHIP mediated ubiquitination and, for p53, even activates ubiquitination *in vitro*. This gives further evidence for two distinguished roles of CHIP function, while it is reported to preferentially target unfolded substrates that are presented by Hsp70, in its direct role, conversely it shows lower affinity and conversion rate for unfolded substrates in the absence of Hsp70. In a cellular context it would be energetically more favourably to refold a protein, rather than for it to be degrades and re-expressed. It is therefore possible, that unfolded proteins are not directly recognised by CHIP, to initially allow binding by the chaperone Hsp70 and only if a protein is misfolded beyond refolding by Hsp70 will it be presented to CHIP and targeted for degradation.

In conclusion, I report here that ubiquitination of specific residues is achieved through the E3 ligase binding site on the substrate and that this is likely to result in modification of several residues in close proximity of the docking site on the substrate; making the modification specific to a subset of lysines residues in a specific domain or region of the protein. Docking of the E3 to its substrate is therefore not only required for ubiquitination but also determines the specificity of the reaction. If the E3 cannot bind to its substrate, for example when IRF-1 is bound to DNA or unfolded, it is not able to mediate DBD ubiquitination. The fact that DNA bound IRF-1 is not recognised and ubiquitinated by its two E3 ligases MDM2 and CHIP suggests a mechanism by which an active pool of IRF-1 is protected from degradation in cells.

Chapter 5: The role of monoubiquitination in the control of p53 and IRF-1 transactivation activity

5.1 Introduction

5.1.1 Ubiquitination in transcriptional control

Regulating the rate of gene transcription is fundamentally important in the control of normal cellular development, differentiation and homeostasis. Therefore, levels and activity of transcription factors are regulated very tightly ensuring fine control of gene expression. Recently the importance of the ubiquitin-proteasome system in regulating transcription factor activity has been illustrated; this can be achieved by proteolytic as well as non-proteolytic functions of both ubiquitin and the proteasome [91].

Most transcription factors have a very short half-life, allowing tight regulation of their steady state cellular levels by small changes in the rate of synthesis and/or degradation. Levels of p53 are kept low by constant ubiquitination followed by degradation in unstressed cells, only in response to certain cellular signals, p53 E3 ligases are prevented from ubiquitinating their target, leading to an increase in p53 levels and its activity. However, the well-studied control of transcription factor activity by destruction is only one of several mechanisms by which the ubiquitin proteasome machinery is involved in transcription control. Several recent studies have highlighted the role of the UPS in the control of different factors of the transcription machinery via non-proteolytic activities. One of the first links between transcription factor activity and ubiquitination was made by Salghetti *et al.* in 1999 [336, 337], and showed that the TAD and degron of the transcription factor Myc are functionally connected, with an overlap of the region that signals for ubiquitin-mediated proteolysis and that which is required to activate transcription. Subsequent studies showed that degron function was a general feature of many activation domains that are rich in acidic residues, and that transcriptional activation potential correlates closely with degron function [91]. There are at least thirty transcription

factors with an overlapping TAD and degron, including IRF-1 and p53 (Fig 5-1) and everal transcription factors are now known to be most active when less abundant. These observations have led to an 'activated by destruction' model of transcription factor activity and taken together these studies suggest a strong link between TA stability and activity. In line with this are results by Salgehtti *at al.*[338], which showed that activation of the synthetic activator LexA-VP16 in yeast is dependent on the E3 ligase Met30, which leads to LexA-VP16 ubiquitination and destruction. This observation is intriguing as one would predict that blocking the E3 ligase that leads to destruction of a specific transcription factor, would increase its levels and thus its activity. However, blocking Met30 inhibits LexA-VP16 activity and this can be rescued by fusion of an ubiquitin molecule to the N-terminus of the protein, demonstrating that ubiquitination of LexA-VP16 is directly required for its activity. The Met30 study therefore indicates a direct connection between ubiquitin modification and enhanced function of transcription factor activity. Several other transcription factor have now also been shown to require activity of their respective E3 enzyme in order to be fully active, including Myc, HPV E2, Gal-4 and Tat [338-341]. The exact mechanism by which ubiquitination can enhance the transactivation potential of a given transcription factor remains elusive. Several different mechanisms have been proposed, including recruitment of parts of the proteasome to the site of transcription, which in turn are suggested to function as activators. An example of this is the transactivator Tat, encoded by the human immunodeficiency virus type 1 (HIV-1). Activity of Tat is dependent on ubiquitination by MDM2, and this was suggested to mediate recruitment of the 19S particle to the HIV-1 promoter, activating Tat-mediated transcription [340]. Another possible mechanism of how ubiquitination could facilitate transcription is through the recruitment of different factors to the site of transcription initiation. For example monoubiquitination of the transcriptional co-activator CIITA, which associates with MHC II transcription factors and the MHC class II promoter to form an active enhanceosome, positively regulates its assembly at the promoter [342].

As ubiquitination can both activate and degrade a number of transcription factors a 'licensing model' was proposed [338], where monoubiquitination leads to activation of the proteins transactivation potential, but is inevitably followed by polyubiquitination and degradation of the protein. This could lead to instant activation of the transcription factor in response to stimuli and also ensure termination of the activity after the signal has ended. However, more research is needed to reveal the physiological significance of this model and to show which factors might be controlled in such a manner. In summary, posttranslational modification of transcription factors by ubiquitin appears to play a major role in regulating their activity by means that are only party understood.

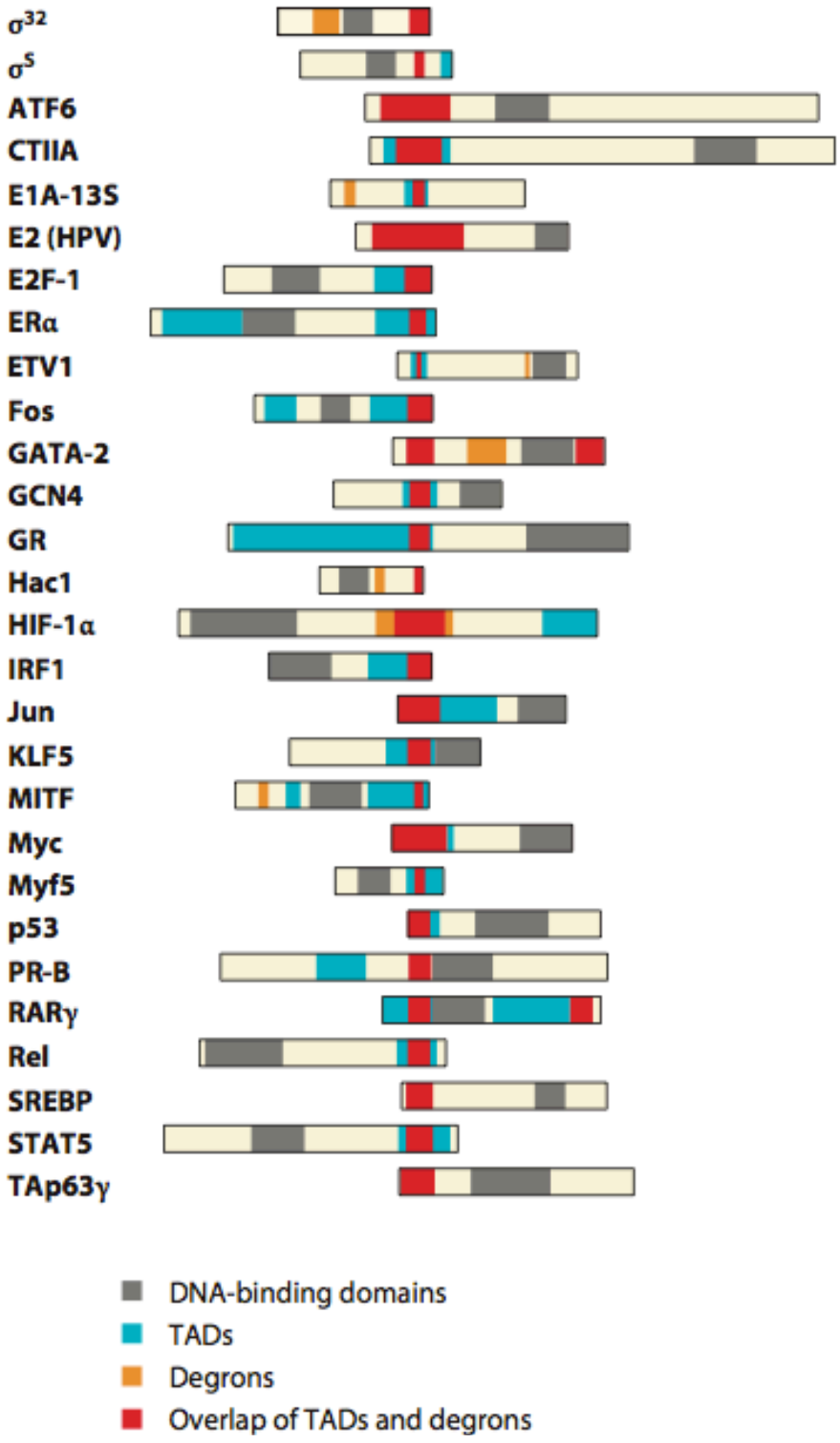

Figure 5-1 Transcriptional regulators with overlapping TAD and degron [91]

Numerous transcription factors with an overlap in the domains involved in their degradation and transactivation have been identified, highlighting the close relationship between these two, seemingly contradictory, functions.

5.2 Results

5.2.1 p53 pathways activation induces its monoubiquitination

The previous chapter of this thesis has focused on the control of the ubiquitination event by accessibility of the E3 ligase. In this chapter I will move on to dissect the effects that ubiquitination has on the transcriptional activity of the tumour suppressors p53 and IRF-1. Novel non-proteolytic functions of ubiquitination are constantly identified, however, the knowledge of how ubiquitination can affect the activity of the transcription factors p53 and IRF-1, besides signalling degradation, is limited. Strikingly, Maki *et al.* have shown in 1997 [230] that IR leads to an increase in ubiquitinated p53 adducts in the cell. Furthermore, the Ball group previously showed that high molecular weight adducts of p53 are induced in cells by treatment with the small molecular activator of p53, Nutlin-3 [198], which leads to an increase in both p53 levels and its transcriptional activity (Fig 5-2), resulting in cell cycle arrest or apoptosis [343]. Nutlins were found in a screen to identify small molecules that could inhibit binding of the MDM2 hydrophobic pocket to a peptide from p53 (Fig 5-2a). Nutlin-3 binds to a p53 binding site in MDM2's hydrophobic pocket, and is generally believed to thereby inhibit MDM2 mediated ubiquitination and degradation of p53 [344].

Intrigued by the possibility of a role of ubiquitination in the p53 activations pathways, I, in a first step, set out to determine the ubiquitination state of transcriptionally active p53. To examine the ubiquitination status of the endogenous proteome under conditions where the p53 pathway is engaged, I started by capturing substrates ubiquitinated in the presence of a His-ubiquitin construct in cells. Briefly, A375 cells, a human malignant melanoma cell line with wild-type p53, were transfected with His-ubiquitin and treated with either the small molecule p53 activator Nutlin-3 or X-ray radiation (IR), both of which are well-characterised activators of the p53-pathway response. Results of the assays show that endogenous p53 ubiquitination is increased in response to activating signals, as several higher molecular weight bands appear following radiation and Nutlin-3 treatment (Fig 5-3). Increase in the levels of p53 transcriptional targets, p21 and MDM2, as a readout of pathway activation could also be observed. These results confirmed the previous

observations made by Maki *et al.* that showed an increase in p53 ubiquitination upon X-Ray and demonstrated that the high molecular weight bands, observed by the Ball group in response to Nutlin-3 treatment, represent ubiquitinated p53.

Interestingly, under these conditions, p53 activation led not only to an increase in the total amount ubiquitinated protein, but also shifted the type of ubiquitination to mainly mono or multi-mono ubiquitinated forms with the first three ubiquitination bands being predominantly present when compared to the control lane (compare lane 4 and 5, Fig 5-2a). This was confirmed by quantifying the first and second monoubiquitin bands (Fig 5-3a; Ub1 and Ub2) relative to the control samples (lane 2 with lane 5; lane 3 with lane 4) in both Nutlin-3 and IR treated cells. This showed (Fig 5-3b) that there was a 5.4- and 3.4-fold increase in the first and second ubiquitin bands in IR-treated cells, respectively; whereas the fold increase in unmodified p53 and the fifth p53-ubiquitin band (Ub5) was 1.5- and 2.3-fold, respectively. Thus, although there is greater increase in the monoubiquitination of p53 in the presence of Nutlin-3 (9.7-fold for Ub1 and 14.1-fold for Ub2, verses 2.2-fold for unmodified p53 and 0.9-fold for Ub5), IR also reproducibly favours the generation of p53-monoubiquitin adducts.

(a)

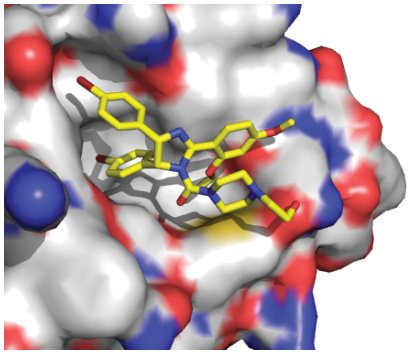

(b)

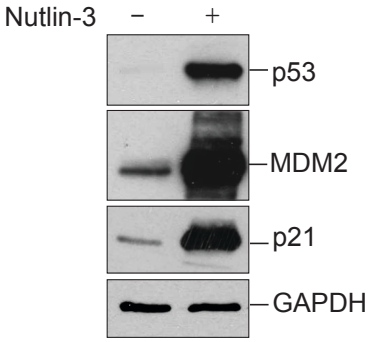

Figure 5-2 Nutlin-3 binds to the E3 ligase MDM2 and thereby activates p53

(a) The small molecular p53 activator nultin-3 (indicated by yellow sticks) crystallised bound to the hydrophobic pocket of MDM2 (shown as surface). (b) A375 cells were treated with 10 μM Nutlin-3 for 8 hours, lysed in Triton-X lysis buffer and analysed by SDS-PAGE/immunoblot with p53, p21, MDM2 and GAPDH monoclonal antibodies. The GI 50 for Nutlin-3 in melanoma cells was shown to be between 5-30 μM [345], therefore a relatively low concentration of Nutlin-3 (10 μM) was used throughout this chapter to reduce unspecific side effects of the drug.

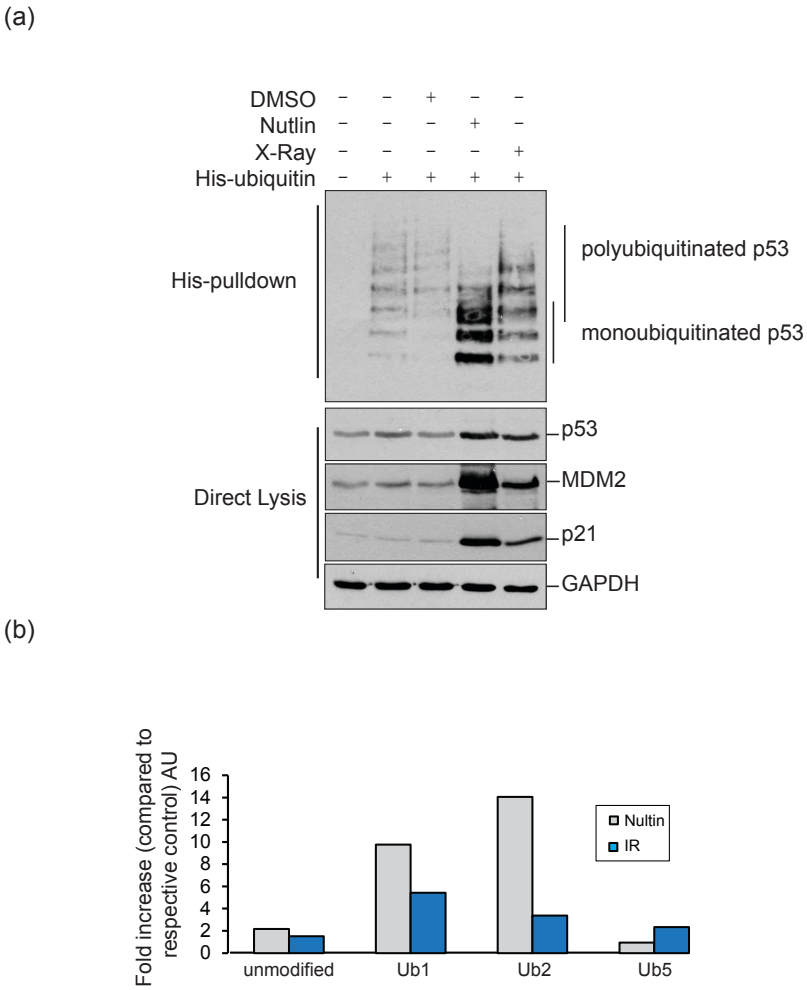

Figure 5-3 p53 is ubiquitinated in response to activation by X-Ray or Nutlin-3 treatment

(a) A375 cells were transfected with His- ubiquitin (0.5 μg) as detailed. Post transfection (24 hours) cells were treated with Nutlin-3 (10 μM) for 8 hours or radiated (5 Gy) and recovered for 3 hours. Subsequently histidine-labelled ubiquitinated protein was isolated using Ni-NTA chromatography and analysed by SDS/PAGE and immunoblot using p53, p21, MDM2 and GAPDH mAb. His-ubiquitinated p53 (upper panel) and total p53, p21, MDM2 and GAPDH in the samples lysed in Tritom-X lysis buffer (lower panel) are shown. (b) Quantification of results from (a) using Image J. The fold increase of unmodified p53 and p53 attached to 1, 2 or 5 ubiquitins in respect to the control samples was calculated and is shown.

5.2.2 p53 and MDM2 form complexes in the presence of Nutlin-3 in cells

In the previous section, I showed that Nutlin-3 leads to a significant increase in p53 monoubiquitination. As Nutlin-3 was previously described as an inhibitor of MDM2's E3 ligase activity, that could prevent the formation of p53:MDM2 complexes and thereby inhibit ubiquitination of p53 by MDM2, we were interested to gain insight into the mechanism by which Nutlin-3 leads to an accumulation of ubiquitinated p53 protein in cells. Therefore, I set out to investigate the effect of Nutlin-3 on binding and ubiquitination of p53 by MDM2 *in vitro* and in cells. To assess the effect of Nultin-3 on binding of p53 to MDM2 *in vitro*, recombinant p53 was coated onto a microtiter plate and incubated with constant amounts of MDM2 that had been pre-incubated with increasing amounts of Nutlin-3. Results of this experiment show that Nutlin-3 interfered with the formation of MDM2:p53 complexes and decreased binding of the two proteins by about 40% *in vitro* (Fig 5-4a, left panel). MDM2 and p53 interact through two distinct motifs. The higher affinity interaction is mediated through residues in the BOX-I motif in p53's N-terminus and the hydrophobic pocket of MDM2, whereas the second weaker binding site is facilitated by the BOX-V motif in the core domain of p53 and the acid domain of MDM2. Interestingly, this second binding site serves as an ubiquitination signal and interaction at this site is required for efficient ubiquitination [198]. As I observed a decrease in binding of p53 and MDM2 in the presence of Nutlin-3 I was interested to determine of this loss is due to disruption of binding at both or one of these interactions sites. Therefore, I carried out peptide binding assays with the BOX-1 or BOX-V p53 peptide immobilised on a streptavidin coated microtiter plate with MDM2, pre-incubated with increasing amounts of Nutlin-3, in the mobile phase. Results of this assay, shown in Figure 5-4a (right panel), are in agreement with previous observations of the Ball group [198] and show that Nutlin-3 inhibits binding of BOX-1 to MDM2, but not between the second binding site of MDM2 and the BOX-1 motif in the p53 core domain, which is required for ubiquitination (Fig 5-6). In fact a small, but reproducible, increase in binding of BOX-V to MDM2 in the presence of Nutlin-3 can be observed. This is an interesting observation as it suggests

that even though Nutlin-3 weakens the interaction between MDM2 and p53, it does not abolish it completely, but shifts binding from one site to another.

To test the effect of Nutlin-3 on the formation of p53:MDM2 complexes in cells, I asked whether MDM2 was detectable in a complex with p53 after Nultin-3 treatment in cells. Specifically, A375 cells were treated with Nutlin-3 for 8 hours, subsequently cells were lysed, and p53 protein was immunoprecipitated from the lysate using a p53 polyclonal antibody. The lysate and immunoprecipitate were analysed by immunoblot, probed for p53 and MDM2. Nutlin-3 treatment resulted in a strong increase in p53 and MDM2 protein levels and MDM2 could be detected in complex with p53 in both control and Nutlin-3 treated cells (Fig 5-4b). The results of the cell based binding assay show that more p53:MDM2 complexes are present in the cell after treatment with Nutlin-3, when compared to control conditions, and that the decrease in binding affinity observed in *in vitro* binding assay is not sufficient to abolish binding of the two proteins *in vivo*. It is difficult to determine if there is a change in relative formation of p53:MDM2 complexes after Nutlin-3 treatment, as the latter results in multiple fold increase of both p53 and MDM2. Taken together these data suggest that binding of p53 to MDM2 by the BOX-V motif, which is stimulated by Nutlin-3, is sufficient for the formation of MDM2/p53 complexes in cells in the presence of Nutlin-3.

In order to investigate whether the increase of p53 ubiquitination is a direct effect of Nutlin-3 binding to MDM2, I assembled an *in vitro* ubiquitination assay with all components of the reaction as purified components and tested the effect of Nutlin-3 on p53 ubiquitination by MDM2 *in vitro*. As shown in Figure 5-5a, Nutlin-3 does not affect the ability of MDM2 to ubiquitinate p53 *in vitro* (under condition where acid domain binding aptamers do inhibit MDM2-activity, right panel). This is in contrast to data obtained in cells, where a time course of Nutlin-3 treatment (50 μM) leads to a gradual increase in p53 ubiquitination (Fig 5-5b), and to the in cell ubiquitination assays, where Nutlin-3 dramatically increases the amount of mono- and diubiquitinated p53 compared to control conditions. Taken together the data demonstrate a novel role for Nutlin-3 in the induction of accumulation of ubiquitin-

p53 adducts in a monoubiquitinated form rather than as polyubiquitin chains. And let me to refine a previous model by the Ball group, where Nutlin-3 acts as an allosteric activator of MDM2-mediated p53 ubiquitination [198], to reflect the fact that Nutlin-3 specifically enhances monoubiquitination, rather than polyubiquitination, of p53 and that Nutlin-3 stimulates the interaction between the acid domain of MDM2 and p53 BOX-V, which is sufficient for complex formation in cells (Fig 5-6).

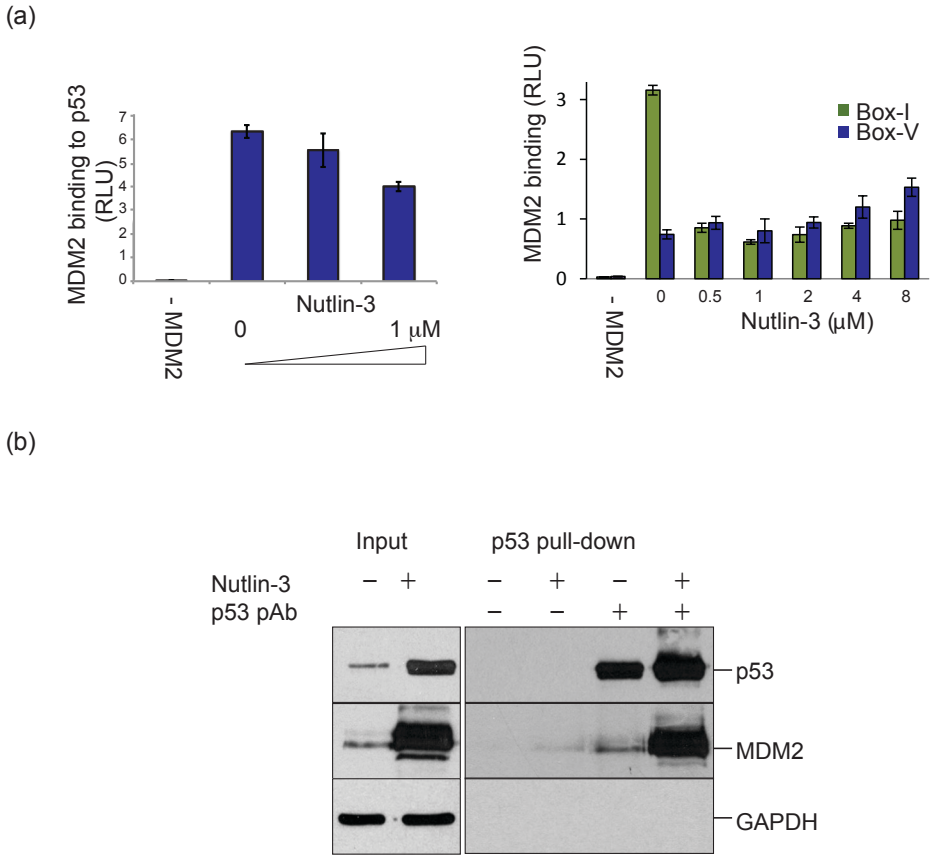

Figure 5-4 Nutlin-3 disrupts the formation of p53:MDM2 complexes *in vitro*, but not cells

(a) p53 (100 ng/well) was immobilized on a microtiter plate and incubated with constant amounts of MDM2 (100 ng) and a titration of Nutlin-3 (0-1 μM). Binding of MDM2 to p53 was detected using an anti-MDM2 mAb (2A10) (b) Co-immunoprecipitation of p53:MDM2 complexes (left panel). Biotin-tagged p53 Box-I (PPLSQETFSDLWKLLP) and Box V (RNSFEVRVCACGRD) peptides were immobilized on a microtitre plate and incubated with 100 ng of MDM2 and a titration of Nutlin-3 (0-8 mM). MDM2 binding to the peptides was detected using an anti-MDM2 mAb (right panel). (b) A375 cells were treated with 10 μM Nutlin-3 for 8 hours and lysed in IP lysis buffer (not denaturing). Lysate was pre-cleared using Sepharose beads and incubated with protein A beads and anti- p53 pAb (CM1) overnight. After washing, proteins bound to the beads were eluted by heating in SDS sample buffer and both lysate and eluate were analysed by SDS-PAGE followed by immunoblotting with anti- p53, MDM2 and GAPDH mAb.

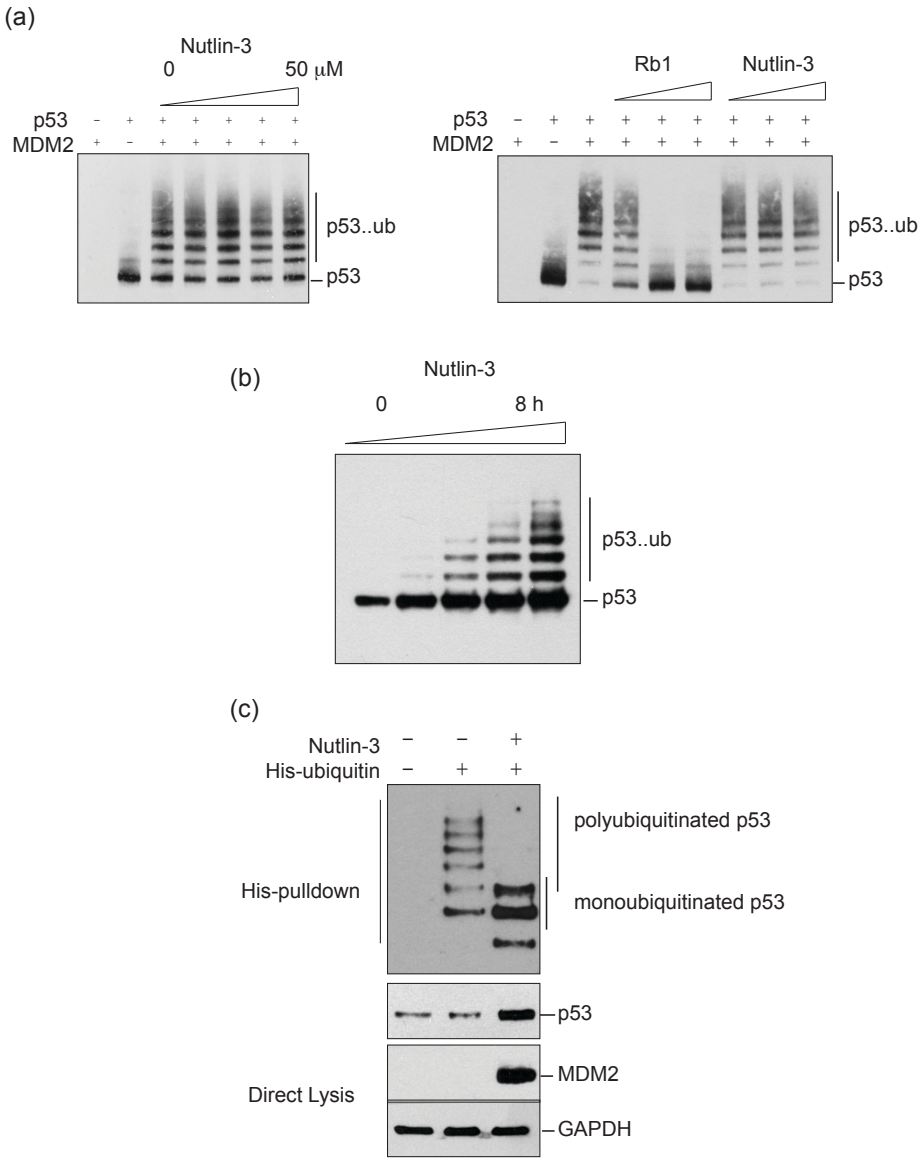

Figure 5-5 Nutlin-3 enhances p53 ubiquitination in cells, but not *in vitro*

(a) *In vitro* ubiquitination assay with p53 as the substrate and a titration of Nutlin-3 (0 -50 μM) (left panel) or a titration (0.5, 5, 10 μM) of Rb1 peptide (DQIMMCSDMYGICKVKNIDLK) and Nutlin-3 (right panel) and MDM2 as the E3 ligase. (b) A375 cells were treated with 10 μM Nultin-3 for 0-8 hours, lysed in urea lysis buffer and analysed by SDS-PAGE/immunoblot using anti- p53 mAb. (c) A375 cells were transfected with His–ubiquitin (0.5 μg) as shown. Post-transfection (20 hours), cells were lysed and histidine-ubiquitinated protein was isolated using Ni-NTA chromatography. Samples were analysed by SDS/PAGE and immunoblotting with the mAbs indicated. Total amounts of p53, MDM2 and GAPDH in the sample extracted using Triton-X lysis buffer (bottom panel) and modified p53 (top panel) are shown.

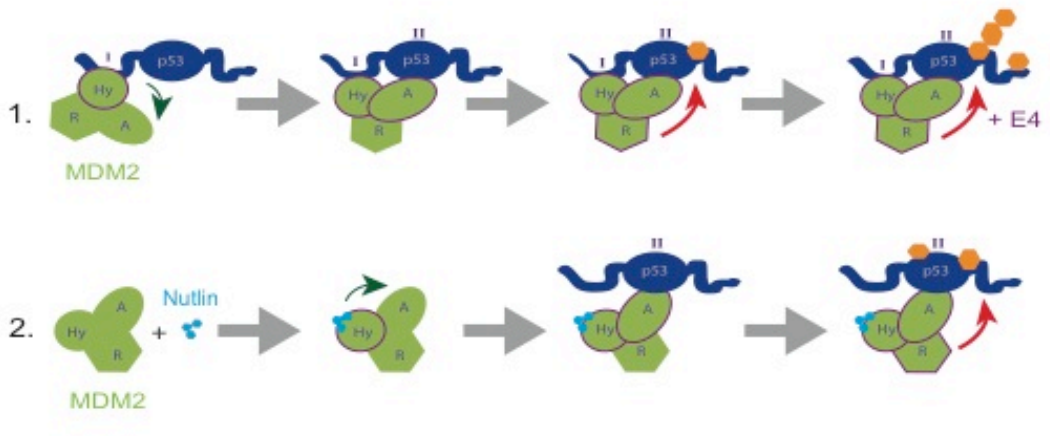

Figure 5-6 Model of Nutlin-3's effect on the p53:MDM2 interaction [198]
MDM2 interacts with two distinct motifs on p53, BOX-I (I) and BOX-V (II). The Box I interaction is of higher affinity, while the interaction through the Box V motif serve as a ubiquitination signal and is required for MDM2 mediated ubiquitination of p53. Nutlin-3 binds to the hydrophobic pocket of MDM2, which interacts with the Box I motif, thereby inhibiting the high affinity interactions. Interaction of the second binding site, which serve as a ubiquitination signal is, however, not affected, and even though the binding affinity is reduced, MDM2 can still stimulate ubiquitination of p53 in the presence of Nutlin-3. In cells, Nutlin-3 treatment shifts the ubiquitination pattern of p53 from polyubiquitination to monoubiquitination. It is known that binding of Nutlin-3 leads to conformational changes in MDM2 [198], one possibility is that this change in conformation could directly shift MDM2 E3 ligase activity towards monoubiquitination. Another possibility is that Nutlin-3 binding alters the set of proteins that interact with MDM2, for example E4 enzymes, and thereby affects the outcome of the ubiquitination event.

5.2.3 p53 ubiquitination and degradation can be uncoupled

The best-studied role of ubiquitination in p53 control, is its role in proteasomal degradation, I therefore asked how activation dependent ubiquitination of p53 affected its half-life. To determine the half-life of p53 under control and activating conditions, cells were treated with the protein synthesis inhibitor cycloheximide and the loss of the protein over a time course of 0 to 90 minutes was followed. Cells were lysed in either Triton X-100 lysis buffer to determine steady state levels or under denaturing conditions in 8 M urea lysis buffer (Fig 5-7a). Lysis in urea buffer preserves the ubiquitinated forms of p53, presumably by inhibiting the activity of DUBs in the lysate. Consistent with observations by others, DNA damage and Nutlin-3 treatment increase the half-life of p53 from 20 ± 5 minutes to over 90 minutes. Strikingly, and as detected in the previous experiment p53 ubiquitination increases after both X-Ray and Nutlin-3 treatment as visible in samples lysed in urea lysis buffer (Fig 5-7a, lower panel), this time in the absence of His-ubiquitin. These results suggest that p53 ubiquitination can be uncoupled from its proteolytic degradation under conditions where p53 is active. Strikingly, the mono- and multi-monoubiquitinated forms of p53 detected in the presence of Nutlin-3 were not subject to turnover and were stable over the 90 minutes course of the experiment (Fig 5-7a; Nutlin-3), whilst, consistent with a mixed population of mono- and polyubiquitinated p53 (Fig 5-7) the higher molecular weight forms of p53 in X-Ray treated cells were degraded whereas the monoubiquitin-adducts persisted.

To expand on this observation, A375 cells were treated with the proteasomal inhibitor lactacystin and lysed under denaturing conditions. In unstressed cells, levels of p53 protein increased and accumulated in an ubiquitinated form, as expected for a short-lived protein that is degraded by the ubiquitin-proteasome pathway. Following p53 pathway activation, however, lactacystin treatment did not lead to the accumulation of Nutlin-3 or IR induced p53 forms, but reproducibly decreased p53 ubiquitination (Fig 5-7b). Proteasome inhibitors are known to lead to deubiquitination of specifically mono- and not polyubiquitinated proteins [346]. Loss of p53 ubiquitination in radiated and Nutlin-3 treated cells, but not control cells, therefore gives further support to the idea that p53 activation results in its

monoubiquitination. Furthermore, this supports the concept that the ubiquitination observed after activation is not coupled to p53 degradation, as otherwise blocking the degradation pathway would lead to an increase in radiation or Nutlin-3 induced ubiquitinated forms of p53.

Taken together, these experiments show that p53 is ubiquitinated, but not degraded, after engagement of the p53 pathway by Nutlin-3 and X-Rays, suggesting a direct role of ubiquitination in the p53 activation pathway.

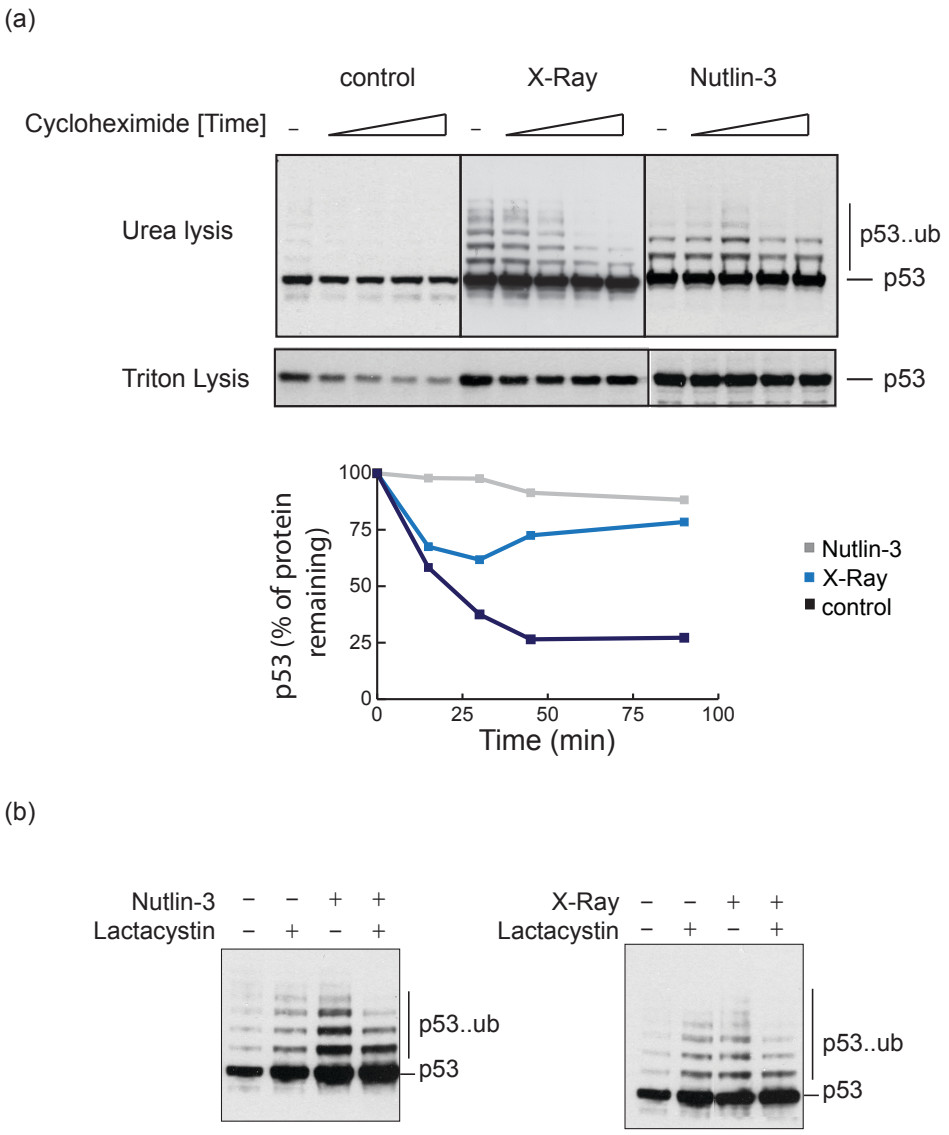

Figure 5-7 p53 ubiquitination in response to activating agents is uncoupled from its degradation

(a) A375 cells were treated with Nutlin-3 (10 μM, 8 hours) or radiated with 5 Gy (3 hours recovery) and additionally treated with 30 μg/ml Cycloheximide prior to harvest at the times shown. Samples were lysed in either Triton-X or urea lysis buffer and analysed by SDS-PAGE/immunoblot, p53 was detected using anti- p53 mAb (lower panel). (b) A375 cells were treated with 10 μM Lactacystin for 4 hours and simultaneously with 10 μM Nutlin-3 (8 hours) or 5 Gy X-radiation followed by 3 hours recovery, as indicated. Cells were lysed in urea lysis buffer and analysed by western blot using anti- p53 mAb.

5.2.4 p53 ubiquitination in response to X-Ray is a direct downstream event in the ATM signalling pathway

IR induced DNA damage leads to activation of p53 by the ATM signalling pathway, to test whether ubiquitination of p53 in response to X-Ray is a direct downstream event of ATM kinase activation, cells were treated with an ATM-Inhibitor and radiated or treated with Nutlin-3. As shown in Figure 5-8, ATM activity is required for increased p53 ubiquitination and p53 dependent expression of p21 and MDM2, after X-Ray, but not Nutlin-3 treatment. This indicates, that ubiquitination of p53 after DNA damage is an event downstream of the ATM signalling pathway. The effect of Nutlin-3 on p53 ubiquitination is not altered by the ATM inhibitor, indicating that Nultin-3, other than radiation, does not lead to activation of this signalling pathway, but rather acts by a direct mechanism through binding to MDM2 (Fig 5-8).

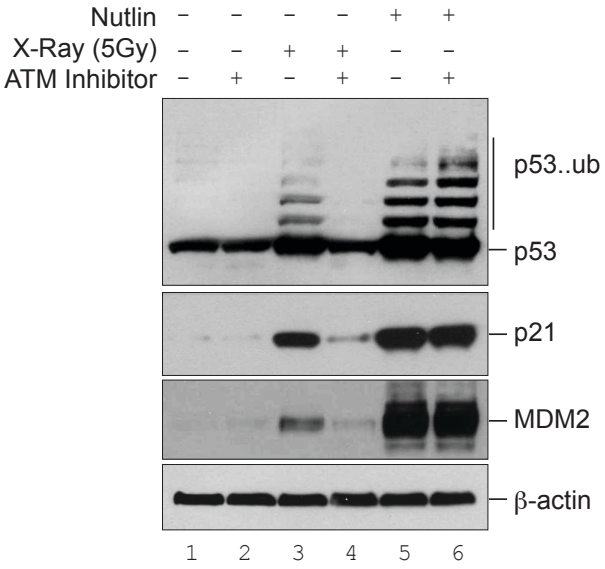

Figure 5-8 ATM Kinase activity is required for increased ubiquitination after X-Ray but not Nutlin-3 treatment

A375 cells were treated with either Nutlin-3 (10 μM, 8 hours) or X-Ray (5 Gy, 3 hours recovery) and ATM inhibitor (KU-55933, 20 μM, 4 hours) and lysed in urea lysis buffer. Samples were analysed by SDS-Page/ immunoblot using p53, p21, MDM2 and β-actin monoclonal antibodies.

5.2.5 Ubiquitinated p53 accumulates in the nucleus in response to Nutlin-3

If p53 was ubiquitinated when in its active form, I would expect it to be located in the nucleus, where p53 functions as a transcriptional activator. As there are no antibodies available that specifically recognise ubiquitinated p53 and as ubiquitin is conjugated to a vast range of cellular proteins, it is not feasible to carry out conventional co-localisation studies to determine the localisation of ubiquitinated p53 following Nutlin-3 treatment. To overcome this technical challenge I used an in situ proximity ligation assay (PLA) to detect endogenous p53 and ubiquitin that were within 40 nm of each other. For this anti-p53 polyclonal (CM1) and anti-ubiquitin monoclonal antibodies were used together with secondary antibodies conjugated to unique short DNA strands, which when in close proximity are amplified and using Duo-link system to produce a fluorescent signal. As a negative control, only one of the primary antibodies was used. To test the functionality of the assay with respect to detection of p53-ubiquitin conjugates, it was carried out in A375 cells that had been treated with Lactacystin an inhibitor of proteasomal degradation that leads to accumulation of ubiquitinated p53 protein in cells. Figure 5-9 shows that whereas in control cells the level of PLA signal is just above the single antibody control background, Lactacystin treatment led to a marked increase in the total number of fluorescent spots, which correspond to ubiquitinated p53. This indicates that the assay is indeed able to detect ubiquitinated p53 in cells. I went on to investigate the effect of Nutlin-3 on the presence of ubiquitinated p53 in the nucleus using this technique. Following Nutlin-3 treatment, a significant increase in the total number of fluorescent spots was detected, and a majority of the signal was located in the nuclear compartment of the cell. This was in contrast to Lactacystin treatment were the majority of spots were located in the cytoplasm (compare Fig 5-9 and 5-10). As an additional control the assay was carried out in HCT-116 p53 wt and HCT-116 p53 -/- cells. No signal was observed in p53 null cells while Nutlin-3 led to an increase in fluorescent signal in HCT-116 p53 wt cells (Fig 5-11). This further supports that the assay specifically detects ubiquitinated p53.

To establish that the nuclear pool of ubiquitinated p53 detected by PLA in the Nutlin-3 treated cells was monoubiquitinated I carried out cellular fractionation. Figure 5-12 shows a pool of monoubiquitinated p53 protein in the nuclear fraction from Nutlin-treated cells. (Note, this assay is not carried out under denaturing conditions and likely therefore under represents the amount of ubiquitinated protein).

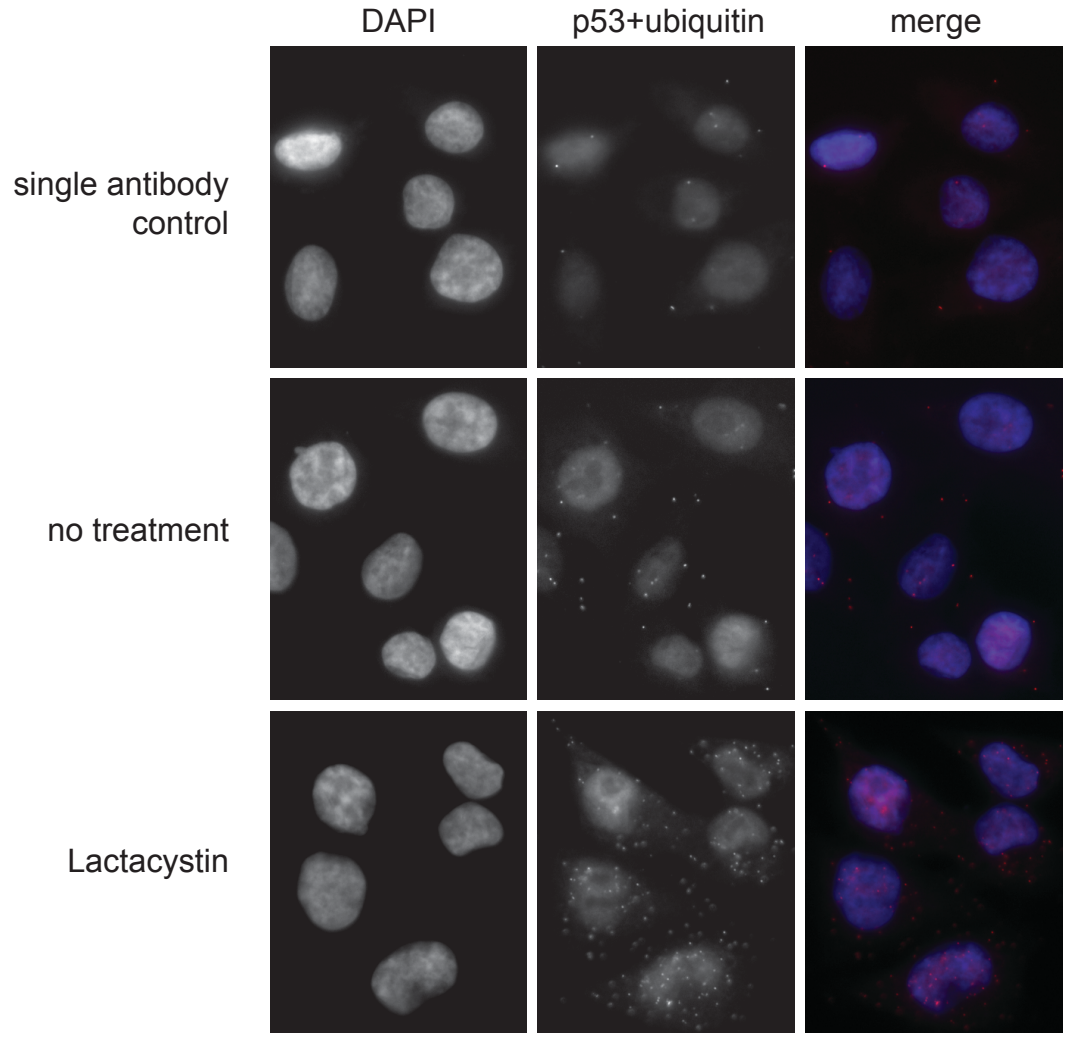

Figure 5-9 Accumulated ubiquitinated p53 in response to lactacystin treatment can be detected using the PLA system

A375 cells were treated with 10 μM Lactacystin for 4 hours, and a proximate ligation assays using either only anti-ubiquitin or both anti-ubiquitin and anti-p53 antibodies was performed. Cells were stained with DAPI (1:5000 in mounting media) and visualised using an Axioplan2 (Zeiss) fluorescent microscope (100 x magnification). Representative PLA images are shown.

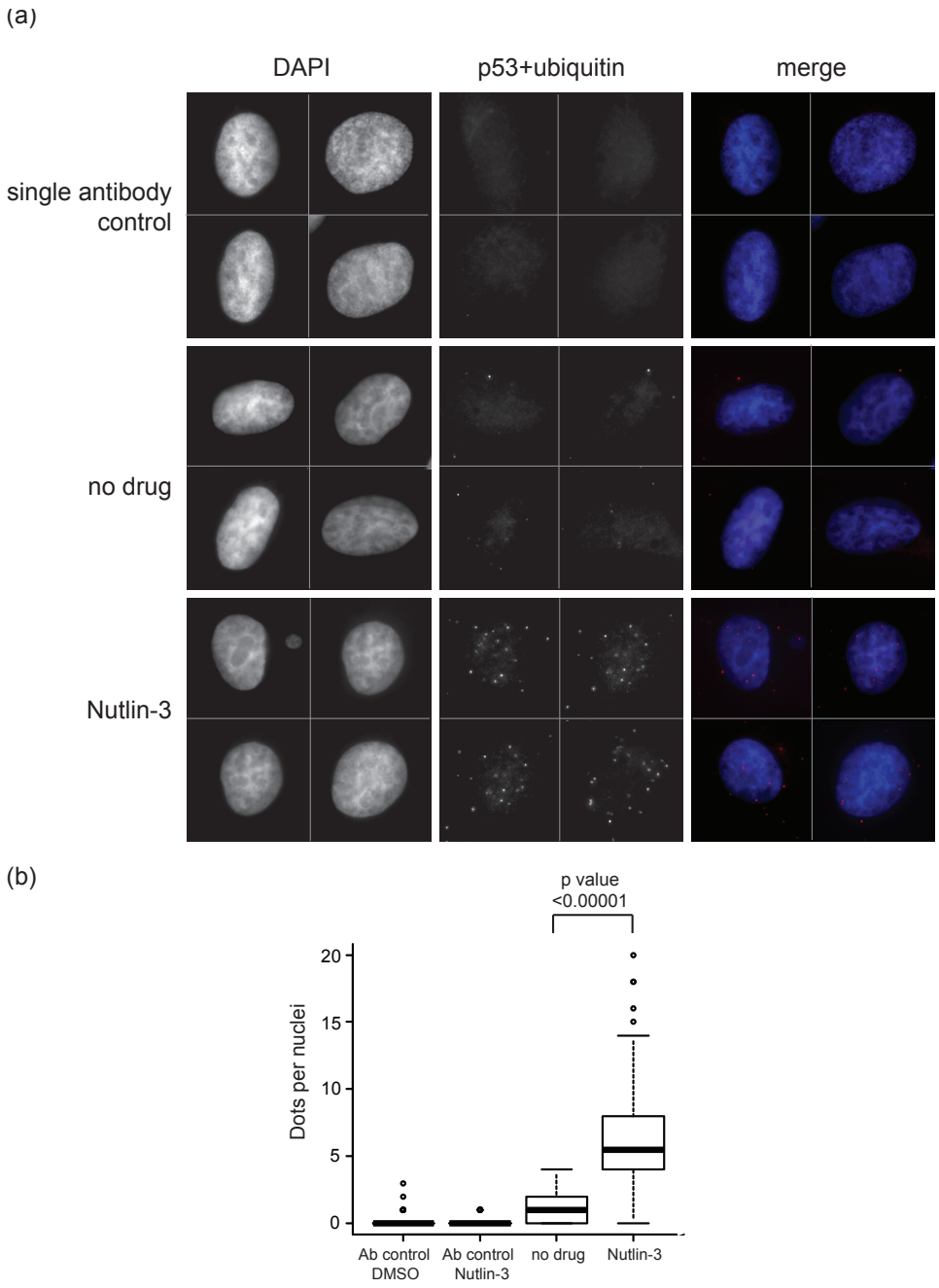

Figure 5-10 Nutlin-3 treatment leads to accumulation of ubiquitinated p53 in the nucleus

(a) A375 cells were treated with 10 μM Nultin-3 for 8 hours, and a proximate ligation assays using either only anti-ubiquitin or both anti-ubiquitin and anti-p53 antibodies were performed. Cells were stained with DAPI (1:5000 in mounting media) and visualised using an Axioplan2 (Zeiss) fluorescent microscope (100 x magnification). Representative PLA images are shown. (b) The numbers of spots in at least 100 cells were counted; the average numbers of spots per cell are shown.

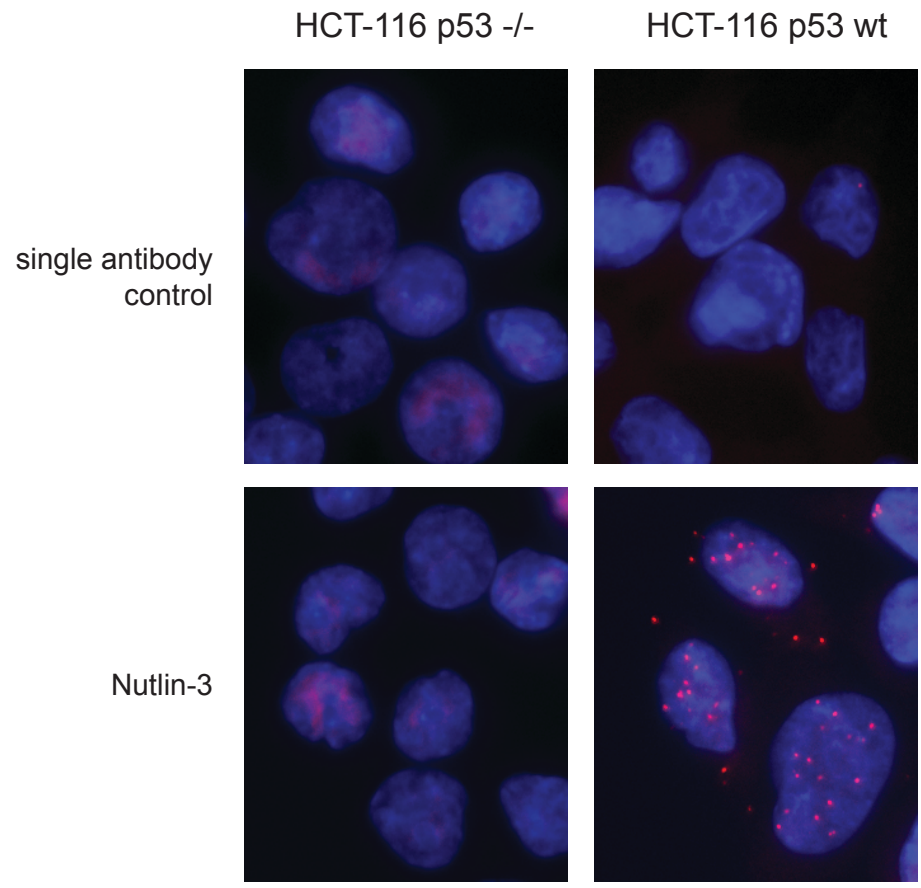

Figure 5-11 The PLA system detects ubiquitinated p53 in HCT-116 p53 wt but not p53 -/- cells

HCT-116 p53 wt or p53 -/- cells were treated with 10 μM Nultin-3 for 8 hours, and a proximate ligation assays using either only anti-ubiquitin or both anti-ubiquitin and anti-p53 antibodies were performed. Cells were stained with DAPI (1:5000 in mounting media) and visualised using an Axioplan2 (Zeiss) fluorescent microscope (100 x magnification). Representative PLA images are shown.

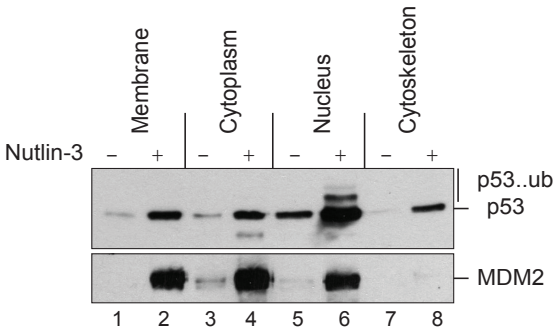

Figure 5-12 Nutlin-3 induces monoubiquitination in nuclear p53

Fractionation of A375 cells treated with Nutlin-3 (10 μM) or DMSO for 8 hours and analysed by Immunoblot with anti p53 and MDM2 (4B2) mAb. The fractionations were carried out using the Proteo Extract Kit (Calbiochem).

5.2.6 Chromatin associated p53 is ubiquitinated

The experiment described above shows that monoubiquitinated p53 accumulated in the nucleus following Nutlin-3 treatment, however it does not tell us whether this pool of protein is associated with the chromosomal DNA or if it is present in the soluble nuclear fraction. As chromatin is insoluble in the buffer conditions used any protein that is associated with the chromatin will be in the insoluble fraction, while chromatin unbound nuclear protein will be present in the soluble fraction. As such I performed a simple fractionation experiments, separating the soluble from the insoluble cellular fraction using hypertonic lysis conditions. To confirm that all the DNA and thus the chromatin was present in the insoluble fraction, DNA content of both fractions was analysed after sonication and RNase treatment of the samples. As expected all DNA was present in the insoluble fraction (Fig 5-13a compare lane S=soluble to P-insoluble fraction). Additionally, analysis of the proteins in the fractions by SDS-PAGE showed that histone-H1, which is associated with the chromatin, was mainly present in the insoluble fraction, providing further confirmation that chromatin associated proteins can be separated from free protein by this method.

To determine if ubiquitinated p53 is associated with the chromatin, MCF7 or A375 cells were treated with Nutlin-3 or X-Ray respectively; subsequently p53 protein in the soluble and insoluble fraction was analysed. After Nutlin-3 treatment an increase in p53 levels together with an increase in the appearance of higher molecular weight bands, indicative ubiquitinated forms of p53, was observed in the soluble and insoluble fraction (Fig 5-13a). Furthermore, radiation (5 Gy) of A375 cells led to the accumulation of ubiquitinated p53 protein in both fractions and this was dependent on ATM kinase activity (Fig 5-13b). This experiment indicates that after engagement of the p53 pathway, ubiquitinated forms of the transcription factor were associated with the chromatin containing fractions. To verify that the higher molecular weight bands represent p53 protein modified by ubiquitin, fractions of radiated samples were incubated with the p53 deubiquitinase HAUSP for 5 minutes at 37°C. The results show a significant decrease in high molecular weight bands in the HAUSP treated samples, when compared to control samples. This confirms that the higher

molecular weight bands correspond to ubiquitinated p53 (Fig 5-13c). It has to be noted that other cellular DUBs are present in the lysates and most likely partially deubiquitinate p53-ubiquitin conjugates present in the sample. The actual ratio of ubiquitinated to unmodified p53 in both fractions is therefore probably underrepresented in the experimental results.

To further confirm that the modified protein is chromatin associated and not in the insoluble fraction through for example membrane association or aggregation, I set up an assay to specifically look at the ubiquitination status of chromatin associated p53 using a 10-50% isokinetic sucrose gradient. Sucrose gradient sedimentation has previously been used to analyse chromatin structures as the sedimentation rate is determined by the mass and hydrodynamic shape of the chromatin fibres [347, 348]. Here, I have adapted this technique to determine whether ubiquitinated p53 is associated with the chromatin structures or present in the free nuclear fraction (See Fig 5-14 for experimental outline).

The nuclei from control, Nutlin-3 and X-ray-irradiated cells were isolated and chromosomal DNA was briefly digested using micrococcal nuclease. After RNase treatment of the samples, to remove any RNA, the nuclei were lysed and the lysate was fractionated using sucrose density gradient centrifugation. UV monitoring and examination of the DNA content of each fraction following phenol/chloroform extraction and subsequent agarose gel analysis, revealed that the chromosomal DNA, and therefore protein associated with it, was mainly present in fractions 6-8 (Fig 5-14b), whereas earlier fractions (1-3) contain nuclear protein that is not associated with chromatin and the remaining fractions contains proteins that are only loosely associated with the chromatin.

Protein analysis of the samples using ethanol precipitation followed by SDS-PAGE, shows that p53 is present in both the soluble nuclear and chromatin associated fraction under all conditions, however, strikingly ubiquitinated protein can only be detected in fractions that are tightly associated with the chromatin and only under conditions where p53 is activated i.e. after Nutlin-3 treatment or radiation. Up to two ubiquitin bands are observed, suggesting that the protein is mono- and diubiquitin

modified or multi mono-ubiquitination (Fig 5-15). Again, the ratio of ubiquitinated to unmodified protein is most likely underrepresented due to activity of DUBs in the lysates.

Taken together, the results presented in this chapter so far show that agents as Nutlin-3 or X-Ray that engage the p53 activation pathway, lead to monoubiquitination of p53, which is uncoupled from its proteolytic degradation. Furthermore, ubiquitinated forms of p53 were shown to be located in the nucleus, associated with the chromatin, indicating that p53 is active in its monoubiquitinated state.

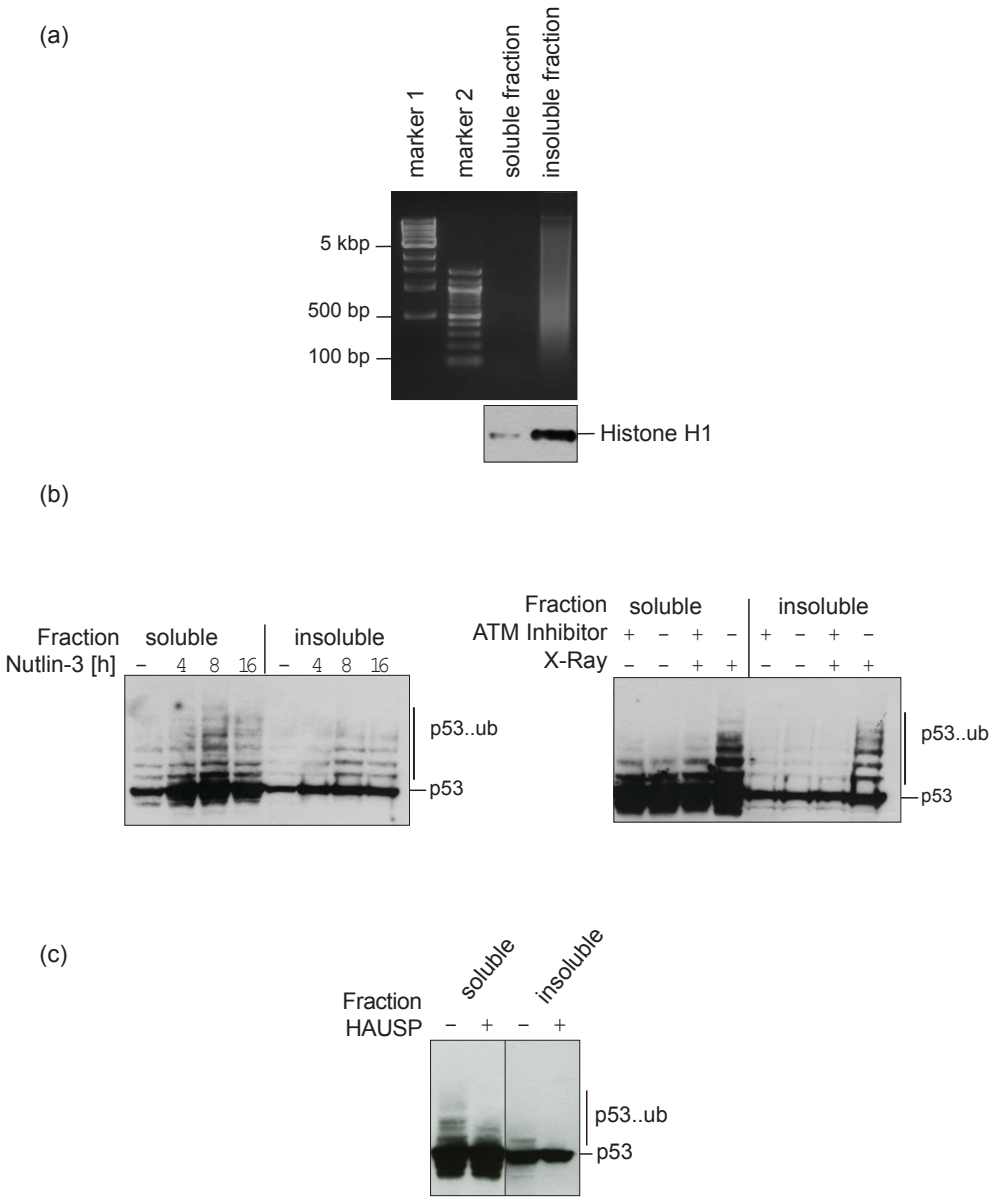

Figure 5-13 Ubiquitinated p53 is present in the insoluble nuclear fraction

(a) MCF7 cells were lysed under hypertonic lysis conditions. The DNA content of the soluble and insoluble fraction was prepared using phenol/chloroform extraction and separated on an agarose gel. Proteins were analysed by SDS-PAGE/immunoblot using anti-p53 and Histone H1 antibodies. (b) MCF7 or A375 cells were treated with 10 μM Nutlin-3 for 0-16 hours (left panel) or 5 Gy followed by 3 hours recovery ± 10 μM ATM inhibitor for 4 hours (right panel) respectively. Cells were fractionated into soluble and insoluble protein and analysed by SDS-PAGE/immunoblot using an anti-p53 antibody. (c) A375 cells were irradiated with 5 Gy of IR, insoluble and soluble fractions were isolated and treated with HAUSP for 5 minutes at 37°C.

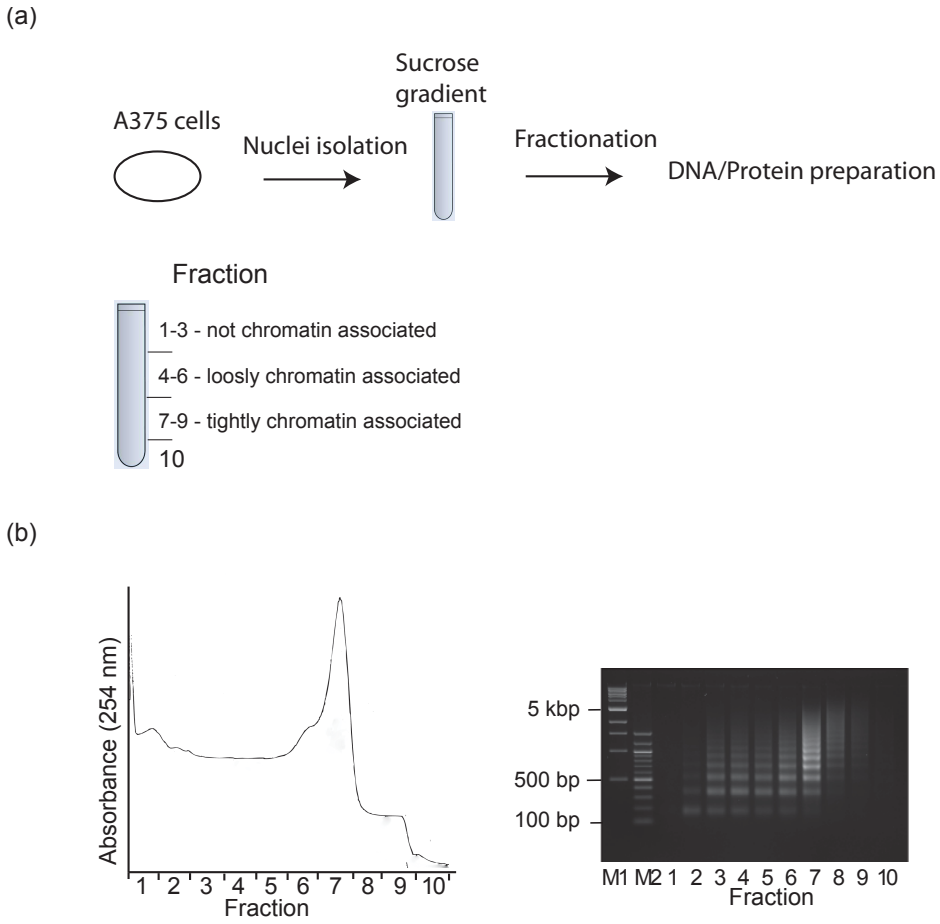

Figure 5-14 Experimental outline of nuclei fractionation using sucrose gradient centrifugation

(a) A375 cells are grown in a tissue culture dish, treated as indicated and harvested at around 90% confluency. Nuclei were isolated, RNA was removed in an RNase step and chromosomal DNA partially digested using micrococcal nuclease. Following digestions, cells were lysed and the lysate was separated using a 10-50% sucrose gradient and ten 0.5 ml fractions collected using a fraction collector. During fraction collection a UV profile of the fractions was recorded. (b) Typical UV trace of a fractionation experiment (left panel), agarose gel representing DNA content of the ten fractions obtained (right panel). DNA was prepared by phenol/chloroform extraction followed by ethanol precipitation.

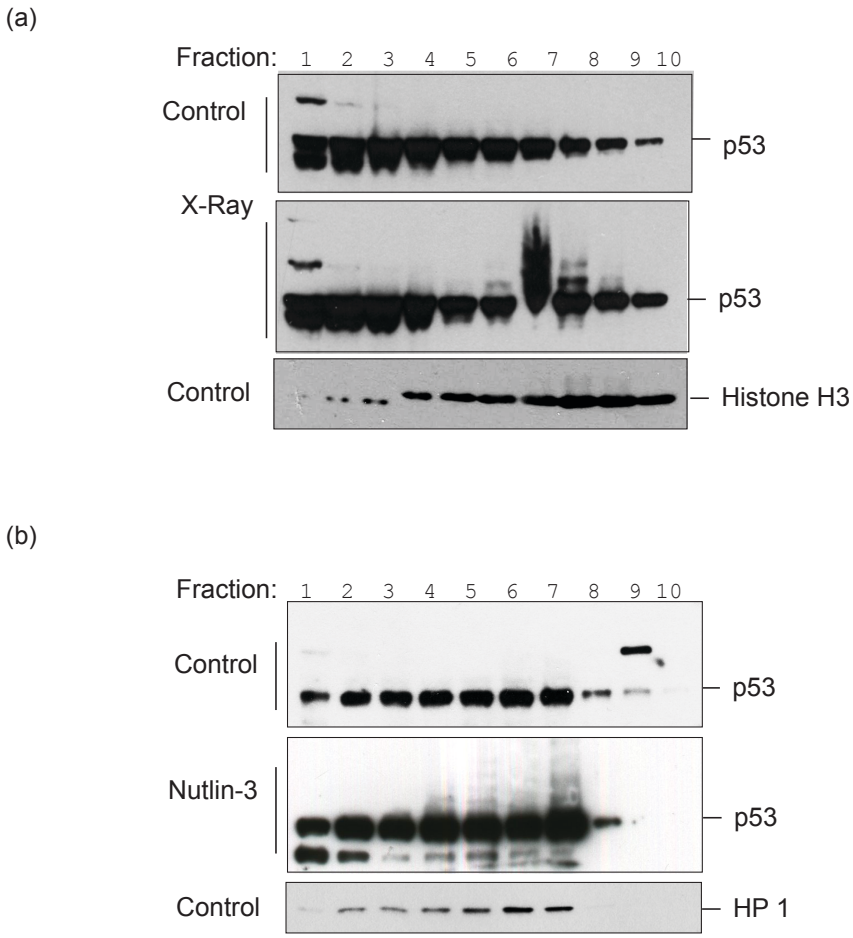

Figure 5-15 X-radiation and Nutlin-3 treatment specifically leads to ubiquitination of chromatin-associated p53

Nuclei of A375 cells treated with 5 Gy IR followed by recovery for 3 hours (a) or with 10 μM Nutlin-3 for 8 hours (b) were fractionated as described in Fig 5-23 and analysed by SDS-PAGE/immunoblot with anti-p53 mAb, Histone-protein 1 pAb, Histone H3 mAb as indicated.

5.2.7 Molecular modeling suggests that direct interactions between ubiquitin and DNA stabilises the TA:DNA complex

The data presented above demonstrate that, following pathway activation, stably monoubiquitinated p53 is in the nucleus where it is tightly associated with chromatin (Fig 5-10 and 5-15). In a next step I therefore to asked whether monoubiquitination directly affected the ability of p53 to bind DNA. We hypothesised that ubiquitin acceptor lysine residues located in the DBD of p53 [349] may be of most interest in respect to DNA-binding, however, multiple ubiquitin acceptor sites have been mapped in a number of p53 domains [232]. Thus, it is difficult to study DBD monoubiquitination in isolation from other p53 ubiquitination events. On the other hand I have shown (chapter 4) that IRF-1 is ubiquitinated exclusively in its DBD (Fig 5-16) making it a good model to study the effects of domain specific monoubiquitination on TA DNA-binding activity.

Interestingly, the DBD ubiquitination sites of both p53 and IRF-1 lie very close to or within the DNA binding interface, suggesting that modification of these residues would affect TA's ability to interact with DNA. To gain insight into the mechanism by which DBD ubiquitination would affect the affinity of their TAs to DNA, I started by generating in silico models of the DBD of both transcription factors in an ubiquitinated state bound to DNA using the Haddock webserver [271, 297]. Models were created for lysine residues that are present in the crystal structure of the DBD of IRF-1 (Lys^{39}, Lys^{50} and Lys^{78}, which I identified as ubiquitin acceptor lysines in chapter 4) and for p53 (Lys^{164} and Lys^{292}) and the C-terminal glycine residue of ubiquitin as active contact residues. The three best structures of the four clusters with the best HADDOCK scores were analysed (see Fig 4-5 for IRF-1 and 5-18 for p53 models). The models were generated in the absence of DNA and later overlaid with the DNA from the respective crystal structure, all complexes exhibiting a major clash between the position of ubiquitin and DNA were discarded, and the models with the best HADDOCK scores were taken forward for subsequent analysis. It should be noted that as shown in Figure 5-18b, even though for the Lys^{292} model the structures with a clash between DNA and ubiquitin were discarded (left panel, upper two molecules), and the remaining one was chosen for MD analysis, during the

simulation the ubiquitin molecule underwent gross movement and resulted in a position very close to the DNA interface and in a similar three dimensional space to the ubiquitin molecules in the other two models (right panel, blue molecule). This shows that the HADDOCK model has to be seen as merely a starting structure, which is refined during the simulation process. Molecular dynamic simulations of the DBD-ubiquitin-DNA complexes were carried out for 40 ns, the complex after the simulation is shown in Figure 5-17 and 5-19. The simulations were run in triplicate for p53 and in duplicate for IRF-1. Interestingly, ubiquitin is positioned at the DNA binding interface in all models and ubiquitin residues directly interact with the DNA in the simulations. An electrostatic surface analysis of the complex using APBS shows that addition of ubiquitin to the DBD strongly increases the positively charged surface area of the transcription factors that faces and binds DNA (Fig 5-17 and 5-19). This suggests that the ubiquitin molecule can contribute to the binding between the transcription factor and DNA and thereby favours the interaction. In fact, analysis of the buried surface on the DNA by the protein shows an increase of 38 – 53 % in the ubiquitinated models when compared to the DBD alone (Fig 5-17 and 5-19). Additionally, the simulations were used to calculate the binding energies between DNA and the p53 DBD, either free or bound to ubiquitin, and this showed a significant decrease in ΔGB of ubiquitinated compared to unmodified TA DBD (Fig 5-17c and 5-19b; left panel). As p53 can be polyubiquitinated in cells, I was interested to examine if addition of more ubiquitins to p53 would further increase the positive surface area. The model of p53 ubiquitinated at Lys^{292} was used as the basis to generate models of tetraubiquitinated p53 with chains linked by K11, K48 or K63. Models of chains linked by K11 and K48 indicate that there might be further interactions between the second ubiquitin molecule, however, there are also steric clashes between the ubiquitin chain and the DNA (Figure 5-20, upper and middle panel). In a model of p53 ubiquitinated by a K63 linked chain, only the first ubiquitin molecule appears to be able to form interaction with DNA (lower panel). Taken together, the models of polyubiquitinated p53, suggest that only the first and possibly the second, but no further ubiquitin molecules, would interact with p53 bound DNA and strengthen the interaction.

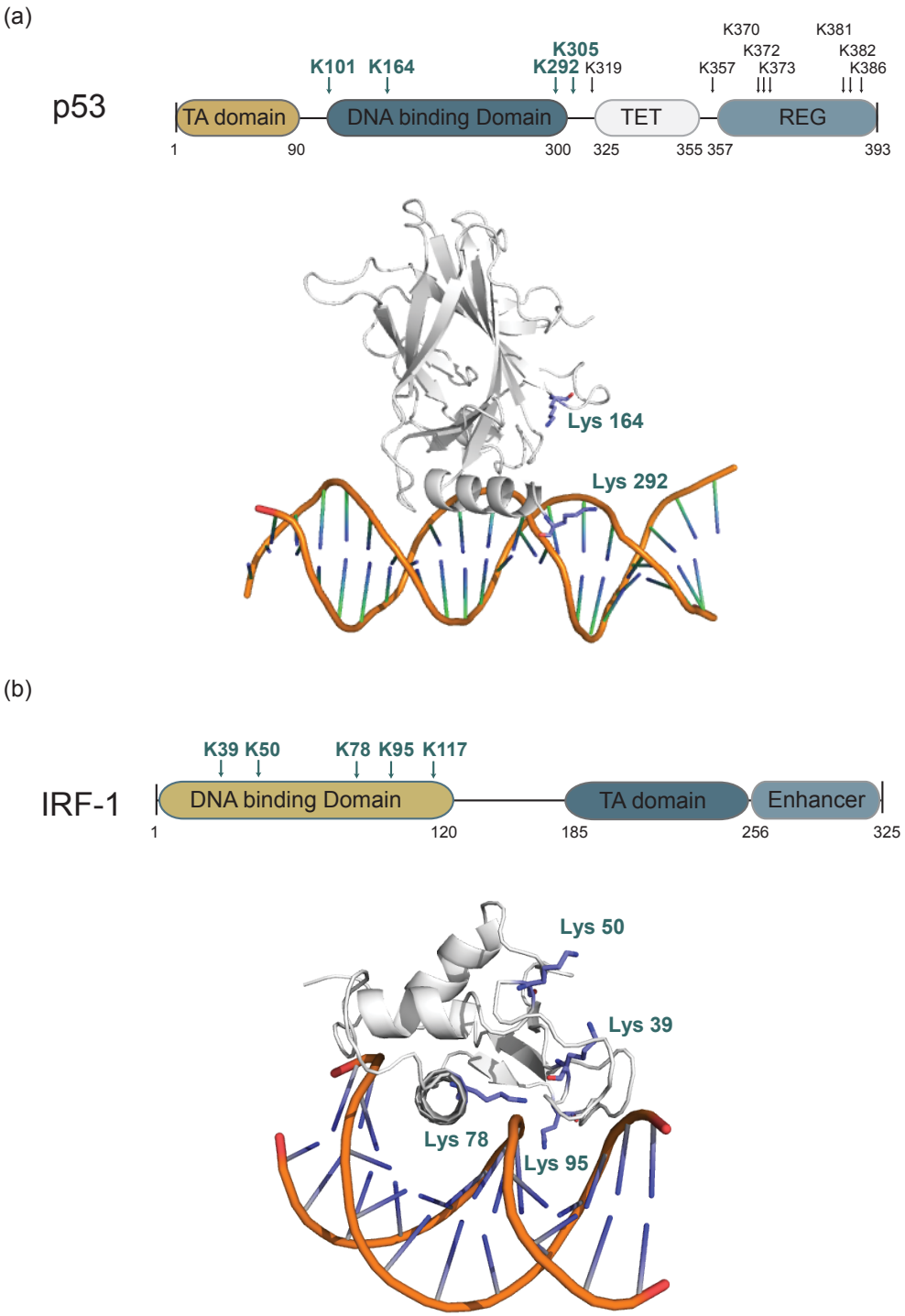

Figure 5-16 Ubiquitination sites on IRF-1 and p53

Domain and crystal structure of (a) IRF-1 and (b) p53 with lysines that are subject to ubiquitination indicated in blue.

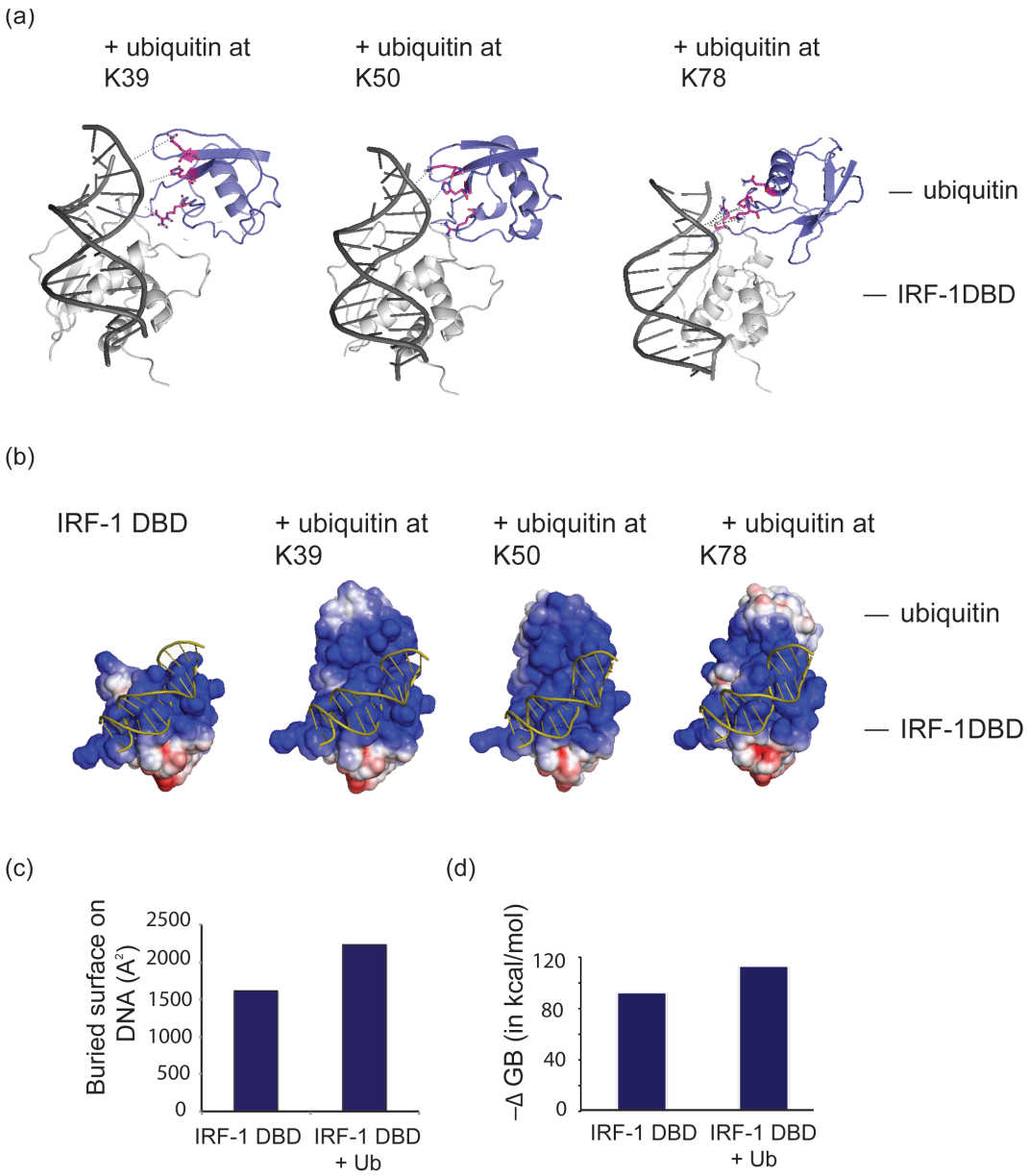

Figure 5-17 Moiecular model of an IRF-1 DBD:DNA:ubiquitin complex

(a) Model of the IRF-1:ubiquitin:DNA complex generated by superimposing the IRF-1:ubiquitin (Fig 3-5) model onto the IRF-1DBD:DNA crystal structure. (b) Electrostatic surface analysis of the ubiquitin:TA model was carried out using the APBS Pymol plugin. Blue indicates positively charged surface, while red shows negatively charged protein surface. (c) Molecular Dynamic Simulations were carried out on the complex of IRF-1 DBD:DNA (PDB:1IF1) and the IRF-1 DBD:DNA:ubiquitin model. The simulations were used to compute the free binding free energy (in kcal/mol) of DNA with IRF-1 DBD +/- ubiquitin (lower panel). (d) The buried surface on IRF-1 DBD alone and in complex with ubiquitin (modeled on Lys^{78}) was calculated using Pymol.

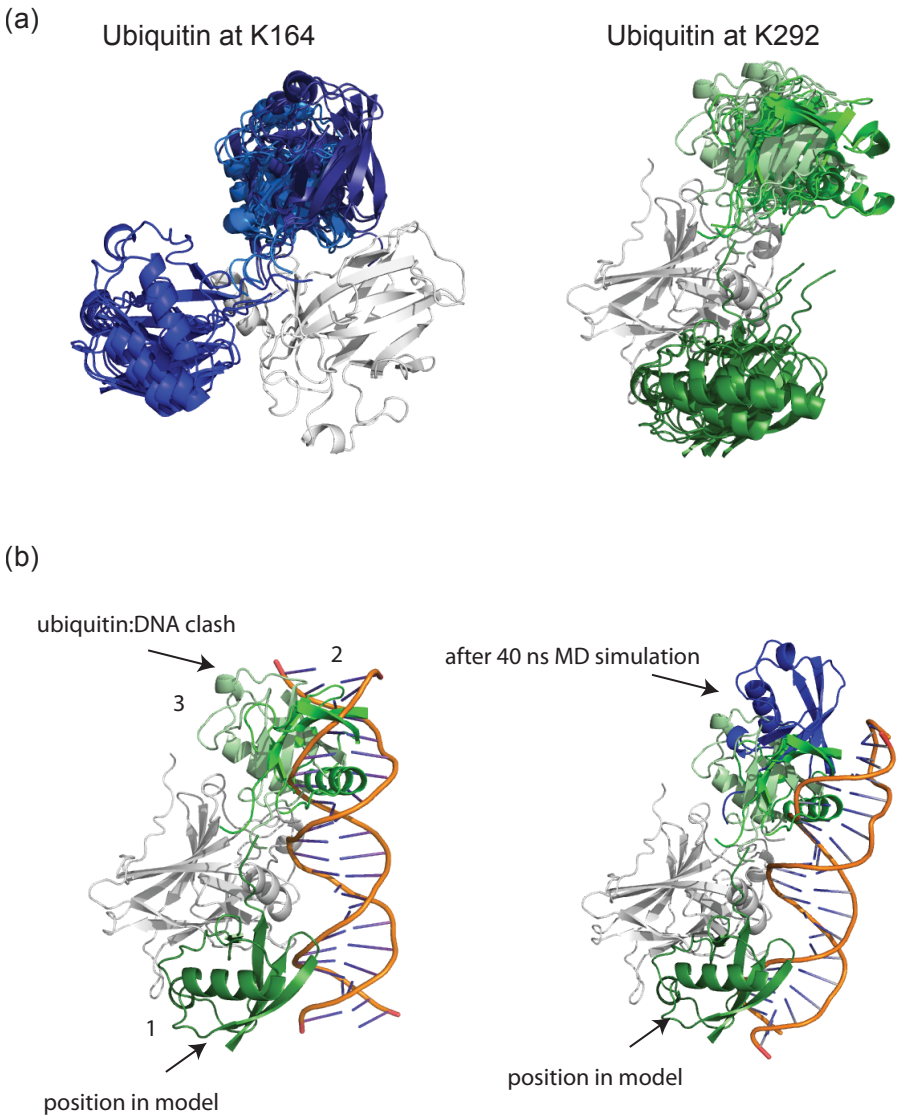

Figure 5-18 Model of monoubiquitinated p53

(a) Ubiquitin was modelled onto the p53 DBD at the ubiquitin receptor lysine residue 292 using the HADDOCK web server. From the results obtained, the four best structures from the three best clusters (1-3) were analysed. The position of ubiquitin (green or blue ribbon) in respect to p53 (white ribbon) in the three models is shown with ubiquitin in structures obtained from different clusters in different green shades.

(b) Models in position 2 and 3 were discarded as they displayed clashes with the DNA. Model 1 was used for subsequent MD simulations (left panel). The ubiquitin molecule underwent conformational changes during the simulation (blue ribbon) that brought it into close proximity to the DNA and in an orientation similar to that of the structures from the other two HADDOCK output clusters (2,3) (right panel), thus suggesting a conversion of the HADDOCK solutions.

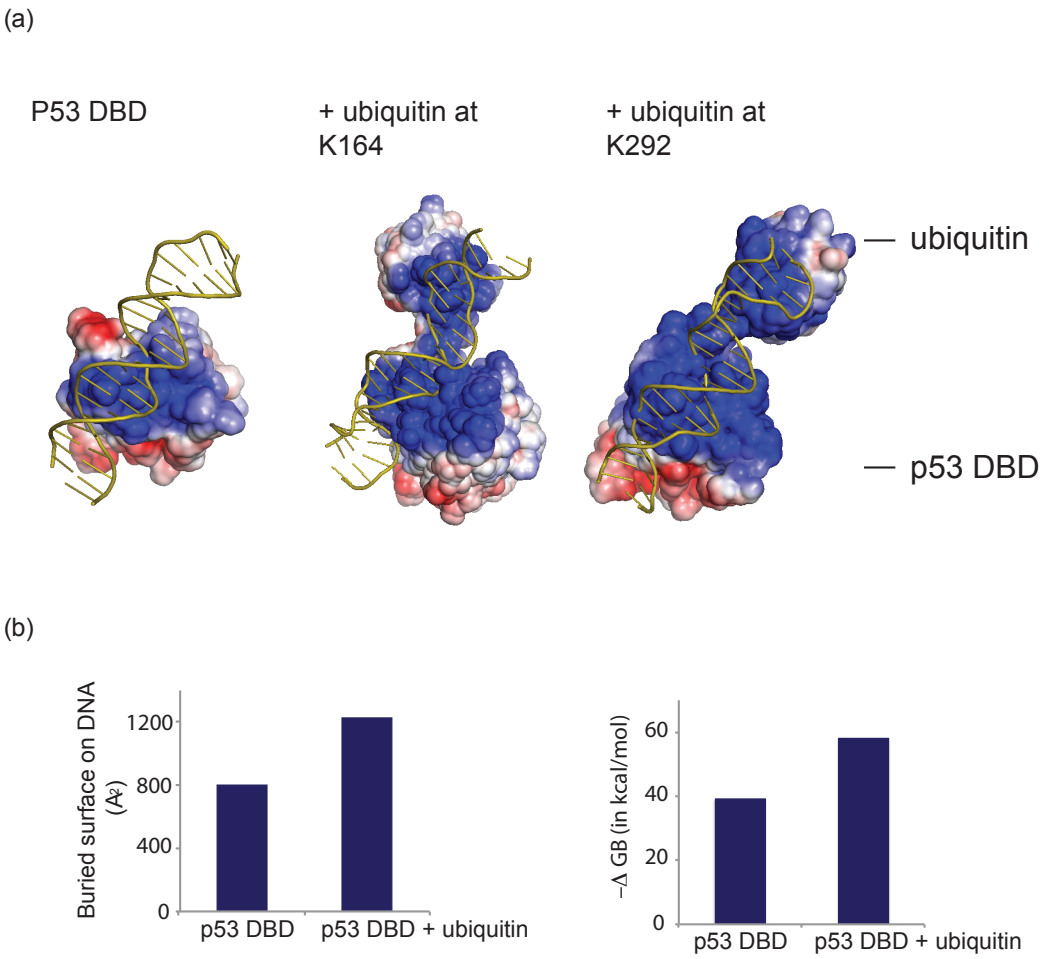

Figure 5-19 Molecular model of a p53 DBD:DNA:ubiquitin complex

(a) Model of the p53:ubiquiti:DNA complex generated by superimposing the p53:ubiquitin model onto the p53:DNA crystal structure (PDB). Electrostatic surface analysis of the ubiquitin:TA model was carried out using the APBS Pymol plugin. Blue indicates positively charged surface, while red shows negatively charged protein surface. (b) The buried surface on p53 was calculated using Pymol (left panel). Binding free energy (in kcal/mol) of DNA with p53 DBD +/- ubiquitin was calculated using MD simulations and is shown on the right.

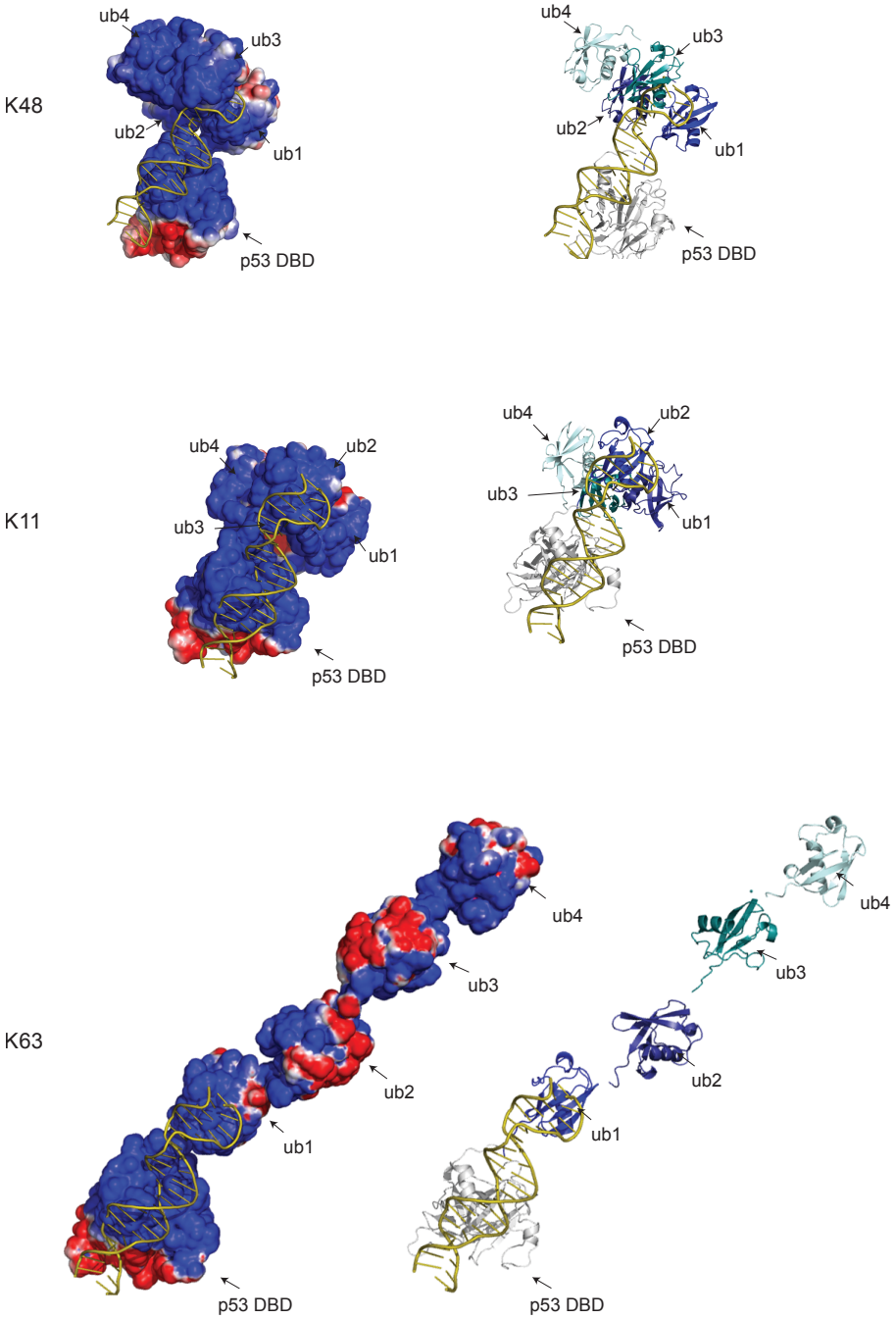

Figure 5-20 Polyubiquitination does not dramatically increase the positive surface area of the p53 DBD:ubiquitin complex

Models of polyubiquitinated p53 were generated on the basis of structures from ubiquitin linked to p53 Lys^{292} (Fig 5-8) and models of tetraubiquitin chains obtained from the respective di-ubiquitin structures (Fig 1-3). Electrostatic surface was generated using Pymol.

5.2.8 IRF-1 and p53 bind DNA more stably when in their ubiquitinated form

In silico modelling suggested a novel role for monoubiquitination in the direct stabilisation of the TA:DNA complex, leading to transcriptional activation. To study this hypothesis experimentally, I first carried out *in vitro* DNA binding assays with recombinant IRF-1 and p53 protein that had been modified by ubiquitin in an *in vitro* ubiquitination reaction containing all components of the ubiquitination cascade as purified compounds. The ubiquitination reactions were carried out with either wild-type ubiquitin, that can result in formation of mono- and polyubiquitination chains or with an ubiquitin mutant, where all lysines are mutated to arginine (NoK), which is unable to form polyubiquitin chains linked by internal ubiquitin lysines (Fig 5-21 and Fig 5-22a). As a control, AMP instead of ATP was added to the *in vitro* reaction (preliminary experiments showed that ADP could in part support ubiquitination where AMP could not). The sequence specific DNA binding ability of either IRF-1 or p53 was examined using an electrophoric mobility shift assay (EMSA) followed by quantification of the resulting bands using Image J. To confirm that the observed bands corresponded to p53 or IRF-1 binding to the probe, anti p53 or IRF-1 antibodies were added to the samples to supershift the protein:DNA complex. For IRF-1, which binds DNA to give a diffuse band in an EMSA, I also set up additional binding assays. Specifically, biotin labelled oligonucleotides that are known to bind to IRF-1 (Chapter 4), were immobilised onto a streptavidin coated microtiter plate, then incubated with a titration of either unmodified or ubiquitinated IRF-1 protein. DNA bound protein was detected using an anti-IRF-1 antibody (Fig 5-21c). In case of p53 the ubiquitination pattern with WT and NoK ubiquitin is relatively similar as MDM2 predominantly acts as a monoubiquitin ligase (Fig 5-23a). Results of the DNA binding assays show that, as predicted by in silico modelling, both IRF-1 and p53 have enhanced DNA-binding activity, when in an ubiquitinated form and that monoubiquitination is sufficient for an increase in DNA binding (Fig 5-21 to 5-23). The increase in DNA binding activity appears to be greater for proteins modified by WT ubiquitin compared to those modified by the NoK ubiquitin mutant. However, the ubiquitin mutant appears to be a poor substrate for the ubiquitination reaction compared to WT ubiquitin and its addition results in less conversion of unmodified

IRF-1 or p53 to the modified product, making a direct comparison of the effects of WT and mutant ubiquitin difficult. Yet, the assays shows very clearly that monoubiquitination of both transcription factors leads to an increase in DNA binding. We can therefore conclude that addition of a single ubiquitin molecule at a given site, rather than a polyubiquitin chain, is sufficient to increase the binding affinity of the transcription factors to their respective consensus sequence. To further confirm that the increase in DNA binding is due to the modification of the TAs by ubiquitin, a timecourse of the ubiquitination reaction for p53 was carried out with incubation times of either 0, 10 or 45 minutes and subsequent DNA binding analysis of the protein was performed by EMSA. As shown in Figure 5-23a the increase in DNA binding activity corresponds to the increase of ubiquitination at a longer incubation time. To determine if this increase in DNA binding activity is exclusive for binding of p53 to the p21 promoter sequence, or if it is a more general phenomenon, the ability of unmodified and ubiquitinated p53 to bind to sequences from the promoter of p21, BAX, MDM2 and PUMA were compared. As shown in Figure 5-24 ubiquitination leads to an increase in binding to all four promoters, indicating that ubiquitination of p53 generally increases the affinity for its target promoters. Taken together, these data provide strong evidence that ubiquitination of p53 and IRF-1 leads to an increase in their ability to bind to DNA and thus function as transcriptional regulators.

The modelling together with DNA binding data thus suggests a direct role for ubiquitin in stabilising the interaction of the DBD with DNA. To identify the main ubiquitin residues that are involved in DNA interactions, I generated an overlay of the position of ubiquitin in respect to DNA in all models (Fig 5-25a). Analysis of the models revealed that ubiquitin contacts the DNA in all models with the same 'positively charged patch', consisting of mainly residues Lys^{6}, Arg^{42} and Lys^{48} (Fig 5-25). Next I wanted to determine, if this positively charged surface is indeed involved in DNA interactions. Therefore, I mutated these three residues and replaced them with either a neutral or negatively charged residue to test if this affected the ability of the mutant to stabilise the p53:DNA complex. A single point mutation of either Lys^{48} or Arg^{42} to either Ala or Gln almost completely abolished the ability of ubiquitin to

serve as a substrate for *in vitro* ubiquitination reactions (Fig 5-25c). Mutation at Lys^{6} to Ala or Gln resulted in a substantial decrease in the ubiquitination efficiently, but some ubiquitination could still be observed, especially with the Ala mutant. Studies in the Hay lab have subsequently shown that all three residues Lys^{6}, Arg^{42} and Lys^{48} are involved in interactions with the E2 in the ubiquitin:E2:E3 complex (structure solved by Plechanonova [46] Figure 1-4) and mutation of these residues most likely disrupts the E2:ubiquitin interaction and thereby prevent the formation of an active complex. Since, I observed some ubiquitination using the lysine 6^{Ala} mutant, I adapted the conditions of the *in vitro* ubiquitination reaction to get a similar amount of ubiquitination with wt and 6^{Ala} ubiquitin, to achieve this both reaction were incubated at 30°C for 45 minutes, but ATP was added to the reaction with WT ubiquitin only for the last 10 minutes, while ATP was present in the reaction with 6^{Ala} ubiquitin for the whole incubation time. The ability of p53 ubiquitinated with either WT or 6^{Ala} ubiquitin to bind to the p21 or Bax promoter was determined using an EMSA. As expected, results of the DNA binding assay show enhanced binding with wt ubiquitin, while ubiquitination with the mutant does not affect binding of p53 to DNA (Fig 5-25c). Because the ubiquitin mutant is not a good substrate for the reaction, the overall ratio of modified to unmodified p53 is quite low and thus the increase in DNA binding of ubiquitinated p53. Therefore, even though the results show a reproducible increase with wt ubiquitin and no increase with the ubiquitin mutant, indicating that interactions between the positively charged Lys and DNA are indeed involved in stabilisation of the DBD:ubiquitn:DNA complex, further experiments are necessary to confirm the role of these specific ubiquitin residues in stabilising the DNA interaction.

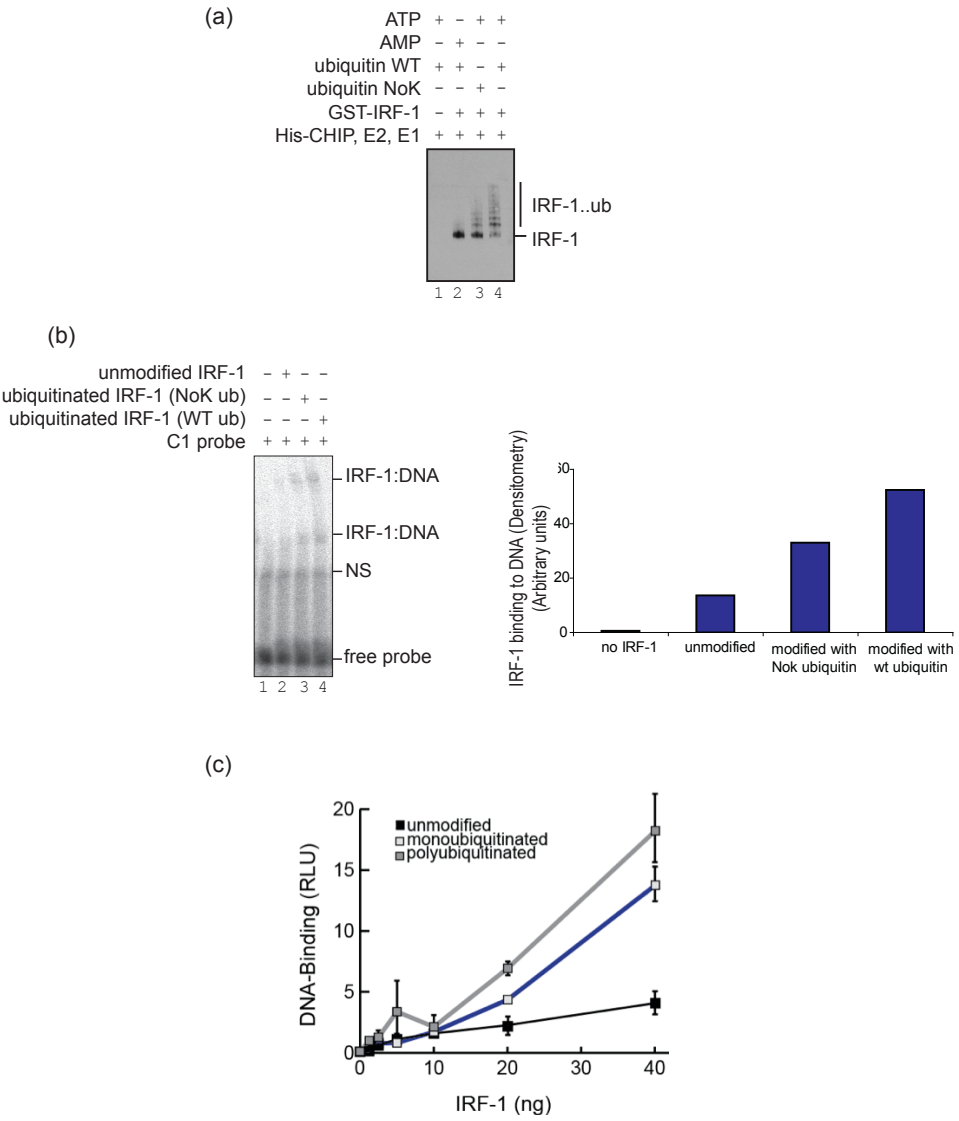

Figure 5-21 (Mono)-ubiquitination increases IRF-1's ability to bind to DNA

(a) IRF-1 was ubiquitinated in an *in vitro* reaction with either wild-type ubiquitin or an ubiquitin mutant (NoK) with all lysines mutated to arginine that cannot form polyubiquitin chains. The reaction was incubated for 45 minutes with 60 ng of His-CHIP and 150 ng of GST-IRF-1 in each reaction. (b) Binding of modified IRF-1 compared to unmodified IRF-1 (from a) to C1 DNA was tested in an EMSA (electrophoretic mobility shift assay) with 100 ng of ubiquitinated or unmodified IRF-1 per reaction, bands were quantified using Image J and are presented in a graph in form of Arbitrary Units (right panel). (c) Binding of the samples (from a) to DNA was determined using a DNA binding assay on a microtiter plate, the plate was saturated with biotin tagged C1 oligonucleotide and incubated with increasing amounts of IRF-1 (0-40 ng) in the mobile phase. Bound IRF-1 was detected using an anti-IRF-1 mAb. (NS = non-specific band)

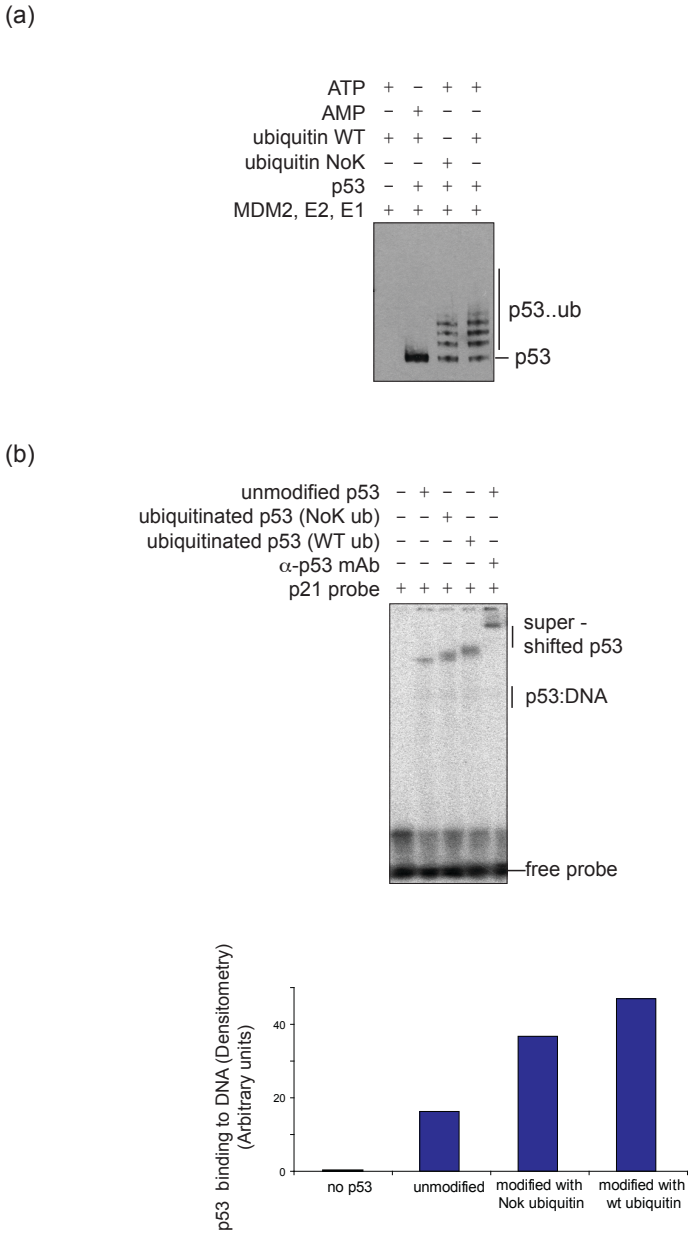

Figure 5-22 (Mono)-ubiquitination increases p53's ability to bind to DNA

(a) p53 was ubiquitinated in an *in vitro* reaction with either wild-type ubiquitin or an ubiquitin mutant (NoK) with all lysines mutated to arginine that cannot form polyubiquitin chains. The reaction was incubated for 45 minutes with 60 ng of MDM2 and 250 ng of p53 in each reaction. (b) Binding of modified compared to unmodified p53 (from a) to p21 promoter DNA was determined by EMSA with 500 ng of ubiquitinated or unmodified p53 per reaction. Where indicated a p53 mAb was added to the sample to supershift the p53:DNA complex. Bands on the EMSA gel were quantified using Image J and are presented in a graphical form below.

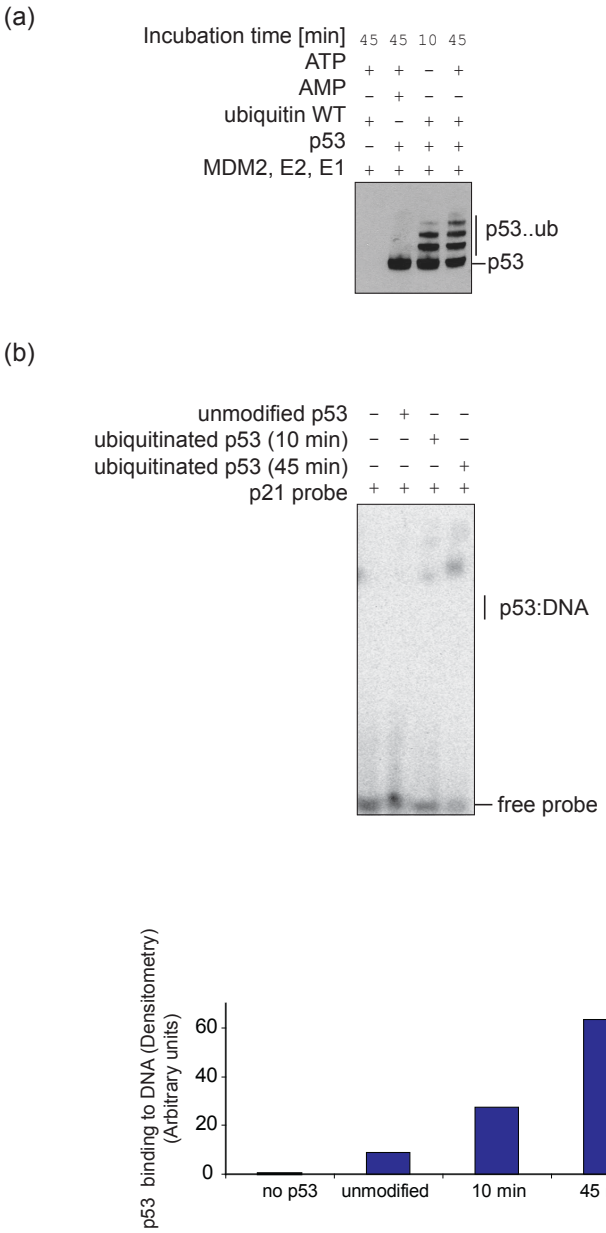

Figure 5-23 Increase in DNA binding ability of p53 correlates with an increase in ubiquitination

(a) p53 was ubiquitinated in an *in vitro* reaction. The reaction was incubated for 0, 10 or 45 minutes with 60 ng of MDM2 and 250 ng of p53 in each reaction. (b) Binding of modified compared to unmodified p53 (from a) to p21 promoter DNA was tested by EMSA with 500 ng of ubiquitinated or unmodified p53. Bands were quantified using Image J and are presented in a graph (lower panel).

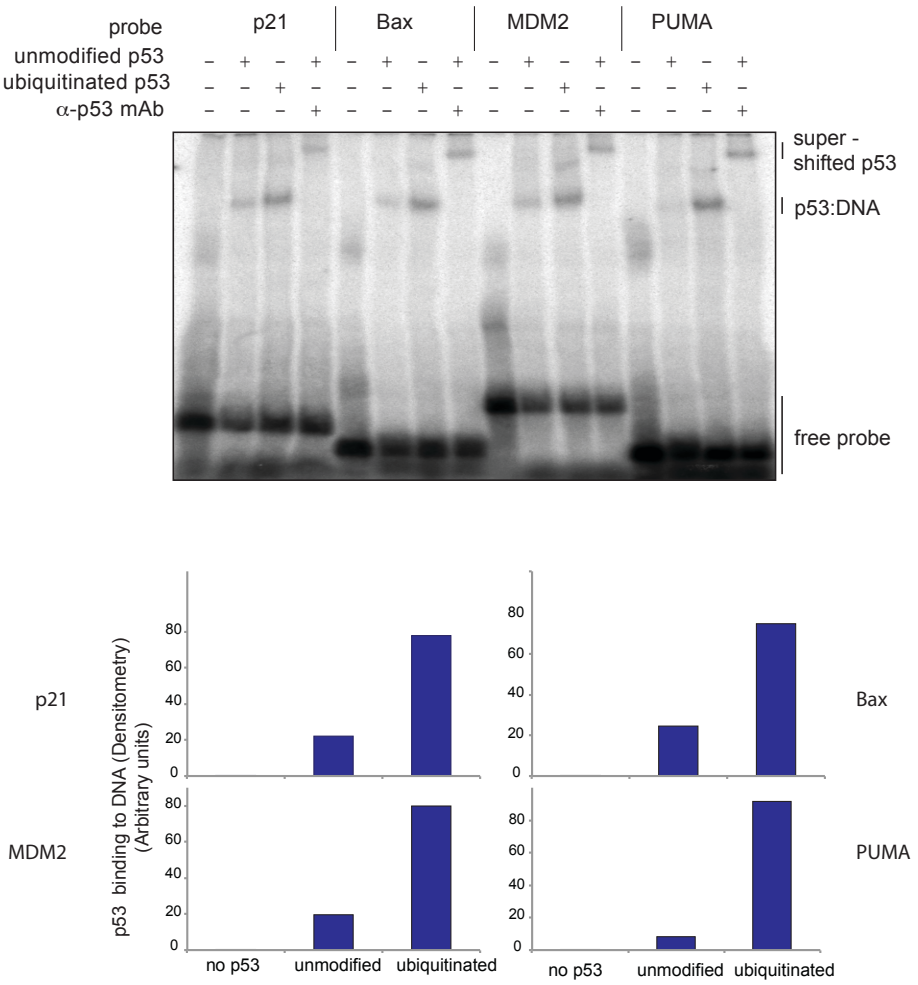

Figure 5-24 Ubiquitination of p53 leads to an increase of binding affinity to several promoters

EMSA comparing binding of 500 ng of *in vitro* ubiquitinated p53 and unmodified p53 to consensus sequences from the p53 target promoters: p21, MDM2, BAX and PUMA. p53 was ubiquitinated in an *in vitro* ubiquitination reaction for 45 minutes with 60 ng MDM2 and 250 ng p53, for the unmodified control AMP instead of ATP was added to the reaction. Bands on the EMSA gel were quantified using Image J (lower panel).

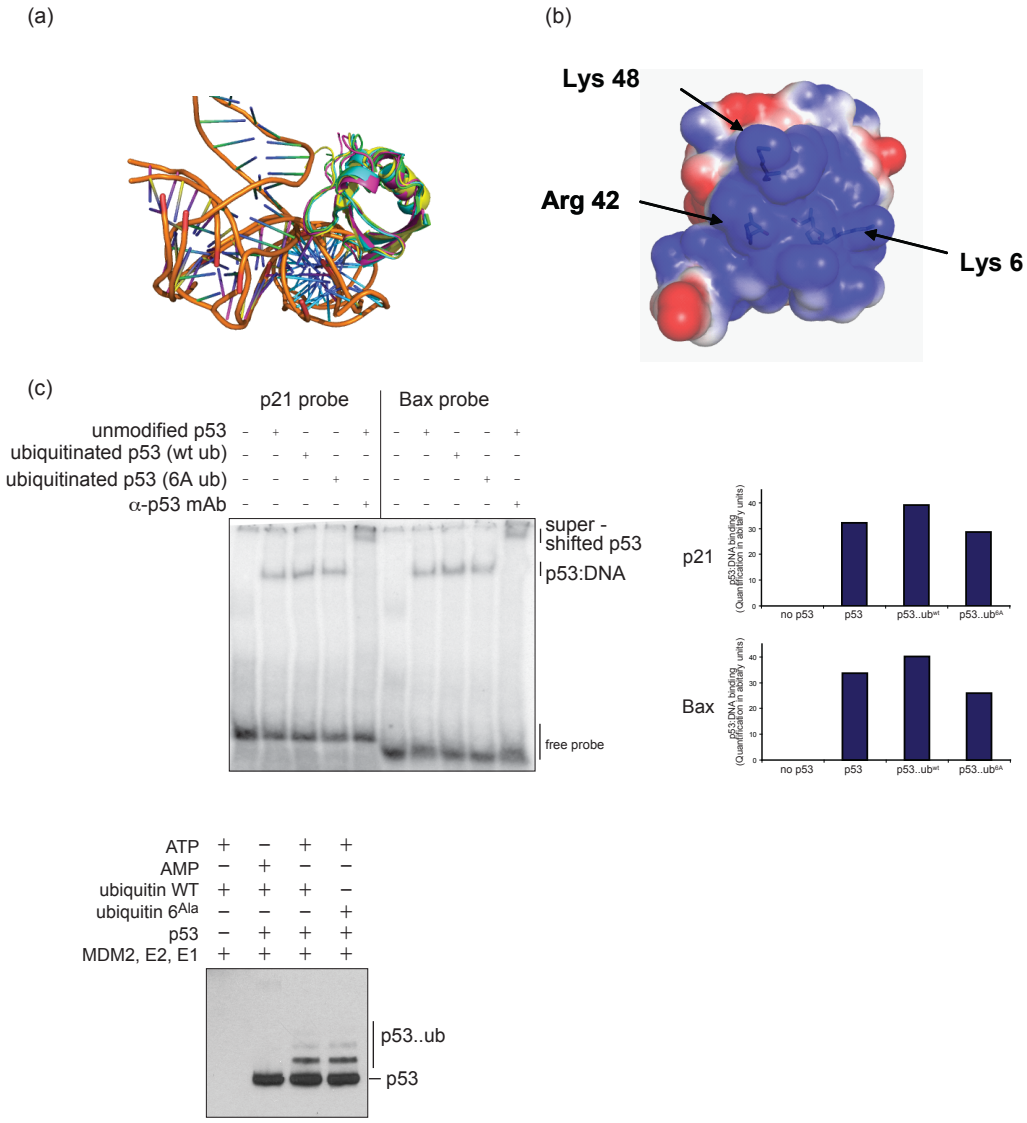

Figure 5-25 Specific residues on the surface of ubiquitin are involved in DNA interaction

(a) Overlay of ubiquitin in all five TA:ubiqutin:DNA models with respect to the DNA sequence. (b) Surface of the ubiquitin facing the DNA in the models. Positively charged residues that appear to interact with the DNA in the MD simulations are highlighted. (c) EMSA comparing binding of 500 ng p53, ubiquitinated with either ubiquitin^{WT} or ubiquitin^{6A} in an *in vitro* ubiquitination assay, to consensus sequences from the p53 target promoters p21 and BAX. p53 was ubiquitinated in an *in vitro* ubiquitination reaction for 45 minutes with 60 ng MDM2 and 250 ng p53. To obtain similar amounts of ubiquitinated p53, ATP was only added to the reaction for the last 10 minutes in the ubiquitin^{WT} sample. For the unmodified control AMP instead of ATP was added to the reaction. Bands on the EMSA gel were quantified using Image J (right panel).

5.2.9 Mutation of ubiquitin acceptor residues impairs the transcriptional of p53 and IRF-1

Results from experimental and *in silico* approaches have provided evidence that monoubiquitination at specific DBD Lys residues of p53 and IRF-1 will increase the ability of these TAs to form stable complexes with DNA and this is supported by the observation that monoubiquitinated p53 is tightly associated with chromatin. If the increase in DNA-binding activity and enhanced chromatin association result in a gain of TA function we would expect that loss of key ubiquitin acceptor Lys would adversely affect the TA activity of p53 and IRF-1. To investigate this, I asked whether the lysine residues within the DBDs of the two proteins that are subject to ubiquitination are required for full transcriptional activity in cells. In detail, I tested the transcriptional activity of both p53 and IRF-1 mutants that contain a mutation from lysine to arginine, at all residues that were shown to be ubiquitinated, in a dual luciferase reporter assay. A mutation from lysine to arginine preserves the charge of the amino acid, but does not allow its modification by ubiquitin.

The ability of the mutants and wild type proteins to modulate the rate of transcription from p21, Bax, PUMA and MDM2 promoters or TRAIL and CDK promoters was tested for p53 and IRF-1 respectively. Therefore, H1299 cells were cotransfected with Renilla luciferase, the reporter construct of interest fused to Firefly luciferase and either p53 or IRF-1. p53 contains ubiquitination sites in both its DNA binding and C-terminal domains. I, therefore, started of by determining the effect of mutations of all four lysines in the DBD and all six C-terminal lysines of p53, on its ability to promote transcription from the Bax and p21 promoters. Strikingly, while mutation of all six C-terminal lysines to arginine did not have any effect on the transcriptional activity of p53, mutation of residues in the DBD almost completely abolished p53 activity using both promoter reporters (Fig 5-26a-d). To investigate exactly which lysines residues were responsible for this effect, single point mutants at all for sites in the DBD were generated and tested in the assay. As shown in Fig 5-26a-d the most significant effect is observed with the mutant that carries a mutation at Lys^{292}, reduced activity was also observed for the protein with a mutation at Lys^{164} whereas and mutation of residues Lys^{305} or Lys^{101} lead to only very small decreases

in p53 transcriptional activity. This implies that ubiquitination of residues Lys^{292} and Lys^{164} is required for p53 activation. Interestingly the Lys^{164} to Arg mutant displayed a significant reduction in TA activity when assayed using MDM2 or BAX reporters, however this mutant was not impaired on the p21-reporter suggesting that there could be some promoter context specificity in the effects with respect to modification at a given DBD site. It is noteworthy, that these are the same sites that were used to model the p53:DNA complex in silico and where ubiquitin linkage lead to an increase in positively charged surface area that interacts wit DNA.

Results for IRF-1 showed that a mutation from Lys^{78} to Arg abolished its transactivation potential on the TRAIL promoter almost completely (Fig 5-26e). Moreover, the mutant was not able to repress transcription from the CDK2 promoter, where IRF-1 functions as a transcriptional repressor (Fig 5-26f). Single site mutations at the other residues lead to only a small change it IRF-1 dependent transactivation/repression, suggesting that ubiquitination at Lys^{78} is important for transcriptional control of IRF-1 under these conditions.

Taken together, the data on p53 and IRF-1 indicate that ubiquitination of the DBD domains in required for full transcriptional activity of both proteins. Furthermore, the results demonstrate that ubiquitination of p53 and IRF-1 can lead to an increase in their affinity for DNA and modelling results suggest that this is due to stabilising interactions between ubiquitin and the promoter DNA. Overall, the results presented in this chapter indicate a complex role for ubiquitination in the control of p53 and IRF-1 activity and stability.

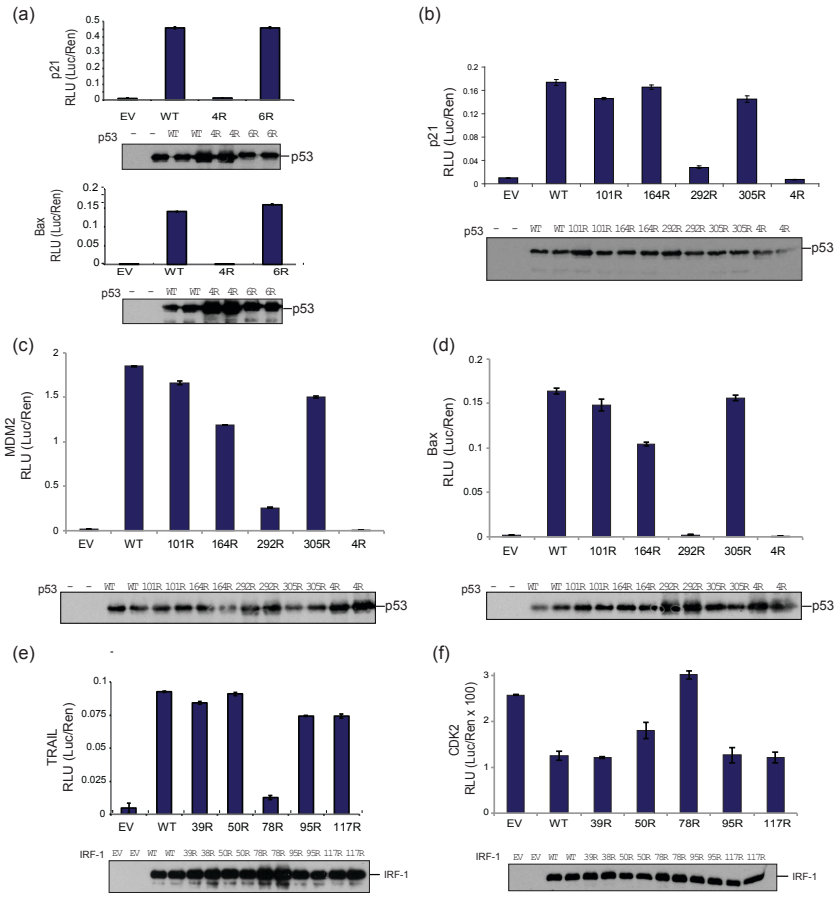

Figure 5-26 Mutation of the ubiquitin acceptor lysines in p53's and IRF-1 DBD decrease their transcriptional activity

(a) H1299 cells were co-transfected with either WT p53 or mutants with all four ubiquitin acceptor lysine in the DBD (4R) or all six C-terminal lysines (6R) mutated to arginine, and a p21 or Bax reporter construct. As a control, promoter activity of a renilla promoter construct was measured. Results are plotted as the normalized firefly luciferase activity over the value of Renilla luciferase and represent the mean of two independent experiments together with standard deviations in relative light units (RLU). (b-d) H1299 cells were transfected with either p53 WT or p53 with a mutation from lysine to arginine at Lys^{101}, Lys^{164}, Lys^{292}, Lys^{305} or with 4R together with a (b) p21, (c) MDM2, or (d) Bax reporter plasmid. Dual luciferase assays were carried out as described above and the transcriptional activity of p53 WT and mutants was compared. (e+f) H1299 cells were co-transfected with 100 ng of either IRF-1 WT or IRF-1 with a mutation from lysine to arginine at Lys^{39}, Lys^{50}, Lys^{78}, Lys^{95} or Lys^{117} and the (e) TRAIL or (f) CDK2 reporter plasmid and renilla. The activity of IRF-1 to activate transcription of the promoter was determined using the dual luciferase assay and activity at the promoters was measured as described above.

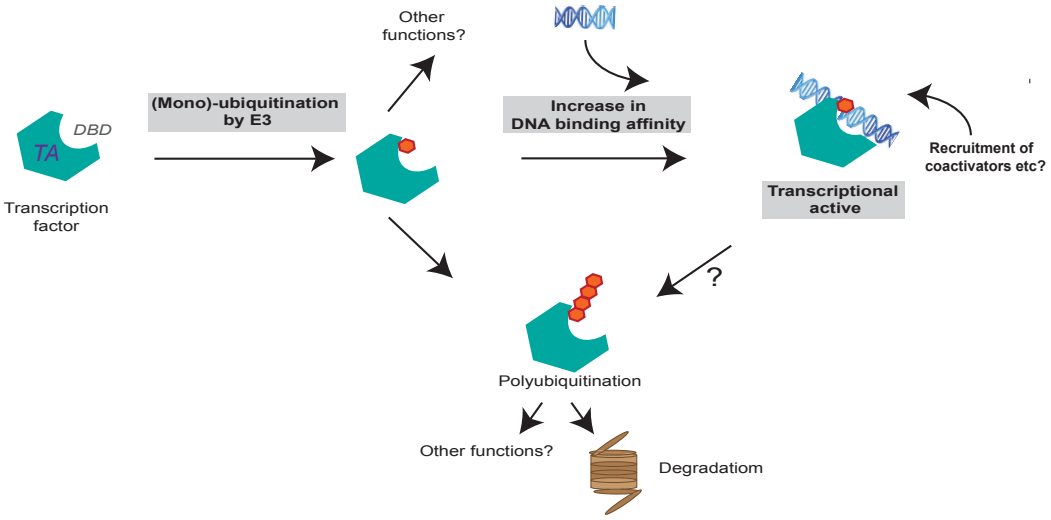

Figure 5-27 Model of role of monoubiquitination in the control of transcriptional activation

5.3 Discussion

Tight control of gene expression is critical for maintenance of cellular homeostasis and thus the prevention of disease development. Therefore, transcription is one of the most highly regulated processes in the eukaryotic cell, including tight control of transcriptional regulator activity. Ubiquitination and subsequent degradation by the proteasome is known to be the primary mechanism by which the stability, and thereby activity, of the transcription factors p53 and IRF-1 is regulated. Here, I demonstrate that (i) the ability of IRF-1 and p53 to bind DNA is increased upon ubiquitination, and that monoubiquitination is sufficient for this gain of function, (ii) increase in p53 ubiquitination occurs in response to activating stimuli and this uncoupled from its degradation, (iii) ubiquitinated forms of p53 are chromatin associated following p53-pathway activation. These results suggest an additional role of ubiquitination in the regulation of the two transcription factors IRF-1 and p53, besides signalling their degradation (see model, Fig 5-27).

A strong link between the UPS and control of several aspects of transcription has become evident in recent time. Ubiquitination of the two viral transcriptional regulators Tat (human immunodeficiency virus type 1) and Human Papillomavirus E2 by MDM2 was shown to be essential for their transactivation function [340, 341]. Fusion of a single ubiquitin molecule to the C-terminal end of Tat bypasses the requirement for MDM2 and provides a fully activate TA, indicating that monoubiquitination by MDM2 is required for the function of Tat as a transcriptional regulator [340]. Additionally, the transcription factors Gal-4 and Myc need to be ubiquitinated in order to be fully active [336, 350, 351]. Several mechanisms have been proposed to explain the link between ubiquitination and TA activation, these mainly involve the recruitment of co-factors to the site of transcriptional initiation, e.g. of the 19S regulatory particle of the proteasome, which exhibits ubiquitin binding ability and is important in transcription elongation by RNA polymerase II [97, 340, 352]. Additionally, it has been argued that in certain cases monoubiquitination can protect promoter bound activators from the unfolding activities of proteasomal ATPases by disrupting TA:ATPase complexes [339]. Ubiquitin can aid in the formation of active enhanceosomes, as seen for the

transcriptional co-regulator CIITA, which in its ubiquitinated form, acts as a scaffold, recruiting several other factors to the site of transcription [342]. Finally, the destruction of the TA as a requirement for further rounds of gene transcription was described by Geng *et al*. (2012) [91] in a model where the TA is phosphorylated by kinases that are associated with the transcriptional machinery. This phosphorylation not only marks the TA as spent and unable to stimulate further rounds of transcription, but also recruits E3 ligases that ubiquitinate the TA leading to its destruction. If ubiquitination/degradation of the TA is inhibited, the inactive TA blocks the promoter binding site, preventing other active regulators to bind and initiate further rounds of transcription [91, 353-355].

Here, I propose an additional mechanism for the activation of TAs by ubiquitin (see model, Fig 5-27). I show that ubiquitination of residues within p53 and within IRF-1 DBD stabilises the interaction of these 2 TAs with their respective consensus sequences. A mutational analysis of ubiquitin acceptor residues in both proteins, indicates that ubiquitination of specific lysine residues within their respective DBD's may be required for full transactivation. Models of the DBD:ubiquitin:DNA complex were computed to get an insight into the binding interface of the apo- compared to the ubiquitinated protein. The computational modelling, together with molecular dynamic simulations, suggests that ubiquitinated residues, mainly Lys^{6}, Arg^{42} and Lys^{48}, directly interact with the promoter DNA, thereby stabilising the protein:ubiquitin:DNA complex. This is confirmed by electrostatic surface analysis of the models, which shows that monoubiquitination leads to a dramatic increase of the positively charged surface area that interacts with the promoter DNA. This observation is intriguing, as even though the role of ubiquitination in promoting protein-protein interactions by providing part of the binding interface is well established, to our knowledge no example has been described where ubiquitin stabilises a DNA-protein interactions by forming part of the protein:DNA interface.

Based on these observations, I propose a mechanism where ubiquitin can directly enhance the affinity of a TA for its target promoter, I also speculate that sequence specificity is determined through the DBD of the TA and that ubiquitin strengthens TA:DNA binding by DNA sequence unspecific electrostatic interactions involving a

highly charged positively patch on its surface. However, even though the modelling data strongly suggest a direct contribution of ubiquitin residues in the TA:DNA interactions, I can not rule out that ubiquitination can lead to conformational changes in the TAs, which increases the affinity of the DBD for DNA through an allosteric mechanism or a combination of direct interactions of ubiquitin with DNA and allosteric changes in the TAs.

The modelling data indicate that the increase of DNA binding is mostly mediated by the first and possibly by the second ubiquitin molecule, but that any further chain elongation would not lead to additional stabilisation of the complex (Fig 5-20). Indeed does ubiquitination of IRF-1 or p53, by an ubiquitin mutant that can only form monoubiquitination, result in an increase in DNA binding, suggesting that (multi) mono/ or di-ubiquitination is sufficient to enhance binding of the transcription factors to DNA. This is in line with my observation, that p53 ubiquitination following its activation does not lead to its degradation. It is commonly believed that at least four ubiquitin molecules are required to mediate degradation, while shorter chains (or chains with different linkages) have been associated with other cellular signals. Nutlin-3 treatment leads to the formation of mainly mono- or di ubiquitinated p53, indicating that under activating conditions p53 ubiquitination can be 'switched' from polyubiquitination linked to degradation to monoubiquitination involved in p53 activation. Nutlin-3 was identified as a small molecular inhibitor of the MDM2-p53 interaction, by binding to the hydrophobic pocket of MDM2 and blocking binding to the Box I motif on p53 [344]. Subsequently, Nutlin-3 was shown to activate p53, leading to apoptosis and it is currently being tested in clinical trials as a novel anti-cancer drug. However, the mechanism by which Nutlin activates the p53 pathway remained a subject of discussion. The most widely accept hypothesis is that Nutlin, by binding to the hydrophobic pocket of MDM2, disrupts its interaction with p53 and thereby inhibits MDM2 mediated ubiquitination and degradation of p53, stabilising its levels and leading to increased transcription of p53 target genes. Conflictingly, however, complete knock-down of MDM2 does not result in an increase of p53 steady state level comparable to the striking up regulation of p53 levels/activity observed in

Nutlin-3 treated cells [356]. This indicates that pure inhibition of MDM2 is not sufficient to explain the activating effect of Nutlin-3 on p53 function. The Ball group has previously reported that Nutlin-3, despite disrupting the high affinity interaction between MDM2 and p53 and releasing the trans-repression activity of MDM2 on p53 [357], Nutlin-3 does not inhibit p53 ubiquitination. In fact they suggested that it leads to conformational changes in MDM2 that can promote interactions between a second MDM2 binding site in the core domain of p53 by the acid domain of MDM2, and that furthermore this interaction is sufficient to facilitate MDM2 mediated ubiquitination of p53. In other words Nutlin-3 acts as an allosteric activator. Here, I built on this model and show that Nutlin-3 can both enhance p53 ubiquitination and modify the ubiquitination pattern, resulting in a pool of monoubiquitinated, active p53 that is localised in the chromatin bound fraction of the nucleus. Even though Nutlin-3 can partially inhibit p53:MDM2 complex formation *in vitro*, more p53:MDM2 complexes can be detected in Nutlin-3 treated cells compared to control cells. This most likely reflects the striking increase in p53 and MDM2 levels in Nutlin-3 treated cells, and shows that interaction of MDM2 with p53's ubiquitination signal in its core domain is sufficient for MDM2:p53 complex formation in cells. As I detect mainly monoubiquitinated p53 in Nutlin-3 treated cells, I postulate that the MDM2:p53 complexes detected lead to p53 monoubiquitination. It would be interesting to determine if a specific ubiquitin-conjugating enzyme preferably interacts with MDM2 in its Nutlin-3 bound conformation, leading to a change in the ubiquitination pattern or if Nutlin-3 can affect the engagement of possible E4 enzymes in p53 ubiquitination.

Ubiquitination of chromatin associated p53 after radiation, but not Nutlin-3 treatment, is dependent on the ATM kinase. ATM is the primary regulator of the double strand break response in cells and leads to p53 activation. It has been shown to directly phosphorylate p53 at Ser^{15} during activation. Furthermore, ATM directly phosphorylates MDM2 at Ser^{395} and indirectly mediates phosphorylation of Tyr^{394} via the c-Abl kinase [358]. It remains to be investigated whether phosphorylation of p53, MDM2 or both by ATM mediate increased ubiquitination of p53. The requirement for ATM function in order for DNA damage to mediate p53

ubiquitination shows that ubiquitination is direct downstream effect of p53 activation via the ATM-pathway.

Interestingly and in line with our results, the E3 ligase E4F1 was shown to lead to p53 polyubiquitination but not degradation [359]. Remarkably, E4F1 promotes p53 dependent transcription of factors involved in cell cycle arrest rather than apoptosis. It would be interesting to determine if ubiquitination of specific residues or by other UBL modifications can change the affinity of p53 for a specific set of promoters and thereby, distinguish between different cellular responses to p53 under specific stress conditions.

The data presented here, suggest that p53 and IRF-1 are members of the class of transcription factors that are activated by ubiquitination, and that this is due to stabilisation of the TA:DNA complex by ubiquitin linked to residues in the proteins DNA binding domain. The importance of the on and off rate of TA binding to their target promoter, in contrast to the pure promoter occupancy, has recently been highlighted by Lickwar *et al.* [360]. This study demonstrates that long residence and thus lower dissociation rates strongly correlate with TA function, while fast binding turnover correlates with shorter residence at the promoter and lower transcriptional activity. We can speculate therefore could that ubiquitin increases promoter occupancy by stabilising the interaction once the transcription factor is bound to DNA and thereby prolonging the residence at the promoter, thus increasing the chances of transcription initiation. A 'licensing' or 'kamikaze model' has also been proposed [137]; where monoubiquitination of TAs lead to their activation but at the same time inevitably results in polyubiquitination and thus TA destruction. In our observations, however, ubiquitinated forms of p53, especially after Nutlin-3 treatment, are very stable and do not appear to lead to polyubiquitination and hence to degradation. This, additionally, shows that active p53 is not ubiquitinated in order to be degraded and 'vacate' a promoter binding site for binding of 'fresh' activators that can initiate another round of transcription, as proposed in the model by Geng *et al.* [91], described earlier. Rather, the results presented here show that under certain conditions p53 ubiquitination can be completely uncoupled from its degradative function and serve purely to activate its transcriptional activity. p53 is an unusual

transcription factor in the sense that its level are almost exclusively regulated through degradation and not by expression. As degradation of p53 is almost completely halted under activating conditions, it is possible that the complete uncoupling of p53 monoubiquitination from degradation forms an exception of TA activation. The levels of the transcription factor IRF-1, on the other hand, are regulated through both, the rate of expression as well degradation. Moreover, the Ball group has previously shown that a reduction in its half-life marks IRF-1 more active [136], making it a *bona fide* example for a transcription factor that is regulated by the 'kamikaze model'. Additionally I showed, in chapter 4, that IRF-1, when in a DNA bound conformation, does not get ubiquitinated (further). It would thus be possible that monoubiquitination stimulates IRF-1 to bind to specific promoters, then, while initiating transcription, IRF-1 is protected from polyubiquitination, and only after DNA dissociation its DBD is accessible for polyubiquitination by E3 ligases that leads to its degradation terminating the signal. To confirm these speculations and to gain complete understanding of the role of monoubiquitination in the control of TA activity and its link to polyubiquitination and degradation, the effects of monoubiquitination on the activity and stability of these and other TAs, as well the E3, E4 and DUB enzymes involved in the process, will have to be studied in more detail.

In summary, I report, for the first time, that ubiquitination of the DNA binding domain of transcription factors can directly enhance binding of the protein to their respective consensus DNA. Furthermore, I show that ubiquitination is involved in activation of p53 and that this can be exploited by the small molecular drug Nutlin-3, which leads to an increase in p53 mono- or multiubiquitination resulting in its association with chromatin and thus activation. More research is necessary to determine how the fate of ubiquitinated p53 is determined. Most likely chain topology and length as well as the specific residue targeted on p53 are involved in determining the outcome of p53 ubiquitination. Importantly, this study highlights the need to further study the role of ubiquitination in the control of p53 activity to fully understand how the UPS is involved in p53 control. Development of small molecular drugs that target p53 E3 ligases to inhibit degradation of the tumour suppressor p53

is a main research interest, however, as shown here modification rather than complete blockage of p53 ubiquitination, as seen for Nutlin-3, might be a more successful approach to restore or activate the tumour suppressive function of p53. In conclusion, the data presented in this chapter indicate a complex role of ubiquitination in the control of the activity of the transcription factors IRF-1 and p53.

Chapter 6: Conclusion and future directions

This thesis aimed to expand our understanding of IRF-1 and p53 ubiquitination by studying two main areas, (i) regulation of the activity and specificity of their E3 ligases (ii) and the implications of ubiquitination on their transcriptional activity. And to thereby gain insight into how ubiquitination of these tumour suppressor proteins is controlled under different conditions to regulate their function.

I presented a novel mechanism by which ubiquitination can be directly involved in the activation of transcription factors by stabilising the interactions with their cognate DNA sequence at target promoters. The fact that both transcription factors studied during my PhD bind DNA more stably when in their ubiquitinated form is intriguing, and indicates that this could be a more general mechanism that is the property of a number of transcriptional regulators. Indeed, several other transcription factors have been shown to require modification by ubiquitin in order to be fully active, including other substrates of MDM2 [340, 361]. It would be interesting to determine if ubiquitination of these transcriptional regulators can stabilise their DNA interactions in a manner similar to that seen of IRF-1 and p53. Further research is necessary to gain an understanding of a possible link between monoubiquitination observed in transcriptional active transcription factors and polyubiquitination leading to their degradation. The 'Kamikaze model' which proposes that ubiquitination could act as a licencing event which activates a TA and at the same time targets it for degradation [137], provides an interesting idea in which a transcription factor is particularly active when very short lived, thus allowing tight control of its activity. This idea is supported by data showing that several transcriptional regulators are most active, when their half-life is reduced, as seen for IRF-1 [136], and that transactivation and degron domains overlap in numerous proteins [91]. The results obtained as part of this study, however, did not reveal a direct link between p53 ubiquitination as part of its activation and that, which signals its destruction. Conversely, I showed that the half-life of active, ubiquitinated p53 is strikingly increased compared to control conditions, implying that the relationship between mono- and polyubiquitination is complex and that once monoubiquitination has occurred, polyubiquitination and

degradation do not inevitably follow. p53 was shown to be targeted by different DUBs, including HAUSP [215]; and it would be interesting to study the role of DUB activity in the regulation of p53 activation. Another question that remains elusive is how the cell controls the outcome of p53 ubiquitination, especially if the same E3 is involved in activation as well as degradation. In the case of MDM2, it has been proposed that the ratio of MDM2 to MDM4 protein, as well as the concentration of MDM2, is involved in the regulation of its activity, tilting MDM2 activity either towards poly- or monoubiquitination [215, 362]. Additionally, ligand binding could influence the outcome of an ubiquitination event. Nutlin-3 induced monoubiquitination of p53 by MDM2 shown here is an example for this. The roles of MDM2, MDM4, other E3 ligases and different E2 enzymes in the activation of p53 upon DNA damage need to be examined in more detail to attain complete understanding of the process. I have carried out preliminary experiments with the aim to identify E3 ligases that are involved in p53 monoubiquitination in response to physiological stress signals. Therefore, chromatin associated proteins were isolated from nuclei of irradiated cells (IR) by sucrose gradient fractionation and analysed by mass spectrometry. The results, which revealed chromatin associated E3 ligases, will need to be validated carefully and the possible implications of these E3 ligases in the control of p53 monoubiquitination remain to be investigated.

One of the main challenges of studying ubiquitination in a cellular context are the limitations to detect specific chain linkages as well to introduce a protein that is ubiquitinated at a specific residue into cells. In contrast to phosphorylation, where a mutation with a negatively charged side chain can be utilised to study its effects *in vivo*, no such modification is available to study ubiquitination. Different studies have utilised ubiquitin fusions protein to either the N- or C-terminus of proteins [363, 364], results of these studies, however, have to be interpreted carefully. It is now clear that different patches on the surface of ubiquitin play distinct roles in interactions with specific ubiquitin binding proteins and that these often interact with residues of both ubiquitin and residues on the surface of the target proteins [8]. Thus, site specificity and orientation of the ubiquitin molecule are important factors in

ubiquitin signalling. In the case of a C-terminal fusion protein, the ubiquitin molecule has a free C-terminus, which is normally linked to a residue on the target protein, while its N-terminal methionine is attached to the target protein. This results in a completely different orientation of the ubiquitin molecule, than if it was linked to a lysine residue on the substrate. Studys by the Gu and Vousden laboratories, for example, suggested that monoubiquitination of p53 signals nuclear export [362-364]; these observations, however, heavily relied on the use of transfected C-terminal ubiquitin fusion proteins in the absence of activating signals.
In my studies, I found it difficult to recapitulate the endogenous p53 pathway using transfections in general, this is most likely due to the fact that introduction of p53 into cells causes growth arrest in the absence of any additional stress signals. To overcome this difficulty, I adapted methods that allowed the detection of the endogenous ubiquitination system, for example sucrose gradient fractionation to study chromatin bound endogenous p53 and PLA to investigate the localisation of endogenous, ubiquitinated p53. Unfortunately, the reagents available to study IRF-1 are not as sensitive as for p53 e.g. antibodies, and it was therefore more difficult to study endogenous ubiquitination of IRF-1 in cells, leading me to focus on p53 at this part of the project.

New technologies are emerging that allow the construction of ubiquitinated proteins or peptides *in vitro*. Most of these advances focus on the introduction of an ubiquitin molecule by chemical modification residues in both a recombinant acceptor protein and the C-terminus of ubiquitin [51]. These techniques could give additional insight into outcomes of ubiquitination at specific lysine residues on a target protein. So could a p53 or IRF-1 construct linked to ubiquitin at specific lysines give insight into how ubiquitination at these exact residues affects its ability to interact with DNA, and furthermore it could reveal if this modification stimulated or inhibited interaction with other proteins. Constructing a CHIP or MDM2 protein that is linked to ubiquitin at one of the acceptors sites I identified using mass spectrometry, could show if and how this modification affects its activity i.e. chain, substrate and E2 specificity.

The study of site-specific ubiquitination *in vivo* remains challenging, linkage- or site-specific antibodies are being developed to investigate effects of specific linkages and ubiquitination at distinct sites, e.g. for H2B [365]. It would be worthwhile generating antibodies that can detect p53 or IRF-1 protein that is specifically ubiquitinated at DBD residues, which are implicated to play a role in their transcriptional control.

Studying the relationship between DNA binding and ubiquitination of IRF-1 further revealed that IRF-1 does not interact with the two ligases MDM2 and CHIP when in a DNA bound conformation and is thus protected from ubiquitination and destruction when in an active conformation. Furthermore, it is unable to interact with other proteins that also bind to its Mf2 domain. This is intriguing and it would be useful to compare the interactome of IRF-1 in a DNA bound compared to a DNA unbound conformation. Other Mf2 binding proteins have regulatory effects on IRF-1 and it would be interesting to determine, if these effects on IRF-1 are inhibited by DNA in a similar manner to that of E3 ligases. It will also be worthwhile to study, if DNA binding introduces allosteric changes in IRF-1, which in addition to blocking interactions with a specific set of proteins, allows other proteins to bind and regulate IRF-1 activity or assists its function.

Lysine acetylation and ubiquitination are two mutual exclusive modifications. Lys^{78} of IRF-1 has previously been shown to be acetylated by the CBP acetyltransferase [325]. The fact that this site is subject to both ubiquitination and acetylation implies that these two posttranslational modifications have interdependent roles, where acetylation could act as a regulator of ubiquitination and vice versa. It would be worthwhile to study the interplay between these two modifications further.

Work presented in this thesis identified ubiquitination sites that were mapped using an *in vitro* mass spectrometry approach. I have evaluated the results for sites identified on IRF-1, but not CHIP and MDM2. It would be useful to verify the autoubiquitination sites on these proteins by a mutational study. The *in vitro* technique to map ubiquitination sites is limited, as it does not give information about how the ubiquitination pattern is regulated by cellular stresses or stimuli. Recently a di-glycine antibody has become available that can be used to isolate peptides that

contain a remnant di-glycine, which is representative for ubiquitinated proteins after trypsin digestion [366]. Using this antibody, ubiquitinated peptides can be enriched from a complex sample, like cell lysates. The antibody however, does not distinguish between modification with ubiquitin and some ubiquitin like modifier, including NEDD8 and ISG 15, which also result in a remnant di-glycine when digested by trypsin [367]. To specifically study the ubiquitinated proteome it would therefore be necessary to isolate ubiquitin modified proteins in an intermediate step before trypsin digestion. This approach would allow a more systematic study of ubiquitination sites from proteins isolated both from cell lysate and *in vitro* reactions and could provide a more detailed understanding of how proteins are modified by ubiquitin under different cellular conditions. It would be worthwhile to dissect how proteins like p53 are ubiquitinated under different conditions to gain an insight into the effect of stimuli like ionising radiation or Nutlin-3 on both the ubiquitination pattern and the lysines residues modified. *In vitro* studies using ligands that bind to E3 ligases and modulate their activity, including the ones presented in this thesis i.e. Hsp70 to CHIP and Nutlin-3 to MDM2 could help us gain understanding of how binding proteins regulate the specificity of E3 ligases. Furthermore, the di-glycine antibody could be employed for a systematic study to detect ubiquitinated transcription factor associated with chromatin and reveal if these are ubiquitinated within or adjacent to their DBD.

In conclusion, in the work presented here, I have started to dissect the complex relationship of E3 ligase regulation and the cellular signal of the modification on the target protein. However, many question on the control and effects of p53 and IRF-1 ubiquitination and how these could possibly be exploited in the use of therapeutics remain to be investigated in future studies.

Bibliography

1. Ciechanover, A., Heller, H., Elias, S., Haas, A.L., and Hershko, A. (1980). ATP-dependent conjugation of reticulocyte proteins with the polypeptide required for protein degradation. Proc Natl Acad Sci U S A *77*, 1365-1368.
2. Hershko, A., Ciechanover, A., Heller, H., Haas, A.L., and Rose, I.A. (1980). Proposed role of ATP in protein breakdown: conjugation of protein with multiple chains of the polypeptide of ATP-dependent proteolysis. Proc Natl Acad Sci U S A *77*, 1783-1786.
3. Finley, D. (2009). Recognition and processing of ubiquitin-protein conjugates by the proteasome. Annu Rev Biochem *78*, 477-513.
4. Spasser, L., and Brik, A. (2012). Chemistry and biology of the ubiquitin signal. Angew Chem Int Ed Engl *51*, 6840-6862.
5. Hochstrasser, M. (2009). Origin and function of ubiquitin-like proteins. Nature *458*, 422-429.
6. Pickart, C.M., and Eddins, M.J. (2004). Ubiquitin: structures, functions, mechanisms. Biochim Biophys Acta *1695*, 55-72.
7. Kirkin, V., and Dikic, I. (2011). Ubiquitin networks in cancer. Curr Opin Genet Dev *21*, 21-28.
8. Komander, D., and Rape, M. (2012). The ubiquitin code. Annu Rev Biochem *81*, 203-229.
9. Xu, P., Duong, D.M., Seyfried, N.T., Cheng, D., Xie, Y., Robert, J., Rush, J., Hochstrasser, M., Finley, D., and Peng, J. (2009). Quantitative proteomics reveals the function of unconventional ubiquitin chains in proteasomal degradation. Cell *137*, 133-145.
10. Ikeda, F., Deribe, Y.L., Skanland, S.S., Stieglitz, B., Grabbe, C., Franz-Wachtel, M., van Wijk, S.J., Goswami, P., Nagy, V., Terzic, J., et al. (2011). SHARPIN forms a linear ubiquitin ligase complex regulating NF-kappaB activity and apoptosis. Nature *471*, 637-641.
11. Ben-Saadon, R., Zaaroor, D., Ziv, T., and Ciechanover, A. (2006). The polycomb protein Ring1B generates self atypical mixed ubiquitin chains required for its in vitro histone H2A ligase activity. Mol Cell *24*, 701-711.
12. Kim, H.T., Kim, K.P., Lledias, F., Kisselev, A.F., Scaglione, K.M., Skowyra, D., Gygi, S.P., and Goldberg, A.L. (2007). Certain pairs of ubiquitin-conjugating enzymes (E2s) and ubiquitin-protein ligases (E3s) synthesize nondegradable forked ubiquitin chains containing all possible isopeptide linkages. J Biol Chem *282*, 17375-17386.
13. Kulathu, Y., and Komander, D. (2012). Atypical ubiquitylation - the unexplored world of polyubiquitin beyond Lys48 and Lys63 linkages. Nat Rev Mol Cell Biol *13*, 508-523.
14. Schimmel, J., Larsen, K.M., Matic, I., van Hagen, M., Cox, J., Mann, M., Andersen, J.S., and Vertegaal, A.C. (2008). The ubiquitin-proteasome system is a key component of the SUMO-2/3 cycle. Mol Cell Proteomics *7*, 2107-2122.

15. Dohmen, R.J., Stappen, R., McGrath, J.P., Forrova, H., Kolarov, J., Goffeau, A., and Varshavsky, A. (1995). An essential yeast gene encoding a homolog of ubiquitin-activating enzyme. J Biol Chem *270*, 18099-18109.
16. Rajagopalan, K.V. (1997). Biosynthesis and processing of the molybdenum cofactors. Biochem Soc Trans *25*, 757-761.
17. Burroughs, A.M., Jaffee, M., Iyer, L.M., and Aravind, L. (2008). Anatomy of the E2 ligase fold: implications for enzymology and evolution of ubiquitin/Ub-like protein conjugation. J Struct Biol *162*, 205-218.
18. Schwartz, A.L., and Ciechanover, A. (2009). Targeting proteins for destruction by the ubiquitin system: implications for human pathobiology. Annu Rev Pharmacol Toxicol *49*, 73-96.
19. Haas, A.L., and Rose, I.A. (1982). The mechanism of ubiquitin activating enzyme. A kinetic and equilibrium analysis. J Biol Chem *257*, 10329-10337.
20. Haas, A.L., Warms, J.V., Hershko, A., and Rose, I.A. (1982). Ubiquitin-activating enzyme. Mechanism and role in protein-ubiquitin conjugation. J Biol Chem *257*, 2543-2548.
21. Hershko, A., and Ciechanover, A. (1998). The ubiquitin system. Annu Rev Biochem *67*, 425-479.
22. Huibregtse, J.M., Scheffner, M., Beaudenon, S., and Howley, P.M. (1995). A family of proteins structurally and functionally related to the E6-AP ubiquitin-protein ligase. Proc Natl Acad Sci U S A *92*, 2563-2567.
23. Nuber, U., Schwarz, S., Kaiser, P., Schneider, R., and Scheffner, M. (1996). Cloning of human ubiquitin-conjugating enzymes UbcH6 and UbcH7 (E2-F1) and characterization of their interaction with E6-AP and RSP5. J Biol Chem *271*, 2795-2800.
24. Ye, Y., and Rape, M. (2009). Building ubiquitin chains: E2 enzymes at work. Nat Rev Mol Cell Biol *10*, 755-764.
25. Koegl, M., Hoppe, T., Schlenker, S., Ulrich, H.D., Mayer, T.U., and Jentsch, S. (1999). A novel ubiquitination factor, E4, is involved in multiubiquitin chain assembly. Cell *96*, 635-644.
26. Jackson, P.K., Eldridge, A.G., Freed, E., Furstenthal, L., Hsu, J.Y., Kaiser, B.K., and Reimann, J.D. (2000). The lore of the RINGs: substrate recognition and catalysis by ubiquitin ligases. Trends Cell Biol *10*, 429-439.
27. Suzuki, H., Chiba, T., Suzuki, T., Fujita, T., Ikenoue, T., Omata, M., Furuichi, K., Shikama, H., and Tanaka, K. (2000). Homodimer of two F-box proteins betaTrCP1 or betaTrCP2 binds to IkappaBalpha for signal-dependent ubiquitination. J Biol Chem *275*, 2877-2884.
28. Passmore, L.A., and Barford, D. (2004). Getting into position: the catalytic mechanisms of protein ubiquitylation. Biochem J *379*, 513-525.
29. McDowell, G.S., Kucerova, R., and Philpott, A. (2010). Non-canonical ubiquitylation of the proneural protein Ngn2 occurs in both Xenopus embryos and mammalian cells. Biochem Biophys Res Commun *400*, 655-660.
30. Tait, S.W., de Vries, E., Maas, C., Keller, A.M., D'Santos, C.S., and Borst, J. (2007). Apoptosis induction by Bid requires unconventional ubiquitination and degradation of its N-terminal fragment. J Cell Biol *179*, 1453-1466.
31. Vosper, J.M., McDowell, G.S., Hindley, C.J., Fiore-Heriche, C.S., Kucerova, R., Horan, I., and Philpott, A. (2009). Ubiquitylation on canonical and non-

canonical sites targets the transcription factor neurogenin for ubiquitin-mediated proteolysis. J Biol Chem *284*, 15458-15468.
32. Peng, J., Schwartz, D., Elias, J.E., Thoreen, C.C., Cheng, D., Marsischky, G., Roelofs, J., Finley, D., and Gygi, S.P. (2003). A proteomics approach to understanding protein ubiquitination. Nat Biotechnol *21*, 921-926.
33. Gerlach, B., Cordier, S.M., Schmukle, A.C., Emmerich, C.H., Rieser, E., Haas, T.L., Webb, A.I., Rickard, J.A., Anderton, H., Wong, W.W., et al. (2011). Linear ubiquitination prevents inflammation and regulates immune signalling. Nature *471*, 591-596.
34. Chen, Z.J., and Sun, L.J. (2009). Nonproteolytic functions of ubiquitin in cell signaling. Mol Cell *33*, 275-286.
35. Skaug, B., Jiang, X., and Chen, Z.J. (2009). The role of ubiquitin in NF-kappaB regulatory pathways. Annu Rev Biochem *78*, 769-796.
36. Vijay-Kumar, S., Bugg, C.E., and Cook, W.J. (1987). Structure of ubiquitin refined at 1.8 A resolution. J Mol Biol *194*, 531-544.
37. Dikic, I., Wakatsuki, S., and Walters, K.J. (2009). Ubiquitin-binding domains - from structures to functions. Nat Rev Mol Cell Biol *10*, 659-671.
38. Shih, S.C., Sloper-Mould, K.E., and Hicke, L. (2000). Monoubiquitin carries a novel internalization signal that is appended to activated receptors. EMBO J *19*, 187-198.
39. Sloper-Mould, K.E., Jemc, J.C., Pickart, C.M., and Hicke, L. (2001). Distinct functional surface regions on ubiquitin. J Biol Chem *276*, 30483-30489.
40. Kamadurai, H.B., Souphron, J., Scott, D.C., Duda, D.M., Miller, D.J., Stringer, D., Piper, R.C., and Schulman, B.A. (2009). Insights into ubiquitin transfer cascades from a structure of a UbcH5B approximately ubiquitin-HECT(NEDD4L) complex. Mol Cell *36*, 1095-1102.
41. Hu, M., Li, P., Li, M., Li, W., Yao, T., Wu, J.W., Gu, W., Cohen, R.E., and Shi, Y. (2002). Crystal structure of a UBP-family deubiquitinating enzyme in isolation and in complex with ubiquitin aldehyde. Cell *111*, 1041-1054.
42. Reyes-Turcu, F.E., Horton, J.R., Mullally, J.E., Heroux, A., Cheng, X., and Wilkinson, K.D. (2006). The ubiquitin binding domain ZnF UBP recognizes the C-terminal diglycine motif of unanchored ubiquitin. Cell *124*, 1197-1208.
43. Jin, L., Williamson, A., Banerjee, S., Philipp, I., and Rape, M. (2008). Mechanism of ubiquitin-chain formation by the human anaphase-promoting complex. Cell *133*, 653-665.
44. Bremm, A., Freund, S.M., and Komander, D. (2010). Lys11-linked ubiquitin chains adopt compact conformations and are preferentially hydrolyzed by the deubiquitinase Cezanne. Nat Struct Mol Biol *17*, 939-947.
45. Cook, W.J., Jeffrey, L.C., Carson, M., Chen, Z., and Pickart, C.M. (1992). Structure of a diubiquitin conjugate and a model for interaction with ubiquitin conjugating enzyme (E2). J Biol Chem *267*, 16467-16471.
46. Plechanovova, A., Jaffray, E.G., Tatham, M.H., Naismith, J.H., and Hay, R.T. (2012). Structure of a RING E3 ligase and ubiquitin-loaded E2 primed for catalysis. Nature *489*, 115-120.
47. Komander, D., Reyes-Turcu, F., Licchesi, J.D.F., Odenwaelder, P., Wilkinson, K.D., and Barford, D. (2009). Molecular discrimination of

structurally equivalent Lys 63-linked and linear polyubiquitin chains. EMBO Rep *10*, 466-473.
48. Behrends, C., and Harper, J.W. (2011). Constructing and decoding unconventional ubiquitin chains. Nat Struct Mol Biol *18*, 520-528.
49. Christensen, D.E., Brzovic, P.S., and Klevit, R.E. (2007). E2-BRCA1 RING interactions dictate synthesis of mono- or specific polyubiquitin chain linkages. Nat Struct Mol Biol *14*, 941-948.
50. Christensen, D.E., and Klevit, R.E. (2009). Dynamic interactions of proteins in complex networks: identifying the complete set of interacting E2s for functional investigation of E3-dependent protein ubiquitination. FEBS J *276*, 5381-5389.
51. Strieter, E.R., and Korasick, D.A. (2012). Unraveling the complexity of ubiquitin signaling. ACS Chem Biol *7*, 52-63.
52. Bosanac, I., Wertz, I.E., Pan, B., Yu, C., Kusam, S., Lam, C., Phu, L., Phung, Q., Maurer, B., Arnott, D., et al. (2010). Ubiquitin binding to A20 ZnF4 is required for modulation of NF-kappaB signaling. Mol Cell *40*, 548-557.
53. Sims, J.J., and Cohen, R.E. (2009). Linkage-specific avidity defines the lysine 63-linked polyubiquitin-binding preference of rap80. Mol Cell *33*, 775-783.
54. Sato, Y., Yoshikawa, A., Mimura, H., Yamashita, M., Yamagata, A., and Fukai, S. (2009). Structural basis for specific recognition of Lys 63-linked polyubiquitin chains by tandem UIMs of RAP80. EMBO J *28*, 2461-2468.
55. Trempe, J.F., Brown, N.R., Lowe, E.D., Gordon, C., Campbell, I.D., Noble, M.E., and Endicott, J.A. (2005). Mechanism of Lys48-linked polyubiquitin chain recognition by the Mud1 UBA domain. EMBO J *24*, 3178-3189.
56. Varadan, R., Assfalg, M., Raasi, S., Pickart, C., and Fushman, D. (2005). Structural determinants for selective recognition of a Lys48-linked polyubiquitin chain by a UBA domain. Mol Cell *18*, 687-698.
57. Vucic, D., Dixit, V.M., and Wertz, I.E. (2011). Ubiquitylation in apoptosis: a post-translational modification at the edge of life and death. Nat Rev Mol Cell Biol *12*, 439-452.
58. Finley, D., Ciechanover, A., and Varshavsky, A. (2004). Ubiquitin as a central cellular regulator. Cell *116*, S29-32, 22 p following S32.
59. Newton, K., Matsumoto, M.L., Wertz, I.E., Kirkpatrick, D.S., Lill, J.R., Tan, J., Dugger, D., Gordon, N., Sidhu, S.S., Fellouse, F.A., et al. (2008). Ubiquitin chain editing revealed by polyubiquitin linkage-specific antibodies. Cell *134*, 668-678.
60. Wertz, I.E., O'Rourke, K.M., Zhou, H., Eby, M., Aravind, L., Seshagiri, S., Wu, P., Wiesmann, C., Baker, R., Boone, D.L., et al. (2004). De-ubiquitination and ubiquitin ligase domains of A20 downregulate NF-kappaB signalling. Nature *430*, 694-699.
61. Komander, D., and Barford, D. (2008). Structure of the A20 OTU domain and mechanistic insights into deubiquitination. Biochem J *409*, 77-85.
62. Cajee, U.F., Hull, R., and Ntwasa, M. (2012). Modification by ubiquitin-like proteins: significance in apoptosis and autophagy pathways. Int J Mol Sci *13*, 11804-11831.

63. Johnson, E.S. (2004). Protein modification by SUMO. Annu Rev Biochem *73*, 355-382.
64. Geiss-Friedlander, R., and Melchior, F. (2007). Concepts in sumoylation: a decade on. Nat Rev Mol Cell Biol *8*, 947-956.
65. Ulrich, H.D. (2009). The SUMO system: an overview. Methods Mol Biol *497*, 3-16.
66. Ulrich, H.D. (2012). Ubiquitin and SUMO in DNA repair at a glance. J Cell Sci *125*, 249-254.
67. Tatham, M.H., Jaffray, E., Vaughan, O.A., Desterro, J.M., Botting, C.H., Naismith, J.H., and Hay, R.T. (2001). Polymeric chains of SUMO-2 and SUMO-3 are conjugated to protein substrates by SAE1/SAE2 and Ubc9. J Biol Chem *276*, 35368-35374.
68. Hardeland, U., Steinacher, R., Jiricny, J., and Schar, P. (2002). Modification of the human thymine-DNA glycosylase by ubiquitin-like proteins facilitates enzymatic turnover. EMBO J *21*, 1456-1464.
69. Steinacher, R., and Schar, P. (2005). Functionality of human thymine DNA glycosylase requires SUMO-regulated changes in protein conformation. Curr Biol *15*, 616-623.
70. Xirodimas, D.P., Saville, M.K., Bourdon, J.C., Hay, R.T., and Lane, D.P. (2004). Mdm2-mediated NEDD8 conjugation of p53 inhibits its transcriptional activity. Cell *118*, 83-97.
71. Petroski, M.D., and Deshaies, R.J. (2005). Function and regulation of cullin-RING ubiquitin ligases. Nat Rev Mol Cell Biol *6*, 9-20.
72. Huang, D.T., and Schulman, B.A. (2005). Expression, purification, and characterization of the E1 for human NEDD8, the heterodimeric APPBP1-UBA3 complex. Methods Enzymol *398*, 9-20.
73. Gong, L., and Yeh, E.T. (1999). Identification of the activating and conjugating enzymes of the NEDD8 conjugation pathway. J Biol Chem *274*, 12036-12042.
74. Soucy, T.A., Dick, L.R., Smith, P.G., Milhollen, M.A., and Brownell, J.E. (2010). The NEDD8 Conjugation Pathway and Its Relevance in Cancer Biology and Therapy. Genes Cancer *1*, 708-716.
75. Thrower, J.S., Hoffman, L., Rechsteiner, M., and Pickart, C.M. (2000). Recognition of the polyubiquitin proteolytic signal. EMBO J *19*, 94-102.
76. Peth, A., Uchiki, T., and Goldberg, A.L. (2010). ATP-dependent steps in the binding of ubiquitin conjugates to the 26S proteasome that commit to degradation. Mol Cell *40*, 671-681.
77. Jacobson, A.D., Zhang, N.Y., Xu, P., Han, K.J., Noone, S., Peng, J., and Liu, C.W. (2009). The lysine 48 and lysine 63 ubiquitin conjugates are processed differently by the 26 s proteasome. J Biol Chem *284*, 35485-35494.
78. Dammer, E.B., Na, C.H., Xu, P., Seyfried, N.T., Duong, D.M., Cheng, D., Gearing, M., Rees, H., Lah, J.J., Levey, A.I., et al. (2011). Polyubiquitin linkage profiles in three models of proteolytic stress suggest the etiology of Alzheimer disease. J Biol Chem *286*, 10457-10465.
79. Xie, Y., and Varshavsky, A. (2000). Physical association of ubiquitin ligases and the 26S proteasome. Proc Natl Acad Sci U S A *97*, 2497-2502.

80. Boutet, S.C., Disatnik, M.H., Chan, L.S., Iori, K., and Rando, T.A. (2007). Regulation of Pax3 by proteasomal degradation of monoubiquitinated protein in skeletal muscle progenitors. Cell *130*, 349-362.
81. Carvallo, L., Munoz, R., Bustos, F., Escobedo, N., Carrasco, H., Olivares, G., and Larrain, J. (2010). Non-canonical Wnt signaling induces ubiquitination and degradation of Syndecan4. J Biol Chem *285*, 29546-29555.
82. Kravtsova-Ivantsiv, Y., and Ciechanover, A. (2012). Non-canonical ubiquitin-based signals for proteasomal degradation. J Cell Sci *125*, 539-548.
83. Lauwers, E., Erpapazoglou, Z., Haguenauer-Tsapis, R., and Andre, B. (2010). The ubiquitin code of yeast permease trafficking. Trends Cell Biol *20*, 196-204.
84. Lauwers, E., Jacob, C., and Andre, B. (2009). K63-linked ubiquitin chains as a specific signal for protein sorting into the multivesicular body pathway. J Cell Biol *185*, 493-502.
85. Terrell, J., Shih, S., Dunn, R., and Hicke, L. (1998). A function for monoubiquitination in the internalization of a G protein-coupled receptor. Mol Cell *1*, 193-202.
86. Nakatsu, F., Sakuma, M., Matsuo, Y., Arase, H., Yamasaki, S., Nakamura, N., Saito, T., and Ohno, H. (2000). A Di-leucine signal in the ubiquitin moiety. Possible involvement in ubiquitination-mediated endocytosis. J Biol Chem *275*, 26213-26219.
87. Haglund, K., Sigismund, S., Polo, S., Szymkiewicz, I., Di Fiore, P.P., and Dikic, I. (2003). Multiple monoubiquitination of RTKs is sufficient for their endocytosis and degradation. Nat Cell Biol *5*, 461-466.
88. Mosesson, Y., Shtiegman, K., Katz, M., Zwang, Y., Vereb, G., Szollosi, J., and Yarden, Y. (2003). Endocytosis of receptor tyrosine kinases is driven by monoubiquitylation, not polyubiquitylation. J Biol Chem *278*, 21323-21326.
89. Kirkin, V., McEwan, D.G., Novak, I., and Dikic, I. (2009). A role for ubiquitin in selective autophagy. Mol Cell *34*, 259-269.
90. Plafker, S.M., Plafker, K.S., Weissman, A.M., and Macara, I.G. (2004). Ubiquitin charging of human class III ubiquitin-conjugating enzymes triggers their nuclear import. J Cell Biol *167*, 649-659.
91. Geng, F., Wenzel, S., and Tansey, W.P. (2012). Ubiquitin and proteasomes in transcription. Annu Rev Biochem *81*, 177-201.
92. Baumann, M., Pontiller, J., and Ernst, W. (2010). Structure and basal transcription complex of RNA polymerase II core promoters in the mammalian genome: an overview. Mol Biotechnol *45*, 241-247.
93. Li, B., Carey, M., and Workman, J.L. (2007). The role of chromatin during transcription. Cell *128*, 707-719.
94. Park, Y.J., and Luger, K. (2008). Histone chaperones in nucleosome eviction and histone exchange. Curr Opin Struct Biol *18*, 282-289.
95. Auld, K.L., Brown, C.R., Casolari, J.M., Komili, S., and Silver, P.A. (2006). Genomic association of the proteasome demonstrates overlapping gene regulatory activity with transcription factor substrates. Mol Cell *21*, 861-871.
96. Ferdous, A., Kodadek, T., and Johnston, S.A. (2002). A nonproteolytic function of the 19S regulatory subunit of the 26S proteasome is required for

efficient activated transcription by human RNA polymerase II. Biochemistry *41*, 12798-12805.
97. Ferdous, A., Gonzalez, F., Sun, L., Kodadek, T., and Johnston, S.A. (2001). The 19S regulatory particle of the proteasome is required for efficient transcription elongation by RNA polymerase II. Mol Cell *7*, 981-991.
98. Gillette, T.G., Gonzalez, F., Delahodde, A., Johnston, S.A., and Kodadek, T. (2004). Physical and functional association of RNA polymerase II and the proteasome. Proc Natl Acad Sci U S A *101*, 5904-5909.
99. Daulny, A., and Tansey, W.P. (2009). Damage control: DNA repair, transcription, and the ubiquitin-proteasome system. DNA Repair (Amst) *8*, 444-448.
100. Bohr, V.A., Smith, C.A., Okumoto, D.S., and Hanawalt, P.C. (1985). DNA repair in an active gene: removal of pyrimidine dimers from the DHFR gene of CHO cells is much more efficient than in the genome overall. Cell *40*, 359-369.
101. Mellon, I., Spivak, G., and Hanawalt, P.C. (1987). Selective removal of transcription-blocking DNA damage from the transcribed strand of the mammalian DHFR gene. Cell *51*, 241-249.
102. Fousteri, M., and Mullenders, L.H. (2008). Transcription-coupled nucleotide excision repair in mammalian cells: molecular mechanisms and biological effects. Cell Res *18*, 73-84.
103. Svejstrup, J.Q. (2007). Contending with transcriptional arrest during RNAPII transcript elongation. Trends Biochem Sci *32*, 165-171.
104. Somesh, B.P., Sigurdsson, S., Saeki, H., Erdjument-Bromage, H., Tempst, P., and Svejstrup, J.Q. (2007). Communication between distant sites in RNA polymerase II through ubiquitylation factors and the polymerase CTD. Cell *129*, 57-68.
105. Bregman, D.B., Halaban, R., van Gool, A.J., Henning, K.A., Friedberg, E.C., and Warren, S.L. (1996). UV-induced ubiquitination of RNA polymerase II: a novel modification deficient in Cockayne syndrome cells. Proc Natl Acad Sci U S A *93*, 11586-11590.
106. Ratner, J.N., Balasubramanian, B., Corden, J., Warren, S.L., and Bregman, D.B. (1998). Ultraviolet radiation-induced ubiquitination and proteasomal degradation of the large subunit of RNA polymerase II. Implications for transcription-coupled DNA repair. J Biol Chem *273*, 5184-5189.
107. Gnatt, A.L., Cramer, P., Fu, J., Bushnell, D.A., and Kornberg, R.D. (2001). Structural basis of transcription: an RNA polymerase II elongation complex at 3.3 A resolution. Science *292*, 1876-1882.
108. Nehyba, J., Hrdlickova, R., Burnside, J., and Bose, H.R., Jr. (2002). A novel interferon regulatory factor (IRF), IRF-10, has a unique role in immune defense and is induced by the v-Rel oncoprotein. Mol Cell Biol *22*, 3942-3957.
109. Miyamoto, M., Fujita, T., Kimura, Y., Maruyama, M., Harada, H., Sudo, Y., Miyata, T., and Taniguchi, T. (1988). Regulated expression of a gene encoding a nuclear factor, IRF-1, that specifically binds to IFN-beta gene regulatory elements. Cell *54*, 903-913.

110. Nguyen, H., Hiscott, J., and Pitha, P.M. (1997). The growing family of interferon regulatory factors. Cytokine Growth Factor Rev *8*, 293-312.
111. Fujii, Y., Shimizu, T., Kusumoto, M., Kyogoku, Y., Taniguchi, T., and Hakoshima, T. (1999). Crystal structure of an IRF-DNA complex reveals novel DNA recognition and cooperative binding to a tandem repeat of core sequences. EMBO J *18*, 5028-5041.
112. Narayan, V., Eckert, M., Zylicz, A., Zylicz, M., and Ball, K.L. (2009). Cooperative regulation of the interferon regulatory factor-1 tumor suppressor protein by core components of the molecular chaperone machinery. J Biol Chem *284*, 25889-25899.
113. Yanai, H., Negishi, H., and Taniguchi, T. (2012). The IRF family of transcription factors: Inception, impact and implications in oncogenesis. Oncoimmunology *1*, 1376-1386.
114. Nozawa, H., Oda, E., Nakao, K., Ishihara, M., Ueda, S., Yokochi, T., Ogasawara, K., Nakatsuru, Y., Shimizu, S., Ohira, Y., et al. (1999). Loss of transcription factor IRF-1 affects tumor susceptibility in mice carrying the Ha-ras transgene or nullizygosity for p53. Genes Dev *13*, 1240-1245.
115. Tamura, T., Ishihara, M., Lamphier, M.S., Tanaka, N., Oishi, I., Aizawa, S., Matsuyama, T., Mak, T.W., Taki, S., and Taniguchi, T. (1997). DNA damage-induced apoptosis and Ice gene induction in mitogenically activated T lymphocytes require IRF-1. Leukemia *11 Suppl 3*, 439-440.
116. Harada, H., Fujita, T., Miyamoto, M., Kimura, Y., Maruyama, M., Furia, A., Miyata, T., and Taniguchi, T. (1989). Structurally similar but functionally distinct factors, IRF-1 and IRF-2, bind to the same regulatory elements of IFN and IFN-inducible genes. Cell *58*, 729-739.
117. Taniguchi, T., Ogasawara, K., Takaoka, A., and Tanaka, N. (2001). IRF family of transcription factors as regulators of host defense. Annu Rev Immunol *19*, 623-655.
118. Ogasawara, K., Hida, S., Azimi, N., Tagaya, Y., Sato, T., Yokochi-Fukuda, T., Waldmann, T.A., Taniguchi, T., and Taki, S. (1998). Requirement for IRF-1 in the microenvironment supporting development of natural killer cells. Nature *391*, 700-703.
119. Duncan, G.S., Mittrucker, H.W., Kagi, D., Matsuyama, T., and Mak, T.W. (1996). The transcription factor interferon regulatory factor-1 is essential for natural killer cell function in vivo. J Exp Med *184*, 2043-2048.
120. Tamura, T., Yanai, H., Savitsky, D., and Taniguchi, T. (2008). The IRF family transcription factors in immunity and oncogenesis. Annu Rev Immunol *26*, 535-584.
121. Taki, S., Sato, T., Ogasawara, K., Fukuda, T., Sato, M., Hida, S., Suzuki, G., Mitsuyama, M., Shin, E.H., Kojima, S., et al. (1997). Multistage regulation of Th1-type immune responses by the transcription factor IRF-1. Immunity *6*, 673-679.
122. Lohoff, M., Ferrick, D., Mittrucker, H.W., Duncan, G.S., Bischof, S., Rollinghoff, M., and Mak, T.W. (1997). Interferon regulatory factor-1 is required for a T helper 1 immune response in vivo. Immunity *6*, 681-689.

123. Tada, Y., Ho, A., Matsuyama, T., and Mak, T.W. (1997). Reduced incidence and severity of antigen-induced autoimmune diseases in mice lacking interferon regulatory factor-1. J Exp Med *185*, 231-238.
124. Escalante, C.R., Yie, J., Thanos, D., and Aggarwal, A.K. (1998). Structure of IRF-1 with bound DNA reveals determinants of interferon regulation. Nature *391*, 103-106.
125. Chouard, T. (2011). Structural biology: Breaking the protein rules. Nature *471*, 151-153.
126. Tompa, P. (2012). Intrinsically disordered proteins: a 10-year recap. Trends Biochem Sci *37*, 509-516.
127. Narayan, V., Halada, P., Hernychova, L., Chong, Y.P., Zakova, J., Hupp, T.R., Vojtesek, B., and Ball, K.L. (2011). A multiprotein binding interface in an intrinsically disordered region of the tumor suppressor protein interferon regulatory factor-1. J Biol Chem *286*, 14291-14303.
128. Spink, J., and Evans, T. (1997). Binding of the transcription factor interferon regulatory factor-1 to the inducible nitric-oxide synthase promoter. J Biol Chem *272*, 24417-24425.
129. Schaper, F., Kirchhoff, S., Posern, G., Koster, M., Oumard, A., Sharf, R., Levi, B.Z., and Hauser, H. (1998). Functional domains of interferon regulatory factor I (IRF-1). Biochem J *335 (Pt 1)*, 147-157.
130. Narayan, V., Pion, E., Landre, V., Muller, P., and Ball, K.L. (2011). Docking-dependent ubiquitination of the interferon regulatory factor-1 tumor suppressor protein by the ubiquitin ligase CHIP. J Biol Chem *286*, 607-619.
131. Kirchhoff, S., Oumard, A., Nourbakhsh, M., Levi, B.Z., and Hauser, H. (2000). Interplay between repressing and activating domains defines the transcriptional activity of IRF-1. Eur J Biochem *267*, 6753-6761.
132. Kim, E.J., Park, C.H., Park, J.S., and Um, S.J. (2003). Functional dissection of the transactivation domain of interferon regulatory factor-1. Biochem Biophys Res Commun *304*, 253-259.
133. Eckert, M., Meek, S.E., and Ball, K.L. (2006). A novel repressor domain is required for maximal growth inhibition by the IRF-1 tumor suppressor. J Biol Chem *281*, 23092-23102.
134. Dornan, D., Eckert, M., Wallace, M., Shimizu, H., Ramsay, E., Hupp, T.R., and Ball, K.L. (2004). Interferon regulatory factor 1 binding to p300 stimulates DNA-dependent acetylation of p53. Mol Cell Biol *24*, 10083-10098.
135. Pion, E., Narayan, V., Eckert, M., and Ball, K.L. (2009). Role of the IRF-1 enhancer domain in signalling polyubiquitination and degradation. Cell Signal *21*, 1479-1487.
136. Moller, A., Pion, E., Narayan, V., and Ball, K.L. (2010). Intracellular activation of interferon regulatory factor-1 by nanobodies to the multifunctional (Mf1) domain. J Biol Chem *285*, 38348-38361.
137. Thomas, D., and Tyers, M. (2000). Transcriptional regulation: Kamikaze activators. Curr Biol *10*, R341-343.
138. Nelson, N., Marks, M.S., Driggers, P.H., and Ozato, K. (1993). Interferon consensus sequence-binding protein, a member of the interferon regulatory

factor family, suppresses interferon-induced gene transcription. Mol Cell Biol *13*, 588-599.
139. Weisz, A., Marx, P., Sharf, R., Appella, E., Driggers, P.H., Ozato, K., and Levi, B.Z. (1992). Human interferon consensus sequence binding protein is a negative regulator of enhancer elements common to interferon-inducible genes. J Biol Chem *267*, 25589-25596.
140. Kirchhoff, S., Schaper, F., Oumard, A., and Hauser, H. (1998). In vivo formation of IRF-1 homodimers. Biochimie *80*, 659-664.
141. Pamment, J., Ramsay, E., Kelleher, M., Dornan, D., and Ball, K.L. (2002). Regulation of the IRF-1 tumour modifier during the response to genotoxic stress involves an ATM-dependent signalling pathway. Oncogene *21*, 7776-7785.
142. Romeo, G., Fiorucci, G., Chiantore, M.V., Percario, Z.A., Vannucchi, S., and Affabris, E. (2002). IRF-1 as a negative regulator of cell proliferation. J Interferon Cytokine Res *22*, 39-47.
143. Taniguchi, T., Tanaka, N., and Taki, S. (1998). Regulation of the interferon system, immune response and oncogenesis by the transcription factor interferon regulatory factor-1. Eur Cytokine Netw *9*, 43-48.
144. Fujita, T., Kimura, Y., Miyamoto, M., Barsoumian, E.L., and Taniguchi, T. (1989). Induction of endogenous IFN-alpha and IFN-beta genes by a regulatory transcription factor, IRF-1. Nature *337*, 270-272.
145. Coccia, E.M., Del Russo, N., Stellacci, E., Orsatti, R., Benedetti, E., Marziali, G., Hiscott, J., and Battistini, A. (1999). Activation and repression of the 2-5A synthetase and p21 gene promoters by IRF-1 and IRF-2. Oncogene *18*, 2129-2137.
146. Wang, Q., and Floyd-Smith, G. (1998). Maximal induction of p69 2', 5'-oligoadenylate synthetase in Daudi cells requires cooperation between an ISRE and two IRF-1-like elements. Gene *222*, 83-90.
147. Beretta, L., Gabbay, M., Berger, R., Hanash, S.M., and Sonenberg, N. (1996). Expression of the protein kinase PKR in modulated by IRF-1 and is reduced in 5q- associated leukemias. Oncogene *12*, 1593-1596.
148. Kirchhoff, S., Koromilas, A.E., Schaper, F., Grashoff, M., Sonenberg, N., and Hauser, H. (1995). IRF-1 induced cell growth inhibition and interferon induction requires the activity of the protein kinase PKR. Oncogene *11*, 439-445.
149. Takaoka, A., and Yanai, H. (2006). Interferon signalling network in innate defence. Cell Microbiol *8*, 907-922.
150. Decker, T., Lew, D.J., and Darnell, J.E., Jr. (1991). Two distinct alpha-interferon-dependent signal transduction pathways may contribute to activation of transcription of the guanylate-binding protein gene. Mol Cell Biol *11*, 5147-5153.
151. Harada, H., Kitagawa, M., Tanaka, N., Yamamoto, H., Harada, K., Ishihara, M., and Taniguchi, T. (1993). Anti-oncogenic and oncogenic potentials of interferon regulatory factors-1 and -2. Science *259*, 971-974.
152. Tanaka, N., Ishihara, M., Lamphier, M.S., Nozawa, H., Matsuyama, T., Mak, T.W., Aizawa, S., Tokino, T., Oren, M., and Taniguchi, T. (1996).

Cooperation of the tumour suppressors IRF-1 and p53 in response to DNA damage. Nature *382*, 816-818.
153. Tamura, T., Ishihara, M., Lamphier, M.S., Tanaka, N., Oishi, I., Aizawa, S., Matsuyama, T., Mak, T.W., Taki, S., and Taniguchi, T. (1995). An IRF-1-dependent pathway of DNA damage-induced apoptosis in mitogen-activated T lymphocytes. Nature *376*, 596-599.
154. Kano, A., Haruyama, T., Akaike, T., and Watanabe, Y. (1999). IRF-1 is an essential mediator in IFN-gamma-induced cell cycle arrest and apoptosis of primary cultured hepatocytes. Biochem Biophys Res Commun *257*, 672-677.
155. Kim, E.J., Lee, J.M., Namkoong, S.E., Um, S.J., and Park, J.S. (2002). Interferon regulatory factor-1 mediates interferon-gamma-induced apoptosis in ovarian carcinoma cells. J Cell Biochem *85*, 369-380.
156. Tomita, Y., Bilim, V., Hara, N., Kasahara, T., and Takahashi, K. (2003). Role of IRF-1 and caspase-7 in IFN-gamma enhancement of Fas-mediated apoptosis in ACHN renal cell carcinoma cells. Int J Cancer *104*, 400-408.
157. Takaoka, A., Tamura, T., and Taniguchi, T. (2008). Interferon regulatory factor family of transcription factors and regulation of oncogenesis. Cancer Sci *99*, 467-478.
158. Tanaka, N., Ishihara, M., Kitagawa, M., Harada, H., Kimura, T., Matsuyama, T., Lamphier, M.S., Aizawa, S., Mak, T.W., and Taniguchi, T. (1994). Cellular commitment to oncogene-induced transformation or apoptosis is dependent on the transcription factor IRF-1. Cell *77*, 829-839.
159. Doherty, G.M., Boucher, L., Sorenson, K., and Lowney, J. (2001). Interferon regulatory factor expression in human breast cancer. Ann Surg *233*, 623-629.
160. Harada, H., Kondo, T., Ogawa, S., Tamura, T., Kitagawa, M., Tanaka, N., Lamphier, M.S., Hirai, H., and Taniguchi, T. (1994). Accelerated exon skipping of IRF-1 mRNA in human myelodysplasia/leukemia; a possible mechanism of tumor suppressor inactivation. Oncogene *9*, 3313-3320.
161. Ogasawara, S., Tamura, G., Maesawa, C., Suzuki, Y., Ishida, K., Satoh, N., Uesugi, N., Saito, K., and Satodate, R. (1996). Common deleted region on the long arm of chromosome 5 in esophageal carcinoma. Gastroenterology *110*, 52-57.
162. Tamura, G., Ogasawara, S., Nishizuka, S., Sakata, K., Maesawa, C., Suzuki, Y., Terashima, M., Saito, K., and Satodate, R. (1996). Two distinct regions of deletion on the long arm of chromosome 5 in differentiated adenocarcinomas of the stomach. Cancer Res *56*, 612-615.
163. Tzoanopoulos, D., Speletas, M., Arvanitidis, K., Veiopoulou, C., Kyriaki, S., Thyphronitis, G., Sideras, P., Kartalis, G., and Ritis, K. (2002). Low expression of interferon regulatory factor-1 and identification of novel exons skipping in patients with chronic myeloid leukaemia. Br J Haematol *119*, 46-53.
164. Tirkkonen, M., Tanner, M., Karhu, R., Kallioniemi, A., Isola, J., and Kallioniemi, O.P. (1998). Molecular cytogenetics of primary breast cancer by CGH. Genes Chromosomes Cancer *21*, 177-184.
165. Forbes, S.A., Bhamra, G., Bamford, S., Dawson, E., Kok, C., Clements, J., Menzies, A., Teague, J.W., Futreal, P.A., and Stratton, M.R. (2008). The

Catalogue of Somatic Mutations in Cancer (COSMIC). Curr Protoc Hum Genet *Chapter 10*, Unit 10 11.
166. Nakagawa, K., and Yokosawa, H. (2000). Degradation of transcription factor IRF-1 by the ubiquitin-proteasome pathway. The C-terminal region governs the protein stability. Eur J Biochem *267*, 1680-1686.
167. Linzer, D.I., and Levine, A.J. (1979). Characterization of a 54K dalton cellular SV40 tumor antigen present in SV40-transformed cells and uninfected embryonal carcinoma cells. Cell *17*, 43-52.
168. Lane, D.P., and Crawford, L.V. (1979). T antigen is bound to a host protein in SV40-transformed cells. Nature *278*, 261-263.
169. DeLeo, A.B., Jay, G., Appella, E., Dubois, G.C., Law, L.W., and Old, L.J. (1979). Detection of a transformation-related antigen in chemically induced sarcomas and other transformed cells of the mouse. Proc Natl Acad Sci U S A *76*, 2420-2424.
170. Joerger, A.C., and Fersht, A.R. (2008). Structural biology of the tumor suppressor p53. Annu Rev Biochem *77*, 557-582.
171. Levine, A.J., Hu, W., and Feng, Z. (2006). The P53 pathway: what questions remain to be explored? Cell Death Differ *13*, 1027-1036.
172. Vogelstein, B., Lane, D., and Levine, A.J. (2000). Surfing the p53 network. Nature *408*, 307-310.
173. Vousden, K.H., and Lu, X. (2002). Live or let die: the cell's response to p53. Nat Rev Cancer *2*, 594-604.
174. Maddocks, O.D., and Vousden, K.H. (2011). Metabolic regulation by p53. J Mol Med (Berl) *89*, 237-245.
175. Li, T., Kon, N., Jiang, L., Tan, M., Ludwig, T., Zhao, Y., Baer, R., and Gu, W. (2012). Tumor suppression in the absence of p53-mediated cell-cycle arrest, apoptosis, and senescence. Cell *149*, 1269-1283.
176. Minakawa, M., Sugimoto, T., Aizawa, S., and Tomooka, Y. (1998). Cerebellar cell lines established from a p53-deficient adult mouse. Brain Res *813*, 172-176.
177. Jacks, T., Remington, L., Williams, B.O., Schmitt, E.M., Halachmi, S., Bronson, R.T., and Weinberg, R.A. (1994). Tumor spectrum analysis in p53-mutant mice. Curr Biol *4*, 1-7.
178. Tyner, S.D., Venkatachalam, S., Choi, J., Jones, S., Ghebranious, N., Igelmann, H., Lu, X., Soron, G., Cooper, B., Brayton, C., et al. (2002). p53 mutant mice that display early ageing-associated phenotypes. Nature *415*, 45-53.
179. Liu, G., McDonnell, T.J., Montes de Oca Luna, R., Kapoor, M., Mims, B., El-Naggar, A.K., and Lozano, G. (2000). High metastatic potential in mice inheriting a targeted p53 missense mutation. Proc Natl Acad Sci U S A *97*, 4174-4179.
180. Olive, K.P., Tuveson, D.A., Ruhe, Z.C., Yin, B., Willis, N.A., Bronson, R.T., Crowley, D., and Jacks, T. (2004). Mutant p53 gain of function in two mouse models of Li-Fraumeni syndrome. Cell *119*, 847-860.
181. Maslon, M.M., and Hupp, T.R. (2010). Drug discovery and mutant p53. Trends Cell Biol *20*, 542-555.

182. Cho, Y., Gorina, S., Jeffrey, P.D., and Pavletich, N.P. (1994). Crystal structure of a p53 tumor suppressor-DNA complex: understanding tumorigenic mutations. Science *265*, 346-355.
183. Butler, J.S., and Loh, S.N. (2003). Structure, function, and aggregation of the zinc-free form of the p53 DNA binding domain. Biochemistry *42*, 2396-2403.
184. Duan, J., and Nilsson, L. (2006). Effect of Zn2+ on DNA recognition and stability of the p53 DNA-binding domain. Biochemistry *45*, 7483-7492.
185. el-Deiry, W.S., Kern, S.E., Pietenpol, J.A., Kinzler, K.W., and Vogelstein, B. (1992). Definition of a consensus binding site for p53. Nat Genet *1*, 45-49.
186. Nagaich, A.K., Zhurkin, V.B., Durell, S.R., Jernigan, R.L., Appella, E., and Harrington, R.E. (1999). p53-induced DNA bending and twisting: p53 tetramer binds on the outer side of a DNA loop and increases DNA twisting. Proc Natl Acad Sci U S A *96*, 1875-1880.
187. Kitayner, M., Rozenberg, H., Kessler, N., Rabinovich, D., Shaulov, L., Haran, T.E., and Shakked, Z. (2006). Structural basis of DNA recognition by p53 tetramers. Mol Cell *22*, 741-753.
188. Sykes, S.M., Mellert, H.S., Holbert, M.A., Li, K., Marmorstein, R., Lane, W.S., and McMahon, S.B. (2006). Acetylation of the p53 DNA-binding domain regulates apoptosis induction. Mol Cell *24*, 841-851.
189. Tang, Y., Luo, J., Zhang, W., and Gu, W. (2006). Tip60-dependent acetylation of p53 modulates the decision between cell-cycle arrest and apoptosis. Mol Cell *24*, 827-839.
190. Chang, J., Kim, D.H., Lee, S.W., Choi, K.Y., and Sung, Y.C. (1995). Transactivation ability of p53 transcriptional activation domain is directly related to the binding affinity to TATA-binding protein. J Biol Chem *270*, 25014-25019.
191. Walker, K.K., and Levine, A.J. (1996). Identification of a novel p53 functional domain that is necessary for efficient growth suppression. Proc Natl Acad Sci U S A *93*, 15335-15340.
192. Toledo, F., Lee, C.J., Krummel, K.A., Rodewald, L.W., Liu, C.W., and Wahl, G.M. (2007). Mouse mutants reveal that putative protein interaction sites in the p53 proline-rich domain are dispensable for tumor suppression. Mol Cell Biol *27*, 1425-1432.
193. Di Lello, P., Jenkins, L.M., Jones, T.N., Nguyen, B.D., Hara, T., Yamaguchi, H., Dikeakos, J.D., Appella, E., Legault, P., and Omichinski, J.G. (2006). Structure of the Tfb1/p53 complex: Insights into the interaction between the p62/Tfb1 subunit of TFIIH and the activation domain of p53. Mol Cell *22*, 731-740.
194. Lu, H., and Levine, A.J. (1995). Human TAFII31 protein is a transcriptional coactivator of the p53 protein. Proc Natl Acad Sci U S A *92*, 5154-5158.
195. Thut, C.J., Chen, J.L., Klemm, R., and Tjian, R. (1995). p53 transcriptional activation mediated by coactivators TAFII40 and TAFII60. Science *267*, 100-104.
196. Gu, W., Shi, X.L., and Roeder, R.G. (1997). Synergistic activation of transcription by CBP and p53. Nature *387*, 819-823.
197. Teufel, D.P., Freund, S.M., Bycroft, M., and Fersht, A.R. (2007). Four domains of p300 each bind tightly to a sequence spanning both

transactivation subdomains of p53. Proc Natl Acad Sci U S A *104*, 7009-7014.
198. Wallace, M., Worrall, E., Pettersson, S., Hupp, T.R., and Ball, K.L. (2006). Dual-site regulation of MDM2 E3-ubiquitin ligase activity. Mol Cell *23*, 251-263.
199. Kussie, P.H., Gorina, S., Marechal, V., Elenbaas, B., Moreau, J., Levine, A.J., and Pavletich, N.P. (1996). Structure of the MDM2 oncoprotein bound to the p53 tumor suppressor transactivation domain. Science *274*, 948-953.
200. Marine, J.C., and Jochemsen, A.G. (2005). Mdmx as an essential regulator of p53 activity. Biochem Biophys Res Commun *331*, 750-760.
201. Schon, O., Friedler, A., Bycroft, M., Freund, S.M., and Fersht, A.R. (2002). Molecular mechanism of the interaction between MDM2 and p53. J Mol Biol *323*, 491-501.
202. Goodman, R.H., and Smolik, S. (2000). CBP/p300 in cell growth, transformation, and development. Genes Dev *14*, 1553-1577.
203. Lai, Z., Auger, K.R., Manubay, C.M., and Copeland, R.A. (2000). Thermodynamics of p53 binding to hdm2(1-126): effects of phosphorylation and p53 peptide length. Arch Biochem Biophys *381*, 278-284.
204. Sakaguchi, K., Saito, S., Higashimoto, Y., Roy, S., Anderson, C.W., and Appella, E. (2000). Damage-mediated phosphorylation of human p53 threonine 18 through a cascade mediated by a casein 1-like kinase. Effect on Mdm2 binding. J Biol Chem *275*, 9278-9283.
205. Clore, G.M., Ernst, J., Clubb, R., Omichinski, J.G., Kennedy, W.M., Sakaguchi, K., Appella, E., and Gronenborn, A.M. (1995). Refined solution structure of the oligomerization domain of the tumour suppressor p53. Nat Struct Biol *2*, 321-333.
206. Jeffrey, P.D., Gorina, S., and Pavletich, N.P. (1995). Crystal structure of the tetramerization domain of the p53 tumor suppressor at 1.7 angstroms. Science *267*, 1498-1502.
207. Lee, W., Harvey, T.S., Yin, Y., Yau, P., Litchfield, D., and Arrowsmith, C.H. (1994). Solution structure of the tetrameric minimum transforming domain of p53. Nat Struct Biol *1*, 877-890.
208. Mittl, P.R., Chene, P., and Grutter, M.G. (1998). Crystallization and structure solution of p53 (residues 326-356) by molecular replacement using an NMR model as template. Acta Crystallogr D Biol Crystallogr *54*, 86-89.
209. Nicholls, C.D., McLure, K.G., Shields, M.A., and Lee, P.W. (2002). Biogenesis of p53 involves cotranslational dimerization of monomers and posttranslational dimerization of dimers. Implications on the dominant negative effect. J Biol Chem *277*, 12937-12945.
210. Bode, A.M., and Dong, Z. (2004). Post-translational modification of p53 in tumorigenesis. Nat Rev Cancer *4*, 793-805.
211. Toledo, F., and Wahl, G.M. (2006). Regulating the p53 pathway: in vitro hypotheses, in vivo veritas. Nat Rev Cancer *6*, 909-923.
212. Lavin, M.F., and Gueven, N. (2006). The complexity of p53 stabilization and activation. Cell Death Differ *13*, 941-950.
213. Mujtaba, S., He, Y., Zeng, L., Yan, S., Plotnikova, O., Sachchidanand, Sanchez, R., Zeleznik-Le, N.J., Ronai, Z., and Zhou, M.M. (2004). Structural

mechanism of the bromodomain of the coactivator CBP in p53 transcriptional activation. Mol Cell *13*, 251-263.
214. Rustandi, R.R., Baldisseri, D.M., and Weber, D.J. (2000). Structure of the negative regulatory domain of p53 bound to S100B(betabeta). Nat Struct Biol *7*, 570-574.
215. Li, M., Chen, D., Shiloh, A., Luo, J., Nikolaev, A.Y., Qin, J., and Gu, W. (2002). Deubiquitination of p53 by HAUSP is an important pathway for p53 stabilization. Nature *416*, 648-653.
216. Weinberg, R.L., Freund, S.M., Veprintsev, D.B., Bycroft, M., and Fersht, A.R. (2004). Regulation of DNA binding of p53 by its C-terminal domain. J Mol Biol *342*, 801-811.
217. Friedler, A., Veprintsev, D.B., Freund, S.M., von Glos, K.I., and Fersht, A.R. (2005). Modulation of binding of DNA to the C-terminal domain of p53 by acetylation. Structure *13*, 629-636.
218. McKinney, K., Mattia, M., Gottifredi, V., and Prives, C. (2004). p53 linear diffusion along DNA requires its C terminus. Mol Cell *16*, 413-424.
219. Espinosa, J.M., and Emerson, B.M. (2001). Transcriptional regulation by p53 through intrinsic DNA/chromatin binding and site-directed cofactor recruitment. Mol Cell *8*, 57-69.
220. Kemp, C.J., Wheldon, T., and Balmain, A. (1994). p53-deficient mice are extremely susceptible to radiation-induced tumorigenesis. Nat Genet *8*, 66-69.
221. Harvey, M., McArthur, M.J., Montgomery, C.A., Jr., Butel, J.S., Bradley, A., and Donehower, L.A. (1993). Spontaneous and carcinogen-induced tumorigenesis in p53-deficient mice. Nat Genet *5*, 225-229.
222. Donehower, L.A., Harvey, M., Slagle, B.L., McArthur, M.J., Montgomery, C.A., Jr., Butel, J.S., and Bradley, A. (1992). Mice deficient for p53 are developmentally normal but susceptible to spontaneous tumours. Nature *356*, 215-221.
223. Joerger, A.C., and Fersht, A.R. (2007). Structure-function-rescue: the diverse nature of common p53 cancer mutants. Oncogene *26*, 2226-2242.
224. Bullock, A.N., and Fersht, A.R. (2001). Rescuing the function of mutant p53. Nat Rev Cancer *1*, 68-76.
225. Vassilev, L.T. (2007). MDM2 inhibitors for cancer therapy. Trends Mol Med *13*, 23-31.
226. Roth, J.A. (2006). Adenovirus p53 gene therapy. Expert Opin Biol Ther *6*, 55-61.
227. Martins, C.P., Brown-Swigart, L., and Evan, G.I. (2006). Modeling the therapeutic efficacy of p53 restoration in tumors. Cell *127*, 1323-1334.
228. Ventura, A., Kirsch, D.G., McLaughlin, M.E., Tuveson, D.A., Grimm, J., Lintault, L., Newman, J., Reczek, E.E., Weissleder, R., and Jacks, T. (2007). Restoration of p53 function leads to tumour regression in vivo. Nature *445*, 661-665.
229. Brown, C.J., Lain, S., Verma, C.S., Fersht, A.R., and Lane, D.P. (2009). Awakening guardian angels: drugging the p53 pathway. Nat Rev Cancer *9*, 862-873.

230. Maki, C.G., and Howley, P.M. (1997). Ubiquitination of p53 and p21 is differentially affected by ionizing and UV radiation. Mol Cell Biol *17*, 355-363.
231. Maki, C.G., Huibregtse, J.M., and Howley, P.M. (1996). In vivo ubiquitination and proteasome-mediated degradation of p53(1). Cancer Res *56*, 2649-2654.
232. Shloush, J., Vlassov, J.E., Engson, I., Duan, S., Saridakis, V., Dhe-Paganon, S., Raught, B., Sheng, Y., and Arrowsmith, C.H. (2011). Structural and functional comparison of the RING domains of two p53 E3 ligases, Mdm2 and Pirh2. J Biol Chem *286*, 4796-4808.
233. Francoz, S., Froment, P., Bogaerts, S., De Clercq, S., Maetens, M., Doumont, G., Bellefroid, E., and Marine, J.C. (2006). Mdm4 and Mdm2 cooperate to inhibit p53 activity in proliferating and quiescent cells in vivo. Proc Natl Acad Sci U S A *103*, 3232-3237.
234. Gu, J., Kawai, H., Nie, L., Kitao, H., Wiederschain, D., Jochemsen, A.G., Parant, J., Lozano, G., and Yuan, Z.M. (2002). Mutual dependence of MDM2 and MDMX in their functional inactivation of p53. J Biol Chem *277*, 19251-19254.
235. Stad, R., Little, N.A., Xirodimas, D.P., Frenk, R., van der Eb, A.J., Lane, D.P., Saville, M.K., and Jochemsen, A.G. (2001). Mdmx stabilizes p53 and Mdm2 via two distinct mechanisms. EMBO Rep *2*, 1029-1034.
236. Barak, Y., Juven, T., Haffner, R., and Oren, M. (1993). mdm2 expression is induced by wild type p53 activity. EMBO J *12*, 461-468.
237. Juven, T., Barak, Y., Zauberman, A., George, D.L., and Oren, M. (1993). Wild type p53 can mediate sequence-specific transactivation of an internal promoter within the mdm2 gene. Oncogene *8*, 3411-3416.
238. Rodriguez, M.S., Desterro, J.M., Lain, S., Lane, D.P., and Hay, R.T. (2000). Multiple C-terminal lysine residues target p53 for ubiquitin-proteasome-mediated degradation. Mol Cell Biol *20*, 8458-8467.
239. Feng, L., Lin, T., Uranishi, H., Gu, W., and Xu, Y. (2005). Functional analysis of the roles of posttranslational modifications at the p53 C terminus in regulating p53 stability and activity. Mol Cell Biol *25*, 5389-5395.
240. Lohrum, M.A., Woods, D.B., Ludwig, R.L., Balint, E., and Vousden, K.H. (2001). C-terminal ubiquitination of p53 contributes to nuclear export. Mol Cell Biol *21*, 8521-8532.
241. Gajjar, M., Candeias, M.M., Malbert-Colas, L., Mazars, A., Fujita, J., Olivares-Illana, V., and Fahraeus, R. (2012). The p53 mRNA-Mdm2 interaction controls Mdm2 nuclear trafficking and is required for p53 activation following DNA damage. Cancer Cell *21*, 25-35.
242. Candeias, M.M., Malbert-Colas, L., Powell, D.J., Daskalogianni, C., Maslon, M.M., Naski, N., Bourougaa, K., Calvo, F., and Fahraeus, R. (2008). P53 mRNA controls p53 activity by managing Mdm2 functions. Nat Cell Biol *10*, 1098-1105.
243. Ballinger, C.A., Connell, P., Wu, Y., Hu, Z., Thompson, L.J., Yin, L.Y., and Patterson, C. (1999). Identification of CHIP, a novel tetratricopeptide repeat-containing protein that interacts with heat shock proteins and negatively regulates chaperone functions. Mol Cell Biol *19*, 4535-4545.

244. McDonough, H., and Patterson, C. (2003). CHIP: a link between the chaperone and proteasome systems. Cell Stress Chaperones *8*, 303-308.
245. Schulman, B.A., and Chen, Z.J. (2005). Protein ubiquitination: CHIPping away the symmetry. Mol Cell *20*, 653-655.
246. Murata, S., Chiba, T., and Tanaka, K. (2003). CHIP: a quality-control E3 ligase collaborating with molecular chaperones. Int J Biochem Cell Biol *35*, 572-578.
247. Kumar, P., Pradhan, K., Karunya, R., Ambasta, R.K., and Querfurth, H.W. (2012). Cross-functional E3 ligases Parkin and C-terminus Hsp70-interacting protein in neurodegenerative disorders. J Neurochem *120*, 350-370.
248. Rosser, M.F., Washburn, E., Muchowski, P.J., Patterson, C., and Cyr, D.M. (2007). Chaperone functions of the E3 ubiquitin ligase CHIP. J Biol Chem *282*, 22267-22277.
249. Tripathi, V., Ali, A., Bhat, R., and Pati, U. (2007). CHIP chaperones wild type p53 tumor suppressor protein. J Biol Chem *282*, 28441-28454.
250. Kajiro, M., Hirota, R., Nakajima, Y., Kawanowa, K., So-ma, K., Ito, I., Yamaguchi, Y., Ohie, S.H., Kobayashi, Y., Seino, Y., et al. (2009). The ubiquitin ligase CHIP acts as an upstream regulator of oncogenic pathways. Nat Cell Biol *11*, 312-319.
251. Zeytuni, N., and Zarivach, R. (2012). Structural and functional discussion of the tetra-trico-peptide repeat, a protein interaction module. Structure *20*, 397-405.
252. Cerveny, L., Straskova, A., Dankova, V., Hartlova, A., Ceckova, M., Staud, F., and Stulik, J. (2013). Tetratricopeptide repeat motifs in the world of bacterial pathogens: role in virulence mechanisms. Infect Immun *81*, 629-635.
253. D'Andrea, L.D., and Regan, L. (2003). TPR proteins: the versatile helix. Trends Biochem Sci *28*, 655-662.
254. Zhang, M., Windheim, M., Roe, S.M., Peggie, M., Cohen, P., Prodromou, C., and Pearl, L.H. (2005). Chaperoned ubiquitylation--crystal structures of the CHIP U box E3 ubiquitin ligase and a CHIP-Ubc13-Uev1a complex. Mol Cell *20*, 525-538.
255. Xu, Z., Devlin, K.I., Ford, M.G., Nix, J.C., Qin, J., and Misra, S. (2006). Structure and interactions of the helical and U-box domains of CHIP, the C terminus of HSP70 interacting protein. Biochemistry *45*, 4749-4759.
256. Graf, C., Stankiewicz, M., Nikolay, R., and Mayer, M.P. (2010). Insights into the conformational dynamics of the E3 ubiquitin ligase CHIP in complex with chaperones and E2 enzymes. Biochemistry *49*, 2121-2129.
257. Esser, C., Scheffner, M., and Hohfeld, J. (2005). The chaperone-associated ubiquitin ligase CHIP is able to target p53 for proteasomal degradation. J Biol Chem *280*, 27443-27448.
258. Haupt, Y., Maya, R., Kazaz, A., and Oren, M. (1997). Mdm2 promotes the rapid degradation of p53. Nature *387*, 296-299.
259. Honda, R., Tanaka, H., and Yasuda, H. (1997). Oncoprotein MDM2 is a ubiquitin ligase E3 for tumor suppressor p53. FEBS Lett *420*, 25-27.

260. Oliner, J.D., Kinzler, K.W., Meltzer, P.S., George, D.L., and Vogelstein, B. (1992). Amplification of a gene encoding a p53-associated protein in human sarcomas. Nature *358*, 80-83.
261. Ofir-Rosenfeld, Y., Boggs, K., Michael, D., Kastan, M.B., and Oren, M. (2008). Mdm2 regulates p53 mRNA translation through inhibitory interactions with ribosomal protein L26. Mol Cell *32*, 180-189.
262. Wawrzynow, B., Zylicz, A., Wallace, M., Hupp, T., and Zylicz, M. (2007). MDM2 chaperones the p53 tumor suppressor. J Biol Chem *282*, 32603-32612.
263. Burch, L., Shimizu, H., Smith, A., Patterson, C., and Hupp, T.R. (2004). Expansion of protein interaction maps by phage peptide display using MDM2 as a prototypical conformationally flexible target protein. J Mol Biol *337*, 129-145.
264. Bottger, V., Bottger, A., Garcia-Echeverria, C., Ramos, Y.F., van der Eb, A.J., Jochemsen, A.G., and Lane, D.P. (1999). Comparative study of the p53-mdm2 and p53-MDMX interfaces. Oncogene *18*, 189-199.
265. Shimizu, H., Burch, L.R., Smith, A.J., Dornan, D., Wallace, M., Ball, K.L., and Hupp, T.R. (2002). The conformationally flexible S9-S10 linker region in the core domain of p53 contains a novel MDM2 binding site whose mutation increases ubiquitination of p53 in vivo. J Biol Chem *277*, 28446-28458.
266. Yu, G.W., Rudiger, S., Veprintsev, D., Freund, S., Fernandez-Fernandez, M.R., and Fersht, A.R. (2006). The central region of HDM2 provides a second binding site for p53. Proc Natl Acad Sci U S A *103*, 1227-1232.
267. Poyurovsky, M.V., Jacq, X., Ma, C., Karni-Schmidt, O., Parker, P.J., Chalfie, M., Manley, J.L., and Prives, C. (2003). Nucleotide binding by the Mdm2 RING domain facilitates Arf-independent Mdm2 nucleolar localization. Mol Cell *12*, 875-887.
268. Linke, K., Mace, P.D., Smith, C.A., Vaux, D.L., Silke, J., and Day, C.L. (2008). Structure of the MDM2/MDMX RING domain heterodimer reveals dimerization is required for their ubiquitylation in trans. Cell Death Differ *15*, 841-848.
269. Tanimura, S., Ohtsuka, S., Mitsui, K., Shirouzu, K., Yoshimura, A., and Ohtsubo, M. (1999). MDM2 interacts with MDMX through their RING finger domains. FEBS Lett *447*, 5-9.
270. Shvarts, A., Steegenga, W.T., Riteco, N., van Laar, T., Dekker, P., Bazuine, M., van Ham, R.C., van der Houven van Oordt, W., Hateboer, G., van der Eb, A.J., et al. (1996). MDMX: a novel p53-binding protein with some functional properties of MDM2. EMBO J *15*, 5349-5357.
271. de Vries, S.J., van Dijk, A.D., Krzeminski, M., van Dijk, M., Thureau, A., Hsu, V., Wassenaar, T., and Bonvin, A.M. (2007). HADDOCK versus HADDOCK: new features and performance of HADDOCK2.0 on the CAPRI targets. Proteins *69*, 726-733.
272. Linares, L.K., Hengstermann, A., Ciechanover, A., Muller, S., and Scheffner, M. (2003). HdmX stimulates Hdm2-mediated ubiquitination and degradation of p53. Proc Natl Acad Sci U S A *100*, 12009-12014.

273. de Graaf, P., Little, N.A., Ramos, Y.F., Meulmeester, E., Letteboer, S.J., and Jochemsen, A.G. (2003). Hdmx protein stability is regulated by the ubiquitin ligase activity of Mdm2. J Biol Chem *278*, 38315-38324.
274. Kawai, H., Wiederschain, D., Kitao, H., Stuart, J., Tsai, K.K., and Yuan, Z.M. (2003). DNA damage-induced MDMX degradation is mediated by MDM2. J Biol Chem *278*, 45946-45953.
275. Pan, Y., and Chen, J. (2003). MDM2 promotes ubiquitination and degradation of MDMX. Mol Cell Biol *23*, 5113-5121.
276. Kostic, M., Matt, T., Martinez-Yamout, M.A., Dyson, H.J., and Wright, P.E. (2006). Solution structure of the Hdm2 C2H2C4 RING, a domain critical for ubiquitination of p53. J Mol Biol *363*, 433-450.
277. Yu, G.W., Allen, M.D., Andreeva, A., Fersht, A.R., and Bycroft, M. (2006). Solution structure of the C4 zinc finger domain of HDM2. Protein Sci *15*, 384-389.
278. Uhrinova, S., Uhrin, D., Powers, H., Watt, K., Zheleva, D., Fischer, P., McInnes, C., and Barlow, P.N. (2005). Structure of free MDM2 N-terminal domain reveals conformational adjustments that accompany p53-binding. J Mol Biol *350*, 587-598.
279. Michelsen, K., Jordan, J.B., Lewis, J., Long, A.M., Yang, E., Rew, Y., Zhou, J., Yakowec, P., Schnier, P.D., Huang, X., et al. (2012). Ordering of the N-terminus of human MDM2 by small molecule inhibitors. J Am Chem Soc *134*, 17059-17067.
280. Poyurovsky, M.V., Katz, C., Laptenko, O., Beckerman, R., Lokshin, M., Ahn, J., Byeon, I.J., Gabizon, R., Mattia, M., Zupnick, A., et al. (2010). The C terminus of p53 binds the N-terminal domain of MDM2. Nat Struct Mol Biol *17*, 982-989.
281. Pettersson, S., Kelleher, M., Pion, E., Wallace, M., and Ball, K.L. (2009). Role of Mdm2 acid domain interactions in recognition and ubiquitination of the transcription factor IRF-2. Biochem J *418*, 575-585.
282. Sdek, P., Ying, H., Chang, D.L., Qiu, W., Zheng, H., Touitou, R., Allday, M.J., and Xiao, Z.X. (2005). MDM2 promotes proteasome-dependent ubiquitin-independent degradation of retinoblastoma protein. Mol Cell *20*, 699-708.
283. Balint, E., Bates, S., and Vousden, K.H. (1999). Mdm2 binds p73 alpha without targeting degradation. Oncogene *18*, 3923-3929.
284. Dobbelstein, M., Wienzek, S., Konig, C., and Roth, J. (1999). Inactivation of the p53-homologue p73 by the mdm2-oncoprotein. Oncogene *18*, 2101-2106.
285. Gu, J., Nie, L., Kawai, H., and Yuan, Z.M. (2001). Subcellular distribution of p53 and p73 are differentially regulated by MDM2. Cancer Res *61*, 6703-6707.
286. Ongkeko, W.M., Wang, X.Q., Siu, W.Y., Lau, A.W., Yamashita, K., Harris, A.L., Cox, L.S., and Poon, R.Y. (1999). MDM2 and MDMX bind and stabilize the p53-related protein p73. Curr Biol *9*, 829-832.
287. Zeng, X., Chen, L., Jost, C.A., Maya, R., Keller, D., Wang, X., Kaelin, W.G., Jr., Oren, M., Chen, J., and Lu, H. (1999). MDM2 suppresses p73 function without promoting p73 degradation. Mol Cell Biol *19*, 3257-3266.

288. Gu, L., Findley, H.W., and Zhou, M. (2002). MDM2 induces NF-kappaB/p65 expression transcriptionally through Sp1-binding sites: a novel, p53-independent role of MDM2 in doxorubicin resistance in acute lymphoblastic leukemia. Blood *99*, 3367-3375.
289. Wade, M., Li, Y.C., and Wahl, G.M. (2012). MDM2, MDMX and p53 in oncogenesis and cancer therapy. Nat Rev Cancer *13*, 83-96.
290. Hupp, T.R., and Lane, D.P. (1994). Allosteric activation of latent p53 tetramers. Curr Biol *4*, 865-875.
291. Patel, S., George, R., Autore, F., Fraternali, F., Ladbury, J.E., and Nikolova, P.V. (2008). Molecular interactions of ASPP1 and ASPP2 with the p53 protein family and the apoptotic promoters PUMA and Bax. Nucleic Acids Res *36*, 5139-5151.
292. Kaku, S., Iwahashi, Y., Kuraishi, A., Albor, A., Yamagishi, T., Nakaike, S., and Kulesz-Martin, M. (2001). Binding to the naturally occurring double p53 binding site of the Mdm2 promoter alleviates the requirement for p53 C-terminal activation. Nucleic Acids Res *29*, 1989-1993.
293. Clarke, N., Jimenez-Lara, A.M., Voltz, E., and Gronemeyer, H. (2004). Tumor suppressor IRF-1 mediates retinoid and interferon anticancer signaling to death ligand TRAIL. EMBO J *23*, 3051-3060.
294. Lace, M.J., Anson, J.R., Klingelhutz, A.J., Harada, H., Taniguchi, T., Bossler, A.D., Haugen, T.H., and Turek, L.P. (2009). Interferon-beta treatment increases human papillomavirus early gene transcription and viral plasmid genome replication by activating interferon regulatory factor (IRF)-1. Carcinogenesis *30*, 1336-1344.
295. Gongora, C., Degols, G., Espert, L., Hua, T.D., and Mechti, N. (2000). A unique ISRE, in the TATA-less human Isg20 promoter, confers IRF-1-mediated responsiveness to both interferon type I and type II. Nucleic Acids Res *28*, 2333-2341.
296. Ruiz-Ruiz, C., Ruiz de Almodovar, C., Rodriguez, A., Ortiz-Ferron, G., Redondo, J.M., and Lopez-Rivas, A. (2004). The up-regulation of human caspase-8 by interferon-gamma in breast tumor cells requires the induction and action of the transcription factor interferon regulatory factor-1. J Biol Chem *279*, 19712-19720.
297. Dominguez, C., Boelens, R., and Bonvin, A.M. (2003). HADDOCK: a protein-protein docking approach based on biochemical or biophysical information. J Am Chem Soc *125*, 1731-1737.
298. Baker, N.A., Sept, D., Joseph, S., Holst, M.J., and McCammon, J.A. (2001). Electrostatics of nanosystems: application to microtubules and the ribosome. Proc Natl Acad Sci U S A *98*, 10037-10041.
299. Monticelli, L., and Tieleman, D.P. (2013). Force fields for classical molecular dynamics. Methods Mol Biol *924*, 197-213.
300. Durrant, J.D., and McCammon, J.A. (2011). Molecular dynamics simulations and drug discovery. BMC Biol *9*, 71.
301. Ravid, T., and Hochstrasser, M. (2007). Autoregulation of an E2 enzyme by ubiquitin-chain assembly on its catalytic residue. Nat Cell Biol *9*, 422-427.
302. Imai, Y., Soda, M., Hatakeyama, S., Akagi, T., Hashikawa, T., Nakayama, K.I., and Takahashi, R. (2002). CHIP is associated with Parkin, a gene

responsible for familial Parkinson's disease, and enhances its ubiquitin ligase activity. Mol Cell *10*, 55-67.
303. Jiang, J., Ballinger, C.A., Wu, Y., Dai, Q., Cyr, D.M., Hohfeld, J., and Patterson, C. (2001). CHIP is a U-box-dependent E3 ubiquitin ligase: identification of Hsc70 as a target for ubiquitylation. J Biol Chem *276*, 42938-42944.
304. Fang, S., Jensen, J.P., Ludwig, R.L., Vousden, K.H., and Weissman, A.M. (2000). Mdm2 is a RING finger-dependent ubiquitin protein ligase for itself and p53. J Biol Chem *275*, 8945-8951.
305. Honda, R., and Yasuda, H. (2000). Activity of MDM2, a ubiquitin ligase, toward p53 or itself is dependent on the RING finger domain of the ligase. Oncogene *19*, 1473-1476.
306. Scaglione, K.M., Zavodszky, E., Todi, S.V., Patury, S., Xu, P., Rodriguez-Lebron, E., Fischer, S., Konen, J., Djarmati, A., Peng, J., et al. (2011). Ube2w and ataxin-3 coordinately regulate the ubiquitin ligase CHIP. Mol Cell *43*, 599-612.
307. Kim, H.T., Kim, K.P., Uchiki, T., Gygi, S.P., and Goldberg, A.L. (2009). S5a promotes protein degradation by blocking synthesis of nondegradable forked ubiquitin chains. EMBO J *28*, 1867-1877.
308. Demand, J., Alberti, S., Patterson, C., and Hohfeld, J. (2001). Cooperation of a ubiquitin domain protein and an E3 ubiquitin ligase during chaperone/proteasome coupling. Curr Biol *11*, 1569-1577.
309. Kundrat, L., and Regan, L. (2010). Balance between folding and degradation for Hsp90-dependent client proteins: a key role for CHIP. Biochemistry *49*, 7428-7438.
310. Pace, C.N., and Scholtz, J.M. (1998). A helix propensity scale based on experimental studies of peptides and proteins. Biophys J *75*, 422-427.
311. Bashford, D., and Case, D.A. (2000). Generalized born models of macromolecular solvation effects. Annu Rev Phys Chem *51*, 129-152.
312. Connell, P., Ballinger, C.A., Jiang, J., Wu, Y., Thompson, L.J., Hohfeld, J., and Patterson, C. (2001). The co-chaperone CHIP regulates protein triage decisions mediated by heat-shock proteins. Nat Cell Biol *3*, 93-96.
313. Cyr, D.M., Hohfeld, J., and Patterson, C. (2002). Protein quality control: U-box-containing E3 ubiquitin ligases join the fold. Trends Biochem Sci *27*, 368-375.
314. Shang, Y., Zhao, X., Xu, X., Xin, H., Li, X., Zhai, Y., He, D., Jia, B., Chen, W., and Chang, Z. (2009). CHIP functions an E3 ubiquitin ligase of Runx1. Biochem Biophys Res Commun *386*, 242-246.
315. Xu, W., Marcu, M., Yuan, X., Mimnaugh, E., Patterson, C., and Neckers, L. (2002). Chaperone-dependent E3 ubiquitin ligase CHIP mediates a degradative pathway for c-ErbB2/Neu. Proc Natl Acad Sci U S A *99*, 12847-12852.
316. Liu, J., and Nussinov, R. (2011). Flexible cullins in cullin-RING E3 ligases allosterically regulate ubiquitination. J Biol Chem *286*, 40934-40942.
317. Ratajczak, T., Carrello, A., Mark, P.J., Warner, B.J., Simpson, R.J., Moritz, R.L., and House, A.K. (1993). The cyclophilin component of the unactivated

estrogen receptor contains a tetratricopeptide repeat domain and shares identity with p59 (FKBP59). J Biol Chem *268*, 13187-13192.
318. Ratajczak, T., Hlaing, J., Brockway, M.J., and Hahnel, R. (1990). Isolation of untransformed bovine estrogen receptor without molybdate stabilization. J Steroid Biochem *35*, 543-553.
319. Parashar, V., Jeffrey, P.D., and Neiditch, M.B. (2013). Conformational change-induced repeat domain expansion regulates Rap phosphatase quorum-sensing signal receptors. PLoS Biol *11*, e1001512.
320. Kim, E.J., Park, J.S., and Um, S.J. (2008). Ubc9-mediated sumoylation leads to transcriptional repression of IRF-1. Biochem Biophys Res Commun *377*, 952-956.
321. Nakagawa, K., and Yokosawa, H. (2002). PIAS3 induces SUMO-1 modification and transcriptional repression of IRF-1. FEBS Lett *530*, 204-208.
322. Lin, R., and Hiscott, J. (1999). A role for casein kinase II phosphorylation in the regulation of IRF-1 transcriptional activity. Mol Cell Biochem *191*, 169-180.
323. Negishi, H., Fujita, Y., Yanai, H., Sakaguchi, S., Ouyang, X., Shinohara, M., Takayanagi, H., Ohba, Y., Taniguchi, T., and Honda, K. (2006). Evidence for licensing of IFN-gamma-induced IFN regulatory factor 1 transcription factor by MyD88 in Toll-like receptor-dependent gene induction program. Proc Natl Acad Sci U S A *103*, 15136-15141.
324. Merika, M., Williams, A.J., Chen, G., Collins, T., and Thanos, D. (1998). Recruitment of CBP/p300 by the IFN beta enhanceosome is required for synergistic activation of transcription. Mol Cell *1*, 277-287.
325. Qi, H., Zhu, H., Lou, M., Fan, Y., Liu, H., Shen, J., Li, Z., Lv, X., Shan, J., Zhu, L., et al. (2012). Interferon regulatory factor 1 transactivates expression of human DNA polymerase eta in response to carcinogen N-methyl-N'-nitro-N-nitrosoguanidine. J Biol Chem *287*, 12622-12633.
326. Masumi, A., Wang, I.M., Lefebvre, B., Yang, X.J., Nakatani, Y., and Ozato, K. (1999). The histone acetylase PCAF is a phorbol-ester-inducible coactivator of the IRF family that confers enhanced interferon responsiveness. Mol Cell Biol *19*, 1810-1820.
327. Drew, P.D., Franzoso, G., Becker, K.G., Bours, V., Carlson, L.M., Siebenlist, U., and Ozato, K. (1995). NF kappa B and interferon regulatory factor 1 physically interact and synergistically induce major histocompatibility class I gene expression. J Interferon Cytokine Res *15*, 1037-1045.
328. Sgarbanti, M., Borsetti, A., Moscufo, N., Bellocchi, M.C., Ridolfi, B., Nappi, F., Marsili, G., Marziali, G., Coccia, E.M., Ensoli, B., et al. (2002). Modulation of human immunodeficiency virus 1 replication by interferon regulatory factors. J Exp Med *195*, 1359-1370.
329. Park, J.S., Kim, E.J., Kwon, H.J., Hwang, E.S., Namkoong, S.E., and Um, S.J. (2000). Inactivation of interferon regulatory factor-1 tumor suppressor protein by HPV E7 oncoprotein. Implication for the E7-mediated immune evasion mechanism in cervical carcinogenesis. J Biol Chem *275*, 6764-6769.
330. Kondo, T., Minamino, N., Nagamura-Inoue, T., Matsumoto, M., Taniguchi, T., and Tanaka, N. (1997). Identification and characterization of

nucleophosmin/B23/numatrin which binds the anti-oncogenic transcription factor IRF-1 and manifests oncogenic activity. Oncogene *15*, 1275-1281.
331. Park, J., Kim, K., Lee, E.J., Seo, Y.J., Lim, S.N., Park, K., Rho, S.B., Lee, S.H., and Lee, J.H. (2007). Elevated level of SUMOylated IRF-1 in tumor cells interferes with IRF-1-mediated apoptosis. Proc Natl Acad Sci U S A *104*, 17028-17033.
332. Hansen, S., Hupp, T.R., and Lane, D.P. (1996). Allosteric regulation of the thermostability and DNA binding activity of human p53 by specific interacting proteins. CRC Cell Transformation Group. J Biol Chem *271*, 3917-3924.
333. Pruneda, J.N., Stoll, K.E., Bolton, L.J., Brzovic, P.S., and Klevit, R.E. (2011). Ubiquitin in motion: structural studies of the ubiquitin-conjugating enzyme approximately ubiquitin conjugate. Biochemistry *50*, 1624-1633.
334. Lipford, J.R., and Deshaies, R.J. (2003). Diverse roles for ubiquitin-dependent proteolysis in transcriptional activation. Nat Cell Biol *5*, 845-850.
335. Leung, A., Geng, F., Daulny, A., Collins, G., Guzzardo, P., and Tansey, W.P. (2008). Transcriptional control and the ubiquitin-proteasome system. Ernst Schering Found Symp Proc, 75-97.
336. Salghetti, S.E., Kim, S.Y., and Tansey, W.P. (1999). Destruction of Myc by ubiquitin-mediated proteolysis: cancer-associated and transforming mutations stabilize Myc. EMBO J *18*, 717-726.
337. Salghetti, S.E., Muratani, M., Wijnen, H., Futcher, B., and Tansey, W.P. (2000). Functional overlap of sequences that activate transcription and signal ubiquitin-mediated proteolysis. Proc Natl Acad Sci U S A *97*, 3118-3123.
338. Salghetti, S.E., Caudy, A.A., Chenoweth, J.G., and Tansey, W.P. (2001). Regulation of transcriptional activation domain function by ubiquitin. Science *293*, 1651-1653.
339. Archer, C.T., Burdine, L., Liu, B., Ferdous, A., Johnston, S.A., and Kodadek, T. (2008). Physical and functional interactions of monoubiquitylated transactivators with the proteasome. J Biol Chem *283*, 21789-21798.
340. Bres, V., Kiernan, R.E., Linares, L.K., Chable-Bessia, C., Plechakova, O., Treand, C., Emiliani, S., Peloponese, J.M., Jeang, K.T., Coux, O., et al. (2003). A non-proteolytic role for ubiquitin in Tat-mediated transactivation of the HIV-1 promoter. Nat Cell Biol *5*, 754-761.
341. Gammoh, N., Gardiol, D., Massimi, P., and Banks, L. (2009). The Mdm2 ubiquitin ligase enhances transcriptional activity of human papillomavirus E2. J Virol *83*, 1538-1543.
342. Greer, S.F., Zika, E., Conti, B., Zhu, X.S., and Ting, J.P. (2003). Enhancement of CIITA transcriptional function by ubiquitin. Nat Immunol *4*, 1074-1082.
343. Vassilev, L.T. (2005). p53 Activation by small molecules: application in oncology. J Med Chem *48*, 4491-4499.
344. Vassilev, L.T., Vu, B.T., Graves, B., Carvajal, D., Podlaski, F., Filipovic, Z., Kong, N., Kammlott, U., Lukacs, C., Klein, C., et al. (2004). In vivo activation of the p53 pathway by small-molecule antagonists of MDM2. Science *303*, 844-848.

345. Ji, Z., Njauw, C.N., Taylor, M., Neel, V., Flaherty, K.T., and Tsao, H. (2012). p53 rescue through HDM2 antagonism suppresses melanoma growth and potentiates MEK inhibition. J Invest Dermatol *132*, 356-364.
346. Kim, W., Bennett, E.J., Huttlin, E.L., Guo, A., Li, J., Possemato, A., Sowa, M.E., Rad, R., Rush, J., Comb, M.J., et al. (2011). Systematic and quantitative assessment of the ubiquitin-modified proteome. Mol Cell *44*, 325-340.
347. Gilbert, N., and Allan, J. (2001). Distinctive higher-order chromatin structure at mammalian centromeres. Proc Natl Acad Sci U S A *98*, 11949-11954.
348. Gilbert, N., Boyle, S., Sutherland, H., de Las Heras, J., Allan, J., Jenuwein, T., and Bickmore, W.A. (2003). Formation of facultative heterochromatin in the absence of HP1. EMBO J *22*, 5540-5550.
349. Chan, W.M., Mak, M.C., Fung, T.K., Lau, A., Siu, W.Y., and Poon, R.Y. (2006). Ubiquitination of p53 at multiple sites in the DNA-binding domain. Mol Cancer Res *4*, 15-25.
350. Archer, C.T., Delahodde, A., Gonzalez, F., Johnston, S.A., and Kodadek, T. (2008). Activation domain-dependent monoubiquitylation of Gal4 protein is essential for promoter binding in vivo. J Biol Chem *283*, 12614-12623.
351. Ferdous, A., O'Neal, M., Nalley, K., Sikder, D., Kodadek, T., and Johnston, S.A. (2008). Phosphorylation of the Gal4 DNA-binding domain is essential for activator mono-ubiquitylation and efficient promoter occupancy. Mol Biosyst *4*, 1116-1125.
352. Gonzalez, F., Delahodde, A., Kodadek, T., and Johnston, S.A. (2002). Recruitment of a 19S proteasome subcomplex to an activated promoter. Science *296*, 548-550.
353. Chi, Y., Huddleston, M.J., Zhang, X., Young, R.A., Annan, R.S., Carr, S.A., and Deshaies, R.J. (2001). Negative regulation of Gcn4 and Msn2 transcription factors by Srb10 cyclin-dependent kinase. Genes Dev *15*, 1078-1092.
354. Chymkowitch, P., Le May, N., Charneau, P., Compe, E., and Egly, J.M. (2011). The phosphorylation of the androgen receptor by TFIIH directs the ubiquitin/proteasome process. EMBO J *30*, 468-479.
355. Muratani, M., Kung, C., Shokat, K.M., and Tansey, W.P. (2005). The F box protein Dsg1/Mdm30 is a transcriptional coactivator that stimulates Gal4 turnover and cotranscriptional mRNA processing. Cell *120*, 887-899.
356. Saville, M.K., Sparks, A., Xirodimas, D.P., Wardrop, J., Stevenson, L.F., Bourdon, J.C., Woods, Y.L., and Lane, D.P. (2004). Regulation of p53 by the ubiquitin-conjugating enzymes UbcH5B/C in vivo. J Biol Chem *279*, 42169-42181.
357. Wawrzynow, B., Pettersson, S., Zylicz, A., Bramham, J., Worrall, E., Hupp, T.R., and Ball, K.L. (2009). A function for the RING finger domain in the allosteric control of MDM2 conformation and activity. J Biol Chem *284*, 11517-11530.
358. Meulmeester, E., Pereg, Y., Shiloh, Y., and Jochemsen, A.G. (2005). ATM-mediated phosphorylations inhibit Mdmx/Mdm2 stabilization by HAUSP in favor of p53 activation. Cell Cycle *4*, 1166-1170.

359. Le Cam, L., Linares, L.K., Paul, C., Julien, E., Lacroix, M., Hatchi, E., Triboulet, R., Bossis, G., Shmueli, A., Rodriguez, M.S., et al. (2006). E4F1 is an atypical ubiquitin ligase that modulates p53 effector functions independently of degradation. Cell *127*, 775-788.
360. Lickwar, C.R., Mueller, F., Hanlon, S.E., McNally, J.G., and Lieb, J.D. (2012). Genome-wide protein-DNA binding dynamics suggest a molecular clutch for transcription factor function. Nature *484*, 251-255.
361. Brenkman, A.B., de Keizer, P.L., van den Broek, N.J., Jochemsen, A.G., and Burgering, B.M. (2008). Mdm2 induces mono-ubiquitination of FOXO4. PLoS ONE *3*, e2819.
362. Li, M., Brooks, C.L., Wu-Baer, F., Chen, D., Baer, R., and Gu, W. (2003). Mono- versus polyubiquitination: differential control of p53 fate by Mdm2. Science *302*, 1972-1975.
363. Carter, S., and Vousden, K.H. (2008). p53-Ubl fusions as models of ubiquitination, sumoylation and neddylation of p53. Cell Cycle *7*, 2519-2528.
364. Carter, S., Bischof, O., Dejean, A., and Vousden, K.H. (2007). C-terminal modifications regulate MDM2 dissociation and nuclear export of p53. Nat Cell Biol *9*, 428-435.
365. Shema, E., Oren, M., and Minsky, N. (2011). Detection and characterization of ubiquitylated H2B in mammalian cells. Methods *54*, 326-330.
366. Xu, G., Paige, J.S., and Jaffrey, S.R. (2010). Global analysis of lysine ubiquitination by ubiquitin remnant immunoaffinity profiling. Nat Biotechnol *28*, 868-873.
367. Shi, Y., Xu, P., and Qin, J. (2011). Ubiquitinated proteome: ready for global? Mol Cell Proteomics *10*, R110 006882.

368. Narayan V., Landré V., Blackburn EA., Joseph LJ., Verma C., Walkinshaw M., and Ball KL. An Inter-domain Allosteric Mechanism for the Control of CHIP E3-ligase Activity (submitted manuscript)

Appendix 1.1 The TPR-domain of Cyp40 regulates its Peptidyl Prolyl Isomerise Activity

As the TPR domain of CHIP allosterically regulates its activity through inter domain communication, we were interested to find out, whether this is a general mechanism by which TPR domains can control enzyme activity or whether this is a phenomenon specific to the E3 ligase CHIP. We therefore, chose to investigate the effects of TPR modulation on the dynamics and activity of Cyp40 (Cyclophilin40), in collaboration with Prof Malcolm Walkinshaw's group (School of Biological Science, University of Edinburgh). Cyp40 is comprised of two domains, an N-terminal PPIase domain and a C-terminal TPR domain, which are joined by a flexible linker. Like CHIP, Cyp40 is known to interact with Hsp90 [1, 2].

I began by modelling a Hsp90-bound form of Cyp40 by superimposing the TPR-domain of the Hsp90-bound CHIP crystal structure (2C2L) onto the TPR domain of Cyp40 (PBD: 1IHG[3]) (Fig A1-1a, right panel) and comparing it to both the wild-type conformation and a mutant form in which Lys^{227} (equivalent to Lys^{30} of CHIP, Fig A1-12a; left panel) was replaced by Ala. MD simulations were performed on all three structures, and the averaged fluctuation of each amino acid over the simulation was analysed. Simulations showed that, similar to CHIP, Cyp40 displays most flexibility when in an unliganded wild-type conformation (Fig A1-1b; left panel). Furthermore, mutation of Lys^{227}, or ligand binding, led to an overall 'tightening' of the structures of both the TPR- and PPIase-domains (Fig A1-1b; centre and right panel). This suggests that modulation of the TPR-domain influences the dynamics of Cyp40's catalytic PPIase domain in a relationship similar to that seen for the U-box and TPR-domains of CHIP. To determine if there was evidence of inter-domain communication I analysed the correlated motions between the averaged fluctuations for all amino acids. A correlated movement between the first α-helix of the TPR-domain and a β-sheet in the PPIase-domain was observed in the case of apo-Cyp40 (Fig A1-2 a left panel, movement A), but this was greatly reduced or lost in the ligand bound and K227A mutant form of Cyp40 (Fig A1-2 a, middle and right panel). Additionally, anti-correlated motions within the first three α-helices of the

TPR-domain were detected, again only in the unliganded form of Cyp40 (Movement B and C). Together the MD data suggest inter-domain cross-talk in Cyp40 and that this is dependent on the status of the TPR-domain. In the case of the E3 ligase CHIP, TPR mediated changes in the flexibility of the protein affects the activity of the U-box domain. To explore, if changes in the dynamics of the Cyp40 PPIase domain observed in MD simulations, effects its catalytic activity in a similar manner to CHIP, Cyp40 wild type or mutant protein, with a single mutation in its TPR domain from Lys to Ala at 227 or 305, were purified and its cis-trans prolyl isomerase activity was tested using a Kofron's optimised peptidyl-prolyl isomerase assay with suc-Ala-Leu-Pro-Phe-pNA as the substrate. Results of this experiment show that the introduction of a mutation at the TPR domain of Cyp40 increases it catalytic activity when compared to the wild type protein. Hence, modulation of the TPR domain of Cyp40, which affects its overall flexibility, modulates the activity of its catalytic domain in a similar manner as observed for CHIP. We speculate that ligands binding to TPR domains of proteins can act as allosteric regulators, changing the dynamic and thus activity of the protein's catalytic domains.

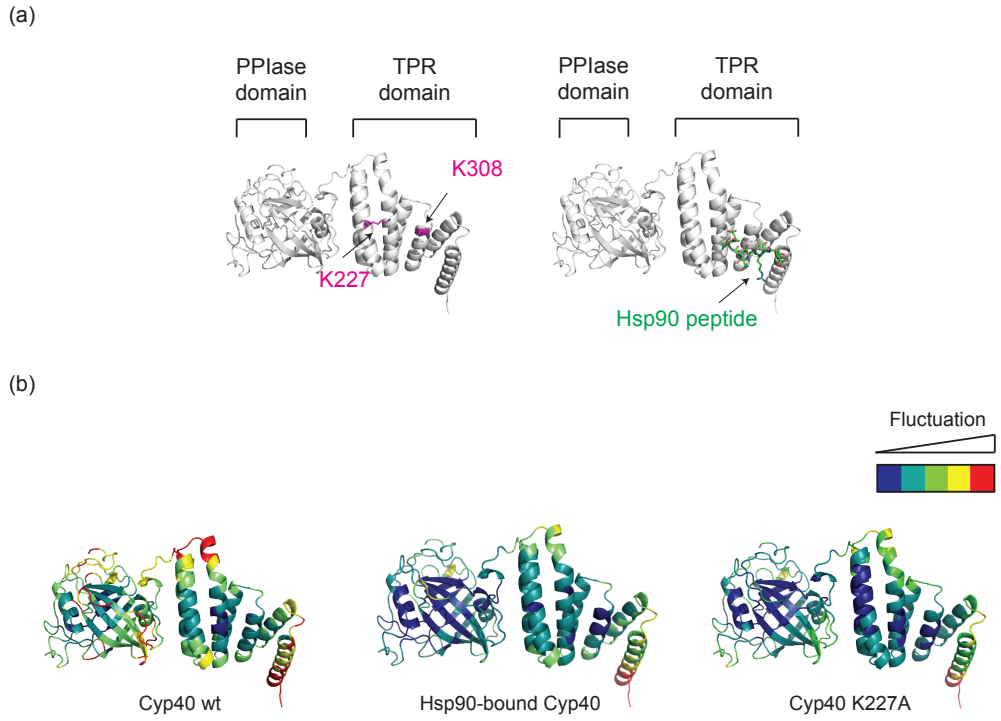

Figure A1-1 Mutation or peptide binding to the Cyp40 TPR leads to an overall loss of protein flexibilty

(a) Crystal structure of Cyp40 shown as cartoon (PBD: 1IHG[3]) with K^{308} and K^{227} indicated in pink. Also shown is a structure of Cyp40 associated with Hsp90 peptide, which was obtained by superimposing the TPR-domain of Hsp90-bound CHIP (from PDB 2C2L) onto the available structure for Cyp40 (PDB 1IHG). (b) Root mean square fluctuation (RMSF) of Cα obtained from the trajectories of 40 ns MD simulations of Cyp40 wild-type ± Hsp90 peptide and the K227A mutant. The score of the positional fluctuation analysis averaged over a 5 ns time frame for each amino acid were colour coded and indicated on the crystal structure**.**

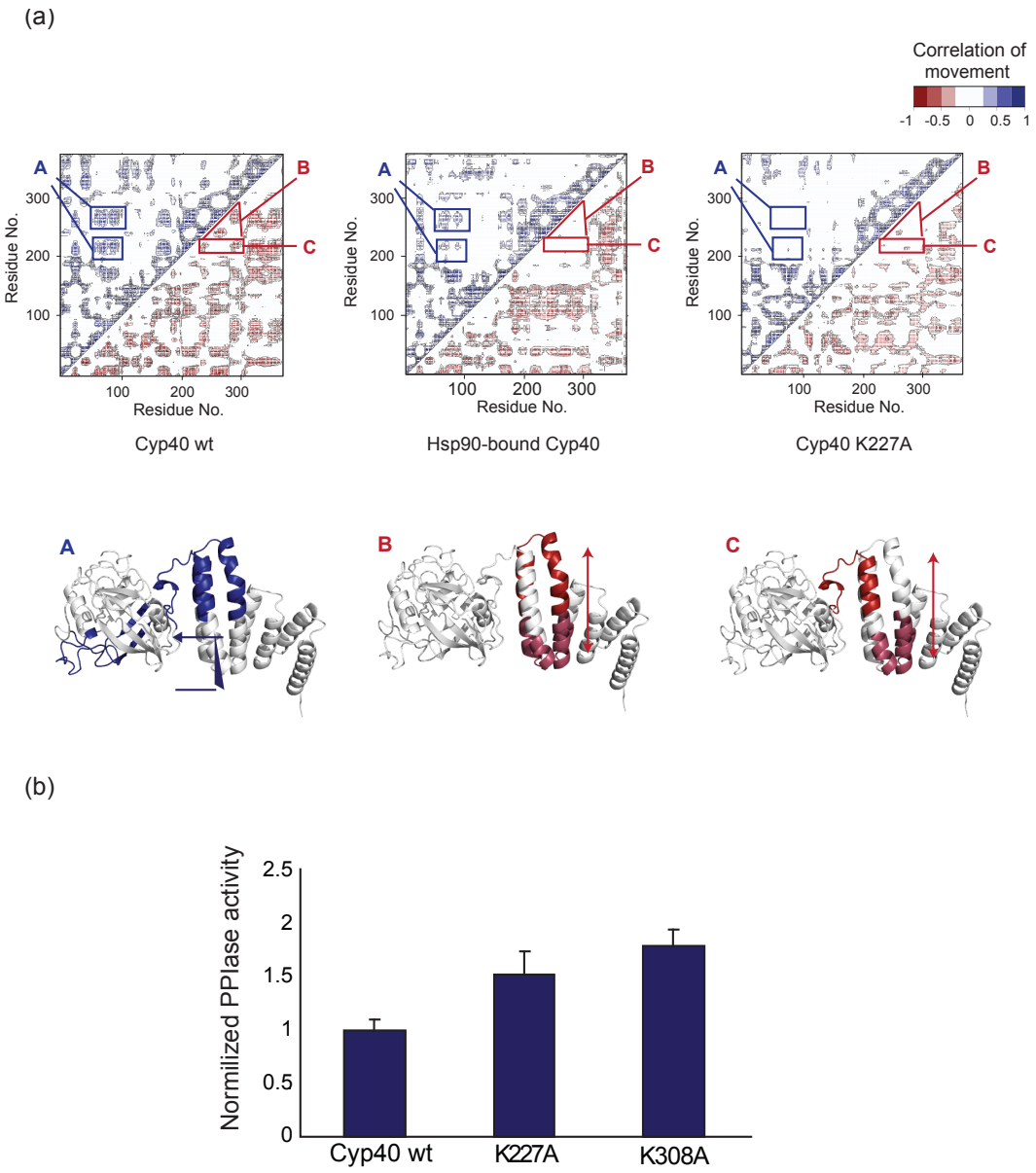

Figure Error! No text of specified style in document.**1-2 Modulation of Cyp40's TPR domain inhibits inter-domain communication and stimulates Cyp40's catalytic activity**

(a) Dynamic cross-correlation maps of Cα atoms for Cyp40 in the presence or absence of Hsp90 peptide and with a K227A point mutation. Correlated movements of the TPR-domain and PPIase-domain [A] and anti-correlated movements within the first three helices of the TPR-domain [B, C] can be seen for the wild-type Cyp40 protein, but are strongly decreased upon Hsp90 peptide binding and in the Lys^{227} mutant. Sections of the wild-type protein coloured in red or blue. (b) Results from a Kofron's optimised peptidyl-prolyl isomerase assay with suc-Ala-Leu-Pro-Phe-pNA as substrate and the indicated Cyp40 proteins. Graphs show PPIase activity normalised to standard error of mean. (b - data courtesy Liz Blackburn)

1. Ratajczak, T., Carrello, A., Mark, P.J., Warner, B.J., Simpson, R.J., Moritz, R.L., and House, A.K. (1993). The cyclophilin component of the unactivated estrogen receptor contains a tetratricopeptide repeat domain and shares identity with p59 (FKBP59). J Biol Chem *268*, 13187-13192.
2. Ratajczak, T., Hlaing, J., Brockway, M.J., and Hahnel, R. (1990). Isolation of untransformed bovine estrogen receptor without molybdate stabilization. J Steroid Biochem *35*, 543-553.
3. Taylor, P., Dornan, J., Carrello, A., Minchin, R.F., Ratajczak, T., and Walkinshaw, M.D. (2001). Two structures of cyclophilin 40: folding and fidelity in the TPR domains. Structure *9*, 431-438.

Appendix 1.2 Chaperone mediated allosteric regulation of the CHIP E3-ubiquitin ligase (submitted manuscript)

Chaperone mediated allosteric regulation of the CHIP E3-ubiquitin ligase

Vikram Narayan[1,4,6], Vivien Landré[1,4], Elizabeth A Blackburn[2], Chandra Verma[3], Malcolm D Walkinshaw[2] and Kathryn L Ball[1,5]

[1]IGMM, University of Edinburgh Cancer Research Centre, Cell Signalling Unit, Crewe Road South, Edinburgh EH4 2XR

[2]CTCB, Institute of Structural and Molecular Biology, University of Edinburgh, The King's Buildings, Mayfield Road, Edinburgh EH9 3JR

[3]Bioinformatics Institute (A*STAR), 30 Biopolis Street, 07-01 Matrix, Singapore 138671; Department of Biological Sciences, National University of Singapore, 14 Science Drive 4, Singapore 117543; School of Biological Sciences, Nanyang Technological University, 60 Nayang Drive, Singapore 637551

[4]These two authors contributed equally to the study reported

[5]To whom correspondence should be addressed (kathryn.ball@ed.ac.uk)

[6]Current address: Wellcome Trust Centre for Gene Regulation & Expression, University of Dundee, Dow Street, Dundee DD1 5EH

Running title: Allostery and cochaperones

Character count with spaces: 50503

Tetratricopeptide repeats (TPRs) are best characterised as scaffolds for the assembly of multiprotein complexes in essential processes such as cell cycle control, host defence and proteostasis. The current study addresses the role of the TPR in regulation of CHIP, a chaperone associated E3-ubiquitin ligase linking molecular chaperones to the ubiquitin proteasome system. We reveal the TPR-domain of CHIP as a binding site for allosteric modulators involved in determining the dynamic conformation and activity of CHIP as an E3-ligase. Molecular dynamic simulations support biochemical and biophysical evidence demonstrating that Hsp70 binding to the TPR, or Hsp70 mimetic mutations, negatively regulates CHIP-mediated ubiquitination of p53 and IRF-1 by preventing U-box catalysed discharge of ubiquitin from UbcH5. Using a second TPR-domain protein, the peptidyl-prolyl isomerase cyclophilin 40, we show that chaperone mediated allostery can activate, as well as inhibit, cochaperone function. Defining chaperone-associated TPR-domains as managers of inter-domain allosteric communication highlights the potential for scaffolding modules to regulate, as well as assemble, complexes that are fundamental to the control of proteostasis by the core molecular chaperone machinery.

Tetratricopeptide repeats are versatile structural modules conserved from *E.coli* to man which function in fundamental processes such as transcriptional control, kinase signalling, protein folding and immunity (Cerveny et al, 2012; D'Andrea & Regan, 2003; Zeytuni & Zarivach, 2012). TPR-domains are composed of two anti-parallel α-helices (containing a total of 34 amino acids) packed in tandem arrays to create a characteristic fold and binding cleft. Cleft formation facilitates protein:protein

interactions and underpins the role of TPR-domains as molecular scaffolds for the assembly of multi-protein complexes (Andrade et al, 2001; Smith, 2004). Although crystallographic studies originally led to the conclusion that TPR-domains were relatively rigid structures with an invariant conformation on ligand binding, a more recently study on bacterial Rap proteins suggests that TPR-domain binding can induce gross conformational changes in the protein as a whole (Parashar et al, 2013). Using NMR (Cliff et al, 2006), CD (Cliff et al, 2005) and HX-MS (Graf et al, 2010) the flexible character of the apo-TPR has been uncovered and this has pointed to an essential role for unstructured or intrinsically disordered TPR-domain regions in a coupled fold-on-binding mechanism. This suggests that flexible TPR-domain structures may be an advantage when it comes to setting up protein interaction networks (Dunker et al, 2005).

A subset of the TPR-domain proteins is known to associate with the Hsp70/Hsp90 family of molecular chaperones through interaction with a conserved C-terminal (EEVD) motif and act as cochaperones. CHIP (Carboxy-terminus of Hsc70-interacting protein) is an E3-ligase with three TPRs within its N-terminus, a central charged domain and a C-terminal U-box that is required for E2-conjugating enzyme binding and E3-ligase activity. CHIP functions as an Hsp70 co-chaperone (Ballinger et al, 1999) that can also interact with Hsp90, and links the molecular chaperones to the ubiquitin proteasome system. In addition CHIP can interact directly with native substrates to facilitate docking dependent ubiquitination[13]. The Cyp40 (cyclophilin-40) cochaperone, comprises an N-terminal peptidyl-prolyl isomerase (PPIase) domain joined by a flexible linker to TPR repeats situated in the C-terminus. Like

CHIP, the TPR-domain of Cyp40 is made up of three helix-turn-helix motifs arranged in pairs to form a super-helical structure that provides a concave binding surface, which in the case of Cyp40, binds preferentially to Hsp90 (Carrello et al, 2004).

Here a dynamic role for TPR-domains in the regulation of co-chaperone structure and function is proposed. By studying CHIP we have defined the TPR-domain as a modulator site for allosteric effectors of its U-box function and E3-ligase activity using physiologically relevant substrates such as p53 and IRF-1 (Narayan et al, 2011; Tripathi et al, 2007). The wider utility of the TPR as a regulatory module that can be employed by the chaperone machinery to maintain protein homeostasis is demonstrated using the immunophilin Cyp40 where stabilisation of TPR-domain conformation stimulates *cis-trans* isomerisation catalysed by the PPIase domain. We discuss inherent flexibility of a TPR-domain and its role in establishing dynamic motions within ensemble proteins and how this can mediate negative and positive allosteric regulation of protein activity in response to chaperone interactions.

Results

Hsp70 Modulates the E3-Ligase Activity of CHIP

We are interested in the role for TPR-domain proteins in maintaining protein homeostasis and particularly in whether the TPR-domain of CHIP plays a role in determining its E3-ligase activity and specificity. CHIP binds to a well-defined consensus motif in the C-terminus of Hsp70/Hsp90 and recent solution studies suggest that the CHIP-TPR attains a more stable conformation on Hsp70 binding whereas in an unliganded state it is highly flexible (Graf et al, 2010). How changes in

conformation affect the activity of CHIP however have not been addressed. Experiments therefore concentrated on determining the E3-ligase activity of CHIP in the apo-form compared to CHIP in which the TPR-domain was stabilised through binding to Hsp70. When the effect of Hsp70 on CHIP-mediated ubiquitination was determined, using a range of well-defined substrates (Demand et al, 2001; Esser et al, 2005; Narayan et al, 2011) and an Hsp70 free *in vitro* ubiquitination assay (Narayan et al, 2011), we found that Hsp70, alone or together with its physiological partner Hsp40 (present at a ratio of 1:10 with Hsp70), could either inhibit or activate CHIP function dependent on the substrate (Fig 1A, B and C). Hsp70 inhibited the ubiquitination of p53 and IRF-1 (1A and 1B; this is not due to binding site competition as native IRF-1 and p53 bind to ΔTPR-CHIP; Narayan et al, 2011; Tripathi et al, 2007) under conditions where it stimulated the modification of BAG-1s (1C). In addition, Hsp70 inhibited CHIP auto-ubiquitination in the presence of either IRF-1 or p53, whereas no inhibition of CHIP auto-ubiquitination was detected in the BAG-1s assay.

The above data suggest that the mechanism by which Hsp70 effects CHIP-mediated ubiquitination may differ dependent on the substrate however interpretation of the data is complicated by the fact that Hsp70 can bind directly to p53, IRF-1 and BAG-1s (Fourie et al, 1997; Narayan et al, 2009; Takayama et al, 1997a) in the absence of CHIP. To extend our analysis we therefore used a C-terminal peptide from Hsp70 (^{634}GPTIEEVD^{641}) that binds exclusively to the TPR-domain of CHIP (Fig 1D and Fig S1) and not to its substrates. When added to the ubiquitination assays, the Hsp70 peptide inhibited ubiquitination of IRF-1, and a mutant peptide with reduced CHIP

binding activity (see Fig S1) also had reduced inhibitory activity (Fig 1E). Ubiquination of p53 (Fig 1F) and CHIP auto-ubiquitination (Fig 1E and F) were also inhibited by the Hsp-peptide mimetic. Interestingly, the Hsp70 peptide was not sufficient to mimic the stimulatory effect of full-length Hsp70/40 on the ubiquitination of BAG-1s and furthermore, Hsp70/40 stimulated ubiquitination of BAG-1s was overcome by the Hsp70 peptide (Fig 1G). Together the data suggest that the mechanism by which Hsp70 promotes the ubiquitination of BAG-1s can be uncoupled from binding to the TPR-domain of CHIP and that it most likely relies on the ability of Hsp70 to bind directly to BAG-1s (Hohfeld & Jentsch, 1997; Takayama et al, 1997b). As a control for peptide specificity in binding to CHIP we show that it has no effect on the activity of the MDM2 E3-ligase in a p53 ubiquitination assay (Fig 1H) where all the components of the assay (with the exception of the E3) were identical to those in Fig 1F.

CHIP-K30A has an Intrinsic Defect in E3-Ubiquitin Ligase Activity

We reasoned that mutation of certain TPR-domain residues to Ala, a residue that encourages helix formation (Pace & Scholtz, 1998b), may mimic the stabilising effect of Hsp70-binding on the TPR-domainwhen[22]. Lys^{30} of CHIP is one of two basic residues (the other being Lys^{95}) that are required to form a dicarboxylate clamp around the C-terminal Asp of Hsp70/90 (Fig 2A), and mutation of this residue to Ala has been predicted to prevent Hsp70 binding. We therefore reasoned that a $Lys^{30}\rightarrow$Ala (K30A) point mutant protein may provide a tool to study the effect of stabilising the TPR-domain in the absence of added ligand.

Following expression, purification and normalization of K30A and wild-type CHIP (Fig S2A), we verified that the K30A mutant was folded and dimeric using a variety of biophysical techniques, we then asked whether the K30A mutation produced protein that was deficient in binding to Hsp70. CHIP-K30A protein was unable to bind to a C-terminal peptide from Hsp70 (Fig 2B) in a real-time AlphaScreen assay under conditions where the wild-type protein bound with a high affinity. As CHIP-K30A constructs have been used extensively in cell-based assays to study the chaperone-dependence of CHIP (Bonvini et al, 2004; Xu et al, 2002; Zhang et al, 2007) we next determined the effect of the Lys^{30} substitution on IRF-1 modification in cells. In-cell ubiquitination assays showed that wild-type CHIP significantly enhanced IRF-1 modification by ubiquitin (Fig 2C, compare lanes 6 and 3) whereas CHIP-K30A did not, rather the mutant had some dominant-negative activity towards endogenous E3-ligases. This result could be interpreted as a requirement for Hsp70 in enhanced substrate ubiquitination, however we also noted that CHIP-K30A did not undergo auto-ubiquitination (Fig 2C; Ub-CHIP) suggestive of differences in its intrinsic activity in a way which, as we predicted, might reflect a stabilisation of the TPR-domain structure by Ala.

To determine if CHIP-K30A E3-ligase activity was affected by the TPR-domain mutation it was assayed alongside that of the wild-type protein. To rule out an effect of the N-terminal His-tag on the structure and activity of the TPR-domain, these experiments were carried out using untagged CHIP (Fig S2B). Strikingly, CHIP-K30A displayed a significant reduction in its E3-ligase activity compared to the wild-type protein using either IRF-1 (Fig 2D) or p53 (Fig 2E) as the substrate. In addition, in

keeping with the cell-based assays (Fig 2C), the CHIP-K30A mutant was severely restricted in its ability to undergo auto-ubiquitination (Fig 2F). As the *in vitro* ubiquitination assay does not contain Hsp70/90 the decrease in CHIP-K30A E3-activity is not due to loss of Hsp70 binding potential.

Evidence of TPR-Mediated Changes in CHIP Conformation

Data presented above suggest that the TPR-domain plays an active role in the regulation of CHIP and that modulation by ligand binding or the introduction of structure stabilising amino acids may result in a shift in the protein ensemble that impacts on the activity of the U-box which is require to bind and allosterically activate the E2-enzyme component of the ubiquitination pathway (Jiang et al, 2001; Ozkan et al, 2005). In addition, as Hsp70 and Hsp70-peptide, or the introduction of a Lys^{30} point mutation within the TPR, have similar effects on the activity of CHIP, we hypothesised that the CHIP-K30A mutation might 'mimic' binding of Hsp70/90 to the ligase. To test our hypothesis we investigated whether CHIP-K30A had different dynamic properties and if these were similar to those of Hsp70-bound CHIP.

We started by determining whether peptide binding and/or Lys^{30} substitution affected the melting temperature (T_m) of full-length CHIP using fluorescence-based thermal shift assays as a measure of TPR secondary-structure and folding. CHIP had a higher melting temperature when bound to the Hsp70 peptide than in the un-liganded state (Fig 3A and B; T_m unbound (DMSO) = 43.5^oC, and bound [wt peptide; GPTIEEVD] = 45.5^oC) or in the presence of the low affinity mutant peptide (Hsp70 mutant peptide; GAAAEEVD, see Fig S1). Strikingly, when wild-type CHIP was

compared to CHIP-K30A, the mutation (Fig 3A and B), like ligand binding, made the protein more resistant to melting, with a T_m for CHIP-K30A of 46^{o}C. The data suggest that substituting Lys^{30} with Ala encourages a more structured or folded conformation to be adopted by the CHIP TPR-domain.

Next, limited proteolysis was used to probe for differences in the conformation of liganded- and apo-CHIP compared to the CHIP-K30A mutant protein. Conditions from preliminary experiments (Fig S3) were used to compare wt- and CHIP-K30A proteins to CHIP in the presence of the active Hsp70- or mutant-peptides (Fig 3C). The results showed a striking similarity between the banding pattern seen over-time for the CHIP-K30A mutant and for liganded CHIP i.e. full-length protein was more resistant to cleavage and no band 2 was generated. On the other hand, the bands generated for the wt protein in the absence of ligand or in the presence of control peptide were similar, with band 2 appearing between 15 and 30 min. Similar data were obtained using trypsin as the protease (Fig S3). Together the data suggest that the CHIP-K30A and Hsp70 peptide bound forms of CHIP have less structural flexibility and are in a more 'ordered' or compact form than wild-type CHIP when in solution.

Striking Similarity between the Structures of Liganded and Mutant CHIP

To gain further insight into how the TPR-domain might mediate changes in the activity and structure of CHIP, MD simulations were carried out using information derived from the crystal structure of mouse CHIP (residues 25-304) with an Hsp90 peptide-bound (PDB code: 2C2L; Fig 5A). To relate the modelling to our experimental data, five mutations were introduced into the crystal structure to obtain human

CHIP. Simulations were run on dimeric CHIP wild-type protein with and without Hsp90 peptide and on the Lys^{30} mutant. Simulations where one CHIP protomer was Hsp90 peptide bound and the other was unbound and where the Hsp90 peptide was replaced with the peptide from Hsp70 (Fig S4) were also run. The results of the simulations demonstrate that the conformation of CHIP in its liganded (Fig 4B; CHIP wt + Hsp90 peptide) or mutant state (Fig 4B; CHIP-K30A) are very similar to each other and are different from the apo-state (Fig 4B; CHIP wt). In the apo-state, the protein adopts a more linear and extended conformation with gross outwards movement of both TPR-domains (supplementary video). In contrast, in both its mutant and peptide bound states the protein adopts a closed conformation that is similar the crystal structure (Fig 4C).

Averaging the fluctuation of each residue in the CHIP structure showed that wild-type unliganded-CHIP (Fig 4D; left panel) was characterized by larger and more widespread fluctuations than peptide-bound (centre panel) or Lys^{30}-mutant CHIP (right panel), suggesting that the dynamics of the apo-state are different from the dynamics of the ligand-bound or mutant states, which in turn are similar to each other. This is in good agreement with HX-MS data showing that apo-CHIP protein is more flexible than the Hsp peptide-bound forms (Graf et al, 2010). Thus, MD agrees with experimental observations showing that CHIP has a lower melting point and is more susceptible to limited proteolysis in its unliganded form, whereas it is more thermostable and less susceptible to proteolysis in the presence of a Lys^{30} mutation or TPR-domain binding ligands.

The striking similarity between CHIP when it is bound to Hsp70/Hsp90 peptides or when it contains an Ala substitution at Lys^{30} confirms that although CHIP-K30A has been studied as a non-chaperone binding mutant of CHIP (Bonvini et al, 2004; Xu et al, 2002; Zhang et al, 2007), its properties are in fact like those of a constitutively Hsp-bound form. The side-chain of Lys^{30} does not appear to make any hydrogen bonds with other protein atoms during the MD simulations and is instead well hydrated. We speculate that, consistent with studies showing alanine residues favour the formation of ordered helical structures (Pace & Scholtz, 1998a), mutation of Lys^{30} to the much smaller and more hydrophobic Ala, will make this region less hydrated and more likely to fold into an ordered structure which is more similar to the peptide bound structure than to the flexible, less ordered structure described for the apo-TPR (Graf et al, 2010).

The TPR-Domain is an Allosteric Modulatory Site which Affects U-Box Activity

When the correlations between the fluctuations for residues in all three of the CHIP simulations (Fig 4D) were examined, a striking anti-correlated movement (Fig 5A) was seen between the TPR-domain of one CHIP wild-type protomer with the U-boxes of both dimer components. This motion was strongly suppressed upon peptide binding and almost completely lost in CHIP-K30A. Additionally, correlated motions were observed between the two U-box domains of the dimer (Fig 5B) in the wild-type conformation and again these were attenuated upon peptide binding or substitution of Lys^{30}. The MD simulations therefore provide strong support for a model where cross-talk between distinct domains of CHIP is likely to underpin its function. Previous studies have concluded that the CHIP dimer is asymmetric and

that the U-box of one of the protomers is unavailable for E2 binding due to the location of its cognate TPR-domain, whereas the U-box from the other protomer remains accessible to the E2 (Zhang et al, 2005) (with only one E2 charged U-box required for CHIP E3-activity). Our MD simulations suggest that changes in TPR-domain and U-box motion would not affect the ratio of E2-binding. We conclude therefore that the loss of anti-correlated motions of the two U-box domains with one of the TPR domains (Fig 5) upon peptide binding or Lys^{30} mutation is evidence that the TPR-domain is acting as a binding-site for allosteric effectors which negatively regulate CHIP activity. In our model loss of anti-correlated motion would impact on the dynamic nature of the U-box rather than altering the accessibility of one, or other, of the U-boxes at any given time.

To seek experimental evidence to support allosteric regulation of the U-box through the TPR-domain of CHIP, E2-binding and E2~Ub-discharge assays were used. The E2-enzyme UbcH5 can act as the catalytic module for CHIP as binding to the U-box (Fig 6A) generates allosteric changes in the UbcH5 which facilitate substrate ubiquitination or the transfer of ubiquitin to other ubiquitin molecules (Pruneda et al, 2012; Xu et al, 2008). To determine if TPR-domain-initiated changes in CHIP conformation and dynamic structure are transmitted to the U-box, we set up an E2-discharge assay and followed the loss of ubiquitin from thiolester-linked E2-ubiquitin (E2~Ub) in response to CHIP (Fig 6B; Cartoon). Whereas increasing amounts of wild-type CHIP stimulated ubiquitin discharge from UbcH5 (Fig 6B; lanes 4 and 5) the CHIP-K30A mutant protein had a significantly reduced ability to stimulate ubiquitin loss from the E2~Ub complex. In fact the activity of the CHIP-K30A mutant was

intermediate between that of wild-type CHIP and a U-box mutant (H260Q) that can no longer interact with the E2. Similarly, whereas ubiquitin was discharged from UbcH5~Ub by CHIP in the presence of both DMSO and a mutant Hsp70 peptide that has a reduced affinity for CHIP (D641A peptide) the wild-type Hsp70-peptide prevented CHIP mediated discharge (Fig 6C).

To ask whether decreased E2 discharge by CHIP-K30A represented a change in the affinity of the U-box for UbcH5, we carried out AlphaScreen assays where binding of UbcH5-donor beads to CHIP-acceptor beads (Fig 6D) was determined at equilibrium. The assays demonstrated that the loss of activity in the ubiquitin-discharge assay for the CHIP-K30A protein (Fig 6B) was due to a significant reduction in the ability of the mutant protein to bind the E2 when compared to wild-type CHIP. The experimental data on E2-discharge and CHIP:E2 binding therefore support a role for the TPR-domain of CHIP as an allosteric modulator site, occupation of which can generate long range inter-domain changes in the affinity and activity of the U-box inhibiting the ability of UbcH5 to catalyse ubiquitin discharge (Fig 6E).

The TPR-domain of Cyp40 Stimulates its Peptidyl Prolyl Isomerise Activity

We next set ourselves the task of determining whether CHIP was an isolated example of a cochaperone protein whose activity could be regulated through the TPR-domain, or whether dynamic conformational changes are more widely employed as a mechanism to affect intra-domain communication in TPR-domain proteins that function in association with Hsp70/Hsp90. A list of proteins that show homology to CHIP was compiled by aligning its TPR-sequence to all human

sequences in the Uniprot Knowledgebase (UniProtKB), and ranking them for homology using five iterations of PSI-BLAST (Altschul et al, 1997). We noted that the top hits were rich in proteins known to act as cochaperones by binding to the C-terminus of Hsp70/Hsp90 (Fig 7A). Once the list was filtered for proteins where structural details were available and that, like CHIP, had 3 TPR repeats plus additional domains with measurable activity, we had prioritized four co-chaperone proteins, namely the protein phosphatase PPP5 plus three immunophilins; Cyp40, FK506 binding protein-51 (FKBP51) and FK506 binding protein-52 (FKBP52). Importantly, all four of these proteins also had conserved Lys residues (equivalent to Lys^{30} and Lys^{95} of CHIP), which form part of a dicarboxylate clamp (Fig 7B). Of these, Cyp40 was an attractive candidate for further analysis as it has a relatively simple two domain structure (Taylor et al, 2001) comprising a C-terminal TPR-domain linked to a catalytically active peptidyl-prolyl isomerase (PPIase) domain (Fig 7C) that is amenable to biochemical characterisation.

We began by modelling an Hsp90-bound form of Cyp40 by superimposing the TPR-domain of the Hsp90-bound CHIP crystal structure onto the TPR-domain of Cyp40 (Fig 7C; lower panel) and comparing it to both the wild-type conformation and a mutant form in which Lys^{227} (equivalent of Lys^{30} of CHIP, Fig 7B and C; upper panel) was replaced by Ala. MD simulations were performed on all three structures and the averaged fluctuation of each amino acid over the simulation was analysed. The simulations showed that, similar to CHIP, Cyp40 displays most flexibility when in an unliganded wild-type conformation (Fig 7D; left panel). Furthermore, mutation of Lys^{227}, or ligand binding, led to an overall 'tightening' of both the TPR- and PPIase-

domains (Fig 7D; centre and right panel). This suggests that modulation of the TPR-domain influences the dynamics of Cyp40's catalytic PPIase-domain in a relationship similar to that seen for the U-box and TPR-domains of CHIP.

As the MD simulations suggested that TPR-domain status could influence the PPIase-domain, we generated Cyp40-K227A (Lys^{227}→Ala) to determine if predicted changes in the flexibility and motion of the PPIase-domain affected its *cis*-trans prolyl isomerase activity. Using a Kofron's optimised peptidyl-prolyl isomerase assay (Kofron et al, 1991) with suc-Ala-Leu-Pro-Phe-pNA as the substrate, we determined that the K227A-Cyp40 protein exhibited increased activity compared to the wild-type protein (153±22% of wt; Fig 7E). We sought to confirm the data by generating a Cyp40-K308A mutant (the second dicarboxylate clamp-forming Lys Fig 7B and C). Like the Cyp40-K227A protein, a Cyp40-K308A protein had enhanced PPIase activity displaying 180±16% of wild-type protein activity (Fig 7E).

The increase in PPIase activity for two independent TPR-domain Cyp40-mutant proteins is consistent with the concept that changes in TPR-domain flexibility regulate distinct cochaperone functions. Further, we have provided evidence that restricting the conformational flexibility of TPR-domain structures can act as a positive regulatory signal, as in the case of Cyp40, or, as with CHIP, can negatively influence the function of other domains.

Discussion

TPR-domains are protein interaction modules present across diverse kingdoms spanning bacteria to mammals that have been studied as scaffolds for the assembly of multiprotein complexes. We demonstrate that the presence of an N- or C-terminal TPR-domain can pave the way for allosteric regulation of distinct cochaperone activities or associated catalytic polypeptides through modulation of conformational dynamics and correlated motions. Thus, in keeping with recent conceptual advances on the potential of scaffolds and intrinsic disorder to support allosteric control of signalling complexes (Motlagh et al, 2012; Nussinov et al, 2013) we show that TPR-flexibility impacts on protein ensembles to regulated cochaperone activity in proteostasis.

Recent biophysical analysis has uncovered a degree of intrinsic disorder or dynamic flexibility in some TPR-domains when they are free in solution or if they are situated within the N-terminus of a protein (Cliff et al, 2006; Graf et al, 2010). Solution studies on the TPR-domain of PP5 using NMR and CD have suggested a mechanism of fold-on-binding to Hsp90 leading to the concept that changes in TPR-structure could contribute to the activation of the enzyme (Cliff et al, 2006; Cliff et al, 2005). However these studies were carried out on the isolated TPRs and have not been confirmed using full-length PP5. Recent crystallographic analysis of the Rap proteins from gram negative bacteria questions the widely held view that TPR domains have an invariant structure on ligand binding by showing that interaction of the RapJ TPR with PhrC generates large changes in the conformation of the protein as a whole (Parashar et al, 2013). Analyse of the TPR-domain in full-length CHIP using HX-MS shows it is 'loosely folded' and that the first 60 amino acids are intrinsically

disordered (Graf et al, 2010). A flexible TPR-domain structure that is readily able to take part in 'fold-on-binding interactions' leading to a change in the conformation and dynamic motions of the protein as a whole is supported by the current study. Fluctuation measurements for individual residues using MD simulations (Fig 4 and 7) for the TPR-domains of both CHIP and Cyp40 reveal a high degree of flexibility which is significantly reduced upon ligand binding or the introduction of structure stabilizing amino acids. In addition we see extensive correlations in motions between groups of residues and protein domains. In CHIP, correlated motions (motion occurring with the same phase) between one TPR and the U-box domains of the dimer and anti-correlated motion (motion occurring in opposite phases) between the two U-box domains (Fig 5) take place. As correlated and anti-correlated motions are linked to mechanisms of enzyme catalysis and protein allostery it is striking that TPR-domain binding suppresses motions within the TPR itself as well as in the U-boxes. Thus, loss of coordinated motion and intrinsic flexibility appear to be key components of allosteric inhibition by TPR-binding ligands such as Hsp70. Although the TPR-domain of Cyp40 is at the C-terminus, rather than the N-terminus, it still has a high degree of flexibility, especially in helix 1, 2 and 7 (Fig 7). In addition, atomic fluctuations suggest that the PPIase-domain of Cyp40 is affected by TPR status. PPIase domains are thought to undergo coordinated conformation changes that are correlated with enzymatic activity (Ramanathan & Agarwal, 2011). The β-barrel core of the PPIase-domain must provide a rigid scaffold to conserve hydrophobic interactions holding proline in the active site whilst loops proximal to the active site must be flexible enough to accommodate proline moving from *cis* to *trans*. Thus, a change in flexibility within the PPIase-domain is likely to influence enzyme activity.

Dynamic protein motion and flexibility are emerging as potential hallmarks of E3-ligase mediated ubiquitination. Studies on cullin-RING E3-ligases have shown that flexibility in substrate-binding proteins and Rbx subunits is required for efficient polyubiquitination. Moreover, the cullins, have recently been described as conformationally labile. Together, the flexible components of the cullin-RING E3-ligase complexes function to facilitate a shortening of the distance between the E2 and the substrate to initiate ubiquitination and an increase in the E2-substrate distance to accommodate polyubiquitination (Liu & Nussinov, 2012). In another model, flexible regions of the yeast E3-ligase San1 (Rosenbaum et al, 2011) and the ribosome-associated ligase Ltn1 (Lyumkis et al, 2013) aid in substrate selection by facilitating the recognition of misfolded or defective nascent-polypeptides. Here, we describe a third route by which E3-ligase structural flexibility can regulate ubiquitination. In this case, changes in the degree of TPR-domain secondary structure, flexibility and motion are transmitted to the U-box of CHIP and impact on the ability of CHIP to form complexes with UbcH5, an E2 catalytic partner. As E2/E3 interactions are critical to the generation of allosteric changes in the E2 which activate the thiolester-linked (Liu & Nussinov, 2012; Ozkan et al, 2005; Plechanovova et al, 2012), CHIP in which the TPR has been stabilized is deficient in its ability to discharge ubiquitin from the E2~Ub thiolester (Fig 6). Thus, the TPR-domain in CHIP appears to provide the plasticity it requires to act as an E3-ligase but can also act as an 'allosteric switch' where the introduction of a more ordered stable structure can 'turn off' its E3-function. Our study therefore supports the hypothesis that site-to-site allosteric coupling is optimized when ID domains are present and when a fold-

on-binding mechanism is employed (Hilser & Thompson, 2011; Ma & Nussinov, 2009), it also demonstrates that intrinsic disorder, scaffolding and allostery can all be linked in a single polypeptide chain as well as in multiprotein complexes.

The current study provides compelling evidence that Hsp70 is not simply acting as a targeting moiety for CHIP in the canonical protein quality control/chaperoning pathways, but is intimately linked to the control of CHIP activity. Support for this comes from studies on Smad1/5 (Wang et al, 2011) where Hsp70 inhibits CHIP-mediated ubiquitination and from α-synuclein where suppression of mono-ubiquitination by BAG-5 is Hsp70-mediated (Kalia et al, 2011). Our data is consistent with the concept that Hsp70 might hold CHIP in an inactive form until a favourable substrate is identified, at which stage CHIP would dissociate and bind directly to its target substrate (Narayan et al, 2011). The cochaperone function of Cyp40 is the *cis* to *trans* isomerisation of Xaa-proline isopeptide bonds (where Xaa is any amino acid) this is a rate limiting step in protein folding, thus the ability of TPR-stabilizing mutations to enhance its PPIase activity suggests that it could be allosterically activated by Hsp90. Alternatively, as Cyp40, has an intrinsic chaperone activity (Mok et al, 2006) misfolded or nascent polypeptides could bind directly to its TPR-domain leading to allosteric auto-activation.

Broadening the function of TPR-domains to include allosteric regulatory roles offers the opportunity to modulate the activity of rate-limiting steps in protein homeostasis pathways that are key to healthy aging and which play a significant role in preventing the development of neurodegenerative diseases and cancer. The ability of TPR-

domains to accommodate ligands with diverse primary and secondary structures (Brinker et al, 2002; Ramsey et al, 2009; Zeytuni & Zarivach, 2012), should encourage us to think that TPR directed biologics and/or small molecules will be identified for specific proteins offering the potential for allosteric drug development.

Methods and Materials

Chemicals, antibodies and peptides

Antibodies were used at 1 µg/ml and were anti-IRF-1 mAb (BD Biosciences), anti-p53 DO- 1, anti-Mdm2 4B2 and anti-CHIP v3.1 mAbs (Moravian Biotechnology), anti-CHIP N-terminal pAb (Sigma), anti-Hsp70 pAb (Stressgen) and anti-His mAb (Novagen). Secondary antibodies were purchased from Dako Cytomation. MG-132 (Calbiochem) was dissolved in DMSO to 10 mM and used as indicated. Peptides were from Chiron Mimotopes and were synthesized with a Biotin-tag and an SGSG spacer at the N-terminus; peptides were solubilized in DMSO. ATP was purchased from Calbiochem and creatine phosphate from Sigma.

Plasmids and purified proteins

pDEST-15-codon optimized IRF-1 (GST-IRF-1) and pET15b-CHIP (His-CHIP; wt, K30A and ΔTPR) were purified using glutathione-sepharose (Amersham GE) and Ni^{2+}-NTA agarose (Qiagen) respectively, according to the manufacturer's instructions. An *NdeI*-codon optimized IRF-1-*EcoRI* fragment was amplified from pDEST-15-IRF-1, ligated into pCOLDI (TaKaRa Bio) to give pCOLDI-IRF-1 (His-IRF-1) and purified as above following expression at 15^{o}C for 15 min by addition of IPTG (1mM). pET3a-CHIP (untagged CHIP; wt and K30A mutant) was sub-cloned from pET15b-CHIP using *NdeI*

and *BamHI*. Recombinant untagged p53 was purified as previously described[50]. Purified recombinant Hsp70 was purchased from Stressgen, ubiquitin and UBE1 from Boston Biochem and creatine phosphokinase from Sigma. Purified His-UbcH5a and His-tag cleaved UbcH5a were produced in house. pcDNA3-IRF-1, pcDNA3-CHIP and His-Ub are as previously described[13]. Purification of untagged CHIP is described in detail in the supplemental text.

Cell Culture

H1299 cells were cultured in RPMI-1640 (Roswell Park Memorial Institute 1640; Invitrogen) supplemented with 10% (v/v) fetal bovine serum (Autogen Bioclear) and 1% (v/v) penicillin-streptomycin mix (Invitrogen), and were maintained at 37°C/5% CO_2. Cells were seeded 24 hours before transfection and DNA transfected into the cells using Attractene (Qiagen) according to the manufacturer's recommendations.

Binding Assays

Purified protein (Hsp70 or UbcH5a; 100 ng) was immobilized on microtitre plates in 0.1 M $NaHCO_3$ (pH 8.6) overnight at 4°C. Following washing in PBS plus 0.1% (v/v) Tween-20, non-reactive sites were blocked using 3% (w/v) BSA in PBS. A titration of the protein of interest (usually 0-100 ng) was added in 1x ELISA Buffer (25 mM HEPES, pH 7.5, 50 mM KCl, 10 mM $MgCl_2$, 5% (v/v) glycerol, 0.1% (v/v) Tween-20) for 1 h at RT. Binding was detected using anti-His mAb and HRP-tagged anti-mouse 2^o or anti-CHIP pAb and HRP-tagged anti-rabbit 2^o, and electrochemical luminescence was quantified using a luminometer. For peptide binding assays, microtitre plates were coated with streptavidin (1 µg/well in PBS) and incubated with enough biotin-tagged

peptide to saturate the streptavidin (~60 pmol). Unbound peptide was removed and non-reactive sites blocked as above. A titration of His-CHIP (wt or K30A or ΔTPR as stated) in 1x ELISA buffer was added for 1 h at RT. Washing and detection was as above using anti-His mAb.

AlphaScreen

Amplified Luminescent Proximity Homogeneous Assays (AlphaScreen) were carried out in white half-area microtitre plates according to the manufacturer's recommendations. In brief, biotin-tagged Hsp70 peptide (GPTIEEVD; 6.25 ng) was linked to streptavidin donor beads (20 µl) diluted 1:100 and incubated with a titration (0-100 ng in 10 µl volume) of His-CHIP wt or K30A mutant conjugated to protein-A acceptor beads (20 µl of 1:100 dilution) using anti-His mAb. The reaction mix was incubated for 1 h at room temperature and quantified using an EnVision fluorescence detector (Perkin Elmer). For His-UbcH5:untagged CHIP AlphaScreen, the assay was performed as above except that His-tagged UbcH5a (50 ng) was anchored onto Nickel-chelate donor beads and a titration (0-100 ng) of untagged CHIP wt or K30A onto protein-A acceptor beads using anti-CHIP N-terminal pAb.

Ubiquitination and PPIase Assays

Cell-based ubiquitination assays were carried out as previously described (Pion et al, 2009). *In vitro* ubiquitination assays (Wallace et al, 2006) were started with His-CHIP (50-100 nM) or untagged CHIP (100-200 nM), incubated for up to 20 min as indicated at 30°C, and stopped by the addition of SDS-PAGE sample buffer. Samples were analyzed using 4–12% NuPAGE gels in a MOPS buffer system/immunoblot. If

required, Hsp70 (1:1 molar ratio with CHIP unless stated otherwise) and/or Hsp40 (at 1:10 ratio of Hsp40:Hsp70) or peptides were added to the ubiquitination mix (see figure legends for details) immediately prior to the incubation at 30°C. Cyp40 was analysed using Kofron's optimised peptidyl-prolyl isomerase assay(Kofron et al, 1991). A solution of 6 mg/ml α-chymotrypsin (CalBiotech) in 10 mM hydrochloric acid was prepared and kept on ice. α-chymotrypsin solution (100 µL) was added to 870 µL of Cyp40 in 50 mM HEPES, pH8, 100 mM NaCl, 1 mM DTT and 0.5 mM EDTA, gently mixed and rapidly added to a cuvette containing 4 mM substrate (30 µL; suc-Ala-Leu-Pro-Phe-pNA; Bachem, UK). The final solution contained 20 nM Cyp40, 0.6 mg/mL α-chymotrypsin, 120 µM substrate, 14 mM lithium chloride, 3% (v/v) 2,2,2-trifluoroethanol. Absorbance at 400 nM was recorded every 0.1 s for 120 s on a JascoV550 UV/VIS spectrophotometer (ε_{400nm} = 10,050 $M^{-1} \cdot cm^{-1}$; *p*-nitroaniline). The rate of the turnover reaction was determined during the steady-state phase.

E2 Discharge Assay

Reactions contained 25 mM HEPES pH 8.0, 10 mM $MgCl_2$, 350 nM ATP, 0.5 mM DTT, 0.05% (v/v) Triton X-100, 0.25 mM benzamidine, 10 µM ubiquitin, 100 nM UBE1 and 1 µM UbcH5a (E2). The E2 was charged for 15 min at 30°C after which His-CHIP (0-200 nM; ±Hsp70 peptide as required) was added and reactions were incubated for a further 15 min at 30°C to discharge the E2. To stop the reaction, SDS-PAGE sample buffer (without DTT, but with 2.5 mM N-ethylmaleimide) was added and the reactions analysed on 4–12% NuPAGE gels/immunoblot.

Thermal Unfolding Assay

SYPRO Orange was diluted to 50X in Buffer S (20 mM Tris, pH 8, 150 mM NaCl) and used at 5X. His-CHIP wt or K30A was diluted to 5 µM in Buffer S before the addition of SYPRO Orange. Hsp70 peptides (or a DMSO control) were added to a final concentration of 5 µM. Samples were loaded on a 96-well PCR plate (50 µl per reaction) and sealed. Unfolding was measured using an iCycler iQ Real-Time PCR system (Bio-Rad) by heating samples from 25°C to 60°C at 1°C increments with a 30 second incubation at each increment. Fluorescence intensity was measured in relative fluorescent units (RFU) using excitation/emission wavelengths of 485 nm/575 nm.

Limited Proteolysis

CHIP protein (2 µg; plus 4 µg peptide if required) was incubated with Glu-C (Roche; 40 ng) in 25 mM ammonium carbonate (pH 7.8) at room temperature as indicated. Reactions were stopped by addition of sample buffer and heating at 85°C for 5 min. Samples were analysed by 4-12% NuPAGE gels and stained with InstantBlue (Expedeon). For tryptic digests, 500 ng CHIP proteins, 5 ng trypsin (Roche) and 1 µg peptide was used, and the incubation carried out in 100 mM Tris-HCl (pH 8.5) at 4°C.

MD Simulations

The crystal structure of mouse CHIP in complex with Hsp90 peptide (PDB code 2C2L, resolved at 3.3 Å(Zhang et al, 2005)) was used as the initial structure for simulations. Five mutations (P77H, T167S, H188D, G192S, I194V - mouse numbering) were introduced into the crystal structure to obtain human CHIP using the WHATIF (http://swift.cmbi.ru.nl/whatif/) program. Simulations were then run on three

systems: the CHIP dimer with Hsp90 pep (chains A,B,E,F from 2C2L where chains A and B are the CHIP dimer and chains E and F are the peptides bound to chains A and B respectively), the CHIP dimer without peptide (chains A,B) and the CHIP dimer with Lys^{30} mutated to Ala (chains A,B). For simulations on Cyp40, the crystal structure of bovine Cyclophilin 40 in its monoclinic form was used (PDB code 1IHG, resolved at 1.8 Å[35]). A mutation was introduced at Lys^{227} to Ala and a Hsp90 peptide bound form was modelled by superimposing the CHIP structure bound to the Hsp90 peptide (2C2L Chain A and E) onto the Cyp40 TPR using Pymol (The PyMOL Molecular Graphics System, Version v1.4.1, Schrödinger, LLC). Simulations were run on the three systems: Cyp40 WT, Cyp40 K227A and Cyp40 bound to Hsp90 (obtained from Chain E of 2C2L). For details of the analyses see supplementary text.

Acknowledgments

VN was funded by a grant to KLB (C377/A6355) from CRUK. VL was funded by a SULSA Studentship. MW and EB were supported by the Wellcome Trust and the BBSRC through funding to the CTCB and Edinburgh Protein Production Facility.

Author contributions

VN, VL, EAB and KLB conceived, designed, executed and analyzed experiments. CV and MDW analyzed data and secured funding for the project. KLB secured funding for the study and wrote the manuscript with the aid of VN, VL and EAB.

Conflict of Interest

There are no conflicts of interest

References

Altschul SF, Madden TL, Schaffer AA, Zhang J, Zhang Z, Miller W, Lipman DJ (1997) Gapped BLAST and PSI-BLAST: a new generation of protein database search programs. *Nucleic acids research* **25:** 3389-3402

Andrade MA, Perez-Iratxeta C, Ponting CP (2001) Protein repeats: structures, functions, and evolution. *J Struct Biol* **134:** 117-131

Ballinger CA, Connell P, Wu Y, Hu Z, Thompson LJ, Yin LY, Patterson C (1999) Identification of CHIP, a novel tetratricopeptide repeat-containing protein that interacts with heat shock proteins and negatively regulates chaperone functions. *Mol Cell Biol* **19:** 4535-4545

Bonvini P, Dalla Rosa H, Vignes N, Rosolen A (2004) Ubiquitination and proteasomal degradation of nucleophosmin-anaplastic lymphoma kinase induced by 17-allylamino-demethoxygeldanamycin: role of the co-chaperone carboxyl heat shock protein 70-interacting protein. *Cancer Res* **64:** 3256-3264

Brinker A, Scheufler C, Von Der Mulbe F, Fleckenstein B, Herrmann C, Jung G, Moarefi I, Hartl FU (2002) Ligand discrimination by TPR domains. Relevance and selectivity of EEVD-recognition in Hsp70 x Hop x Hsp90 complexes. *The Journal of biological chemistry* **277:** 19265-19275

Carrello A, Allan RK, Morgan SL, Owen BA, Mok D, Ward BK, Minchin RF, Toft DO, Ratajczak T (2004) Interaction of the Hsp90 cochaperone cyclophilin 40 with Hsc70. *Cell stress & chaperones* **9:** 167-181

Cerveny L, Straskova A, Dankova V, Hartlova A, Ceckova M, Staud F, Stulik J (2012) Tetratricopeptide Repeat Motifs in the World of Bacterial Pathogens; Role in Virulence Mechanisms. *Infection and immunity*

Cliff MJ, Harris R, Barford D, Ladbury JE, Williams MA (2006) Conformational diversity in the TPR domain-mediated interaction of protein phosphatase 5 with Hsp90. *Structure* **14:** 415-426

Cliff MJ, Williams MA, Brooke-Smith J, Barford D, Ladbury JE (2005) Molecular recognition via coupled folding and binding in a TPR domain. *J Mol Biol* **346:** 717-732

D'Andrea LD, Regan L (2003) TPR proteins: the versatile helix. *Trends Biochem Sci* **28:** 655-662

Demand J, Alberti S, Patterson C, Hohfeld J (2001) Cooperation of a ubiquitin domain protein and an E3 ubiquitin ligase during chaperone/proteasome coupling. *Curr Biol* **11:** 1569-1577

Dunker AK, Cortese MS, Romero P, Iakoucheva LM, Uversky VN (2005) Flexible nets. The roles of intrinsic disorder in protein interaction networks. *Febs J* **272:** 5129-5148

Esser C, Scheffner M, Hohfeld J (2005) The chaperone associated ubiquitin ligase CHIP is able to target p53 for proteasomal degradation. *J Biol Chem*

Fourie AM, Hupp TR, Lane DP, Sang BC, Barbosa MS, Sambrook JF, Gething MJ (1997) HSP70 binding sites in the tumor suppressor protein p53. *J Biol Chem* **272:** 19471-19479

Graf C, Stankiewicz M, Nikolay R, Mayer MP Insights into the conformational dynamics of the E3 ubiquitin ligase CHIP in complex with chaperones and E2 enzymes. *Biochemistry* **49:** 2121-2129

Graf C, Stankiewicz M, Nikolay R, Mayer MP (2010) Insights into the conformational dynamics of the E3 ubiquitin ligase CHIP in complex with chaperones and E2 enzymes. *Biochemistry* **49:** 2121-2129

Hilser VJ, Thompson EB (2011) Structural dynamics, intrinsic disorder, and allostery in nuclear receptors as transcription factors. *The Journal of biological chemistry* **286:** 39675-39682

Hohfeld J, Jentsch S (1997) GrpE-like regulation of the hsc70 chaperone by the anti-apoptotic protein BAG-1. *Embo J* **16:** 6209-6216

Jiang J, Ballinger CA, Wu Y, Dai Q, Cyr DM, Hohfeld J, Patterson C (2001) CHIP is a U-box-dependent E3 ubiquitin ligase: identification of Hsc70 as a target for ubiquitylation. *J Biol Chem* **276:** 42938-42944

Kalia LV, Kalia SK, Chau H, Lozano AM, Hyman BT, McLean PJ (2011)Ubiquitinylation of alpha-synuclein by carboxyl terminus Hsp70-interacting protein (CHIP) is regulated by Bcl-2-associated athanogene 5 (BAG5). *PLoS One* **6:** e14695

Kofron JL, Kuzmic P, Kishore V, Colon-Bonilla E, Rich DH (1991) Determination of kinetic constants for peptidyl prolyl cis-trans isomerases by an improved spectrophotometric assay. *Biochemistry* **30:** 6127-6134

Liu J, Nussinov R (2012) The role of allostery in the ubiquitin-proteasome system. *Crit Rev Biochem Mol Biol*

Lyumkis D, Doamekpor SK, Bengtson MH, Lee JW, Toro TB, Petroski MD, Lima CD, Potter CS, Carragher B, Joazeiro CA (2013) Single-particle EM reveals extensive

conformational variability of the Ltn1 E3 ligase. *Proceedings of the National Academy of Sciences of the United States of America* **110:** 1702-1707

Ma B, Nussinov R (2009) Amplification of signaling via cellular allosteric relay and protein disorder. *Proceedings of the National Academy of Sciences of the United States of America* **106:** 6887-6888

Mok D, Allan RK, Carrello A, Wangoo K, Walkinshaw MD, Ratajczak T (2006) The chaperone function of cyclophilin 40 maps to a cleft between the prolyl isomerase and tetratricopeptide repeat domains. *FEBS letters* **580:** 2761-2768

Motlagh HN, Li J, Thompson EB, Hilser VJ (2012) Interplay between allostery and intrinsic disorder in an ensemble. *Biochemical Society transactions* **40:** 975-980

Narayan V, Eckert M, Zylicz A, Zylicz M, Ball KL (2009) Cooperative regulation of the interferon regulatory factor-1 tumor suppressor protein by core components of the molecular chaperone machinery. *J Biol Chem* **284:** 25889-25899

Narayan V, Pion E, Landre V, Muller P, Ball KL (2011) Docking dependent ubiquitination of the interferon regulatory factor-1 tumour suppressor protein by the ubiquitin ligase chip. *J Biol Chem*

Nussinov R, Ma B, Tsai CJ (2013) A broad view of scaffolding suggests that scaffolding proteins can actively control regulation and signaling of multienzyme complexes through allostery. *Biochimica et biophysica acta*

Ozkan E, Yu H, Deisenhofer J (2005) Mechanistic insight into the allosteric activation of a ubiquitin-conjugating enzyme by RING-type ubiquitin ligases. *Proceedings of the National Academy of Sciences of the United States of America* **102:** 18890-18895

Pace CN, Scholtz JM (1998a) A helix propensity scale based on experimental studies of peptides and proteins. *Biophysical journal* **75:** 422-427

Pace CN, Scholtz JM (1998b) A helix propensity scale based on experimental studies of peptides and proteins. *Biophys J* **75:** 422-427

Parashar V, Jeffrey PD, Neiditch MB (2013) Conformational change-induced repeat domain expansion regulates Rap phosphatase quorum-sensing signal receptors. *PLoS biology* **11:** e1001512

Pion E, Narayan V, Eckert M, Ball KL (2009) Role of the IRF-1 enhancer domain in signalling polyubiquitination and degradation. *Cell Signal* **21:** 1479-1487

Plechanovova A, Jaffray EG, Tatham MH, Naismith JH, Hay RT (2012) Structure of a RING E3 ligase and ubiquitin-loaded E2 primed for catalysis. *Nature* **489:** 115-120

Pruneda JN, Littlefield PJ, Soss SE, Nordquist KA, Chazin WJ, Brzovic PS, Klevit RE (2012) Structure of an E3:E2~Ub complex reveals an allosteric mechanism shared among RING/U-box ligases. *Mol Cell* **47:** 933-942

Ramanathan A, Agarwal PK (2011) Evolutionarily conserved linkage between enzyme fold, flexibility, and catalysis. *PLoS biology* **9:** e1001193

Ramsey AJ, Russell LC, Chinkers M (2009) C-terminal sequences of hsp70 and hsp90 as non-specific anchors for tetratricopeptide repeat (TPR) proteins. *The Biochemical journal* **423:** 411-419

Rosenbaum JC, Fredrickson EK, Oeser ML, Garrett-Engele CM, Locke MN, Richardson LA, Nelson ZW, Hetrick ED, Milac TI, Gottschling DE, Gardner RG (2011) Disorder targets misorder in nuclear quality control degradation: a disordered ubiquitin ligase directly recognizes its misfolded substrates. *Molecular cell* **41:** 93-106

Smith DF (2004) Tetratricopeptide repeat cochaperones in steroid receptor complexes. *Cell stress & chaperones* **9:** 109-121

Takayama S, Bimston DN, Matsuzawa S, Freeman BC, Aime-Sempe C, Xie Z, Morimoto RI, Reed JC (1997a) BAG-1 modulates the chaperone activity of Hsp70/Hsc70. *Embo J* **16:** 4887-4896

Takayama S, Bimston DN, Matsuzawa S, Freeman BC, Aime-Sempe C, Xie Z, Morimoto RI, Reed JC (1997b) BAG-1 modulates the chaperone activity of Hsp70/Hsc70. *The EMBO journal* **16:** 4887-4896

Taylor P, Dornan J, Carrello A, Minchin RF, Ratajczak T, Walkinshaw MD (2001) Two structures of cyclophilin 40: folding and fidelity in the TPR domains. *Structure* **9:** 431-438

Tripathi V, Ali A, Bhat R, Pati U (2007) CHIP chaperones wild type p53 tumor suppressor protein. *J Biol Chem* **282:** 28441-28454

Wallace M, Worrall E, Pettersson S, Hupp TR, Ball KL (2006) Dual-Site Regulation of MDM2 E3-Ubiquitin Ligase Activity. *Mol Cell* **23:** 251-263

Wang L, Liu YT, Hao R, Chen L, Chang Z, Wang HR, Wang ZX, Wu JW (2011) Molecular mechanism of the negative regulation of Smad1/5 protein by carboxyl terminus of Hsc70-interacting protein (CHIP). *The Journal of biological chemistry* **286:** 15883-15894

Xu W, Marcu M, Yuan X, Mimnaugh E, Patterson C, Neckers L (2002) Chaperone-dependent E3 ubiquitin ligase CHIP mediates a degradative pathway for c-ErbB2/Neu. *Proc Natl Acad Sci U S A* **99:** 12847-12852

Xu Z, Kohli E, Devlin KI, Bold M, Nix JC, Misra S (2008) Interactions between the quality control ubiquitin ligase CHIP and ubiquitin conjugating enzymes. *BMC Struct Biol* **8:** 26

Zeytuni N, Zarivach R (2012) Structural and functional discussion of the tetra-trico-peptide repeat, a protein interaction module. *Structure* **20:** 397-405

Zhang L, Nephew KP, Gallagher PJ (2007) Regulation of death-associated protein kinase. Stabilization by HSP90 heterocomplexes. *J Biol Chem* **282:** 11795-11804

Zhang M, Windheim M, Roe SM, Peggie M, Cohen P, Prodromou C, Pearl LH (2005) Chaperoned ubiquitylation--crystal structures of the CHIP U box E3 ubiquitin ligase and a CHIP-Ubc13-Uev1a complex. *Mol Cell* **20:** 525-538

Figure legends

Figure 1. Hsp70 differentially modulates CHIP-dependent ubiquitination. (**A**) Immunoblot of *in vitro* ubiquitination reactions assembled using ATP, ubiquitin, UBE1, UbcH5a, His-CHIP and GST-IRF-1 in the presence of a titration of Hsp70 and/or Hsp40 (at either a 1:1 and 1:2 molar ratio of Hsp70 with CHIP) as indicated. (**B, C**) Immunoblot of *in vitro* ubiquitination assays assembled as in (**A**) except using untagged p53 (**B**) or GST-BAG-1s (**C**) as substrate, in the presence of Hsp70 and Hsp40. (**D**) Snapshot of the crystal structure of mCHIP dimer (protomers in shades of grey) in complex with Hsp90 peptide (yellow sticks; PDB code 2C2L) generated using PyMOL v1.4.1. Lys30 is highlighted in blue. (**E, F**) Immunoblot of *in vitro* ubiquitination reactions assembled using ATP, ubiquitin, UBE1, UbcH5a, His-CHIP and His-IRF-1 (**E**) or untagged p53 (**F**) in the presence of a titration of Hsp70 peptides as indicated (wt: GPTIEEVD; mut: GAAAEEVD). A carrier only control (DMSO) was included. (**G**) As above except that GST-BAG-1s was used as the substrate and both full-length Hsp70/Hsp40 as well as Hsp70 wt peptides were included in the assay as indicated. (**H**) As in (**F**) except using GST-Mdm2 as the E3 ligase.

Figure 2. CHIP-K30A is intrinsically defective in E3-ligase activity. (**A**) Close-up of the Hsp90 binding site on CHIP extracted from the crystal structure of mCHIP dimer (protomers in shades of grey) in complex with Hsp90 peptide (yellow sticks; PDB code 2C2L) generated using PyMOL v1.4.1. Lys30 on CHIP and Asp732 on Hsp90 are highlighted in blue and green respectively. (**B**) An AlphaScreen assay was set up (see cartoon) to measure binding dynamics of His-CHIP wt or K30A mutant with biotin-tagged Hsp70 peptide (GPTIEEVD) in solution. (**C**) Ubiquitination of exogenous IRF-1 in H1299 cells transiently transfected with plasmids encoding CHIP wt or K30A mutant and His-ubiquitin. Immunoblots show ubiquitinated protein (His-pulldown) and total protein (direct lysis). (**D, E**) *In vitro* ubiquitination assays were assembled using ATP, ubiquitin, UBE1, UbcH5a, untagged CHIP wt or K30A, and His-IRF-1 (**D**) or untagged p53 (**E**) as substrate. Reactions were analyzed by 4-12% NuPAGE/immunoblot. (**F**) Immunoblot of *in vitro* ubiquitination assays assembled as above except in the absence of substrate to study auto-ubiquitination of untagged CHIP wt or K30A proteins over time.

Figure 3. CHIP-K30A and Hsp70-bound CHIP are conformationally distinct from the wild-type protein. (**A**) Graph showing the unfolding of His-CHIP wt or K30A mutant (left panel) or His-CHIP wt pre-incubated with the indicated peptides based on Hsp70 (right panel) as a function of temperature change measured by the uptake of the fluorescent dye SYPRO Orange. Shown is the mean ± standard error of mean of 3 experiments. (**B**) Table listing the mid-point temperature of phase transition (Tm) of each sample in (**A**) that was calculated by plotting the gradient of protein unfolding

against the temperature gradient [d(RFU)/dT]. (**C**) InstantBlue stained gel of untagged CHIP wt or K30A (left panel) digested with Glu-C. FL is the full-length protein and band 1 is a cleavage product that persists in the K30A mutant. Band 2 is only observed in digests of the wt protein. Also shown is a Glu-C digest of His-CHIP wt protein in complex with wt or mutant Hsp70 peptides (right panel).

Figure 4. CHIP-K30A and Hsp70-bound CHIP have similar equilibrium structures. (**A-D**) Images were generated using PyMOL v.1.4.1. (**A**) Crystal structure of murine CHIP dimer (monomers in shades of blue) in complex with Hsp90 peptide (pink sticks; adapted from PDB 2C2L). (**B**) Overlay of the CHIP dimer before (blue ribbon) and after (grey mesh) 20 ns MD simulations for unliganded CHIP wt (left), CHIP wt in complex with Hsp90 peptide (centre) and CHIP-K30A (right). (**C**) Overlaid snapshots of the CHIP dimer in apo and liganded forms and with Lys30 mutated to Ala after 20 ns MD simulations (from (B)). (**D**) Root mean square fluctuation (RMSF) of Cα obtained from the trajectories of the 20 ns simulations of CHIP wt ± peptide and the CHIP-K30A mutant. The score of the positional fluctuation analysis averaged over amino acid were colour coded and indicated on the crystal structure.

Figure 5. Coordinated movements between the TPR and U-box domains of CHIP are reduced when Hsp90 binds to the TPR domain. (**A**) Dynamic cross-correlation map (left panel) of Cα atoms for the un-liganded wt CHIP dimer. Correlated motions are represented above the diagonal in blue and anti-correlated below in red. Correlated movements of the CHIP U-boxes are indicated by a blue box. Anti-correlated movements of the TPR domain (right panel in brown) with both U-boxes (right panel

in green) are indicated with red boxes. Cartoon of CHIP dimer (right panel) was generated using PyMOL v.1.4.1. (**B**) As above except the dynamic cross-correlation maps of Cα atoms are for Hsp90 peptide bound wt CHIP dimer (left panel) and the K30A mutant CHIP dimer (right panel).

Figure 6. Modulation of the TPR-domain of CHIP affects U-box function. (**A**) Snapshot of the crystal structure of zebrafish CHIP-Ubox in complex with UbcH5 (from PDB 2OXQ) superimposed onto the crystal structure of mouse CHIP (from PDB 2C2L). The image, showing a single CHIP monomer, was generated using PyMOL v1.4.1. Blue ribbon: CHIP; red ribbon: UbcH5; TPR tetratricopeptide repeat. (**B**) His-UbcH5a was charged with ubiquitin (Ub~E2; thiolester linkage) by incubating with UBE1 and ubiquitin in the presence of ATP, following which ubiquitin discharge from the E2 by His-CHIP wt or K30A mutant was monitored. The E2-binding-defective mutant H260Q was included as a control. Shown is an immunoblot probed for CHIP and the E2. (**C**) Immunoblot of E2 discharge assay as above except using a titration of His-CHIP wt protein that had been pre-incubated with a fixed amount (3 μM) of Hsp70 wt peptide or D641A mutant peptide or DMSO control prior to addition into the assay. Ub~E2 represents the E2:Ub species linked by a thiolester bond while * indicates the E2:Ub species linked by an isopeptide bond (Ub-E2 or ubiquitinated E2). (**D**) An AlphaScreen assay was set up (see cartoon) to measure binding dynamics of untagged CHIP wt or K30A mutant with His-tagged UbcH5a in solution. (**E**) A model for CHIP regulation where the whole of the apo-protein (i) is more flexible and where there are regions of intrinsic disorder in the TPR(Graf et al, 2010). Upon binding to the E2~Ub complex the U-box of apo-CHIP generates a conformational change in

UbcH5 that facilitates Ub discharge. Alternatively (ii), when the TPR-domain binds to certain ligands (or is stabilised by mutations) it becomes more ridged and there is a decrease in dynamic motions throughout the whole protein. In the ligand bound form of CHIP the U-box is less able to for complexes with UbcH5 and Ub is therefore discharged inefficiently.

Figure 7. The TPR-domain of Cyp40 allosterically enhances its peptidyl proline isomerase activity. (**A**) List of human TPR-containing proteins in the UniProt Knowledgebase bearing homology to CHIP's TPR domain and ranked for homology using five iterations of PSI-BLAST. Proteins that, like CHIP, had three TPR motifs based on available structural information and additional domains with measurable enzymatic activity are highlighted in bold. (**B**) Sequence alignment of the three TPR motifs in the indicated proteins with the highly conserved Lys residues that interact with the dicarboxylate clamp of Hsp70/Hsp90 marked in blue. (**C**) Snapshot of the crystal structure of Cyp40 (PBD 1IHG ; upper panel) with the dicarboxylate clamp residues K227 and K308 in pink. Also shown is a snapshot of the structure obtained by superimposing the TPR-domain of Hsp90-bound CHIP (from PDB 2C2L) onto the available structure for Cyp40 (PDB 1IHG ; lower panel). (**D**) Root mean square fluctuation (RMSF) of Cα obtained from the trajectories of 40 ns MD simulations of Cyp40 wt ± Hsp90 peptide and the K227A mutant. The score of the positional fluctuation analysis averaged over amino acid were colour coded and indicated on the crystal structure. (**E**) Results from a Kofron's optimised peptidyl-prolyl isomerase assay with suc-Ala-Leu-Pro-Phe-pNA as substrate and the indicated Cyp40 proteins. Graphs show PPIase activity with standard error of the mean.

Figure 1

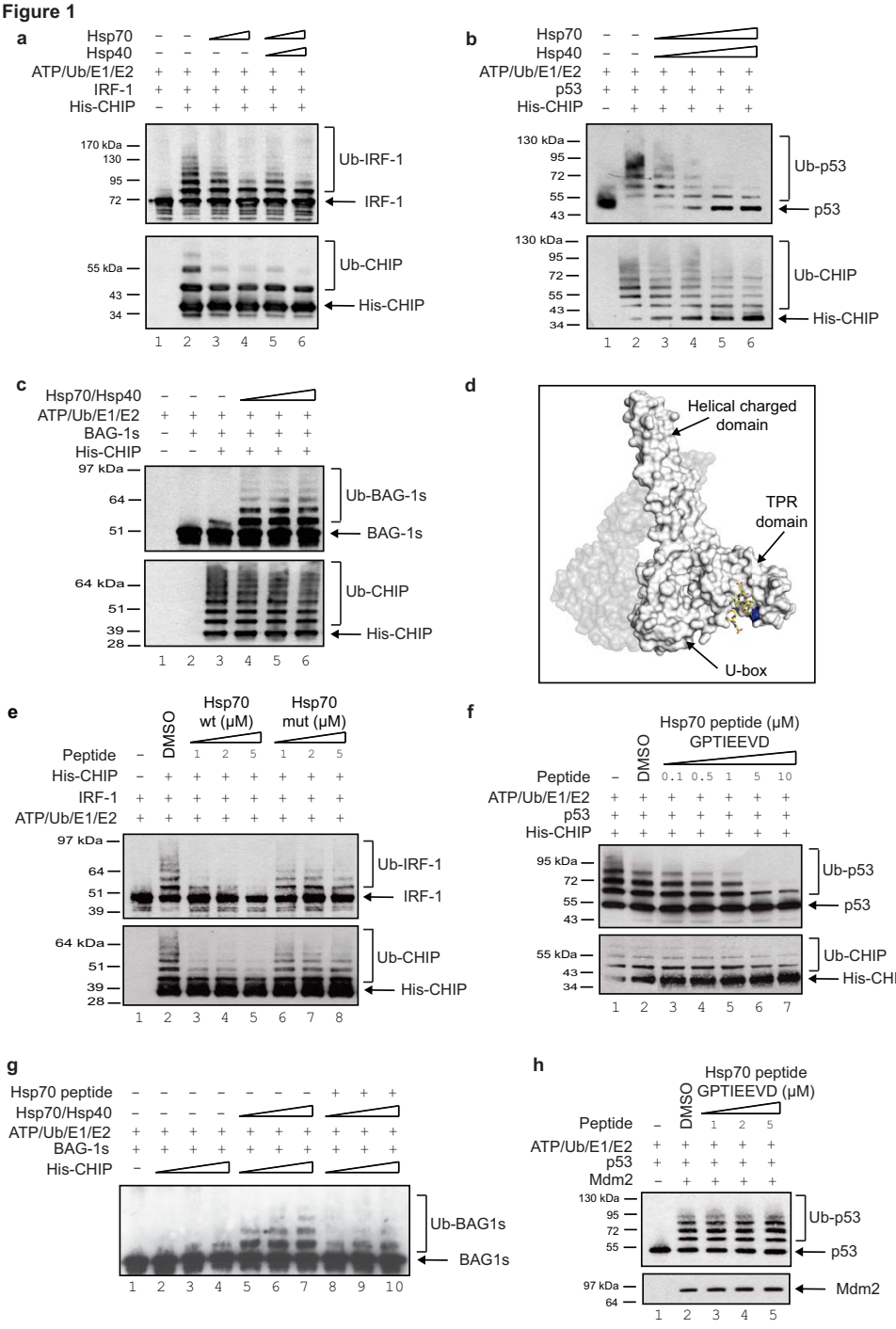
a
Hsp70
Hsp40
ATP/Ub/E1/E2
IRF-1
His-CHIP
170 kDa
130
95
72
Ub-IRF-1
IRF-1
55 kDa
43
34
Ub-CHIP
His-CHIP
1 2 3 4 5 6
b
Hsp70
Hsp40
ATP/Ub/E1/E2
p53
His-CHIP
130 kDa
95
72
55
43
Ub-p53
p53
130 kDa
95
72
55
43
34
Ub-CHIP
His-CHIP
1 2 3 4 5 6
c
Hsp70/Hsp40
ATP/Ub/E1/E2
BAG-1s
His-CHIP
97 kDa
64
51
Ub-BAG-1s
BAG-1s
64 kDa
51
39
28
Ub-CHIP
His-CHIP
1 2 3 4 5 6
d
Helical charged domain
TPR domain
U-box
e
DMSO
Hsp70 wt (μM)
Hsp70 mut (μM)
1 2 5 1 2 5
Peptide
His-CHIP
IRF-1
ATP/Ub/E1/E2
97 kDa
64
51
39
Ub-IRF-1
IRF-1
64 kDa
51
39
28
Ub-CHIP
His-CHIP
1 2 3 4 5 6 7 8
f
Hsp70 peptide (μM) GPTIEEVD
DMSO
0.1 0.5 1 5 10
Peptide
ATP/Ub/E1/E2
p53
His-CHIP
95 kDa
72
55
43
Ub-p53
p53
55 kDa
43
34
Ub-CHIP
His-CHIP
1 2 3 4 5 6 7
g
Hsp70 peptide
Hsp70/Hsp40
ATP/Ub/E1/E2
BAG-1s
His-CHIP
Ub-BAG1s
BAG1s
1 2 3 4 5 6 7 8 9 10
h
Hsp70 peptide GPTIEEVD (μM)
DMSO
1 2 5
Peptide
ATP/Ub/E1/E2
p53
Mdm2
130 kDa
95
72
55
Ub-p53
p53
97 kDa
64
Mdm2
1 2 3 4 5

Figure 2

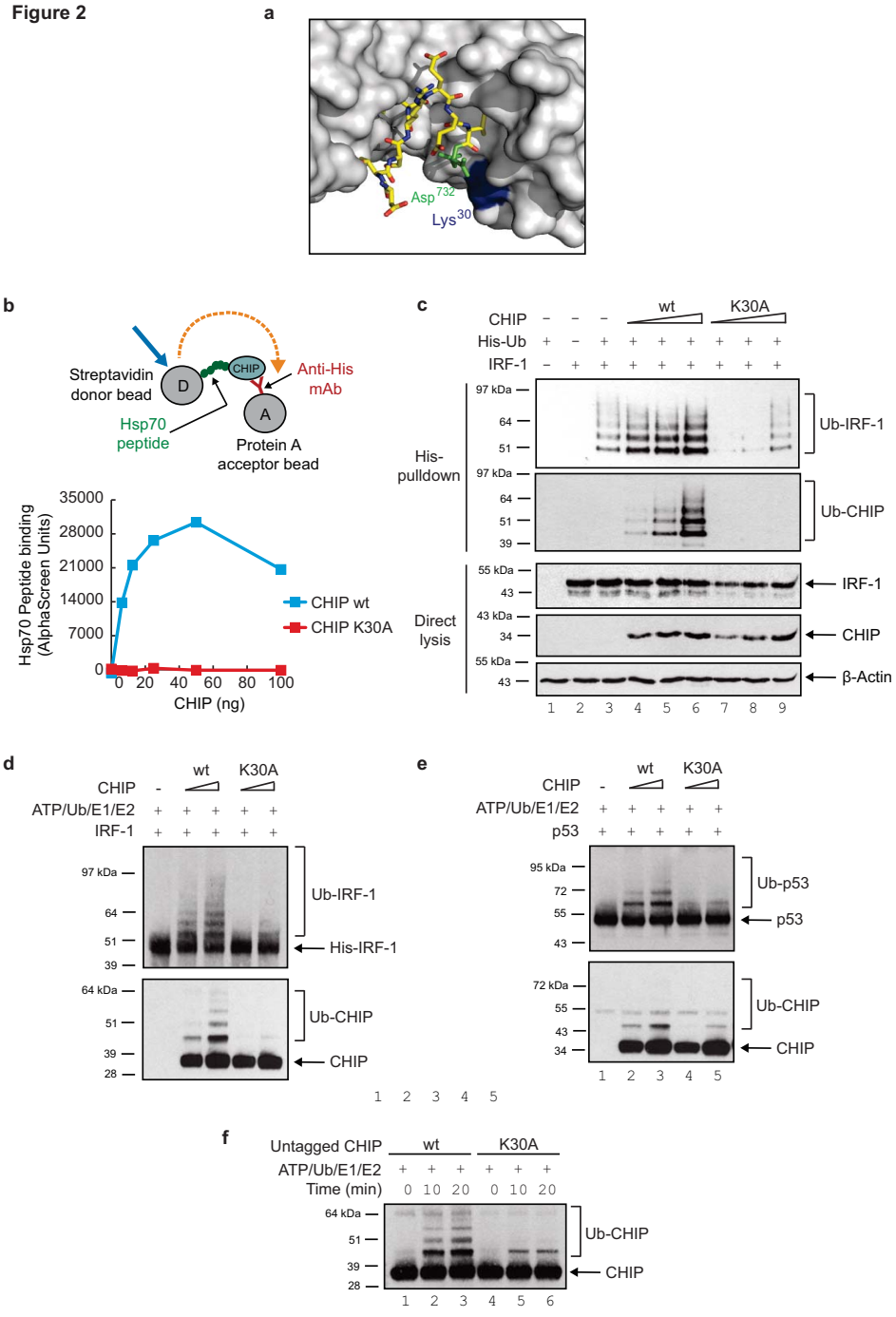
a
Asp732
Lys30
b
Streptavidin donor bead
CHIP
D
A
Anti-His mAb
Hsp70 peptide
Protein A acceptor bead
Hsp70 Peptide binding (AlphaScreen Units)
35000
28000
21000
14000
7000
0
0 20 40 60 80 100
CHIP (ng)
CHIP wt
CHIP K30A
c
CHIP
His-Ub
IRF-1
wt
K30A
His-pulldown
Direct lysis
97 kDa
64
51
39
55 kDa
43
43 kDa
34
Ub-IRF-1
Ub-CHIP
IRF-1
CHIP
β-Actin
1 2 3 4 5 6 7 8 9
d
CHIP
ATP/Ub/E1/E2
IRF-1
wt
K30A
97 kDa
64
51
39
64 kDa
28
Ub-IRF-1
His-IRF-1
Ub-CHIP
CHIP
1 2 3 4 5
e
CHIP
ATP/Ub/E1/E2
p53
wt
K30A
95 kDa
72
55
43
34
Ub-p53
p53
Ub-CHIP
CHIP
1 2 3 4 5
f
Untagged CHIP
wt
K30A
ATP/Ub/E1/E2
Time (min)
0 10 20 0 10 20
64 kDa
51
39
28
Ub-CHIP
CHIP
1 2 3 4 5 6

Figure 3

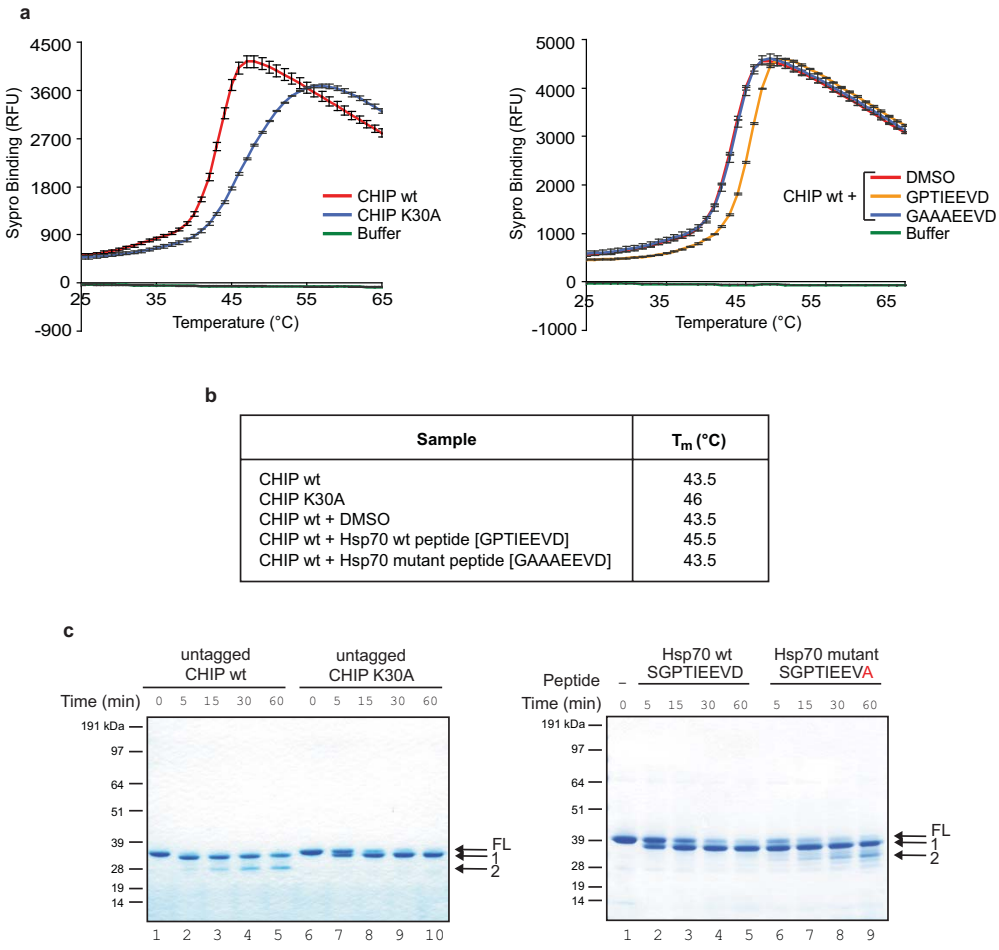

b

Sample	T_m (°C)
CHIP wt	43.5
CHIP K30A	46
CHIP wt + DMSO	43.5
CHIP wt + Hsp70 wt peptide [GPTIEEVD]	45.5
CHIP wt + Hsp70 mutant peptide [GAAAEEVD]	43.5

Figure 4

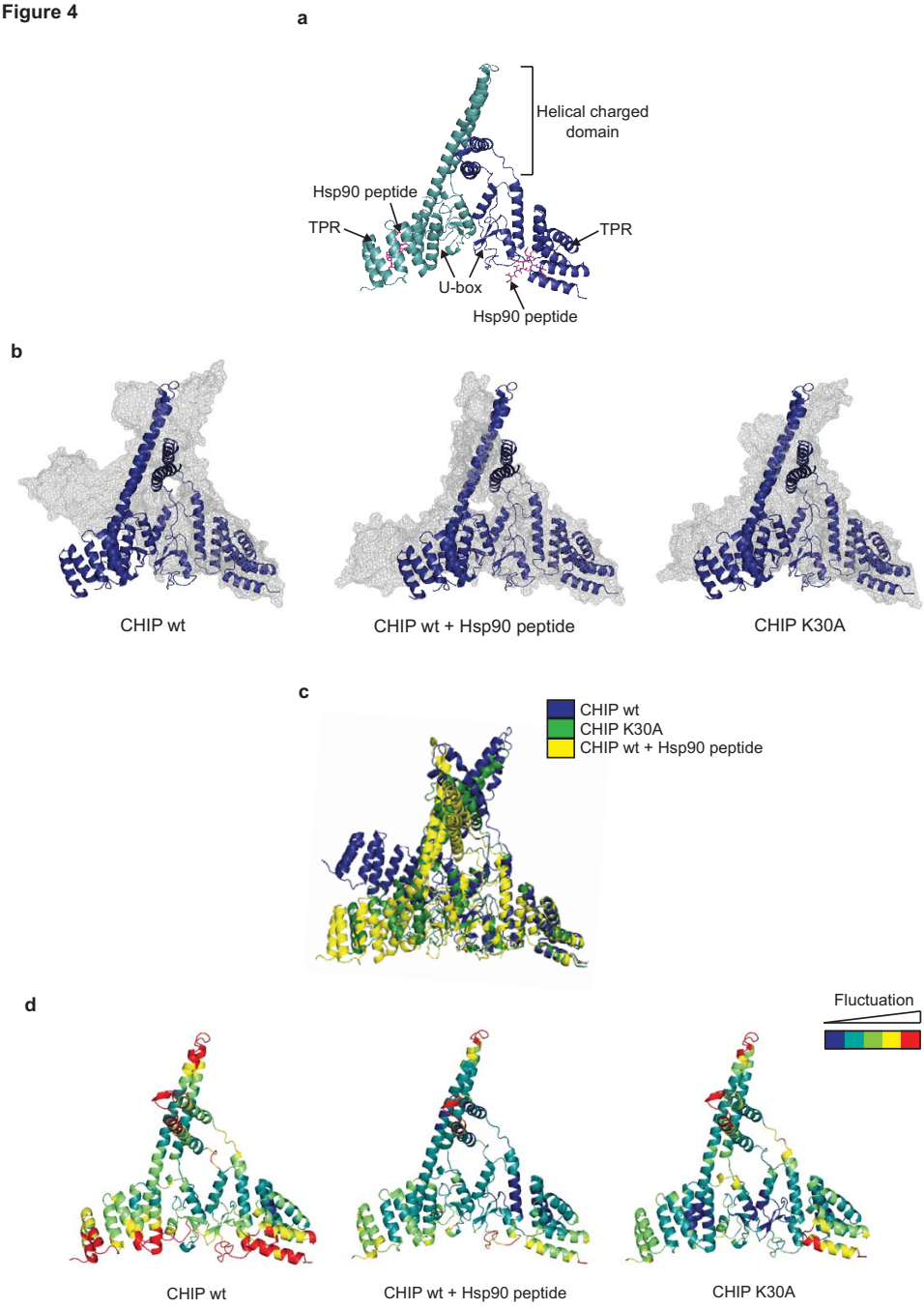
a
Helical charged domain
Hsp90 peptide
TPR
TPR
U-box
Hsp90 peptide
b
CHIP wt
CHIP wt + Hsp90 peptide
CHIP K30A
c
CHIP wt
CHIP K30A
CHIP wt + Hsp90 peptide
d
Fluctuation
CHIP wt
CHIP wt + Hsp90 peptide
CHIP K30A

Figure 5

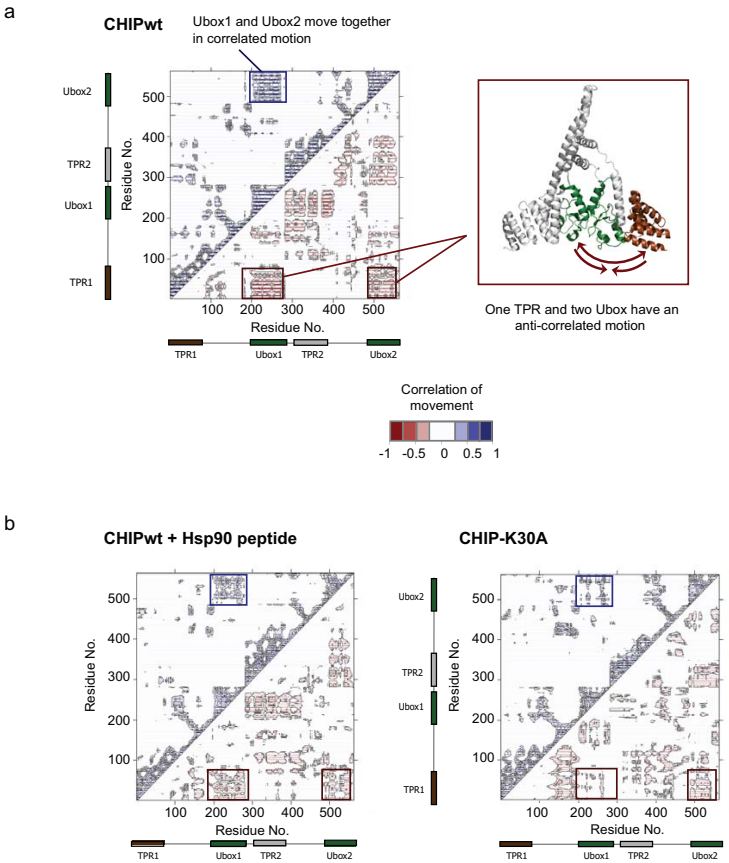
a
CHIPwt
Ubox1 and Ubox2 move together in correlated motion
Ubox2
TPR2
Ubox1
TPR1
Residue No.
100 200 300 400 500
One TPR and two Ubox have an anti-correlated motion
Correlation of movement
-1 -0.5 0 0.5 1
b
CHIPwt + Hsp90 peptide
CHIP-K30A

Figure 6

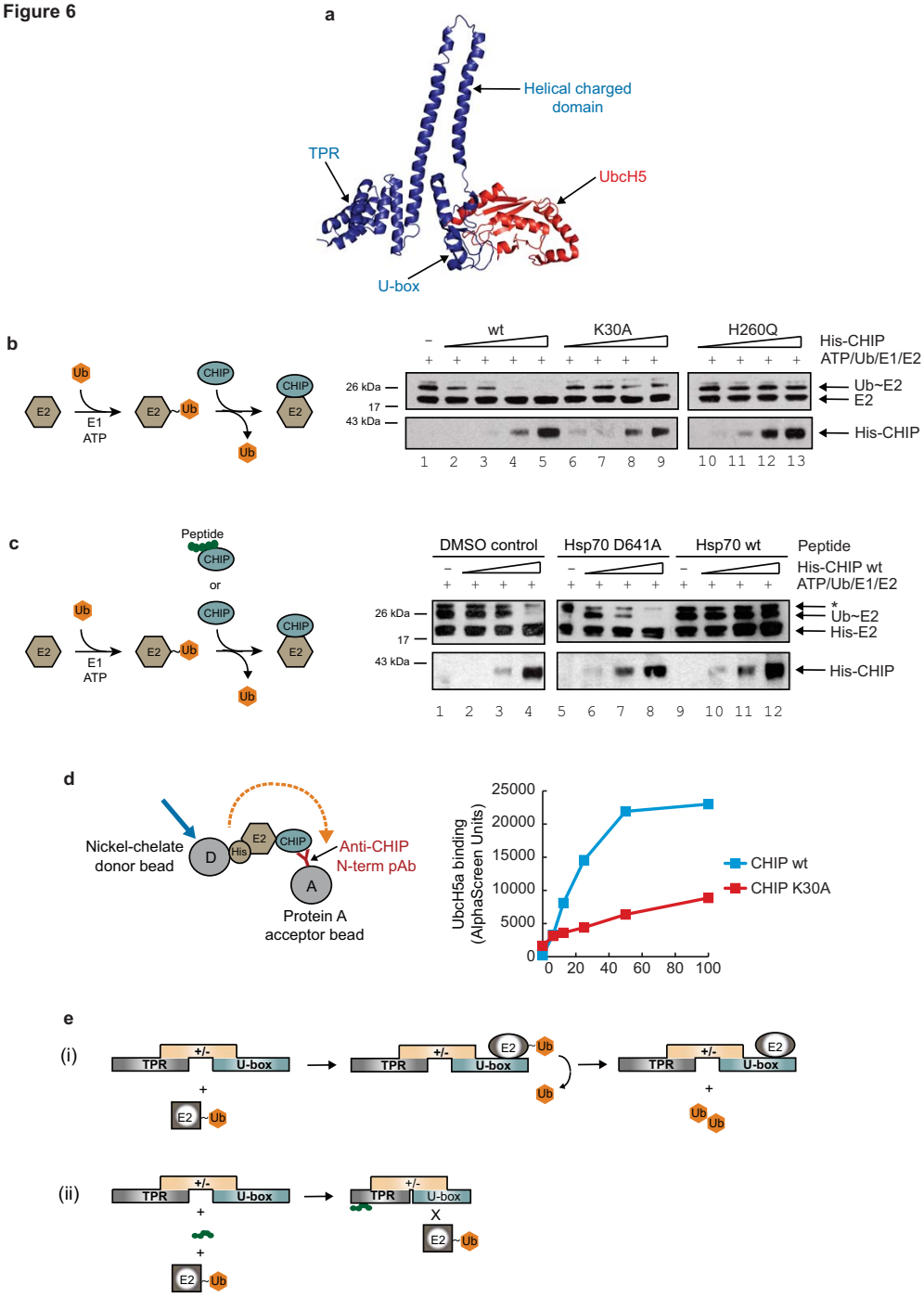
a
Helical charged domain
TPR
UbcH5
U-box
b
Ub
E2
E1
ATP
CHIP
wt
K30A
H260Q
His-CHIP
ATP/Ub/E1/E2
26 kDa
17
43 kDa
Ub~E2
E2
His-CHIP
1 2 3 4 5 6 7 8 9 10 11 12 13
c
Peptide
or
DMSO control
Hsp70 D641A
Hsp70 wt
His-CHIP wt
*
Ub~E2
His-E2
1 2 3 4 5 6 7 8 9 10 11 12
d
Nickel-chelate donor bead
D
His
Anti-CHIP N-term pAb
A
Protein A acceptor bead
UbcH5a binding (AlphaScreen Units)
25000
20000
15000
10000
5000
0
0 20 40 60 80 100
CHIP wt
CHIP K30A
e
(i)
(ii)
TPR
+/-
U-box
X

Figure 7

a

	Protein	Uniprot	No.TPR	Protein evidence	Function/Enzymatic activity	Hsp90
	CHIP	Q9UNE7	3	YES	E3 ubiquitin-ligase	YES
1	SGTA-beta	Q96EQ0	4	YES	co-chaperone	YES
2	SGTA-alpha	O43765	3	YES	co-chaperone	YES
3	PPP5C	P53041	3	YES	serine/threonine phosphatase	YES
4	TTC12	Q9H892	3	NO	not known	
5	UNC-45A	Q9H3U1	3	YES	co-chaperone	YES
6	RPAP3	Q9H6T3	7	YES	chaperone/scaffolding protein for RNA polymerase	YES
7	Cyp40	Q08752	3	YES	peptidyl-prolyl isomerase, co-chaperone	YES
8	TOMM34	Q15785	6	YES	import of preproteins into mitochondria	YES
9	SPAG1	Q07617	9	YES	GTPase activity	
10	TTC3	P53804	4	YES	E3 ubiquitin-ligase	
11	LONRF3	Q496Y0	4	YES	not known	
12	TTC31	Q49AM3	3	NO	not known	
13	UNC45B	Q8IWX7	3	NO	not known	
14	TTC28	Q96AY4	28	YES	not known	
15	HOP	P31948	9	YES	co-chaperone	YES
16	WDTC1	Q8N5D0	2	YES	associates with proteins of Ub-prot. system	
17	TOMM70A	O94826	10	YES	component of mitochondrial translocase complex	YES
18	TTC1	Q99614	3	YES	interacts with GAP-domain of NF1	
19	TANC1	Q9C0D5	3	YES	scaffold protein?	
20	Wisp39	Q9UIM3	3	YES	regulates p21 protein stability by binding to Hsp90	YES
21	FKBP51	Q13451	3	YES	peptidyl-prolyl isomerase, co-chaperone	YES
22	FKBP52	Q02790	3	YES	peptidyl-prolyl isomerase, co-chaperone	YES
23	OGT	O15294	13	YES	N-acetylglucosamine transferase	
24	TANC2	Q9HCD6	3	YES	not known	
25	CDC27 hom.	P30260	9	YES	E3 ubiquitin-ligase	

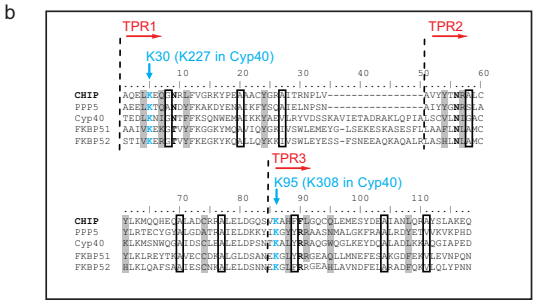

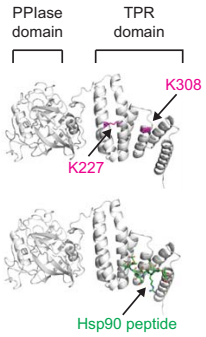

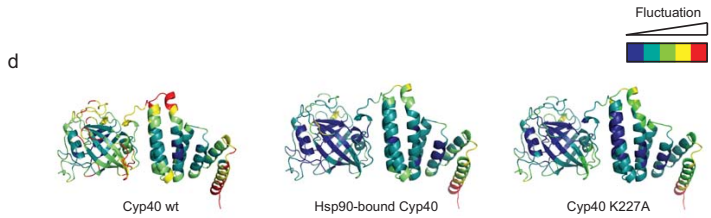

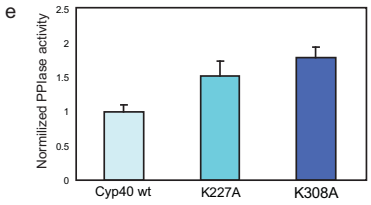

Appendix 1.3 Selected Publication: DNA-binding regulates site-specific ubiquitination of IRF-1

Biochem. J. (2013) **449**, 707–717 (Printed in Great Britain) doi:10.1042/BJ20121076

DNA-binding regulates site-specific ubiquitination of IRF-1

Vivien LANDRÉ*, Emmanuelle PION*[1], Vikram NARAYAN*, Dimitris P. XIRODIMAS† and Kathryn L. BALL*[2]

*Cell Signalling Unit, Edinburgh Cancer Research Centre, MRC Institute of Genetics and Molecular Medicine, University of Edinburgh, Crewe Rd South, Edinburgh EH4 2XR, U.K., and †Centre de Recherche de Biochimie Macromoléculaire, UMR 5237, CNRS, Montpellier, France

Understanding the determinants for site-specific ubiquitination by E3 ligase components of the ubiquitin machinery is proving to be a challenge. In the present study we investigate the role of an E3 ligase docking site (Mf2 domain) in an intrinsically disordered domain of IRF-1 [IFN (interferon) regulatory factor-1], a short-lived IFNγ-regulated transcription factor, in ubiquitination of the protein. Ubiquitin modification of full-length IRF-1 by E3 ligases such as CHIP [C-terminus of the Hsc (heat-shock cognate) 70-interacting protein] and MDM2 (murine double minute 2), which dock to the Mf2 domain, was specific for lysine residues found predominantly in loop structures that extend from the DNA-binding domain, whereas no modification was detected in the more conformationally flexible C-terminal half of the protein. The E3 docking site was not available when IRF-1 was in its DNA-bound conformation and cognate DNA-binding sequences strongly suppressed ubiquitination, highlighting a strict relationship between ligase binding and site-specific modification at residues in the DNA-binding domain. Hyperubiquitination of a non-DNA-binding mutant supports a mechanism where an active DNA-bound pool of IRF-1 is protected from polyubiquitination and degradation.

Key words: C-terminus of the heat-shock cognate 70-interacting protein (CHIP), DNA binding, interferon regulatory factor 1 (IRF-1), murine double minute 2 (MDM2), transcription, ubiquitination.

INTRODUCTION

Protein ubiquitination was first described as part of the proteasomal degradation pathway and has since been shown to play a major role in regulating a wide range of cellular pathways. Cell-cycle progression, DNA damage and repair, and transcription are all subject to fine control by the ubiquitin pathway. The ubiquitin transfer cascade comprises three enzymes, E1, E2 and E3. In the initial step, ubiquitin is activated by the E1 (ubiquitin-activating enzyme) and subsequently transferred to the E2 (ubiquitin-conjugating enzyme) which forms a complex with the E3 (ubiquitin ligase) and the substrate [1]. The main class of E3 ligases [RING including PHD (plant homeodomain) and U-box domain proteins] act by facilitating the transfer of ubiquitin from the E2 to one, or several, lysine residues in the substrate. The outcome of ubiquitination depends on the type of modification (mono- compared with poly-), the configuration of the chain linkages and the position of the modified residue in the primary amino acid sequence of the protein. The E3 is believed to determine substrate specificity and interplay between the E3 and E2 results in different chain linkages [2]. Ubiquitin contains seven lysine residues (Lys^6, Lys^{11}, Lys^{27}, Lys^{29}, Lys^{33}, Lys^{48} and Lys^{63}); any one of these lysine residues, in addition to the N-terminal methionine residue, can be connected to another ubiquitin molecule resulting in the formation of di- or poly-ubiquitin chains with a variety of different linkages [2,3]. Additionally, ubiquitin chains with mixed linkages and branches have been observed, adding to the overall complexity of the system [4]. While Lys^{48} chains are associated with protein degradation, Lys^{63} has roles in processes such as the response to stress, membrane trafficking and endocytosis. Lys^{11} signals proteasomal degradation and can alter subcellular localization, cell division and protein activity [5]. Although progress is being made on understanding the cellular roles of linkage-specific ubiquitination, the mechanisms involved in ubiquitin transfer, and particularly the selection of specific ubiquitin-acceptor residues, remain elusive. In contrast with phosphorylation, where specific peptide motifs are known to serve as phosphorylation signals for different kinases, no such definite sequence motifs have been identified for E3 ligases and prediction of lysine residues that are subject to modification remains difficult [6].

IRF-1 [IFN (interferon) regulatory factor-1] is an IFN-regulated transcription factor and a key effector of IFNγ-activated changes in gene expression. IRF-1 has a strong link to human health with loss of function leading to the development of some cancers [7,8], whereas its overexpression is associated with chronic autoimmune diseases [9–12]. Like many other transcription factors, IRF-1 is turned over very rapidly, with a half-life of approximately 20–30 min in cultured cells, and it is degraded via the ubiquitin–proteasome pathway [13,14]. We formerly reported that CHIP [C-terminus of the Hsc (heat-shock cognate) 70-interacting protein] binds to a central intrinsically disordered domain (Mf2 domain) of IRF-1 and mediates its ubiquitination under certain stress conditions [15]. This led us to ask (i) whether ligase docking plays a role in selecting lysine residues for modification, and (ii) what would be the outcome if the E3 could no longer dock to the Mf2 domain. We report in the present paper that IRF-1 ubiquitination by CHIP is proximal to its binding site and that only selected lysine residues in the structured DBD (DNA-binding domain) of IRF-1 were able to act as ubiquitin-acceptor sites. We characterize MDM2 (murine double minute 2) as a second Mf2-domain-binding ligase and show that it also mediates DBD

Abbreviations used: CHIP, C-terminus of the Hsc (heat-shock cognate) 70-interacting protein; DBD, DNA-binding domain; DTT, dithiothreitol; EMSA, electrophoretic mobility-shift assay; GST, glutathione transferase; IFN, interferon; IRF-1, IFN regulatory factor-1; mAb, monoclonal antibody; MDM2, murine double minute 2; MS/MS, tandem MS; Ni-NTA, Ni^{2+}-nitrilotriacetate; NP40, Nonidet P40; pAb, polyclonal antibody; TA, transcriptional activator; TRAIL, TNF (tumour-necrosis-factor)-related apoptosis-inducing ligand; WT, wild-type.

[1] Present address: Centre de Recherche de Biochimie Macromoléculaire, UMR 5237, CNRS, Montpellier, France.
[2] To whom correspondence should be addressed (email Kathryn.Ball@igmm.ed.ac.uk).

ubiquitination. In addition, we show that IRF-1 is only available for E3 docking and ubiquitination when in a DNA-unbound state, leading us to propose a mechanism by which IRF-1 degradation is partly controlled by its ability to bind DNA.

MATERIALS AND METHODS

Cell culture, transfection, FLAG pull-down, half-life and immunoblotting

HCT-116 cells were maintained in McCoy's medium (Invitrogen). Medium was supplemented with 5 % (v/v) FBS (fetal bovine serum; Biosera) and 1 % (v/v) penicillin/streptomycin (Invitrogen), and cells were grown at 37 °C with 5 % CO_2. At 80 % confluence, cells were transfected using Attractene (Invitrogen) following the manufacturer's instructions. FLAG pull-down and half-life determination was carried out as described previously [13,16]. Immunoblotting was performed as described previously [17].

Reagents, plasmids and protein preparation

The antibodies used were anti-IRF-1 mAb (monoclonal antibody) (BD Biosciences) and anti-IRF-1 C20 pAb (polyclonal antibody) (Santa Cruz Biotechnology), DO1 mAb (anti-p53; Moravian Biotechnology), anti-FLAG M2 mAb (Sigma), 4B2 mAb (anti-MDM2) and anti-CHIP 3.1 (a gift from Dr Borek Vojtesek, Masaryk Memorial Cancer Institute, Brno, Czech Republic). Secondary antibodies were purchased from Dako. Antibodies were used at the concentrations indicated by the supplier and at 1 μg/ml for DO1 and anti-CHIP. pDEST15-IRF-1 [GST (glutathione transferase)–IRF-1] mutants were constructed using a QuikChange® site-directed mutagenesis kit (Stratagene) with primers designed for a codon change from tryptophan to arginine or lysine to arginine (Sigma). GST–IRF-1 and GST–MDM2 were purified using glutathione–Sepharose (GE Healthcare) following the manufacturer's instructions. The GST tag was cleaved off MDM2 using Prescission Protease (GE Healthcare) following the manufacturer's instructions. His–CHIP, His–UbcH5 and His–SET (pET-26b-SET was from J. Libermann and T. Tuschi via Addgene [18]) were purified using Ni-NTA (Ni^{2+}-nitrilotriacetate) agarose (Qiagen) following the manufacturer's instructions. Kap-1 was purified as described previously [16] (pGEX-4T1-Kap-1 was a gift from Dr A. Ivanov, West Virginia University, Morgantown, West Virginia, U.S.A. [19]). Untagged p53 purified from insect cells was a gift from Dr Jennifer Fraser and Professor Ted Hupp (both from the University of Edinburgh, Edinburgh, Scotland, U.K.).

Ubiquitination assay

In vitro ubiquitination assays were performed as described previously [20] using 25 ng of substrate [GST–IRF-1^{WT}, GST–IRF-1^{W11R} or p53 as indicated; WT is wild-type] and His–CHIP or MDM2 as indicated. Reactions were incubated at 30 °C for 15 min unless otherwise indicated. The reactions were terminated by the addition of SDS sample buffer and analysed on a 4–12 % NuPAGE gel in a Mops buffer system (Invitrogen) followed by immunoblotting.

In vivo ubiquitination assays were carried out as described previously [20]. Briefly, HCT-116 cells were transfected with the indicated amounts of His–ubiquitin, IRF-1 and MDM2 or CHIP and treated with 50 μM MG-132 for 4 h. Cells were harvested and 20 % was lysed directly in 0.1 % NP40 (Nonidet P40) lysis buffer [25 mM Hepes (pH 7.5), 0.1 % NP40, 150 mM KCl, 5 mM DTT (dithiothreitol), 50 mM NaF and protease inhibitor mix] and separated by PAGE (12 % gel) followed by immunoblot analysis; for the remaining cells, His–ubiquitin conjugates were isolated using Ni-NTA agarose as described previously [20].

EMSA (electrophoretic mobility-shift assay) and ELISA

EMSAs were carried out as described previously [21]. Briefly, 100–300 ng of GST–IRF-1^{WT} or GST–IRF-1^{W11R} was incubated with either 40 ng of ^{32}P-labelled C1 probe [21], the ISRE (IFN-stimulated response element) sequences from the promoter sequences of caspase 8 [22], ISG-15 [23], ISG-20 [24], TRAIL [TNF (tumour-necrosis-factor)-related apoptosis-inducing ligand] [25] or an oligonucleotide from the p53-binding site on the 21 promoter [26] in EMSA buffer [20 mM Hepes (pH 7.5), 50 mM KCl, 5 % glycerol, 0.4 mM DTT, 0.1 mg/ml BSA, 0.5 % Triton X-100, 0.125 mg/ml poly(dI-dC) and 0.04 mg/ml salmon sperm DNA] for 30 min at room temperature (24 °C). After the addition of 6× loading buffer samples were analysed by PAGE (5 % gel) and radiolabelled bands were detected using a Storm840 phosphoimager (GE Healthcare).

Protein-binding assays (ELISAs) detecting protein–protein or protein–peptide binding were carried out as described previously [15].

MS analysis

Samples were analysed by 4–12 % gradient SDS/PAGE. The gel track was excised and divided into approximately 15 sections. Each section was cut into 1 mm cubes. These were then subjected to in-gel digestion using trypsin; samples were loaded on to a C18 column in 0.05 % TFA (trifluoroacetic). Peptides were eluted using acetonitrile in formic acid (2 % acetonitrile in 0.01 % formic acid to 90 % acetonitrile in 0.08 % formic acid). The eluate was sprayed on to an Ultimate 3000 nLC (Dionex) column coupled to a LTQ Orbitrap XL (Thermo Scientific) and the Top 5 Method was used: FT (Fourier transform)-MS plus five IT (ion trap)-MS/MS (tandem MS) (95 min acquisition). Orbitrap XL RAW data files were extracted with Raw2MSM (Version 1.7.2007.04.11) to generate a Mascot generic file (.msm). Extracted data was searched against the IPI (International Protein Index) human database (date 20100502) using the Mascot search engine (version 2.2). The following parameters were used: type of search, MS/MS ion search; enzyme, trypsin/P; fixed modifications, carbamidomethyl (C); variable modifications, acetyl (N-term), dioxidation (M), Gln→pyro-Glu (N-term Q), GlyGly (K), GlyGly (N-term), oxidation (M); mass values, monoisotopic; protein mass, unrestricted; peptide mass tolerance, $\pm$10 p.p.m. (#^{13}C = 2); fragment mass tolerance, $\pm$0.6 Da; and maximum missed cleavages, two. Hits with a Mascot score under ten were discarded. Two separate analyses, using different batches of CHIP-ubiquitinated IRF-1, were carried out in the proteomics facility in the College of Life Sciences, University of Dundee, Dundee, U.K.

Generation of models using HADDOCK

The 'Easy Interface' of the HADDOCK web server [27,28] was used to generate models of the IRF-1 DBD conjugated to ubiquitin. The C-terminal glycine residue of ubiquitin (Gly^{76}) was selected as the active residue on ubiquitin (structure obtained from PDB code 1UBQ, chain A [29]) and either Lys^{39}, Lys^{50}, Lys^{78} or Lys^{95} was chosen on the DBD as the active residue in the IRF-1 structure PDB code 1IF1, chain B. No passive residues

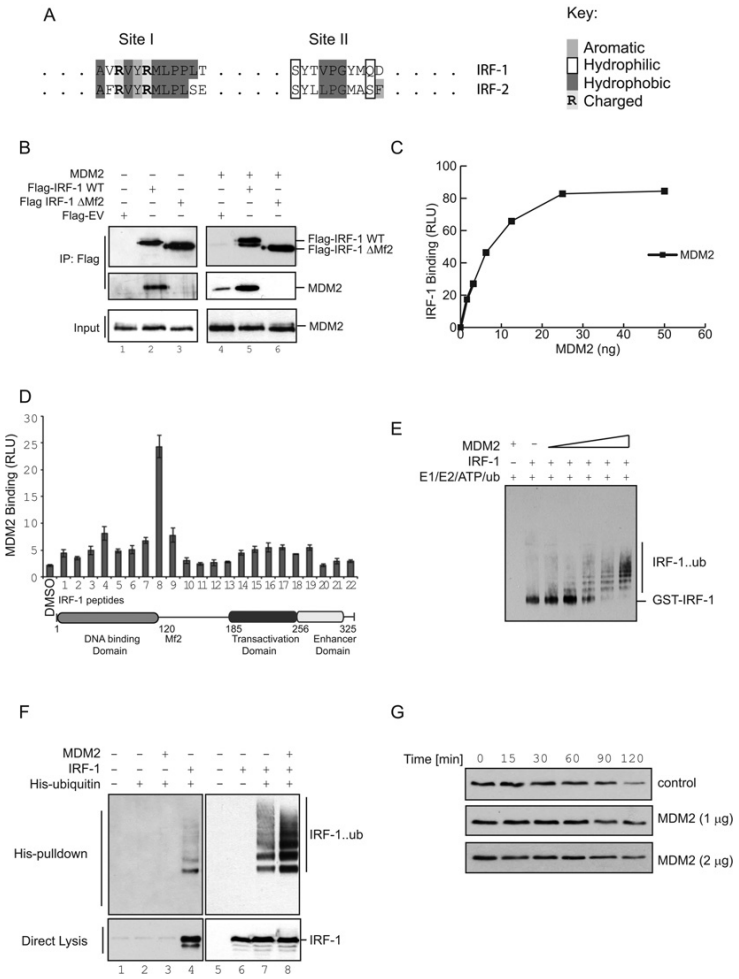

Figure 1 MDM2 can act as an E3 ligase for IRF-1 *in vitro* and in cells

(**A**) Alignment of the two MDM2-binding motifs on IRF-2 with the homologous regions from IRF-1. (**B**) HCT-116 cells were co-transfected with 2 μg of pcDNA3-MDM2 or pcDNA3-empty vector and 2 μg of FLAG–IRF-1^{WT}, IRF-1$^{\Delta M2}$ or empty vector. FLAG conjugates were immunoprecipitated using anti-FLAG-M2 agarose. After elution, samples and lysate (25 μg) were analysed by immunoblotting using an anti-MDM2 mAb and anti-FLAG mAb. (**C**) GST–IRF-1 (100 ng) was immobilized on a microtitre plate and incubated with a titration (0–100 ng) of MDM2. Protein binding was detected using an anti-MDM2 mAb and the protein amount against binding is expressed as relative light units (RLU). The results are representative of at least three independent experiments. (**D**) Biotin-tagged IRF-1 peptides (20 amino acids with a five amino acid overlap) were immobilized on a microtitre plate and incubated with 100 ng of MDM2. MDM2 binding to the peptides was detected using an anti-MDM2 mAb. The data are representative of three individual experiments. (**E**) An *in vitro* ubiquitination assay was carried out using GST–IRF-1 as the substrate and increasing amounts of MDM2 as the E3 ligase (0–160 ng) and incubated for 15 min. The samples were analysed using SDS/PAGE and immunoblotting with an anti-IRF-1 mAb. Results are representative of two separate experiments. (**F**) HCT-116 cells were co-transfected with pcDNA3-IRF-1 (0.5 μg), His–ubiquitin (0.5 μg) and pcDNA3-MDM2 (2 μg) as shown. Post-transfection (20 h), cells were treated with MG132 (50 μM) for 4 h and histidine-labelled ubiquitinated protein was isolated using Ni-NTA chromatography. Samples were analysed by SDS/PAGE and immunoblotting using an anti-IRF-1 mAb. Total amounts of IRF-1 in the sample (bottom panel) and modified IRF-1 (top panel) are shown. The results are representative of three individual experiments. (**G**) Immunoblot analysis of HCT-116 cells transfected with the indicated amounts of pcDNA3-MDM2 following cycloheximide (30 μg/ml) treatment. Cells were harvested at the times shown and analysed (60 μg/lane) by SDS/PAGE (10% gel) and immunoblotting. IRF-1 was detected using an anti-IRF-1 mAb. Results are representative of at least three separate experiments. IP, immunoprecipitation; ub, ubiquitin.

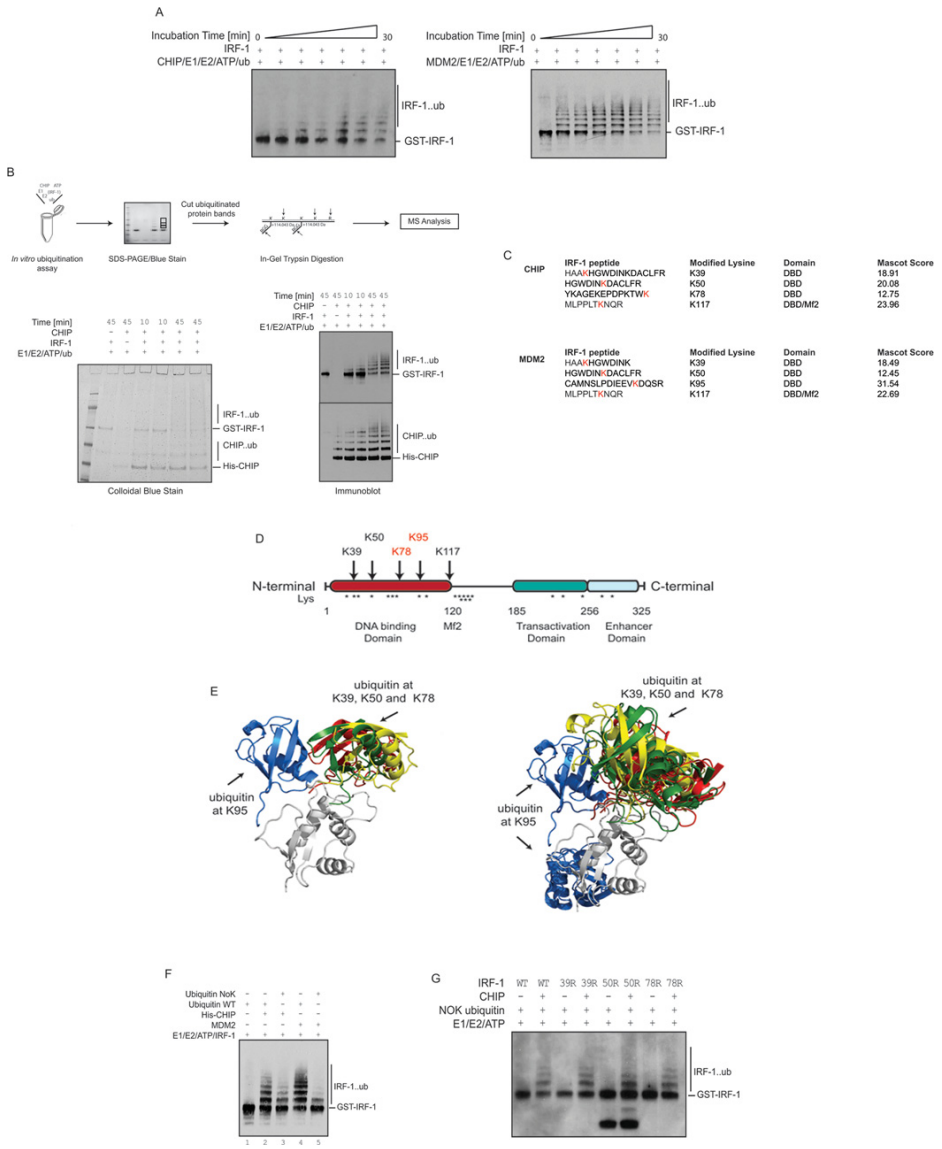

Figure 2 IRF-1 is ubiquitinated specifically in its DBD

(**A**) Time course (0–30 min) of an *in vitro* ubiquitination assay of IRF-1 modified by His–CHIP (50 ng) (left-hand panel) and MDM2 (80 ng) (right-hand panel). Results are representative of at least three separate experiments. (**B**) Schematic illustration of the procedure used to map the ubiquitination sites on IRF-1 by MS (top panel). GST–IRF-1 was ubiquitinated using an *in vitro* ubiquitination assay with CHIP as the E3 ligase and isolated from the reaction mix using glutathione beads. A Colloidal-Blue-stained gel before band excision for MS analysis (bottom left-hand panel)

were selected. The best four structures in the three clusters with the best HADDOCK score were analysed.

RESULTS

MDM2 can act as an E3 ligase for IRF-1 *in vitro* and in cells

CHIP, a U-box E3 ligase, docks to a multi-protein-binding interface in the intrinsically disordered Mf2 domain of IRF-1 and this interaction is required for efficient modification of IRF-1 by CHIP in cells [16]. Interestingly, a domain with homology with the Mf2 is involved in ubiquitination of IRF-2 (Figure 1A), a close relative of IRF-1, by the RING E3 ligase MDM2 [30], suggesting that the Mf2 may comprise a general docking site for IRF-1 and IRF-2 E3 ligases. Thus, in order to acquire additional E3 ligase tools to study the role of the Mf2 in ubiquitination, we determined whether MDM2 could act as a docking-dependent ligase for IRF-1.

We first overexpressed FLAG–IRF-1 in HCT-116 cells and asked whether MDM2 was detectable after isolation of IRF-1 complexes using a FLAG pull-down, and whether loss of the Mf2 domain affected binding. The results show that WT IRF-1 forms a complex containing MDM2 in cells (Figure 1B, lanes 2 and 5), whereas an IRF-1 Mf2 mutant (Δ106–140) is not associated with MDM2 (lanes 3 and 6). To establish whether MDM2 could bind directly to IRF-1 or whether other cellular factors were required for complex formation, protein interaction assays were carried out using purified components. GST–IRF-1 was immobilized on a microtitre plate and incubated with a titration of MDM2 in the mobile phase. Results of this assay showed that MDM2 bound to IRF-1 in a dose-dependent manner (Figure 1C). To identify the binding interface between MDM2 and IRF-1, a peptide–protein interaction assay was used. An overlapping IRF-1 peptide library (Supplementary Figure S1 at http://www.biochemj.org/bj/449/bj4490707add.htm) was immobilized and incubated with a constant amount of MDM2 in the mobile phase; binding was then detected using an anti-MDM2 antibody. MDM2 bound to an IRF-1 peptide from within the Mf2 domain (peptide 8, VRVYRMLPPLTKNQRKERKS; Figure 1D) with homology with the MDM2-binding site-I of IRF-2 (Figure 1A).

Whether formation of MDM2–IRF-1-containing complexes was sufficient to signal IRF-1 ubiquitination was determined using *in vitro* and cell-based approaches. Using a minimal ubiquitination assay employing only purified components, we established that IRF-1 could act as a substrate for MDM2 and that there was a positive correlation between the efficiency of IRF-1 ubiquitination and the concentration of MDM2 added to the assay (Figure 1E). In-cell ubiquitination assays using His–ubiquitin, IRF-1 and MDM2 (Figure 1F) were assembled in HCT-116 cells. After isolation and analysis of His-ubiquitinated proteins, an increase in the amount of ubiquitinated IRF-1 was seen in the presence of MDM2 (Figure 1F; compare lane 7 with lane 8). It should be noted that ubiquitination of IRF-1 seen in lane 7 (Figure 1F) is mediated by endogenous E3-ligase activity. To determine whether ubiquitination of IRF-1 by MDM2 had an effect on its half-life, HCT-116 cells were transfected with MDM2 and treated with the protein synthesis inhibitor cycloheximide. The loss of IRF-1 protein was then monitored over time by immunoblot analysis (Figure 1G). The results show that MDM2 overexpression did not lead to a decrease in the half-life of IRF-1, rather it gave a slight, but reproducible, increase in its half-life. This is in agreement with the idea that MDM2 is a monoubiquitin ligase that can only polyubiquitinate its substrates under specific conditions or in the presence of an E4 ligase [31]; it also suggests that MDM2 may be involved in the regulation of IRF-1 activity rather than its rate of degradation.

Mf2 docking directs DBD ubiquitination by CHIP and MDM2

In order to investigate whether binding of E3 ligases to the Mf2 domain facilitates ubiquitination at specific lysine residues, IRF-1 ubiquitin-acceptor sites modified in the presence of either CHIP or MDM2 were determined using MS. First, optimal conditions for IRF-1 ubiquitination were established by performing a time course of ubiquitination *in vitro* over 30 min with either CHIP (Figure 2A, left-hand panel) or MDM2 (right-hand panel). For identification of ubiquitination sites by MS, IRF-1 was ubiquitinated for either 10 or 45 min and discrete ubiquitinated intermediates were excised and subjected to in-gel digestion using trypsin (Figure 2B). Ubiquitin-modified residues are protected from trypsin cleavage, resulting in a distinct cleavage pattern for the ubiquitinated protein. Furthermore, ubiquitin that is attached to the protein is cleaved off at a C-terminal arginine residue leaving a di-glycine peptide remnant that adds 114.043 Da to the ubiquitinated peptide. The modified cleavage pattern, together with the mass additions, facilitate identification, by MS, of peptides that have been ubiquitinated (Figure 2B).

Although there are a total of 23 lysine residues in the primary amino acid sequence of IRF-1, only a subset of those were detected by MS as being ubiquitin-acceptor sites for the Mf2-binding ligases CHIP or MDM2 (Figures 2C and 2D). Strikingly, IRF-1 was predominantly ubiquitinated in, or adjacent to, the DBD and no modified residues from within the C-terminal half of the protein were detected with either of the E3 ligases. Although both MDM2 and CHIP modified Lys^{39}, Lys^{50} and Lys^{117}, in the two independent analyses of CHIP-ubiquitinated IRF-1 Lys^{95} modification was not detected, whereas this residue was modified when MDM2 provided the E3 activity. Similarly, Lys^{78} was detected only in the CHIP-ubiquitinated samples. Although this difference in specificity remains to be confirmed using a second analytical technique, the existing data suggest that although Mf2-directed ubiquitination of IRF-1 is specific for the DBD, there could be subtle differences in the exact residues targeted by MDM2 and CHIP.

and immunoblot analysis of the samples blotted for IRF-1 and CHIP (bottom right-hand panel) are shown. CHIP was co-purified from the reaction with IRF-1 as a result of IRF-1–CHIP protein interactions. Results are indicative of two separate experiments utilising CHIP and MDM2 as E3 ligases for the ubiquitination reaction. (**C**) Results of MS analysis of modified peptides in IRF-1. Lysine residues that were shown to be modified by ubiquitin are highlighted in red. (**D**) Modified lysine residues are indicated on a schematic IRF-1 domain structure. Lysine residues that are modified by only MDM2 or CHIP are shown in red, whereas residues that are modified by both are shown in black. (**E**) Model of ubiquitinated IRF-1. Ubiquitin was modelled on to the available crystal structure of the IRF-1 DBD (PDB code 1IF1) (white) using the HADDOCK web server at Lys^{39} (green), Lys^{50} (yellow), Lys^{78} (red) and Lys^{95} (blue), the structure that obtained the highest score for each site (left-hand panel) and the three structures obtaining the highest score in one of the three best clusters for each site (right-hand panel) are shown. (**F**) *In vitro* ubiquitination of IRF-1 with CHIP and MDM2 as E3 ligases and either WT or NoK ubiquitin (in which all lysine residues are mutated to arginine). Reactions with WT ubiquitin were incubated for 10 min, whereas the reactions with no E3 ligase and NoK ubiquitin were incubated for 60 min. The results are representative of two independent experiments. (**G**) *In vitro* ubiquitination assay with GST–IRF-1 containing the indicated mutation at one of the ubiquitin-acceptor lysine residues, NoK ubiquitin and CHIP as the E3 ligase; the reactions were incubated for 45 min. Immunoblots were probed with an anti-IRF-1 pAb. ub, ubiquitin.

Using the HADDOCK web server [27,28], a model of the ubiquitinated IRF-1 DBD was generated with ubiquitin docked to the ubiquitin-acceptor sites identified (only sites present in the crystal structure [32], amino acids 7–111 are shown; Figure 2E and Supplementary Figure S2 at http://www.biochemj.org/bj/449/bj4490707add.htm). Interestingly, modelling suggests that modification at three of the five ubiquitination sites identified (Lys^{39}, Lys^{50} and Lys^{78}) would result in ubiquitin occupying an overlapping three-dimensional space. Thus ubiquitination at any one of these three sites could potentially block ubiquitination at the other two sites. In order to investigate this model experimentally *in vitro* ubiquitination assays, using either WT ubiquitin or an ubiquitin mutant in which all of the lysine residues were mutated to arginine (NoK ubiquitin), were used. For the majority of E3 ligases NoK ubiquitin can only result in the formation of monoubiquitinated residues as chain elongation is not possible (linear ubiquitin chain formation by SHARPIN [33] is an exception to this). We found that the ubiquitin mutant was, in general, a poor substrate for *in vitro* ubiquitination with slower conversion of IRF-1 into its monoubiquitinated form than is seen in the presence of WT ubiquitin. However, when assay conditions were adapted to facilitate ubiquitination we saw that monoubiquitination provided a maximum of three ubiquitins added per IRF-1 molecule, and in the case of MDM2 a single ubiquitinated form was predominant (Figure 3E, bottom panel; compare lanes 3 and 5 with lanes 2 and 4), suggesting that a maximum of three out of the five ubiquitin-acceptor sites identified can be modified at any one time.

If the modelling is correct we would predict that mutation of Lys^{39}, Lys^{50} and Lys^{78} individually would not be sufficient to affect IRF-1 DBD monoubiquitination. Therefore to complement the above approach a series of IRF-1 point mutant proteins was generated in which Lys^{39}, Lys^{50} and Lys^{78} were individually mutated to arginine. When the mutant proteins were used as substrates for CHIP in the presence of NoK ubiquitin, loss of Lys^{39} and Lys^{78} did not produce qualitative or quantitative changes in monoubiquitination of IRF-1, consistent with the idea that ubiquitination at either one of these residues produces a similar outcome and that ubiquitination at these two sites is mutually exclusive. Although mutation of Lys^{50} did have an effect on monoubiquitination, with loss of the slowest migrating ubiquitinated form of IRF-1, this mutant was susceptible to cleavage during expression and the cleavage product was also a substrate for CHIP, making the data difficult to interpret. Unfortunately, we were not able to test the modelling data using double and triple mutants as the introduction of multiple lysine point mutations produced proteins that were extremely susceptible to cleavage during expression.

Taken as a whole, the data in this section support the modelling data and suggest that ubiquitination of Lys^{39} and Lys^{78}, and potentially Lys^{50}, are mutually exclusive and might therefore result in the generation of a very similar 'molecular signature'.

DNA-bound IRF-1 is protected from ubiquitination *in vitro*

When the ubiquitin-modified residues were mapped on to the available IRF-1 DBD crystal structure, we found that Lys^{39}, Lys^{50} and Lys^{95} were located in exposed loops (L1, L2 and L3), whereas Lys^{78} was positioned within the α3-helix which forms the second helix of the HTH (helix–turn–helix) homologous motif (Figure 3A). As the ubiquitin-acceptor sites are all located within the DBD, with Lys^{78} and Lys^{95} being at the DNA-binding interface (Figure 3A), we reasoned that modification may be affected by the sequence-specific DNA-binding activity of IRF-1. To test this, IRF-1 was pre-incubated with a consensus site DNA oligonucleotide (C1), which we show can bind to GST–IRF-1^{WT} (Figure 3B, lanes 3–5), but not a DNA-binding mutant, IRF-1^{W11R} (lanes 6–9), in an EMSA and is supershifted by an anti-IRF-1 mAb. A control oligonucleotide that does not interact with IRF-1 (p21c) was used as a negative control (Figure 3B, lanes 7–10). Whereas control DNA (p21c) had no significant effect on the ubiquitination of IRF-1 by CHIP (Figure 3C, left-hand panel) or MDM2 (right-hand panel), addition of IRF-1 consensus site DNA (C1) almost completely suppressed ubiquitination. To control for non-specific effects of DNA on IRF-1 we used a non-DNA-binding mutant (IRF-1^{W11R}; Figure 3B) and asked whether this was refractive to the effects of DNA. Figure 3(C) shows that whereas C1 oligonucleotides inhibit the ubiquitination of wild-type IRF-1 (lanes 4 and 5) they had no significant effect on the ubiquitination of IRF-1^{W11R} (lanes 9 and 10). As an additional control we showed that C1 DNA did not affect CHIP activity directly as there was no effect on the ability of CHIP to mediate autoubiquitination (Figure 3C, bottom panel). Ubiquitination of p53, a second well-characterized substrate for both CHIP (Figure 3D, left-hand panel) and MDM2 (Figure 3D, right-hand panel), was not affected by p53 binding to DNA from the p21 promoter (p21c DNA), suggesting that protection of IRF-1 from ubiquitination by DNA is not a property of all transcription factors (Figure 3D).

To expand on the observation described above, which used an optimized IRF-1 consensus DNA oligonucleotide, a range of oligonucleotide probes based on naturally occurring binding elements from IRF-1 target gene promoters was examined. Elements from all of the IRF-1 target genes tested were able to inhibit CHIP- and MDM2-mediated ubiquitination and there was good agreement between the ability of IRF-1 to bind DNA in an EMSA (Figure 3E, bottom panel) and the ability of the oligonucleotide to inhibit ubiquitination of IRF-1 in an *in vitro* ubiquitination assay (Figure 3E, top panels). For example, IRF-1 binds only weakly to an oligonucleotide based on the *TRAIL* promoter and this probe is a weak inhibitor of IRF-1 ubiquitination (Figure 3E, bottom panel, lane 5).

IRF-1 bound to DNA is unable to associate with proteins that interact with its Mf2 domain

We reasoned that there were two possible mechanisms to explain the loss of IRF-1 ubiquitination when in its DNA-bound form; first the targeted lysine residues may be 'cryptic' and therefore inaccessible to the ligases, or secondly, the ability of IRF-1 to bind to CHIP or to MDM2 may be impaired. As the available structural data for the DBD of IRF-1 bound to its cognate DNA element [32] suggests that at least some of the required lysine residues are still available for ubiquitination (Figure 3A; for example Lys^{50}), we concentrated on the second option, i.e. a change in the affinity of IRF-1 for Mf2-binding proteins. To address the effects of IRF-1 DNA binding on its ability to interact with components of the ubiquitination system, we used protein-interaction assays to measure CHIP binding to IRF-1 protein that had been pre-incubated with either C1 oligonucleotide or control DNA (p21c). Initial titrations demonstrated binding of native unliganded IRF-1 in solution to immobilized CHIP in a dose-dependent manner (Figure 4A, left-hand panel). On the basis of this assay a fixed amount of CHIP was immobilized and incubated with a constant amount of IRF-1 that had been pre-incubated with a titration of either C1 or p21c. Figure 4(A) (right-hand panel) shows that whereas IRF-1 binding to CHIP was largely unaffected by p21c, titration of C1 into the assay inhibited CHIP binding. The

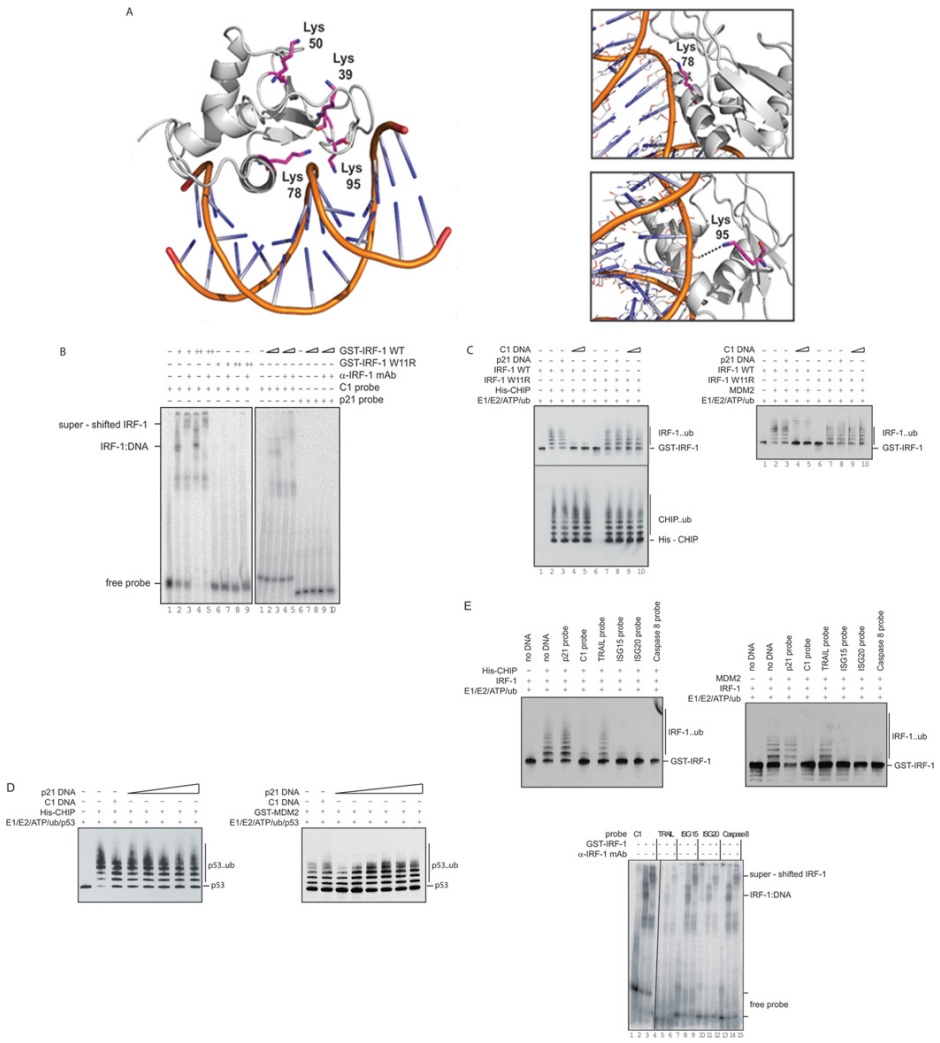

Figure 3 DNA-bound IRF-1 is protected from ubiquitination *in vitro*

(**A**) Crystal structure of the IRF-1 DBD (PDB code 1IF1) with lysine residues that were shown to be modified indicated by sticks. (**B**) EMSA showing binding of a titration (100 and 300 ng) of purified GST–IRF-1^{WT} or of the DNA-binding mutant GST–IRF-1^{W11R} to a ^{32}P-labelled DNA probe of C1 DNA (left-hand panel) or binding of GST-IRF-1^{WT} to the C1 probe compared with the non-binding control probe (p21c) (right-hand panel). When indicated an anti-IRF-1 mAb was added to the reaction to supershift the protein–DNA complex. (**C**) *In vitro* ubiquitination assay using GST–IRF-1^{WT} and GST–IRF-1^{W11R} as substrate with a titration of either C1 oligonucleotides or p21c DNA (0.25 and 1 μM) using CHIP (left-hand panel) or MDM2 (right-hand panel) as the E3 ligase. Results are representative of at least three separate experiments. (**D**) *In vitro* ubiquitination assay with p53 as the substrate and a titration of p21 promoter DNA (10 nm–1 μM) or C1 DNA (500 nM) with either CHIP (left-hand panel) or MDM2 (right-hand panel) as the E3 ligase. (**E**) The effects of oligonucleotides from promoters of different IRF-1-inducible genes (3 μM) were tested on the *in vitro* ubiquitination of IRF-1 by CHIP (top left-hand panel) and MDM2 (top right-hand panel) and compared with the ability of GST–IRF-1 (300 ng) to bind to the oligonucleotides in a band-shift assay (bottom panel). Where indicated, an anti-IRF-1 antibody was added to the reaction to supershift the complex. The results are representative of two independent experiments.

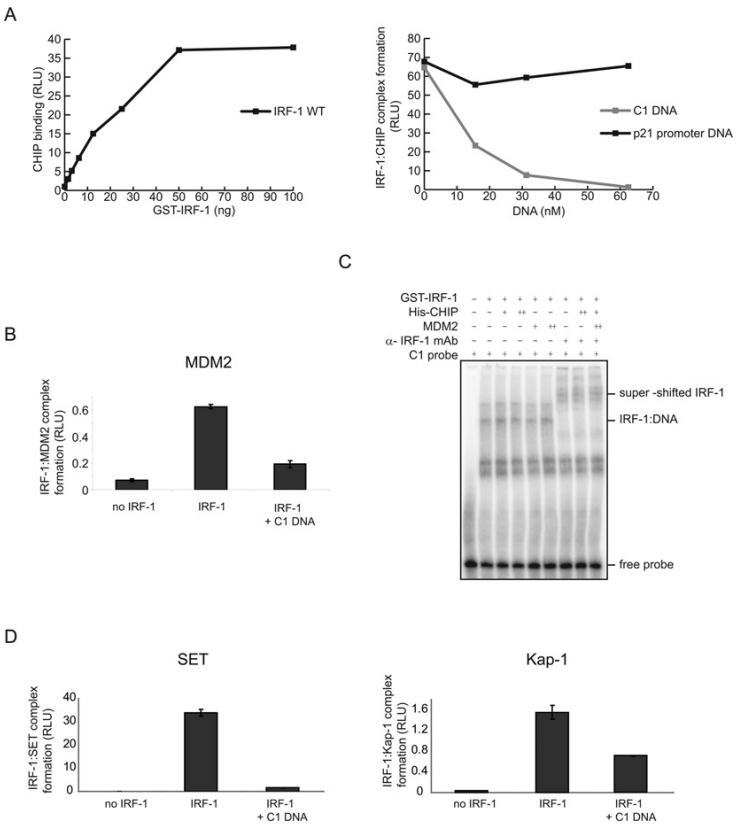

Figure 4 IRF-1 bound to DNA is unable to associate with proteins that interact with its Mf2 domain

(**A**) His–CHIP (100 ng) was immobilized on a microtitre plate and incubated with either a titration of purified GST–IRF-1 alone (0–100 ng) (left-hand panel) or with constant amounts of GST–IRF-1 (100 ng) and a titration of C1 DNA or p21c DNA (right-hand panel). Results are representative of at least three separate experiments. (**B**) MDM2 (100 ng) was immobilized on a microtitre plate and incubated with GST–IRF-1 (100 ng) and C1 or p21c DNA (100 nM). Binding was detected using an anti-IRF-1 mAb. The results are representative of two individual experiments. (**C**) EMSA presenting binding of 300 ng of purified GST–IRF-1^{WT} to a ^{32}P-labelled DNA probe of C1 DNA in the presence of 0.3 or 1.5 μg of purified His–CHIP or MDM2 as shown. When indicated an anti-IRF-1 mAb was added to the reaction to supershift the protein–DNA complex. (**D**) Different Mf2-domain-binding proteins, SET and Kap-1, were immobilized on a microtitre plate (100 ng) and incubated with GST–IRF-1 (100 ng) and C1 or p21c DNA (100 nM). Binding was detected using an anti-IRF-1 mAb. Results are representative of at least two separate experiments. RLU, relative light unit.

results of this assay suggest that stable binding of CHIP to IRF-1 is severely restricted when IRF-1 is in its DNA-bound form.

Similarly, when we tested binding of MDM2 to IRF-1 in its DNA-bound and -unbound form, MDM2 bound preferentially to the unbound form of IRF-1 (Figure 4B). To test whether CHIP and MDM2 binding had a reciprocal effect on DNA binding we examined whether the ligases could compete with DNA for binding to IRF-1 using an EMSA (Figure 4C). Neither CHIP nor MDM2 had any effect on the ability of IRF-1 to bind to DNA, suggesting that IRF-1 has a higher affinity for DNA than for the Mf2-binding protein. As we have shown that the Mf2 domain is a multi-protein-binding site that interacts with a number of other IRF-1 regulators, we also tested the effect of DNA binding on the interaction of IRF-1 with Kap-1 and SET [16]. Figure 4(D) shows reduced binding of IRF-1 to both Kap-1 and SET when in its DNA-bound state.

The crystal structure of the IRF-1 DBD in complex with its cognate promoter-binding element suggests that residues from within the Mf2 domain are not required for DNA binding [30], thus the results of the present study can be interpreted to suggest that access to the Mf2 interface is controlled through changes in the conformation of IRF-1 rather than through direct competition

for binding to DNA. However, as deletion of the Mf2 domain prevents IRF-1 from binding to DNA (Supplementary Figure S3 at http://www.biochemj.org/bj/449/bj4490707add.htm) we cannot completely rule out the possibility that residues from the Mf2 contribute to binding through a direct contact with the DNA.

In summary the experiments presented here suggest that Mf2-domain-binding partners are likely to function only on the unliganded form of the protein. Furthermore, the observation that neither MDM2 nor CHIP is able to ubiquitinate IRF-1 unless they are bound to the protein lends strong support for a direct relationship between E3-ligase binding, ubiquitination and site-specificity.

Ubiquitination of IRF-1 in cells is enhanced in a DNA-binding mutant

Taken together, the above observations led us to hypothesize that IRF-1 is 'protected' from ubiquitination, and therefore presumably from degradation, when it is in its transcriptionally active DNA-bound conformation. To lend support to this hypothesis, we determined whether a non-DNA-binding mutant of IRF-1 was more or less prone to ubiquitination than the wild-type protein. We first confirmed that specific DNA does not inhibit binding of CHIP to IRF-1^{W11R} *in vitro* using a protein–protein interaction assay. CHIP was coated on to a microtitre plate and incubated with IRF-1 and a titration of C1 DNA (Figure 5A). As expected, C1 DNA inhibited binding of IRF-1^{WT} to CHIP, whereas binding of CHIP to IRF-1^{W11R} was not affected by the presence of DNA. To ensure that the kinetics of ubiquitination of IRF-1^{WT} compared with IRF-1^{W11R} by CHIP was not significantly different, we performed *in vitro* ubiquitination assays with a titration of CHIP in the absence of any DNA. CHIP ubiquitinated both IRF-1^{WT} and IRF-1^{W11R} to a similar extent *in vitro* (Figure 5B). Next *in vivo* ubiquitination assays were carried out in HCT-116 cells using IRF-1^{WT} and IRF-1^{W11R}. When histidine-labelled ubiquitinated proteins were isolated from cells that had been transfected with either IRF-1^{WT} or IRF-1^{W11R} together with His–ubiquitin we found that the IRF-1^{W11R} mutant was hyperubiquitinated when compared with the WT protein (Figure 5C, compare lanes 3 and 4), supporting the idea that IRF-1 which is not associated with the chromatin is more 'available' for ubiquitination by endogenous Mf2-domain-interacting ligases. Thus although CHIP ubiquitinates IRF-1^{WT} and IRF-1^{W11R} to a similar extent *in vitro*, in cells the Trp^{11} mutant is preferentially ubiquitinated, supporting the concept that free IRF-1 may be turned over more rapidly than the pool of IRF-1 that is bound, or able to bind, to DNA.

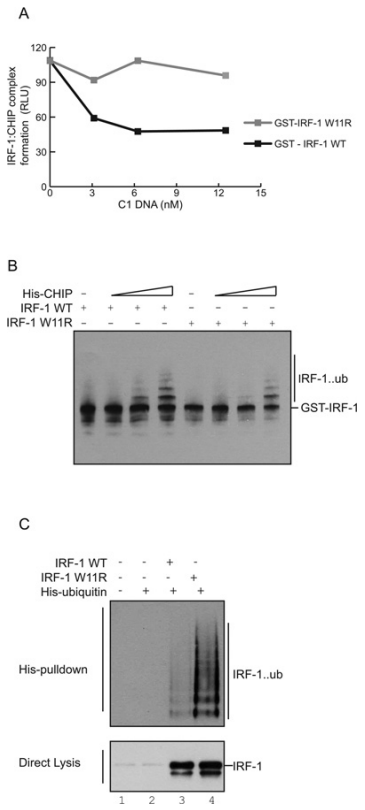

Figure 5 Ubiquitination of IRF-1 in cells is enhanced in a DNA-binding mutant

(**A**) His–CHIP (100 ng) was immobilized on a microtitre plate and incubated with constant amounts of either GST–IRF-1^{WT} or GST–IRF-1^{W11R} (100 ng) and a titration of C1 or p21c probe. The results are representative of four separate experiments. (**B**) *In vitro* ubiquitination assay using GST–IRF-1^{WT} or GST–IRF-1^{W11R} as substrate with a titration of His–CHIP (0–60 ng). Results are representative of three independent experiments. (**C**) HCT-116 cells were co-transfected with pcDNA3-IRF-1^{WT} or pcDNA3-IRF-1^{W11R} (0.5 μg) and His–ubiquitin (0.5 μg) as shown. At 20 h post-transfection cells were treated with MG132 (50 μM) for 4 h and histidine-labelled ubiquitinated protein was isolated using Ni-NTA chromatography and analysed by SDS/PAGE and immunoblotting. Total amounts of IRF-1 in the sample (bottom panel) and modified IRF-1 (top panel) are shown. The results are representative of three separate experiments.

DISCUSSION

In recent years, ubiquitination has been linked to a growing number of cellular processes and it is now apparent that ubiquitin modification is involved not only in proteasomal degradation, but serves as a common mechanism for executing a wide variety of signalling events [1,2]. This raises the question of how the ubiquitin reaction is controlled at multiple levels in order to generate distinct outcomes. Differences in the result of ubiquitination can be achieved by the position of the target lysine residue in the acceptor protein [34], as well as by the use of different linkages and length of the ubiquitin chain. Yet, our understanding of ubiquitin-acceptor site selection lags behind a growing structural and mechanistic understanding of chain elongation and linkage determination [2]. One of the mechanisms proposed for ubiquitin-acceptor site specificity is that the E3 positions the charged E2 in close proximity to the target lysine residue and thereby determines which residues are subject to modification [35]. Thus while artificial 'tethering' of some E2s to their targets in the absence of an E3 is sufficient to signal substrate ubiquitination, this process is fairly non-discriminatory leading to promiscuous modification of lysine residues. In the presence of the E3, however, only a subset of the lysine modified by the E2 alone are ubiquitinated [36], suggesting that, as well as stimulating discharge of the ubiquitin from the E2 through allosteric mechanisms [37,38], E3 ligases may also act

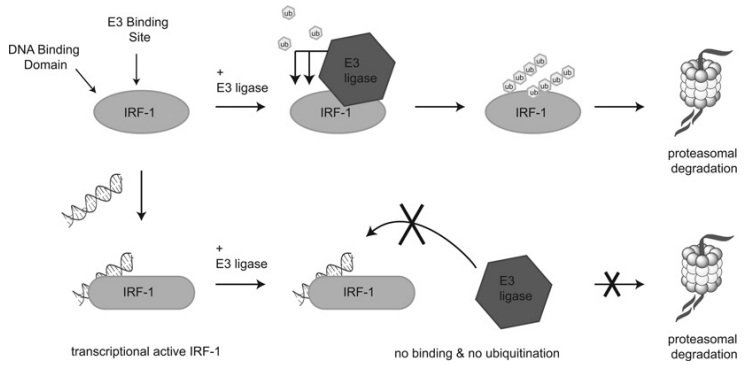

Figure 6 Model of interplay between DNA binding of IRF-1 and interaction with its E3 ligases followed by ubiquitination

The Mf2 domain is a multi E3-ligase-docking site in close proximity to the DBD of IRF-1. Binding of E3 ligases to the Mf2 domain results in ubiquitination of the proximal DBD and this leads to the proteasomal degradation of IRF-1. In complex with DNA, however, IRF-1 is unable to bind E3 ligases and other Mf2-binding partners and is not ubiquitinated and thus protected from degradation. ub, ubiquitin.

to restrain the E2, ensuring that only specific target residues are modified. Analysis of the UbcH5c–ubiquitin complex by both NMR and SAXS (small-angle X-ray scattering) [39] has shown that the conjugate is very flexible and can exhibit a range of conformations in solution, explaining how one E3 ligase can mediate ubiquitination of several different residues within a target protein. The results of the present study are in good agreement with this mechanism; we propose that IRF-1 ubiquitination is specific to its DBD and that this is achieved through docking of E3 ligases to its Mf2 domain followed by ubiquitination of the lysine residues in close proximity. However, we also note that other DBD lysine residues as well as lysine residues in the Mf2 domain itself are not ubiquitinated by either MDM2 or CHIP, suggesting that ubiquitination of these residues is sterically unfavourable.

The observation that DNA binding protects IRF-1 from ubiquitination is intriguing as it suggests a mechanism by which turnover of this transcription factor might decrease when it is in an active state, i.e. when part of a pre-initiation complex. In recent years it has become clear that the ubiquitin–proteasome system and the transcriptional machinery are intimately linked, and that ubiquitin-mediated proteolysis can enhance the activity of TAs (transcriptional activators). This is known as the 'activation by destruction' mechanism [40] and was first indicated by the observation that the transactivation domain and the region required for degradation (degron) overlap in many TAs, including IRF-1 [41]. Furthermore, factors that affect the rate of turnover for this group of transcription factors typically also affect their transactivation potential [40,42]. In keeping with this we have developed nanobodies to a negative regulatory domain of IRF-1 and, in addition to activating the TA activity of endogenous IRF-1 by up to 8-fold, they also modulate the rate of IRF-1 degradation [40]. The most popular hypothesis to explain the connection between degradation and TA function in gene expression is based on a 'suicide' model where activator degradation is somehow required as part of the activation mechanism and potentially also to terminate the signal [42]. Implicit in this model is that the TA is not subject to degradation prior to completing its function or when part of an active DNA-bound complex [42]. In the present study we show that DNA-bound IRF-1 has a cryptic or inaccessible E3-binding site, and that a non-DNA binding mutant of IRF-1 is hyperubiquitinated in comparison with the WT protein (Figure 6). These data support the idea that IRF-1 is 'protected' from degradation when it is part of an active pre-initiation complex, but can be rapidly degraded when it is not functional or when it has completed its function. How the 'suicide' model fits in with recent findings that TAs take part in 'tread-milling' rapidly on and off the chromatin [43] has not been explained. It will therefore be of interest to further dissect the role of polyubiquitination and its interplay with other forms of post-translational modification in the regulation of IRF-1 activity as a transcription factor.

In conclusion, in the present paper we report that ubiquitination of residues in the DBD of IRF-1 is achieved through E3-ligase binding to an adjacent multi-protein docking site resulting in the selective modification of several lysine residues. Docking of the E3 to its substrate is therefore not only required for ubiquitination, but also determines the specificity of the reaction. If the E3 cannot bind to its substrate, for example when IRF-1 is bound to DNA, it is not able to mediate DBD ubiquitination, suggesting a mechanism by which an active pool of IRF-1 might be protected from degradation in cells.

AUTHOR CONTRIBUTION

Vivien Landré carried out all of the experiments and contributed significantly to their design, analysed the data, generated the Figures and made a significant contribution to writing the manuscript. Kathryn Ball aided in planning and design of experiments, interpreted data and, with Vivien Landré, wrote the paper. Emmanuelle Pion contributed to Figure 1(F), generated some reagents and carried out preliminary experiments (results not shown). Vikram Narayan provided reagents, aided in the design of some experiments and contributed to discussions. Dimitris Xirodimas aided in the design and analysis of MS studies and, together with Kathryn Ball, obtained funding.

ACKNOWLEDGEMENTS

We thank Susanne Pettersson for her technical support.

FUNDING

This work was supported by Cancer Research UK [programme grant number C377/ A6355 (to K.L.B.)]. V.L. receives a Ph.D. studentship from the Scottish Universities Life Sciences Alliance (SULSA).

REFERENCES

1 Pickart, C. M. and Eddins, M. J. (2004) Ubiquitin: structures, functions, mechanisms. Biochim. Biophys. Acta **1695**, 55–72
2 Komander, D. and Rape, M. (2012) The ubiquitin code. Annu. Rev. Biochem. **81**, 203–229
3 Metzger, M. B. and Weissman, A. M. (2010) Working on a chain: E3s ganging up for ubiquitylation. Nat. Cell Biol. **12**, 1124–1126
4 Kim, H. T., Kim, K. P., Lledias, F., Kisselev, A. F., Scaglione, K. M., Skowyra, D., Gygi, S. P. and Goldberg, A. L. (2007) Certain pairs of ubiquitin-conjugating enzymes (E2s) and ubiquitin-protein ligases (E3s) synthesize nondegradable forked ubiquitin chains containing all possible isopeptide linkages. J. Biol. Chem. **282**, 17375–17386
5 Wickliffe, K. E., Williamson, A., Meyer, H. J., Kelly, A. and Rape, M. (2011) K11-linked ubiquitin chains as novel regulators of cell division. Trends Cell Biol. **21**, 656–663
6 Catic, A., Collins, C., Church, G. M. and Ploegh, H. L. (2004) Preferred *in vivo* ubiquitination sites. Bioinformatics **20**, 3302–3307
7 Liebermann, D. A. and Hoffman, B. (2009) Good and bad IRF-1: role in tumor suppression versus autoimmune disease. Leuk. Res. **33**, 1301–1302
8 Ren, Z., Wang, Y., Tao, D., Liebenson, D., Liggett, T., Goswami, R., Clarke, R., Stefoski, D. and Balabanov, R. (2011) Overexpression of the dominant-negative form of interferon regulatory factor 1 in oligodendrocytes protects against experimental autoimmune encephalomyelitis. J. Neurosci. **31**, 8329–8341
9 Willman, C. L., Sever, C. E., Pallavicini, M. G., Harada, H., Tanaka, N., Slovak, M. L., Yamamoto, H., Harada, K., Meeker, T. C., List, A. F. et al. (1993) Deletion of IRF-1, mapping to chromosome 5q31.1, in human leukemia and preleukemic myelodysplasia. Science **259**, 968–971
10 Tamura, G., Ogasawara, S., Nishizuka, S., Sakata, K., Maesawa, C., Suzuki, Y., Terashima, M., Saito, K. and Satodate, R. (1996) Two distinct regions of deletion on the long arm of chromosome 5 in differentiated adenocarcinomas of the stomach. Cancer Res. **56**, 612–615
11 Green, W. B., Slovak, M. L., Chen, I. M., Pallavicini, M., Hecht, J. L. and Willman, C. L. (1999) Lack of IRF-1 expression in acute promyelocytic leukemia and in a subset of acute myeloid leukemias with del(5)(q31). Leukemia **13**, 1960–1971
12 Wang, Y., Liu, D. P., Chen, P. P., Koeffler, H. P., Tong, X. J. and Xie, D. (2007) Involvement of IFN regulatory factor (IRF)-1 and IRF-2 in the formation and progression of human esophageal cancers. Cancer Res. **67**, 2535–2543
13 Pion, E., Narayan, V., Eckert, M. and Ball, K. L. (2009) Role of the IRF-1 enhancer domain in signalling polyubiquitination and degradation. Cell. Signalling **21**, 1479–1487
14 Nakagawa, K. and Yokosawa, H. (2000) Degradation of transcription factor IRF-1 by the ubiquitin-proteasome pathway. The C-terminal region governs the protein stability. Eur. J. Biochem. **267**, 1680–1686
15 Narayan, V., Pion, E., Landre, V., Muller, P. and Ball, K. L. (2011) Docking-dependent ubiquitination of the interferon regulatory factor-1 tumor suppressor protein by the ubiquitin ligase CHIP. J. Biol. Chem. **286**, 607–619
16 Narayan, V., Halada, P., Hernychova, L., Chong, Y. P., Zakova, J., Hupp, T. R., Vojtesek, B. and Ball, K. L. (2011) A multiprotein binding interface in an intrinsically disordered region of the tumor suppressor protein interferon regulatory factor-1. J. Biol. Chem. **286**, 14291–14303
17 Pamment, J., Ramsay, E., Kelleher, M., Dornan, D. and Ball, K. L. (2002) Regulation of the IRF-1 tumour modifier during the response to genotoxic stress involves an ATM-dependent signalling pathway. Oncogene **21**, 7776–7785
18 Beresford, P. J., Zhang, D., Oh, D. Y., Fan, Z., Greer, E. L., Russo, M. L., Jaju, M. and Lieberman, J. (2001) Granzyme A activates an endoplasmic reticulum-associated caspase-independent nuclease to induce single-stranded DNA nicks. J. Biol. Chem. **276**, 43285–43293
19 Ivanov, A. V., Peng, H., Yurchenko, V., Yap, K. L., Negorev, D. G., Schultz, D. C., Psulkowski, E., Fredericks, W. J., White, D. E., Maul, G. G. et al. (2007) PHD domain-mediated E3 ligase activity directs intramolecular sumoylation of an adjacent bromodomain required for gene silencing. Mol. Cell **28**, 823–837
20 Wallace, M., Worrall, E., Pettersson, S., Hupp, T. R. and Ball, K. L. (2006) Dual-site regulation of MDM2 E3-ubiquitin ligase activity. Mol. Cell **23**, 251–263
21 Fujita, T., Kimura, Y., Miyamoto, M., Barsoumian, E. L. and Taniguchi, T. (1989) Induction of endogenous IFN-α and IFN-β genes by a regulatory transcription factor, IRF-1. Nature **337**, 270–272
22 Ruiz-Ruiz, C., Ruiz de Almodovar, C., Rodriguez, A., Ortiz-Ferron, G., Redondo, J. M. and Lopez-Rivas, A. (2004) The up-regulation of human caspase-8 by interferon-γ in breast tumor cells requires the induction and action of the transcription factor interferon regulatory factor-1. J. Biol. Chem. **279**, 19712–19720
23 Lace, M. J., Anson, J. R., Klingelhutz, A. J., Harada, H., Taniguchi, T., Bossler, A. D., Haugen, T. H. and Turek, L. P. (2009) Interferon-β treatment increases human papillomavirus early gene transcription and viral plasmid genome replication by activating interferon regulatory factor (IRF)-1. Carcinogenesis **30**, 1336–1344
24 Gongora, C., Degols, G., Espert, L., Hua, T. D. and Mechti, N. (2000) A unique ISRE, in the TATA-less human Isg20 promoter, confers IRF-1-mediated responsiveness to both interferon type I and type II. Nucleic Acids Res. **28**, 2333–2341
25 Clarke, N., Jimenez-Lara, A. M., Voltz, E. and Gronemeyer, H. (2004) Tumor suppressor IRF-1 mediates retinoid and interferon anticancer signaling to death ligand TRAIL. EMBO J. **23**, 3051–3060
26 Walerych, D., Kudla, G., Gutkowska, M., Wawrzynow, B., Muller, L., King, F. W., Helwak, A., Boros, J., Zylicz, A. and Zylicz, M. (2004) Hsp90 chaperones wild-type p53 tumor suppressor protein. J. Biol. Chem. **279**, 48836–48845
27 Dominguez, C., Boelens, R. and Bonvin, A. M. (2003) HADDOCK: a protein–protein docking approach based on biochemical or biophysical information. J. Am. Chem. Soc. **125**, 1731–1737
28 de Vries, S. J., van Dijk, A. D., Krzeminski, M., van Dijk, M., Thureau, A., Hsu, V., Wassenaar, T. and Bonvin, A. M. (2007) HADDOCK versus HADDOCK: new features and performance of HADDOCK2.0 on the CAPRI targets. Proteins **69**, 726–733
29 Vijay-Kumar, S., Bugg, C. E., Wilkinson, K. D., Vierstra, R. D., Hatfield, P. M. and Cook, W. J. (1987) Comparison of the three-dimensional structures of human, yeast, and oat ubiquitin. J. Biol. Chem. **262**, 6396–6399
30 Pettersson, S., Kelleher, M., Pion, E., Wallace, M. and Ball, K. L. (2009) Role of Mdm2 acid domain interactions in recognition and ubiquitination of the transcription factor IRF-2. Biochem. J. **418**, 575–585
31 Wang, X., Wang, J. and Jiang, X. (2011) MdmX protein is essential for Mdm2 protein-mediated p53 polyubiquitination. J. Biol. Chem. **286**, 23725–23734
32 Escalante, C. R., Yie, J., Thanos, D. and Aggarwal, A. K. (1998) Structure of IRF-1 with bound DNA reveals determinants of interferon regulation. Nature **391**, 103–106
33 Gerlach, B., Cordier, S. M., Schmukle, A. C., Emmerich, C. H., Rieser, E., Haas, T. L., Webb, A. I., Rickard, J. A., Anderton, H., Wong, W. W. et al. (2011) Linear ubiquitination prevents inflammation and regulates immune signalling. Nature **471**, 591–596
34 Meier, F., Abeywardana, T., Dhall, A., Marotta, N. P., Varkey, J., Langen, R., Chatterjee, C. and Pratt, M. R. (2012) Semisynthetic, site-specific ubiquitin modification of α-synuclein reveals differential effects on aggregation. J. Am. Chem. Soc. **134**, 5468–5471
35 Passmore, L. A. and Barford, D. (2004) Getting into position: the catalytic mechanisms of protein ubiquitylation. Biochem. J. **379**, 513–525
36 David, Y., Ternette, N., Edelmann, M. J., Ziv, T., Gayer, B., Sertchook, R., Dadon, Y., Kessler, B. M. and Navon, A. (2011) E3 ligases determine ubiquitination site and conjugate type by enforcing specificity on E2 enzymes. J. Biol. Chem. **286**, 44104–44115
37 Ozkan, E., Yu, H. and Deisenhofer, J. (2005) Mechanistic insight into the allosteric activation of a ubiquitin-conjugating enzyme by RING-type ubiquitin ligases. Proc. Natl. Acad. Sci. U.S.A. **102**, 18890–18895
38 Das, R., Mariano, J., Tsai, Y. C., Kalathur, R. C., Kostova, Z., Li, J., Tarasov, S. G., McFeeters, R. L., Altieri, A. S., Ji, X. et al. (2009) Allosteric activation of E2-RING finger-mediated ubiquitylation by a structurally defined specific E2-binding region of gp78. Mol. Cell **34**, 674–685
39 Pruneda, J. N., Stoll, K. E., Bolton, L. J., Brzovic, P. S. and Klevit, R. E. (2011) Ubiquitin in motion: structural studies of the ubiquitin-conjugating enzyme approximately ubiquitin conjugate. Biochemistry **50**, 1624–1633
40 Lipford, J. R. and Deshaies, R. J. (2003) Diverse roles for ubiquitin-dependent proteolysis in transcriptional activation. Nat. Cell Biol. **5**, 845–850
41 Leung, A., Geng, F., Daulny, A., Collins, G., Guzzardo, P. and Tansey, W. P. (2008) Transcriptional control and the ubiquitin-proteasome system. Ernst Schering Found. Symp. Proc., 75–97
42 Geng, F., Wenzel, S. and Tansey, W. P. (2012) Ubiquitin and proteasomes in transcription. Annu. Rev. Biochem. **81**, 177–201
43 Lickwar, C. R., Mueller, F., Hanlon, S. E., McNally, J. G. and Lieb, J. D. (2012) Genome-wide protein-DNA binding dynamics suggest a molecular clutch for transcription factor function. Nature **484**, 251–255

Received 5 July 2012/31 October 2012; accepted 8 November 2012
Published as BJ Immediate Publication 8 November 2012, doi:10.1042/BJ20121076

Biochem. J. (2013) **449**, 707–717 (Printed in Great Britain) doi:10.1042/BJ20121076

online data

SUPPLEMENTARY ONLINE DATA

DNA-binding regulates site-specific ubiquitination of IRF-1

Vivien LANDRÉ*, Emmanuelle PION*[1], Vikram NARAYAN*, Dimitris P. XIRODIMAS† and Kathryn L. BALL*[2]

*Cell Signalling Unit, Edinburgh Cancer Research Centre, MRC Institute of Genetics and Molecular Medicine, University of Edinburgh, Crewe Rd South, Edinburgh EH4 2XR, U.K., and †Centre de Recherche de Biochimie Macromoléculaire, UMR 5237, CNRS, Montpellier, France

IRF-1 peptides

1:	MPITRMRMRPWLEMQINSNQ	12:	VPGYMQDLEVEQALTPALSP
2:	INSNQIPGLIWINKEEMIFQ	13:	PALSPCAVSSTLPDWHIPVE
3:	EMIFQIPWKHAAKHGWDINK	14:	HIPVEVVPDSTSDLYNFQVS
4:	WDINKDACLFRSWAIHTGRY	15:	NFQVSPMPSTSEATTDEDEE
5:	HTGRYKAGEKEPDPKTWKAN	16:	DEDEEGKLPEDIMKLLEQSE
6:	TWKANFRCAMNSLPDIEEVK	17:	LEQSEWQPTNVDGKGYLLNE
7:	IEEVKDQSRNKGSSAVRVYR	18:	YLLNEPGVQPTSVYGDFSCK
8:	VRVYRMLPPLTKNQRKERKS	19:	DFSCKEEPEIDSPGGDIGLS
9:	KERKSKSSRDAKSKAKRKSC	20:	DIGLSLQRVFTDLKNMDATW
10:	KRKSCGDSSPDTFSDGLSSS	21:	MDATWLDSLLTPVRLPSIQA
11:	GLSSSTLPDDHSSYTVPGYM	22:	LDSLLTPVRLPSIQAIPCAP

Figure S1 IRF-1 peptides

List of the IRF-1 peptide library used in the protein–peptide binding assay in Figure 1(D) of the main text.

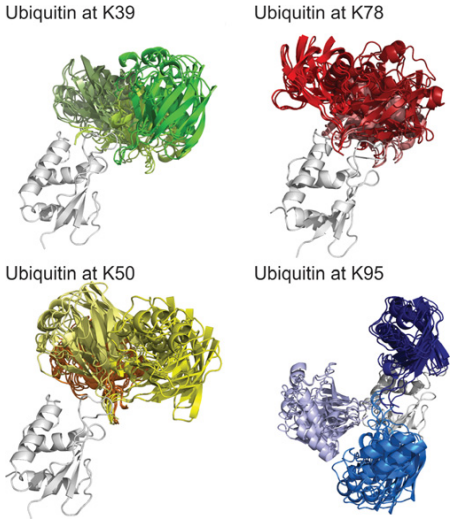

Figure S2 Model of monoubiquitinated IRF-1

Ubiquitin was modelled on to the IRF-1 DBD at the ubiquitin receptor lysine residues present in the crystal structure [Lys^{39} (K39), Lys^{50} (K50), Lys^{78} (K78) and Lys^{95} (K95)] using the HADDOCK web server. From the results obtained the four best structures from the three best clusters were analysed. The overlay of the ubiquitin position in respect to IRF-1 for each lysine residue are shown, with ubiquitin in structures obtained from different clusters in different colours.

[1] Present address: Centre de Recherche de Biochimie Macromoléculaire, UMR 5237, CNRS, Montpellier, France.
[2] To whom correspondence should be addressed (email Kathryn.Ball@igmm.ed.ac.uk).

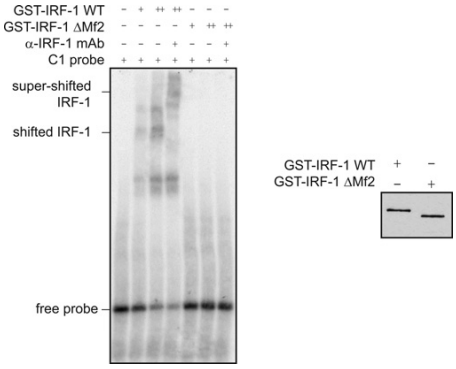

Figure S3 An IRF-1 Mf2 domain deletion mutant is DNA-binding-deficient

EMSA showing binding of a titration (100 and 300 ng) of purified GST–IRF-1^{WT} or GST–IRF-$1^{\Delta Mf2}$ to a ^{32}P-labelled DNA probe of C1 DNA; an anti-IRF-1 mAb was included in the reaction where indicated to supershift the complex (left-hand panel). Purified GST–IRF-1^{WT} or GST–IRF-$1^{\Delta Mf2}$ was separated by SDS/PAGE and analysed by immunoblotting using an anti-IRF-1 pAb.

Received 5 July 2012/31 October 2012; accepted 8 November 2012
Published as BJ Immediate Publication 8 November 2012, doi:10.1042/BJ20121076